VOLUME 26 (1961) No. 3

NUCLEAR PHYSICS

JOURNAL DEVOTED TO THE EXPERIMENTAL AND THEORETICAL STUDY OF THE FUNDAMENTAL CONSTITUENTS OF MATTER AND THEIR INTERACTIONS

EDITOR: L. ROSENFELD - COPENHAGEN

HELMUT JAHN, Die Darstellungen der starken Kopplung und das Resonanzproblem der Meson-Nucleon Streuung 353

E. A. SANDERSON, Excitation of the giant dipole resonance by inelastic proton scattering on carbon 420

D. W. LANG, Analysis of recent measurement of nuclear level density parameters 434

R. M. FREEMAN, The magnetic moment of the second excited state of F^{19} . 446

A. I. SOLOMON, The new particles and the baryon mass spectrum 452

J. M. FERGUSON and F. M. TOMNOVEC, Gamma-ray spectrum of Te^{131} . . . 457

E. W. SCHMID and K. WILDERMUTH, Phase shift calculations on α-α scattering 463

J. S. R. CHISHOLM, Change of variables in quantum field theories 469

H. E. GOVE, A. E. LITHERLAND and R. BATCHELOR, Proton capture gamma rays in the giant resonance region in light nuclei 480

F. LACOSTE and G. R. BISHOP, Experimental study of the charge distribution of O^{16} and O^{18} by electron scattering 511

Errata 527

August 1961

NORTH-HOLLAND PUBLISHING COMPANY - AMSTERDAM

EDITORIAL BOARD

AUSTRALIA & NEW ZEALAND:	H. Messel (Sydney), M. L. Oliphant (Canberra)
AUSTRIA:	B. Karlik (Vienna), H. Thirring (Vienna)
BELGIUM:	M. de Hemptinne (Louvain), J. Verhaeghe (Ghent)
CANADA:	G. Volkoff (Vancouver)
DENMARK:	C. Møller (Copenhagen), S. Rozental (Copenhagen), G. E. Brown (Copenhagen)
FINLAND:	L. Simons (Helsinki)
FRANCE:	A. Berthelot (Saclay), S. Gorodetzky (Strasbourg)
GERMANY (DEM. REP.):	G. Hertz (Leipzig)
GERMANY (FED. REP.):	W. Gentner (Freiburg i. B.), J. H. D. Jensen (Heidelberg)
GREAT BRITAIN:	W. E. Burcham (Birmingham), T. H. R. Skyrme (Harwell)
HUNGARY:	L. Janossy (Budapest)
INDIA:	H. Bhabha (Bombay), R. Ramanna (Trombay)
IRISH REPUBLIC:	J. McConnell (Maynooth)
ISRAEL:	G. Racah (Jerusalem)
ITALY:	E. Amaldi (Rome)
JAPAN:	S. Kikuchi (Tokay), S. Tomonaga (Tokyo)
MEXICO:	M. Moshinsky (Mexico)
NETHERLANDS:	H. Brinkman (Groningen), S. R. de Groot (Leiden)
NORWAY:	E. Hylleraas (Oslo), A. Lundby (Oslo), H. Wergeland (Trondheim)
POLAND:	L. Infeld (Warsaw), J. Werle (Warsaw)
PORTUGAL:	J. M. Araújo (Porto), J. R. de Almeida Santos (Coimbra)
SOUTH AMERICA:	G. Beck (Saõ Paulo), J. Leite Lopes (Rio de Janeiro)
SPAIN:	J. M. Otero (Madrid), C. Sanchez del Rio (Madrid)
SWEDEN:	O. Klein (Stockholm), K. Siegbahn (Uppsala), I. Waller (Uppsala)
SWITZERLAND:	P. Huber (Basel), P. Scherrer (Zürich)
U.A.R. & ARAB COUNTRIES:	F. El Bedewi (Cairo), M. G. Nooh (Cairo)
U.S.A.:	H. H. Barschall (Madison, Wisconsin), S. Devons (New York), V. F. Weisskopf (Cambridge, Mass.)
U.S.S.R.:	M. A. Markov (Moscow), I. S. Shapiro (Moscow), D. V. Skobeltzyn (Moscow)
YUGOSLAVIA:	I. Supek (Zagreb)

CONTRIBUTIONS may be sent to the Editor, Professor L. Rosenfeld, NORDITA, Blegdamsvej 17, Copenhagen Ø, either directly, or preferably through the intermediary of one of the members of the Editorial Board of the country or region in which the author is working. They may be written in English, French or German.

NUCLEAR PHYSICS is published in fortnightly issues. The subscription price per volume of 700 pages is fl 57.00; 114s; $ 15.00. Post-free.

SUBSCRIPTIONS should be sent to the publishers, **NORTH-HOLLAND PUBLISHING COMPANY** P.O. Box 103, Amsterdam or to any subscription-agent.

BOOKS FOR REVIEW should be sent to Professor Rosenfeld.

No part of this issue may be reproduced in any form, by print, photoprint, microfilm or any other means without permission from the publisher.

Printed in the Netherlands

8.C

Nuclear Physics **26** (1961) 353—419; © *North-Holland Publishing Co., Amsterdam*

Not to be reproduced by photoprint or microfilm without written permission from the publisher

DIE DARSTELLUNGEN DER STARKEN KOPPLUNG UND DAS RESONANZPROBLEM DER MESON-NUCLEON-STREUUNG

HELMUT JAHN

Max-Planck-Institut für Physik und Astrophysik, München †

Eingegangen am 2. Januar 1961

Abstract: This paper deals with the completion of the strong-coupling method in meson field theory. By means of a canonical and non-linear transformation of variables the original meson field is split into a free meson part and a self field part of the nucleon. The transformation is defined so that the interaction between the compound nucleon system thus arising and the free mesons vanishes in the case of infinitely strong coupling. It is shown that there exists a family of transformations satisfying the conditions. A system of equations for certain transformation functions is stated as the consequence of the conditions. The solutions of the field-splitting problem are investigated. The general scheme for a strong-coupling approximation method based on this field splitting is derived, and the problem of calculating the pion-nucleon resonance scattering from the strong coupling theory is treated on this basis. A special approximation is made for calculations near the resonance. Numerical results obtained from such a calculation are discussed. For the sake of simplicity the symmetric scalar fixed-source meson theory is used. But the principle of the method will be the same in the more essential but more complicated symmetric pseudoscalar case. Thus the present considerations will serve to guide an analogous investigation using the symmetric pseudoscalar theory.

1. Einleitung

Gegenstand dieser Arbeit †† ist das Problem der Weiterentwicklung der Methode der starken Kopplung der Meson-Feldtheorie. Diese Methode ist schon vor längerer Zeit von Wentzel [1, 2]), Oppenheimer u. Schwinger [3]) und Pauli u. Dancoff [4]) begründet [5]) ††† und danach von einer Reihe von Autoren [6–16]) ‡, zuletzt von Pais u. Serber [17, 18]), Landovitz u. Margolis [19]), Nickle u. Serber [20]) und Chun [7]) weitergeführt worden. Einige Ergebnisse der in der hier vorliegenden Arbeit entwickelten Transformationsmethode sind vom Verfasser bereits bei Untersuchungen über die Durchführung einer Näherung der starken

† Anschließend am Institut für Theoretische Physik der Universität Hamburg. Gegenwärtige Adresse: Institute for Advanced Study, Princeton, New Jersey, USA.

†† Gekürzte Veröffentlichung eines Preprints vom Februar 1959. Alle in der hier vorliegenden Arbeit gegebenen Formulierungen sind schon in diesem Preprint enthalten.

††† Eine auf einer klassischen Behandlungsweise basierende Vorstufe dazu, die aber noch nicht die Isobaren berücksichtigt, wurde schon von Heisenberg angegeben; siehe Ref. [5]). Halbklassisch-korrespondenzmäßige Untersuchungen mit Berücksichtigung der Isobaren, wurden von Tomonaga (siehe Ref. [5])) und Pauli durchgeführt (siehe Ref. [11])).

‡ Funktionalanalytische Methoden wurden auf diesem Problemkreis von Hamilton [16]) und Edwards [16]) angewandt. Für die Behandlung der Kernkräfte siehe man Ref. [7]).

Kopplung des Chew-Low-Formalismus benutzt worden [21]), sodaß aus der hier vorliegenden Arbeit die Herleitung dieser Ergebnisse zu entnehmen ist.

Schon in den früheren der eben genannten Arbeiten waren die als Nukleonisobaren bezeichneten Anregungszustände des bei starker Kopplung durch Bindung von Mesonen an ein Nukleon sich bildenden Compoundnukleonsystems im Rahmen des Modells der festen Quelle [22])† gefunden worden[23])††, und Landovitz u. Margolis haben zusätzlich dazu noch weitere Zustände errechnet [19]). Die Formulierung der Ankopplung des Teilsystems der freien Mesonen an diese Nukleonisobaren ist aber bisher noch nicht bis zu dem Grade gelungen, daß so wichtige Probleme wie der Fall der Instabilität der Isobaren und die daraus sich ergebende Berechnungsmöglichkeit der π-Meson-Nukleon-Resonanzstreuung in einer Näherung der starken Kopplung hätten behandelt werden können. Eine solche Näherung wäre gemäß Goebel [24]) und dem Verfasser [21]) verschieden von der inzwischen von Chew u. Low [25]) und für den geladenen skalaren Fall von Lee u. Serber [26]) entwickelten Ein-Meson-Näherung der π-Meson-Nukleon-Streuintegralgleichung von Low [27]) und würde einer bestimmten Art von Mehr-Meson-Näherung derselben entsprechen [21, 24]).

Eine bestimmte Art der bisherigen Behandlungsweise der Methode der starken Kopplung ist dadurch gekennzeichnet, daß zur Beschreibung der Isobaren Operatoren der Integrale der Bewegung des Gesamtsystems als Endergebnis eines dazu dienenden Transformationsprozesses in den Hamiltonoperator des Modells der festen Quellen eingeführt werden. Diese Behandlungsweise wurde in Weiterentwicklung des von Wentzel [1]), Serber u. Dancoff [6]), Tomonaga [9]) und Kaufman [13]) eingeschlagenen Weges bisher am weitgehendsten von Pais u. Serber [17, 18]) und Nickle u. Serber [20]) durchgeführt. Dabei sind Kaufman [13]) und Pais u. Serber [17]) im Fall des Modells der festen Quellen der geladenen skalaren Theorie bis zur Berechnung von Streuprozessen mit Anregung von stabilen Isobaren bei endlicher, großer Kopplungskonstanten gelangt, während Nickle u. Serber [20]) die Korrekturen zum Isobarenenergiespektrum bis zur Ordnung g^{-4} berechnet und ihre Einbeziehbarkeit in die Renormierung des bisherigen Spektrums gefunden haben. Chun [7]) hat beim Zwei-Nukleon Problem der geladenen skalaren Theorie mit dieser Behandlungsweise gezeigt, daß beim Übergang von großen zu kleinen Nukleonabständen die Kopplungskonstante der Kernkräfte von der renormierten zur unrenormierten Kopplungskonstanten übergeht. Es scheint aber bei der geladenen skalaren Theorie nur schwer möglich zu sein, zur Instabilität der Isobaren zu kommen [17, 21, 24]), sondern diese ist erst bei der stärkeren cut-off-Abhängigkeit, wie sie die pseudoskalare Theorie aufweist, erreichbar. Pais u. Serber [18]) haben

† Überlegungen zur Frage der über das Modell der festen Quellen hinausgehende Erweiterung der Methode der starken Kopplung findet man in Ref. [22]).

†† Eine obere Grenze der Kopplungskonstanten für den Beginn der Bildung solcher Isobaren wurde unabhängig von einer speziellen Näherung von Ruderman u. Gasiorowics bestimmt (siehe Ref. [23])).

ihre zunächst bei der geladenen skalaren Theorie entwickelten Behandlungsweise auch auf die symmetrische pseudoskalare Theorie übertragen. Sie sind dabei bis zu der dafür charakteristischen expliziten Einführung der Isospin- und Drehimpulsoperatoren des Gesamtsystems in den Hamiltonoperator des Modells der festen Quellen zur Beschreibung der Isobaren gelangt. Ganz entsprechend zu ihrer Behandlung des geladenen skalaren Falles haben sie eine geschlossen angebbare Transformation hergeleitet, mittels der dies exakt möglich ist. Die Spezialisierung auf den Fall der starken Kopplung ist dabei noch nicht vorausgesetzt, sodaß diese Transformation auch über den Zweck der Entwicklung des Näherungsverfahrens der starken Kopplung hinaus von Bedeutung ist.

Statt der Einführung von Operatoren der Integrale der Bewegung des Gesamtsystems zur Beschreibung der Isobaren, wie sie für die eben genannte Behandlungsweise in Ref. [1, 6, 9, 12, 13, 17, 18, 20]) charakteristisch war, kann es aber für die Behandlung solcher Probleme wie des oben genannten Instabilitäts- und Resonanzproblems zweckmäßiger sein, die zur Beschreibung der Isobaren dienenden Operatoren nur auf das Compoundnukleon als Teilsystem zu beziehen, um sie so auch als Operatoren der instabilen Isobaren beim Übergang zum instabilen Fall verwenden zu können [42]). Dem entspricht auch schon das Vorgehen der älteren Arbeiten von Pauli u. Dancoff [4]), Wentzel [2]) und Houriet [8]) im Rahmen des Modells der festen Quellen der symmetrischen pseudoskalaren u. vektoriellen Theorie (siehe die Zusammenfassungen in Ref. [10, 11]). In diesen Arbeiten dienen aber zur Beschreibung des Teilsystems der freien Mesonen noch Operatoren mit nichtkanonischen Vertauschungsrelationen, mit denen man keine Erzeugungs- u. Vernichtungsoperatoren zum Aufbau eines Basissystems für ein systematisches Näherungsverfahren in der gewöhnlichen Weise bilden kann. Vielmehr würden dazu erst noch weitere Transformationen erforderlich sein, die in diesen Arbeiten noch nicht durchgeführt sind. Daher konnten Probleme wie das Instabilwerden der Anregungszustände des Compoundnukleons, und die Berechnung der π-Meson-Nukleon-Resonanz-Streuung mit der Methode der starken Kopplung auch auf diesem Wege bisher noch nicht behandelt werden. Weiterhin treten bei den eben genannten Arbeiten auch Freiheitsgrade von 0-ter Ordnung auf, die formal als zur Mesonwolke gehörend eingeführt wurden, von denen aber schon bei Pauli u. Dancoff [4]) zum Ausdruck gebracht wird, daß sie eigentlich zu den freien Mesonen zu rechnen sind. Kopplungsterme zwischen diesen Freiheitsgraden und den freien Mesonen treten ebenfalls in 0-ter Ordnung auf und stören daher bei der Entwicklung eines Näherungsverfahrens, wo sie, etwa störungstheoretisch betrachtet, zu ein und derselben Ordnung in der Kopplungskonstanten Beiträge von beliebig hohen Näherungen liefern würden.

In den folgenden Ausführungen wollen wir daher außer der Einführung von Operatoren für das Teilsystem des Compoundnukleons, auch die Einführung

von Erzeugungs- und Vernichtungsoperatoren für das Teilsystem der freien Mesonen mittels einer Variablentransformation durchführen und zwar so, daß die eben erwähnten Freiheitsgrade und Kopplungsterme der 0-ten Ordnung in der Kopplungskonstanten nicht mehr auftreten. Wir erreichen dies durch die Forderung, daß die Wechselwirkung zwischen den beiden Teilsystemen der freien Mesonen und des Compoundnukleons im Grenzfall $g \to \infty$ verschwinden soll (Bedingung 4, Absatz 2.1.6), die wir die Bedingung der starken Kopplung nennen.

Die einzelnen Schritte sind dabei folgende: Zuerst stellen wir die Operatoren der Teilsysteme der freien Mesonen und des Compoundnukleons auf (Absatz 2.1.3. u. 4), wobei wir letztere lediglich auf Grund der Symmetrieeigenschaften des verwendeten Modells der festen Quellen konstruieren (Absatz 2.1.4.) Dann leiten wir den einfachsten Ansatz für eine Variablensubstitution her, die die ursprünglichen Feldvariablen durch derartige Variablen der freien Mesonen und des Compoundnukleons substituiert, und damit das ursprüngliche Gesamtsystem in die beiden so definierten Teilsysteme der freien Mesonen und des Compoundnukleons aufspaltet (Absätze 2.2.1. bis 2.2.4). Die Erfüllung der Vertauschungsrelationen aller dabei vorkommenden Operatoren, sowie die exakte Aufspaltung ohne gemischte Terme für jedes g der außer der Energie noch in Frage kommenden Erhaltungsgrößen wie des Isospinoperators, wird garantiert durch Bedingungen, die an die dabei auftretenden noch unbekannten Transformationsfunktionen zu stellen sind (Absätze 2.1.6 und 2.2.2 bis 2.2.4). Diese Transformationsfunktionen sind dadurch aber noch nicht bestimmt. Somit haben wir noch die Freiheit, die eben genannte Bedingung der starken Kopplung zu stellen. Aber auch nach Stellung der Bedingung der starken Kopplung bekommen wir noch eine ganze Schar von Transformationen des eben genannten einfachsten Ansatzes, die mit der Bedingung der starken Kopplung zusammen allen eben genannten Bedingungen genügen (Absätze 2.4.1 bis 2.4.3). Für zwei spezielle Vertreter aus dieser Schar schreiben wir die durch die Variablensubstitution sich ergebende, in freie-Meson-Terme, Compoundnukleonterme u. Wechselwirkungsterme neu aufgespaltene Form des Hamiltonoperators an, deren Wechselwirkungsterme die Bedingung der starken Kopplung erfüllen (Abschnitt 2.5). Die Entwicklung der Eigenzustände des Gesamthamiltonoperators nach den Eigenzuständen des wechselwirkungsfreien Anteils der neu aufgespaltenen Form des Gesamthamiltonoperators nennen wir dabei eine Darstellung der starken Kopplung. Mit Hilfe einer solchen Darstellung der starken Kopplung kann dann das Schema eines auf dieser Neuaufspaltung des Hamiltonoperators basierenden Näherungsverfahrens der starken Kopplung entwickelt werden (Teil 3).

Um möglichst einfache Verhältnisse zu haben, sind diese Untersuchungen der vorliegenden Arbeit hier zunächst am Modell der festen Quelle für den Fall der symmetrischen skalaren Theorie durchgeführt. Das Prinzip der Methode

ist aber ebenso auch auf den physikalisch wichtigereren, jedoch komplizierteren Fall der symmetrischen pseudoskalaren Theorie übertragbar [41]).

2. Transformation zur Aufspaltung des Mesonfeldes in freies Mesonfeld und Nukleoneigenfeld

2.1. AUSGANGSGLEICHUNGEN, VARIABLEN FÜR FREIEN FELDANTEIL UND EIGENFELDANTEIL

2.1.1. *Ausgangsgleichungen*

Wie soeben erläutert wurde, entwickeln wir das Verfahren hier zunächst am Modell eines an ein vorgegebenes Nukleon unter Vernachlässigung von dessen Rückstoß gekoppelten symmetrischen skalaren Mesonfeldes, wie es für die Methode der starken Kopplung schon von Miyazima, Tati u. Tomonaga [11]) benutzt wurde. Demgemäß lautet der Hamiltonoperator

$$H = \tfrac{1}{2}\sum_{\rho}\int\{\pi_\rho{}^2(\mathbf{r})+\varphi_\rho(\mathbf{r})(-\Delta+\kappa^2)\varphi_\rho(\mathbf{r})\}\,\mathrm{d}\mathbf{r}+g(2\pi)^{\frac{1}{2}}\sum_{\rho}\tau_\rho\int K(\mathbf{r})\varphi_\rho(\mathbf{r})\mathrm{d}\mathbf{r}$$

mit den kanonisch konjugierten Hermiteschen Feldoperatoren $\varphi_\rho(\mathbf{r})$ und $\pi_\rho(\mathbf{r})$ des Mesonfeldes der Masse κ, deren Vertauschungsrelationen

$$i[\pi_{\rho'}(\mathbf{r}'),\varphi_\rho(\mathbf{r})]=\delta_{\rho'\rho}\delta(\mathbf{r}'-\mathbf{r}),\qquad[\pi_{\rho'}(\mathbf{r}'),\pi_\rho(\mathbf{r})]=[\varphi_{\rho'}(\mathbf{r}'),\varphi_\rho(\mathbf{r})]=0$$

lauten, und deren auf den Isospinraum bezogenen Vektorindex ρ die Zuordnung zu der jeweiligen Ladungssorte beschreibt, und zwar mit $\rho = 1{,}2$ für die geladenen Mesonen und $\rho = 3$ für die neutralen Mesonen, wenn $\rho = 3$ die Ladungsachse bezeichnet.

Das nackte Nukleon wird beschrieben durch die kugelsymmetrische Quellfunktion $K(\mathbf{r})$ mit der Normierung $\int K(\mathbf{r})\,\mathrm{d}\mathbf{r} = 1$ und einer radialen Ausdehnung von etwa der Größenordnung der Proton-Comptonwellenlänge. Seine einzige dynamische Variable ist sein Isospinvektoroperator τ_ρ, dessen Komponenten $\rho = 1{,}2$ die Übergänge zwischen den nackten Proton- u. Neutronzuständen beschreiben, während $\frac{1}{2}(1+\tau_3)$ den Ladungsoperator mit Eigenwerten 1 oder 0 darstellt.

Übergang in den Impulsraum ergibt

$$H=\tfrac{1}{2}\sum_{\rho}\int\{p^*_{\rho\mathbf{k}}p_{\rho\mathbf{k}}+\varepsilon^2q^*_{\rho\mathbf{k}}q_{\rho\mathbf{k}}\}\mathrm{d}\mathbf{k}+\frac{g}{2\pi}\sum_{\rho}\tau_\rho\int v(k)q_{\rho\mathbf{k}}\mathrm{d}\mathbf{k},\tag{1}$$

wobei

$$q_{\rho\mathbf{k}}=(2\pi)^{-\frac{3}{2}}\int\varphi_\rho(\mathbf{r})\mathrm{e}^{-\mathrm{i}\mathbf{k}\cdot\mathbf{r}}\mathrm{d}\mathbf{r},\quad p_{\rho\mathbf{k}}=(2\pi)^{-\frac{3}{2}}\int\pi_\rho(\mathbf{r})\mathrm{e}^{\mathrm{i}\mathbf{k}\cdot\mathbf{r}}\mathrm{d}\mathbf{r},$$

$$v(k)=\int K(\mathbf{r})\mathrm{e}^{\mathrm{i}\mathbf{k}\cdot\mathbf{r}}\mathrm{d}\mathbf{r},\tag{2}$$

$$\varepsilon^2=k^2+\kappa^2,\tag{2a}$$

$$i[\dot{p}_{\rho'\mathbf{k}'}, q_{\rho\mathbf{k}}] = \delta_{\rho'\rho}\delta(\mathbf{k}'-\mathbf{k}), \qquad [\dot{p}_{\rho'\mathbf{k}'}, \dot{p}_{\rho\mathbf{k}}] = [q_{\rho'\mathbf{k}'}, q_{\rho\mathbf{k}}] = 0. \tag{3}$$

Aus der Normierung der Quellfunktion folgt

$$v(0) = \int K(\mathbf{r})\mathrm{d}\mathbf{r} = 1, \tag{4}$$

und der Übergang zur Punktquelle wird beschrieben durch

$$K(\mathbf{r}) \to \delta(\mathbf{r}), \qquad v(k) \to \text{Konst.} = 1. \tag{5}$$

Wegen der Hermitizität von $\varphi_\rho(\mathbf{r})$ und $\pi_\rho(\mathbf{r})$ muß gelten

$$q^*_{\rho\mathbf{k}} = q_{\rho-\mathbf{k}}, \qquad \dot{p}^*_{\rho\mathbf{k}} = \dot{p}_{\rho-\mathbf{k}}, \tag{6}$$

und der Gesamtisospinoperator des Systems lautet

$$\mathcal{I}_{\rho\sigma} = \int (q_{\rho\mathbf{k}}\dot{p}_{\sigma\mathbf{k}} - q_{\sigma\mathbf{k}}\dot{p}_{\rho\mathbf{k}})\mathrm{d}\mathbf{k} + \tfrac{1}{2}\tau_{\rho\sigma}. \tag{7}$$

2.1.2. *Definition der Methode*

Den Ausführungen der Einleitung entsprechend (siehe insbesondere was dort gesagt wird über die Operatoren für das Teilsystem des Compoundnukleons) definieren wir die Methode der starken Kopplung wie folgt.

Die ursprünglichen Mesonfeldoperatoren sind durch die Operatoren der im Compoundnukleon gebundenen Mesonwolke — im Folgenden stets "Eigenfeld" genannt — und durch die Erzeugungs- u. Vernichtungsoperatoren des freien Feldanteiles in möglichst einfacher Weise zu substituieren. Nach Einsetzen dieser Substitution in den ursprünglichen Gesamthamiltonoperator sind dessen dadurch sich ergebende neue Bestandteile zu ordnen in einen nur Compoundnukleonoperatoren enthaltenen Anteil H^{0c}, einen nur Operatoren des freien Feldanteiles bilinear enthaltenden Anteil H^{0f} und einen nur aus gemischten Termen bestehenden Wechselwirkungshamiltonoperator zwischen Compoundnukleonanteil und freiem Feldanteil H^{W}. Für diesen neuen Wechselwirkungsterm

$$H^{W} = H - (H^{0c} + H^{0f}) \tag{8}$$

soll dann die störungstheoretische Reihe

$$f_N(n) = \delta_{Nn} + \frac{(n|H^{W}|N)}{E_N - E_n^0} + \sum_{n'} \frac{(n|H^{W}|n')(n'|H^{W}|N)}{(E_N - E_n^0)(E_N - E_{n'}^0)} + \ldots, \tag{9}$$

die gemäß der Entwicklung

$$\chi_N = \sum_n f_N(n)\theta_n \tag{10}$$

der Eigenzustände von H nach den Eigenzuständen von $H^{0f}+H^{0c}$ gebildet ist, mit stark anwachsender Kopplung bei festgehaltenem endlichen Abstand

der Energie E_N von der Energie E_0 des Grundzustandes auf δ_{Nn} zusammenschrumpfen, sodaß

$$f_N(n) \to \delta_{Nn} \text{ für } g \to \infty. \tag{11}$$

Dabei ist E_N der Eigenwert von H zum Eigenzustand χ_N und E_n^0 derjenige von $H^{0f}+H^{0c}$ zum Eigenzustand θ_n. Die Reihe (9) ist also die störungstheoretische Reihe der starken Kopplung im Unterschied zur störungstheoretischen Reihe der schwachen Kopplung, die bei verschwindender Kopplungskonstanten auf δ_{Nn} zusammenschrumpft. Mit den $f_N(n)$ ist somit durch (10) die Darstellung der starken Kopplung von χ_N gegeben. Die Forderung (11) nennen wir die Bedingung der starken Kopplung (siehe die Zusammenstellung in Absatz 2.1.6).

2.1.3. *Beschreibung des freien Feldanteiles*

Der freie Feldanteil werde durch die Erzeugungs- und Vernichtungsoperatoren $a^*_{\rho_0\mathbf{k}_0}$ und $a_{\rho_0\mathbf{k}_0}$ eines Systems von harmonischen Feldoscillatoren mit dem kontinuierlichen Impulsparameter $\mathbf{k}_0$, dem auf den Isospinraum bezogenen Vektorindex ρ_0, und den Vertauschungsrelationen

$$[a_{\rho'_0\mathbf{k}'_0}, a^*_{\rho_0\mathbf{k}_0}] = \delta_{\rho'_0\rho_0}\delta(\mathbf{k}'_0-\mathbf{k}_0), \tag{12}$$

$$[a_{\rho'_0\mathbf{k}'_0}, a_{\rho_0\mathbf{k}_0}] = [a^*_{\rho'_0\mathbf{k}'_0}, a^*_{\rho_0\mathbf{k}_0}] = 0 \tag{13}$$

beschrieben. Der Hamiltonoperator des freien Feldanteiles sei demgemäß

$$H^{0f} = \sum_{\rho_0}\int \varepsilon_0 \langle a^*_{\rho_0\mathbf{k}_0} a_{\rho_0\mathbf{k}_0}\rangle \mathrm{d}\mathbf{k}_0, \tag{14}$$

und sein Isospintensor

$$\mathcal{I}^{\mathrm{f}}_{\rho\sigma} = \frac{1}{i}\sum_{\rho_0,\sigma_0}\int (\delta_{\rho\rho_0}\delta_{\sigma\sigma_0}-\delta_{\sigma\rho_0}\delta_{\rho\sigma_0}) a^*_{\rho_0\mathbf{k}_0} a_{\rho_0\mathbf{k}_0}\mathrm{d}\mathbf{k}_0, \tag{15}$$

wobei $\langle\rangle$ das symmetrisierte Produkt bedeutet.

2.1.4. *Beschreibung des Eigenfeldes*

Das Eigenfeld kann bei dem der Gl. (2) entsprechenden Modell nur Isospinfreiheitsgrade besitzen, da der Kopplungsterm der Gl. (2) nur die Aufnahme von Isospin auf Grund der in ihm enthaltenen τ_ρ-Operatoren, nicht aber von Drehimpuls (wegen der Kugelsymmetrie der Quellfunktion) oder von Quantitäten anderer physikalischer Größen gestattet.

Demgemäß führen wir den Isospinoperator des Eigenfeldes mit den Komponenten $\mathcal{I}^{\mathrm{e}}_{\rho\sigma}$ und den Einheitsvektor

$$S_\rho \equiv (\sin\theta\cos\varphi;\ \sin\theta\sin\varphi;\ \cos\theta) \tag{16}$$

der die Richtung des Eigenfeldes im Isospinraum angibt †, als die einzigen

† Vom formalen Standpunkt aus sind die Operatoren S_ρ notwendig, um von Zuständen eines bestimmten $\mathcal{I}^{\mathrm{e}2} = \frac{1}{2}\Sigma_{\rho,\sigma}\mathcal{I}^{\mathrm{e}2}_{\rho\sigma}$ zu solchen mit einem anderen $\mathcal{I}^{\mathrm{e}2}$ gelangen zu können.

dynamischen Variablen des Eigenfeldes ein. Hierbei sei φ der Drehwinkel des Vektors S_ρ um die Ladungsachse und θ der Winkel, der von der Ladungsachse und dem Vektor S_ρ eingeschlossen wird. Die $\mathcal{T}^{\mathrm{e}}_{\rho\sigma}$ können wir darstellen als die Drehoperatoren des Richtungsvektoroperators S_ρ, also

$$\begin{aligned}\mathcal{T}^{\mathrm{e}}_{12} &= \frac{1}{i}\frac{\partial}{\partial\varphi},\\ \mathcal{T}^{\mathrm{e}}_{23} &= -\sin\varphi\frac{1}{i}\frac{\partial}{\partial\theta}-\cos\varphi\frac{\cos\theta}{\sin\theta}\frac{1}{i}\frac{\partial}{\partial\varphi},\\ \mathcal{T}^{\mathrm{e}}_{31} &= +\cos\varphi\frac{1}{i}\frac{\partial}{\partial\theta}-\sin\varphi\frac{\cos\theta}{\sin\theta}\frac{1}{i}\frac{\partial}{\partial\varphi}.\end{aligned} \tag{17}$$

Die Winkel φ und θ zusammen mit ihren kanonischen konjugierten „Impulsen" $-i\,\partial/\partial\varphi$ und $-i\,\partial/\partial\theta$ wären dann als die kanonischen Variablen des Eigenfeldes anzusehen. Der Operator $-i\,\partial/\partial\varphi = \mathcal{T}^{\mathrm{e}}_{12}$ ist der Ladungsoperator des Eigenfeldes. Die Vertauschungsrelationen der $\mathcal{T}^{\mathrm{e}}_{\rho\sigma}$ und S_ρ sind

$$i[\mathcal{T}^{\mathrm{e}}_{\rho'\sigma'}, \mathcal{T}^{\mathrm{e}}_{\rho\sigma}] = \delta_{\sigma'\rho}\mathcal{T}^{\mathrm{e}}_{\rho'\sigma}+\delta_{\rho'\sigma}\mathcal{T}^{\mathrm{e}}_{\sigma'\rho}-\delta_{\rho'\rho}\mathcal{T}^{\mathrm{e}}_{\sigma'\sigma}-\delta_{\sigma'\sigma}\mathcal{T}^{\mathrm{e}}_{\rho'\rho}, \tag{18}$$

$$[S_{\rho'}, S_\rho] = 0, \tag{19}$$

$$i[\mathcal{T}^{\mathrm{e}}_{\rho\sigma}, S_{\rho'}] = \delta_{\sigma\rho'}S_\rho-\delta_{\rho\rho'}S_\sigma. \tag{20}$$

Dabei ist

$$\sum_\rho S_\rho^2 = 1 \tag{21}$$

eine c-Zahl. In Achsialvektorschreibweise ($\mathcal{T}^{\mathrm{e}}_{\rho}$ statt $\mathcal{T}^{\mathrm{e}}_{\rho\sigma}$) gilt außerdem

$$\sum_\rho S_\rho\mathcal{T}^{\mathrm{e}}_{\rho} = \sum_\rho \mathcal{T}^{\mathrm{e}}_{\rho}S_\rho = 0, \tag{22}$$

wie es aus den Gln. (16) u. (17) ersichtlich ist.

Die von den Mesonfeldoperatoren $q_{\rho\mathbf{k}}$ und $p_{\rho\mathbf{k}}$ (siehe Gl. (2)) abzuspaltenden Eigenfeldanteile nennen wir nun $q^{\mathrm{e}}_{\rho\mathbf{k}}$ und $p^{\mathrm{e}}_{\rho\mathbf{k}}$ und identifizieren die Richtung von $q^{\mathrm{e}}_{\rho\mathbf{k}}$ im Isospinraum mit S_ρ. Für den Eigenfeldanteil $p^{\mathrm{e}}_{\rho\mathbf{k}}$ des Mesonfeldoperators $p_{\rho\mathbf{k}}$ bilden wir einen weiteren polaren Hermiteschen Vektoroperator mit den Komponenten

$$p_\rho = -\tfrac{1}{2}\sum_\sigma(S_\sigma\mathcal{T}^{\mathrm{e}}_{\rho\sigma}+\mathcal{T}^{\mathrm{e}}_{\rho\sigma}S_\sigma) = -\sum_\sigma\langle S_\sigma\mathcal{T}^{\mathrm{e}}_{\rho\sigma}\rangle, \tag{23}$$

sodaß bei Berücksichtigung von (22)

$$S_\rho p_\sigma - S_\sigma p_\rho = \mathcal{T}^{\mathrm{e}}_{\rho\sigma}. \tag{24}$$

Dann gilt auf Grund von (20)

$$i[p_\rho, S_{\rho'}] = -i[\tfrac{1}{2}\sum_\sigma(S_\sigma\mathcal{T}^{\mathrm{e}}_{\rho\sigma}+\mathcal{T}^{\mathrm{e}}_{\rho\sigma}S_\sigma), S_{\rho'}] = (\delta_{\rho\rho'}-S_\rho S_{\rho'}) \tag{25}$$

und auf Grund von (18)

$$i[\mathfrak{p}_{\rho'}, \mathfrak{p}_{\rho}] = \mathcal{T}^{e}_{\rho'\rho}. \tag{26}$$

Aus (23) folgt ferner wegen der Antisymmetrie von $\mathcal{T}^{e}_{\rho\sigma}$ bei Berücksichtigung von (25) bzw. (17), daß

$$\sum_{\rho} S_{\rho}\mathfrak{p}_{\rho} = -\sum_{\rho} \mathfrak{p}_{\rho}S_{\rho} = i \tag{27}$$

eine c-Zahl ist, bzw.

$$\sum_{\rho} \langle S_{\rho}\mathfrak{p}_{\rho}\rangle = 0, \tag{28}$$

wobei $\langle\rangle$ das symmetrisierte Produkt bedeutet.

Wir machen nun für das Eigenfeld den Ansatz

$$q^{e}_{\rho\mathbf{k}} = u_{\mathbf{k}}S_{\rho}, \qquad \mathfrak{p}^{e}_{\rho\mathbf{k}} = v_{\mathbf{k}}\mathfrak{p}_{\rho} = -v_{\mathbf{k}}\tfrac{1}{2}\sum_{\sigma}(S_{\sigma}\mathcal{T}^{e}_{\rho\sigma} + \mathcal{T}^{e}_{\rho\sigma}S_{\rho}). \tag{29}$$

Hierbei sind $u_{\mathbf{k}}$ und $v_{\mathbf{k}}$ c-Zahlfunktionen von $\mathbf{k}$, die nachher im Ansatz für die kanonischen Aufspaltungstransformation naturgemäß eine wesentliche Rolle spielen und sich im Folgenden z.T. aus den Aufspaltungsbedingungen, z.T. durch Spezialisierung auf eine Darstellung der starken Kopplung ergeben werden. Wegen der Kugelsymmetrie des Kopplungsterms in Gl. (2) sind $u_{\mathbf{k}}$ und $v_{\mathbf{k}}$ ebenfalls kugelsymmetrisch und wegen der Hermitizitätsbedingung (Gl. (6)) sind $u_{\mathbf{k}}$ und $v_{\mathbf{k}}$ reell. Stellen wir für $u_{\mathbf{k}}$ und $v_{\mathbf{k}}$ die Bedingung

$$\int u_{\mathbf{k}}\, v_{\mathbf{k}}\, \mathrm{d}\mathbf{k} = 1, \tag{30}$$

so wird auf grund von Gl. (29) u. (24)

$$\mathcal{T}^{e}_{\rho\sigma} = \int (q^{e}_{\rho\mathbf{k}}\mathfrak{p}^{e}_{\sigma\mathbf{k}} - q^{e}_{\sigma\mathbf{k}}\mathfrak{p}^{e}_{\rho\mathbf{k}})\mathrm{d}\mathbf{k}, \tag{31}$$

wie wir es auch gemäß Gl. (7) zu erwarten haben.

2.1.5. *Compoundnukleon*

Für den Hamiltonoperator H^{0C} des aus Eigenfeld und nacktem Nukleon zusammengesetzten Compoundnukleonsystems ergibt sich durch Einsetzen von $q^{e}_{\rho\mathbf{k}}$ und $\mathfrak{p}^{e}_{\rho\mathbf{k}}$ in (1)

$$H^{0C} = \tfrac{1}{2}\int |v_{\mathbf{k}}|^2 \mathrm{d}\mathbf{k}\mathcal{T}^{e^2} + \frac{g}{2\pi}\int v(k)u_{\mathbf{k}}\mathrm{d}\mathbf{k}\sum_{\rho}\tau_{\rho}S_{\rho} + \tfrac{1}{2}\int \varepsilon^2 |u_{\mathbf{k}}|^2 \mathrm{d}\mathbf{k} \tag{32}$$

mit

$$\mathcal{T}^{e^2} = \tfrac{1}{2}\sum_{\rho,\sigma}\mathcal{T}^{e^2}_{\rho\sigma} = \sum_{\rho}\mathcal{T}^{e^2}_{\rho}. \tag{33}$$

Seine Eigenwerte lassen sich mit den Quantenzahlen T des Compoundnukleon-

gesamtisospins

$$\mathscr{T}_{\rho\sigma} = \mathscr{T}^{e}_{\rho\sigma} + \tfrac{1}{2}\tau_{\rho\sigma} = \mathscr{T}^{e}_{\rho\sigma} + \tfrac{1}{2}\sum_{\rho',\sigma'} \bar{\tau}_{\rho'\sigma'} S_{\rho'\rho} S_{\sigma'\sigma} \tag{34}$$

exakt angeben und lauten

$$E_T = \tfrac{1}{2}\int |v_{\mathbf{k}}|^2 \mathrm{d}\mathbf{k}(T+\tfrac{1}{2})^2 \pm \sqrt{\tfrac{1}{4}(\int |v_{\mathbf{k}}|^2 \mathrm{d}\mathbf{k})^2 (T+\tfrac{1}{2})^2 + \left(\frac{g}{2\pi}\int v(k) u_{\mathbf{k}} \mathrm{d}\mathbf{k}\right)^2}. \tag{35}$$

Für unsere Zwecke interessiert besonders eine dem Fall der starken Kopplung gemäße Formulierung von H^{0C}. In diesem Fall wird τ_ρ so stark an das Eigenfeld gekoppelt, daß der Isospinvektor $\boldsymbol{\tau} \equiv \{\tau_\rho\}$ sich in Richtung von $\mathbf{S} \equiv \{\mathbf{S}_\rho\}$ einstellt und der relativen Kleinheit des $\mathscr{T}^{e^2}$-Terms entsprechend met S mitrotiert. Das bedeutet formal ausgedrückt, daß der Energieabstand der Eigenwerte des $\sum_\rho \tau_\rho S_\rho$-Terms groß ist gegen den Energieabstand benachbarter Niveaus des $\mathscr{T}^{e^2}$-Terms in H^{0C} also †:

$$\int |v_{\mathbf{k}}|^2 \mathrm{d}\mathbf{k}\, \frac{\Delta \mathscr{T}^{e^2}}{2} \ll \frac{g}{\pi}\int v(k) u_{\mathbf{k}} \mathrm{d}\mathbf{k}, \tag{36}$$

wobei der $\mathscr{T}^{e^2}$ Term im Grenzfall $g \to \infty$ überhaupt zu vernachlässigen ist als Ausdruck davon, daß dann überhaupt keine Rotation von S_ρ mehr stattfindet (Statischer Grenzfall). Gemäß (8) bis (11) sind in diesem Grenzfall auch die Eigenwertkorrekturen von H^W zu vernachlässigen, sodaß in diesem Grenzfall der tiefste Eigenwert von H^{0C} mit $\sum_\rho \tau_\rho S_\rho = -1$ zugleich auch der tiefste Eigenwert von Gesamt-H ist, und die Funktion, die ihn zum Minimum macht sich zu

$$u_{\mathbf{k}} = \frac{g}{2\pi}\frac{v(k)}{\varepsilon^2} \tag{37}$$

ergibt. Diese Spezifizierung von $u_{\mathbf{k}}$ wird aus der Bedingung der starken Kopplung (4) von Absatz 2.1.6 zwangsläufig folgen (siehe Gl. (117), (118)). Wie (30) zeigt, wird dann $v_{\mathbf{k}}$ mindestens wie $1/g$ gehen müssen. Wir substituieren dementsprechend die Funktion $v_{\mathbf{k}}$ durch die Funktion $v^1(k)$ gemäß

$$v_{\mathbf{k}} = \frac{2\pi}{gb} v^1(k) \tag{38}$$

mit der Konstanten

$$b = \int \frac{[v(k)]^2}{\varepsilon^2}\, \mathrm{d}\mathbf{k}, \tag{39}$$

† Dies entspricht dem Hundschen Kopplungsfall der Molekülphysik, bei dem sich der Spin der Leuchtelektronen zur rotierenden Molekülachse einstellt [28]). Auf die Ähnlichkeit mit den Verhältnissen bei der Molekülphysik hat zuerst Tomonaga hingewiesen [5, 9]).

sodaß (30) die Form

$$\int v^1(k)\,\frac{v(k)}{\varepsilon^2}\,\mathrm{d}\mathbf{k} = b = \int \frac{[v(k)]^2}{\varepsilon^2}\,\mathrm{d}\mathbf{k} \tag{40}$$

bzw.

$$\int [v^1(k) - v(k)]\,\frac{v(k)}{\varepsilon^2}\,\mathrm{d}\mathbf{k} = 0 \tag{41}$$

annimmt. Die spezielle Form dieser Substitution (38) wird sich für später als zweckmäßig erweisen.

Die dem Fall der starken Kopplung gemäße Formulierung von H^{0C} erhält man, wenn man mit S_ρ mitbewegte Komponenten von $\boldsymbol{\tau}$ einführt gemäß

$$\bar{\tau}_{\rho'} = \sum_{\rho} s_{\rho'\rho}\tau_\rho, \qquad \tau_\rho = s_{\rho'\rho}\bar{\tau}_{\rho'}, \qquad s_{3\rho} = S_\rho, \tag{42}$$

mit

$$s_{\rho'\rho} = \begin{pmatrix} \cos\theta\cos\varphi & \cos\theta\sin\varphi & -\sin\theta \\ -\sin\varphi & \cos\varphi & 0 \\ \sin\theta\cos\varphi & \sin\theta\sin\varphi & \cos\theta \end{pmatrix} \tag{43}$$

und in H^{0C} die τ_ρ und $\mathscr{T}^{e}_{\rho\sigma}$ vollständig durch die $\bar{\tau}_{\rho\sigma}$ und die mit $\bar{\tau}_3$ vertauschbaren Gesamtisospin des Compoundnukleonsystems (34) ausdrückt. Mit den obigen Substitutionen (37) u. (38) wird dann

$$H^{0C} = \left(\frac{2\pi}{g}\right)^2 \frac{\eta_1^2}{2b}\left[\mathscr{T}^2 - 2\sum_{s,s'\sigma} \bar{\tau}_{\rho'3}\langle\langle S_\sigma \mathscr{T}_{\rho\sigma}\rangle s_{\rho'\rho}\rangle + \tfrac{3}{4}\right] + \left(\frac{g}{2\pi}\right)^2 b(\bar{\tau}_3 + \tfrac{1}{2}), \tag{44}$$

wobei

$$\eta_1^2 = \int [v^1(k)]^2 \mathrm{d}\mathbf{k}. \tag{45}$$

In (44) hat H^{0C} die dem niedrigsten Entwicklungsglied der Wurzel von (35) nach $1/g^2$ entsprechende Diagonalform bis auf den zweiten Term in der eckigen Klammer. Dieser Term enthält wegen (23) u. (25) — d.h. letzten Endes wegen (22) — nicht $\bar{\tau}_3$ sondern nur die antidiagonalen Matrizen $\bar{\tau}_{\rho'}$ mit $\rho' \neq 3$ und bewirkt somit nur Übergänge zwischen den für starke Kopplung weit auseinanderliegenden Niveaus der Eigenwerte von $\bar{\tau}_3$. Folglich verschwindet sein Erwartungswert in bezug auf die Eigenzustände von $\mathscr{T}^2$ u. $\bar{\tau}_3$, während die von ihm herrührende Eigenwertkorrektur in zweiter störungstheoretischer Näherung $\approx 1/bg^4$ und somit im Sinne der starken Kopplung gegen das $\mathscr{T}^2$ und $\bar{\tau}_3$ Glied zu vernachlässigen ist. Dann beschreibt der Isospinoperator des Compoundnukleons $\mathscr{T}_{\rho\sigma}$ nicht nur das physikalische Proton-Neutron ($\mathscr{T}_{12} = \pm\frac{1}{2}$, $\bar{\tau}_3 = -1$), sondern auch Zustände mit höherem Isospin- und höherer Ladung, deren Massen durch die $\mathscr{T}^2$-Abhängigkeit in H^{0C} gegeben sind. Im Fall der starken Kopplung liegen die Niveaus der $\bar{\tau}_3 = +1$-Termsystems sehr hoch

über denen des $\bar{\tau}_3 = -1$-Termsystems. Im Gegensatz dazu wird im Fall der schwachen Kopplung, der durch weitgehende Entkopplung von τ-Spin- und Eigenfeldbewegung charakterisiert und dem die Formulierung (32) gemäß ist, durch den τ-Spin nur das Proton-Neutron-Niveau beschrieben, während die $\mathcal{T}^{e^2}$-Niveaus dann ihrerseits sehr hoch darüber liegen.

Im Unterschied zu $u_{\mathbf{k}}$ wird die Funktion $v_{\mathbf{k}}$ bzw. $v^1(k)$, wie wir auch später sehen werden, — außer der Tatsachen daß $v_{\mathbf{k}}$ mindestens wie $1/g$ gehen muß bzw. $v^1(k)$ nicht mit g anwachsen darf — durch die Bedingung der starken Kopplung weniger scharf bestimmt, sodaß noch eine ganze Schar von Transformationen die Bedingung der starken Kopplung erfüllt. Ausgezeichnete Fälle sind in Übereinstimmung mit (30) bzw. (40) u. (41)

$$v^1(k) = v(k), \tag{46}$$

d.h. $v^1(k)$ ist gleich der Fouriertransformierten der Quellfunktion, und

$$v^1(k) = \frac{b}{W}\frac{v(k)}{\varepsilon^2}, \qquad W = \int \frac{[v(k)]^2}{\varepsilon'^4}\,\mathrm{d}\mathbf{k}, \tag{47}$$

d.h. $v^1(k)$ hat dieselbe k-Abhängigkeit wie $u_{\mathbf{k}}$. Diesen zweiten Fall haben wir schon bei den Untersuchungen über die Durchführung der Näherung der starken Kopplung des Chew-Low-Formalismus benutzt [21]), und auch Nickle u. Serber [20]) haben mit der Gleichsetzung von Verteilungsfunktion und Eigenfeldfunktion des Formalismus von Pais u. Serber den analogen Fall dazu für diesen Formalismus behandelt.

Dieser eben genannte Fall (47) zeichnet sich nun dadurch aus, daß vom Kopplungsterm mit dem freien Feldanteil herrührende Eigenwertkorrekturen zu den Anregungsenergieen des Compoundnukleons, für $\bar{\tau}_3 = -1$ erst von der Ordnung g^{-4} an abwärts auftreten, wie in Refn. [17, 20, 21]) gezeigt wurde, sodaß die Anregungsenergieen des Compoundnukleons für $\bar{\tau}_3 = -1$ bis zur Ordnung g^{-2} herab vollständig durch H^{0C} gegeben sind, während man dieses im Fall $v^1(k) = v(k)$ erst nach Einbeziehung der niedrigsten Eigenwertkorrektur des Kopplungsterms mit dem freien Feldanteil bekommt (siehe die Bemerkungen nach Gln. (197), (245) u. (270)). Somit scheint der Fall (47) die Bedingung der starken Kopplung besser zu erfüllen als der Fall (46), jedoch hat auch der letztere, wie wir im Folgenden sehen werden, hinsichtlich der Bedingung der starken Kopplung gewisse Vorzüge. Ein Hauptmerkmal des Falles (47) ist ferner, daß er die Rolle der cut-off-Abhängigkeit bei der hier verwendeten skalaren Theorie deutlicher hervortreten läßt. In

$$H^{0C} = \left(\frac{2\pi}{g}\right)^2 \frac{1}{2W}\left[\mathcal{T}^2 - 2\sum_{\rho,\rho',\sigma} \bar{\tau}_{\rho' 3} \langle\langle S_\sigma, \mathcal{T}_{\rho\sigma}\rangle S_{\rho'\rho}\rangle + \tfrac{3}{4}\right] + \left(\frac{g}{2\pi}\right)^2 b(\bar{\tau}_3 + \tfrac{1}{2}) \tag{48}$$

rücken nämlich mit zunehmender Lokalisierung die $\bar{\tau}_3 = +1$-Niveaus wegen $b \to \infty$ immer höher, sodaß dann der Fall der starken Kopplung auch bei

irgendeinem endlichen g immer besser erfüllt wird, während das $\mathcal{T}^2$-Spektrum mit $W \to \pi^2/\kappa$ — bei Verschwinden der Eigenwertkorrekturen des zweiten Terms der Klammer [ ] von H^{0C} mit $1/b$ — dem Grenzwert

$$E_T = \frac{2\kappa}{g^2} T(T+1) + \text{konst.} \tag{49}$$

zustrebt. Wie Nickle u. Serber [20]) für die geladene, skalare Theorie gezeigt haben, divergieren dann die vom Kopplungsterm mit den freien Mesonen herrührenden Eigenwertkorrekturen der Ordnung g^{-4} zu den Anregungsenergieen dieses Spektrums mit logarithmischer cut-off-Abhängigkeit und können in die Renormierung von g beim vorstehenden Spektrum mit einbezogen werden, was auch mit den Ergebnissen der Durchführung des Chew-Low-Formalismus bei der geladenen skalaren Theorie in Einklang steht [26, 24, 21]).

2.1.6. *Die Aufspaltungsbedingungen*

Bei der Aufspaltung des Mesonfeldes in den freien Feldanteil und den Eigenfeldanteil mit den vorstehend eingeführten Operatoren $a^*_{\rho_0 \mathbf{k}_0}$ und $a_{\rho_0 \mathbf{k}_0}$ für den freien Feldanteil (siehe (12) u. (13)) und S_ρ, p_ρ für den Eigenfeldanteil (siehe (16), (17), (19) u. (23)) müssen nun folgende Aufspaltungsbedingungen berücksichtigt werden, auf deren Einhaltung wir bei der Aufstellung eines geeigneten Ansatzes für die gemäß Absatz 2.1.2 durchzuführende kanonische Variablensubstitution notwendig zu achten haben:

(1) *Isospinaufspaltungsbedingung.* Der Ausdruck des Isospintensors (7) muß unabhängig von g in den freien Feldanteil $\mathcal{I}^{\mathrm{f}}_{\rho\sigma}$ (15) und den Eigenfeldanteil $\mathcal{T}^{\mathrm{e}}_{\rho\sigma}$ (17) so aufspalten, daß für jedes g exakt gilt

$$\mathcal{I}_{\rho\sigma} = \mathcal{I}^{\mathrm{f}}_{\rho\sigma} + \mathcal{T}^{\mathrm{e}}_{\rho\sigma} + \tfrac{1}{2}\tau_{\rho\sigma}, \tag{50}$$

bzw. gemäß (34)

$$\mathcal{I}_{\rho\sigma} = \mathcal{I}^{\mathrm{f}}_{\rho\sigma} + \mathcal{T}_{\rho\sigma}. \tag{51}$$

(2) *Kanonizitätsbedingungen.* Die Kanonizität der Transformation muß sicher gestellt werden, was am naheliegensten durch die Forderung geschieht, daß die kanonischen Vertauschungsregeln (3) erhalten bleiben, d.h. die Vertauschungsrelationen (3) müssen sich also ergeben als Konsequenz der Vertauschungsrelationen (12), (13), (19), (18), (20) mit (21) und

$$[a_{\rho_0 \mathbf{k}_0}, S_\rho] = [a^*_{\rho_0 \mathbf{k}_0}, S_\rho] = [a_{\rho_0 \mathbf{k}_0}, \mathcal{T}^{\mathrm{e}}_{\rho\sigma}] = [a^*_{\rho_0 \mathbf{k}_0}, \mathcal{T}^{\mathrm{e}}_{\rho\sigma}] = 0. \tag{52}$$

Dabei garantieren die Kommutatoren (52), daß die Variablen des freien Feldanteiles und des Eigenfeldanteiles voneinander unabhängig, und somit die Zustände des freien Feldanteiles und des Eigenfeldanteiles aufeinander orthogonal sind.

(3) *Umkehrbarkeitsbedingung* Die Transformation soll umkehrbar sein. D.h. die $a_{\rho_0 \mathbf{k}_0}$, $a^*_{\rho_0 \mathbf{k}_0}$, S_ρ und p_ρ sollen durch die $p_{\rho \mathbf{k}}$ und $q_{\rho \mathbf{k}}$ ausgedrückt werden können.

Schließlich müssen wir noch diejenige Bedingung anschreiben, die gemäß dem Grundgedanken der Methode der vorliegenden Arbeit die eigentliche Bedingung der starken Kopplung ist und speziell zu den Darstellungen der starken Kopplung führt. Wir haben sie schon in Absatz 2.1.2, formuliert. Also:

(4) *Bedingung der starken Kopplung*, formuliert in Absatz 2.1.2, siehe insbesondere die Gleichungen (8) bis (11).

2.2. EINFACHSTER AUFSPALTUNGSANSATZ FÜR DIE KANONISCHE VARIABLEN-SUBSTITUTION

Wir wenden uns nun der Aufstellung eines geeigneten Ansatzes für die gemäß der Einleitung und Absatz 2.1.2 durchzuführende kanonische Aufspaltungstransformation zu. Mittels dieses Transformationsansatzes müssen den vorstehenden Ausführungen zufolge die kanonischen Mesonfeldoperatoren $q_{\rho \mathbf{k}}$ und $p_{\rho \mathbf{k}}$ von Gl. (2) durch die Erzeugungs- und Vernichtungsoperatoren $a^*_{\rho_0 \mathbf{k}_0}$ und $a_{\rho_0 \mathbf{k}_0}$ der harmonischen Feldoscillatoren des freien Mesonfeldes einerseits und durch die Operatoren S_ρ und $\mathcal{T}^{\mathrm{e}}_{\rho\sigma}$ des Eigenfeldes andererseits so substituiert werden, daß die soeben formulierten Aufspaltungsbedingungen (1) bis (4) erfüllt sind. Dabei kann natürlich die Substitution der $q_{\rho \mathbf{k}}$ u. $p_{\rho \mathbf{k}}$ durch die $a^*_{\rho_0 \mathbf{k}_0}$, $a_{\rho_0 \mathbf{k}_0}$, S_ρ und $\mathcal{T}^{\mathrm{e}}_{\rho\sigma}$ noch in mannigfacher Weise durchgeführt werden. Wir wollen uns deshalb darauf spezialisieren, den einfachsten Ansatz aufzustellen, der sich in Einklang mit den Aufspaltungsbedingungen bilden läßt, und zwar wollen wir darunter einen Ansatz verstehen, der die $a_{\rho_0 \mathbf{k}_0}$, $a^*_{\rho_0 \mathbf{k}_0}$, S_ρ und $\mathcal{T}^{\mathrm{e}}_{\rho\sigma}$ so linear wie möglich enthält. Eine vollkommene Linearität des Ansatzes läßt sich allerdings nicht erzielen, wofür der Grund darin liegt, daß die Kommutatoren der Eigenfeldvariablen, soweit sie nicht verschwinden, im Unterschied zu den Kommutatoren der $q_{\rho \mathbf{k}}$ und $p_{\rho \mathbf{k}}$ sowie auch der $a_{\rho_0 \mathbf{k}_0}$ und $a^*_{\rho_0 \mathbf{k}_0}$ keineswegs c-Zahlen sind, sondern ebenfalls noch die Eigenfeldvariablen teils linear, teils bilinear oder quadratisch mit enthalten (siehe (25) u. (18)).

Im vorliegenden Abschnitt betrachten wir nun zunächst den allgemeinen Fall eines derartigen Tranformationsansatzes, bei dem zwar die Aufspaltungsbedingungen (1) bis (3) erfüllt sind, der jedoch der Bedingung (4), der Bedingung der starken Kopplung, noch nicht unterworfen ist.

2.2.1. *Herleitung der Transformationsgleichungen aus einem linearen Ausgangspunkt*

Um den Ansatz mit der größtmöglichen Linearität zu erhalten, beginnen wir damit, die kanonischen Mesonfeldoperatoren $q_{\rho \mathbf{k}}$ und $p_{\rho \mathbf{k}}$ der Gl. (2) linear aufzuspalten und zwar in der Weise, daß die abgespaltenen Anteile zu den mit

den Gleichungen (29) u. (30) eingeführten Eigenfeldfunktionen $u_{\mathbf{k}}$ und $v_{\mathbf{k}}$ proportional sind:

$$q_{\rho\mathbf{k}} = q_{1\rho\mathbf{k}} + u_{\mathbf{k}}\mathring{q}_\rho, \qquad \mathring{p}_{\rho\mathbf{k}} = \mathring{p}_{1\rho\mathbf{k}} + v_{\mathbf{k}}\mathring{p}_\rho. \tag{53}$$

Sollen dabei die $q_{1\rho\mathbf{k}}$, $\mathring{p}_{1\rho\mathbf{k}}$ und die $\mathring{q}_\rho$, $\mathring{p}_\rho$ voneinander unabhängig sein, so muß gelten

$$[\mathring{p}_{\rho'}, q_{1\rho\mathbf{k}}] = [\mathring{p}_{1\rho'\mathbf{k}'}, \mathring{q}_\rho] = [\mathring{p}_{\rho'}, \mathring{p}_{1\rho\mathbf{k}}] = [\mathring{q}_{\rho'}, q_{1\rho\mathbf{k}}] = 0. \tag{54}$$

Diese Vertauschungsrelationen (54) sind bei Gültigkeit der Vertauschungsregeln (2) für die $q_{\rho\mathbf{k}}$ und $\mathring{p}_{\rho\mathbf{k}}$ und der Bedingung (30) für die $u_{\mathbf{k}}$ und $v_{\mathbf{k}}$ erfüllt, wenn gemäß (53)

$$\mathring{q}_\rho = \int v_{\mathbf{k}} q_{\rho\mathbf{k}}\,\mathrm{d}\mathbf{k}, \qquad \mathring{p}_\rho = \int u_{\mathbf{k}}\mathring{p}_{\rho\mathbf{k}}\,\mathrm{d}\mathbf{k}, \tag{55}$$

und somit

$$q_{1\rho\mathbf{k}} = \int (\delta(\mathbf{k}-\mathbf{k}') - u_{\mathbf{k}}v_{\mathbf{k}'})q_{\rho\mathbf{k}'}\,\mathrm{d}\mathbf{k}', \qquad \mathring{p}_{1\rho\mathbf{k}} = \int (\delta(\mathbf{k}-\mathbf{k}') - v_{\mathbf{k}}u_{\mathbf{k}'})\mathring{p}_{\rho\mathbf{k}'}\,\mathrm{d}\mathbf{k}'. \tag{56}$$

Daraus folgt weiterhin auf Grund von (2) und (30)

$$\begin{aligned} &i[\mathring{p}_{1\rho'\mathbf{k}'}, q_{1\rho\mathbf{k}}] = \{\delta(\mathbf{k}'-\mathbf{k}) = v_{\mathbf{k}'}u_{\mathbf{k}}\}\delta_{\rho'\rho}, \qquad i[\mathring{p}_{\rho'}, \mathring{q}_\rho] = \delta_{\rho'\rho}, \\ &[\mathring{p}_{\rho'}, \mathring{p}_\rho] = [\mathring{q}_{\rho'}, \mathring{q}_\rho] = [\mathring{p}_{1\rho'\mathbf{k}}, \mathring{p}_{1\rho\mathbf{k}}] = [q_{1\rho'\mathbf{k}'}, q_{1\rho\mathbf{k}}] = 0, \end{aligned} \tag{57}$$

$$\int v_{\mathbf{k}} q_{1\rho\mathbf{k}}\,\mathrm{d}\mathbf{k} = 0, \qquad \int u_{\mathbf{k}}\mathring{p}_{1\rho\mathbf{k}}\,\mathrm{d}\mathbf{k} = 0. \tag{58}$$

Mit (53) und (58) ergibt sich dann für die Aufspaltung des Isospinoperators (7)

$$\int (q_{\rho\mathbf{k}}\mathring{p}_{\sigma\mathbf{k}} - q_{\sigma\mathbf{k}}\mathring{p}_{\rho\mathbf{k}})\,\mathrm{d}\mathbf{k} = \int (q_{1\rho\mathbf{k}}\mathring{p}_{1\sigma\mathbf{k}} - q_{1\sigma\mathbf{k}}\mathring{p}_{1\rho\mathbf{k}})\,\mathrm{d}\mathbf{k} + \mathring{q}_\rho\mathring{p}_\sigma - \mathring{q}_\sigma\mathring{p}_\rho \tag{59}$$

Wir zerlegen nun $\mathring{q}_\rho$ u. $\mathring{p}_\rho$ in einen Betragsanteil und einen Richtungsanteil in Bezug auf den Isospinraum ganz analog zum Übergang von karstesischen Koordinaten auf Polarkoordinaten bei der Beschreibung eines Massenpunktes im gewöhnlichen Raum,

$$\mathring{q}_\rho = \mathring{q}\mathring{S}_\rho, \tag{60a}$$

$$\mathring{p}_\rho = \mathring{p}\mathring{S}_\rho - \frac{\frac{1}{2}\sum_\sigma (\mathring{S}_\sigma\mathring{\mathcal{T}}_{\rho\sigma} + \mathring{\mathcal{T}}_{\rho\sigma}\mathring{S}_\sigma)}{\mathring{q}} \tag{60b}$$

mit

$$\sum_\rho \mathring{S}_\rho^{\,2} = 1, \qquad \mathring{q} = \sqrt{\sum_\rho \mathring{q}_\rho^{\,2}}, \tag{61}$$

wobei

$$\mathring{\mathcal{T}}_{\rho\sigma} = \mathring{q}_\rho\mathring{p}_\sigma - \mathring{q}_\sigma\mathring{p}_\rho \tag{62}$$

und

$$\begin{aligned} &i[\mathring{p}, \mathring{q}] = 1, \\ &[\mathring{p}, \mathring{p}] = [\mathring{q}, \mathring{q}] = [\mathring{p}, \mathring{S}_\rho] = [\mathring{p}, \mathring{\mathcal{T}}_{\rho\sigma}] = [\mathring{q}, \mathring{S}_\rho] = [\mathring{q}, \mathring{\mathcal{T}}_{\rho\sigma}] = 0. \end{aligned} \tag{63}$$

Miteinander haben die $\mathring{\mathcal{T}}_{\rho\sigma}$ und $\mathring{S}_\rho$ dieselben Vertauschungseigenschaften wie die durch Gleichungen (16) und (17) eingeführten Eigenfeldoperatoren $\mathcal{T}^{\mathrm{e}}_{\rho\sigma}$ und S_ρ.

Identifizieren wir nun die $\mathring{S}_\rho$ mit den Eigenfeldoperatoren S_ρ und setzen außerdem

$$q'_{\rho\mathbf{k}} = q_{1\rho\mathbf{k}} + u_{\mathbf{k}}(\mathring{q}-1)S_\rho, \qquad p'_{\rho\mathbf{k}} = p_{1\rho\mathbf{k}} + v_{\mathbf{k}}\mathring{p}S_\rho, \tag{64}$$

so hätten wir die Abspaltung des Eigenfeldanteiles (29) von $q_{\rho\mathbf{k}}$ gewonnen. Bei Zusammenfassung der vorstehend durchgeführten Substitutionen (53), (55), (60) und (64) bekommen wir dann nämlich

$$\begin{aligned} &\text{a)} \quad q_{\rho\mathbf{k}} = q'_{\rho\mathbf{k}} + u_{\mathbf{k}} S_\rho, \\ &\text{b)} \quad p_{\rho\mathbf{k}} = p'_{\rho\mathbf{k}} - v_{\mathbf{k}} \frac{\frac{1}{2}\sum_\sigma (S_\sigma \mathring{\mathcal{T}}_{\rho\sigma} + \mathring{\mathcal{T}}_{\rho\sigma} S_\sigma)}{1 + \sum_{\rho'} S_{\rho'} \int v_{\mathbf{k}'} q'_{\rho'\mathbf{k}'} \mathrm{d}\mathbf{k}'}, \end{aligned} \tag{65}$$

wobei sich für die Operatoren $q'_{\rho\mathbf{k}}$, $p'_{\rho\mathbf{k}}$, $\mathring{\mathcal{T}}_{\rho\sigma}$ und S_ρ gemäß (54), (57), (63) und (64) die Vertauschungsrelationen

$$i[p'_{\rho'\mathbf{k}'}, q'_{\rho\mathbf{k}}] = \delta(\mathbf{k}'-\mathbf{k})\delta_{\rho'\rho} - v_{\mathbf{k}'} u_{\mathbf{k}} (\delta_{\rho'\rho} - S_{\rho'} S_\rho), \tag{66}$$

$$[q'_{\rho'\mathbf{k}'}, q'_{\rho\mathbf{k}}] = [p'_{\rho'\mathbf{k}'}, p'_{\rho\mathbf{k}}] = 0, \tag{67}$$

$$[q'_{\rho\mathbf{k}}, S_{\rho'}] = [p'_{\rho\mathbf{k}}, S_\rho] = 0, \tag{68}$$

$$i[\mathring{\mathcal{T}}_{\rho\sigma}, q'_{\rho'\mathbf{k}'}] = u_{\mathbf{k}'} \overbrace{\sum_{\rho''} S_{\rho''} \int v_{\mathbf{k}''} q'_{\rho''\mathbf{k}''} \mathrm{d}\mathbf{k}''}^{\mathring{q}-1} (\delta_{\sigma\rho'} S_\rho - \delta_{\rho\rho'} S_\sigma), \tag{69}$$

$$i[\mathring{\mathcal{T}}_{\rho\sigma}, p'_{\rho'\mathbf{k}'}] = v_{\mathbf{k}'} \overbrace{\sum_{\rho''} S_{\rho''} \int u_{\mathbf{k}''} p'_{\rho''\mathbf{k}''} \mathrm{d}\mathbf{k}''}^{\mathring{p}} (\delta_{\sigma\rho'} S_\rho - \delta_{\rho\rho'} S_\sigma), \tag{70}$$

$$[\mathring{\mathcal{T}}_{\rho\sigma}, \sum_\rho S_\rho \int v_{\mathbf{k}} q'_{\rho\mathbf{k}} \mathrm{d}\mathbf{k}] = [\mathring{\mathcal{T}}_{\rho\sigma}, \sum_\rho S_\rho \int u_{\mathbf{k}} p'_{\rho\mathbf{k}} \mathrm{d}\mathbf{k}] = 0 \tag{71}$$

ergeben als Konsequenz der kanonischen Vertauschungsrelationen für die $q_{\rho\mathbf{k}}$ und $p_{\rho\mathbf{k}}$ (siehe (3)). Anstelle der Gleichung (58) erhalten wir außerdem

$$\sum_{\rho'} (\delta_{\rho\rho'} - S_\rho S_{\rho'}) \int v_{\mathbf{k}'} q'_{\rho'\mathbf{k}'} \mathrm{d}\mathbf{k}' = 0 \tag{72}$$

und

$$\sum_{\rho'}(\delta_{\rho\rho'}-S_\rho S_{\rho'})\int u_{\mathbf{k}'}\dot{p}'_{\rho'\mathbf{k}'}\,\mathrm{d}\mathbf{k}'=0, \tag{73}$$

und da gemäß Gl. (64)

$$\int(q_{1\rho\mathbf{k}}\dot{p}_{1\sigma\mathbf{k}}-q_{1\sigma\mathbf{k}}\dot{p}_{1\rho\mathbf{k}})\,\mathrm{d}\mathbf{k}=\int(q'_{\rho\mathbf{k}}\dot{p}'_{\sigma\mathbf{k}}-q'_{\sigma\mathbf{k}}\dot{p}'_{\rho\mathbf{k}})\,\mathrm{d}\mathbf{k} \tag{74}$$

ergibt sich statt Gl. (59)

$$\int(q_{\rho\mathbf{k}}\dot{p}_{\sigma\mathbf{k}}-q_{\sigma\mathbf{k}}\dot{p}_{\rho\mathbf{k}})\mathrm{d}\mathbf{k}=\int(q'_{\rho\mathbf{k}}\dot{p}'_{\sigma\mathbf{k}}-q'_{\sigma\mathbf{k}}\dot{p}'_{\rho\mathbf{k}})\mathrm{d}\mathbf{k}+\dot{\mathcal{T}}_{\rho\sigma}. \tag{75}$$

Auf Grund von (72) und (73) können die Vertauschungsrelationen (71) auch unmittelbar aus den Vertauschungsrelationen (69) und (70) gefolgert werden. Ferner ist naturgemäß (71) auch mit der Vertauschbarkeit des Zählers mit dem Nenner rechts in (65b) in Einklang.

Für die Transformationsformeln Gl. (65) gilt nun auch das Umgekehrte des vorstehend Ausgesagten, nämlich, daß die kanonischen Vertauschungsrelationen Gl. (3) sowie die Isospinaufspaltungsgleichung (75) erfüllt sind, wenn die Gültigkeit der Vertauschungsrelationen (66) bis (70) sowie der Beziehungen (72) und (73) für die $q'_{\rho\mathbf{k}}$, $\dot{p}'_{\rho\mathbf{k}}$, S_ρ und $\dot{\mathcal{T}}_{\rho\sigma}$ vorausgesetzt wird, und wenn die $\dot{\mathcal{T}}_{\rho\sigma}$ und S_ρ miteinander dieselben Vertauschungsrelationen und Eigenschaften haben wie die $\mathcal{T}^{\mathrm{e}}_{\rho\sigma}$ und S_ρ (siehe Gln. (17)—(29)).

Die Bestätigung hierfür läßt sich durch Einsetzen von (65) in (2) und (75) auf Grund der vorstehenden Relationen (66) bis (73) sowie der Gln. (16) bis (27) leicht erbringen, weshalb wir sie nicht im Einzelnen vorführen wollen. Doch wollen wir die weitere Herleitung der Transformation auf der vorstehenden Feststellung aufbauen.

2.2.2. *Einführung der Variablen des freien Feldanteiles und des Eigenfeldanteiles*

Wir wollen jetzt in den Transformationsformeln (65) die Operatoren $q'_{\rho\mathbf{k}}$, $\dot{p}'_{\rho\mathbf{k}}$ und $\dot{\mathcal{T}}_{\rho\sigma}$ durch die Operatoren des freien Feldanteiles $a^*_{\rho_0\mathbf{k}_0}$ und $a_{\rho_0\mathbf{k}_0}$ und die Eigenfeldoperatoren $\mathcal{T}^{\mathrm{e}}_{\rho\sigma}$ und S_ρ (siehe Seite 8/9) ausdrücken, und zwar muß dies zur Erfüllung der Kanonizität in der Weise geschehen, daß alle Vertauschungsrelationen und Beziehungen für die $q'_{\rho\mathbf{k}}$, $\dot{p}'_{\rho\mathbf{k}}$, S_ρ, und $\dot{\mathcal{T}}_{\rho\sigma}$ (siehe Absatz 2.1.4) sowie die mit $\dot{\mathcal{T}}_{\rho\sigma}$ an Stelle von $\mathcal{T}^{\mathrm{e}}_{\rho\sigma}$ geschriebenen Vertauschungsrelationen sich nun als Konsequenz der Vertauschungsrelationen für die $a^*_{\rho_0\mathbf{k}_0}$, $a_{\rho_0\mathbf{k}_0}$, S_ρ und $\mathcal{T}^{\mathrm{e}}_{\rho\sigma}$ (siehe (12) bis (27) und (52)) ergeben.

Die Operatoren $\dot{S}_\rho$ hatten wir ja schon durch die Eigenfeldoperatoren S_ρ in unseren Transformationsformeln (65) ersetzt. Mit dieser Gleichsetzung von $\dot{S}_\rho$ mit S_ρ ist jedoch nicht gesagt, daß auch die $\dot{\mathcal{T}}_{\rho\sigma}$ dementsprechend mit den Isospintensorkomponenten $\mathcal{T}^{\mathrm{e}}_{\rho\sigma}$ des Eigenfeldes identifiziert werden können,

sondern es ergibt sich zunächst aus dem Vergleich der Isospinaufspaltungsgleichung (75) mit der Isospinaufspaltungsbedingung (50) (siehe hierzu auch (7) und (15)):

$$\mathring{\mathcal{T}}_{\rho\sigma} = \mathcal{J}^{\mathrm{i}}_{\rho\sigma} - \int (q'_{\rho\mathbf{k}} p'_{\sigma\mathbf{k}} - q'_{\sigma\mathbf{k}} p'_{\rho\mathbf{k}}) \mathrm{d}\mathbf{k} + \mathcal{T}^{\mathrm{e}}_{\rho\sigma}. \tag{76}$$

Durch (76) ist somit dafür gesorgt, daß unserer Transformationsformeln (65) die Isospinaufspaltungsbedingung (50) bzw. (51) erfüllen.

Der in (76) auftretende Isospinoperator $\mathcal{J}^{\mathrm{i}}_{\rho\sigma}$ des freien Feldanteiles ist aus den Operatoren $a^*_{\rho_0\mathbf{k}_0}$ und $a_{\rho_0\mathbf{k}_0}$ des freien Feldanteiles entsprechend (15) gebildet. Demgemäß haben wir mit (76) die $\mathring{\mathcal{T}}_{\rho\sigma}$ durch die $a^*_{\rho_0\mathbf{k}_0}$, $a_{\rho_0\mathbf{k}_0}$, $\mathcal{T}^{\mathrm{e}}_{\rho\sigma}$, $q'_{\rho\mathbf{k}}$ und $p'_{\rho\mathbf{k}}$ ausgedrückt. Zur weiteren und vollständigen Durchführung der Substitution müssen wir daher jetzt nur noch die Operatoren $q'_{\rho\mathbf{k}}$ und $p'_{\rho\mathbf{k}}$ durch die Operatoren des freien Feldanteiles und des Eigenfeldanteiles ausdrücken. Wir tun dies durch den in $a_{\rho_0\mathbf{k}_0}$ und $a^*_{\rho_0\mathbf{k}_0}$ linearen Ansatz

$$\begin{aligned} \text{a)}\quad & q'_{\rho\mathbf{k}} = \sum_{\rho_0} \int (2\varepsilon_0)^{-\frac{1}{2}} (u_{\substack{\mathbf{k}\mathbf{k}_0\\ \rho\rho_0}} a_{\rho_0\mathbf{k}_0} + u^*_{\substack{-\mathbf{k}\mathbf{k}_0\\ \rho\rho_0}} a^*_{\rho_0\mathbf{k}_0}) \mathrm{d}\mathbf{k}_0, \\ \text{b)}\quad & p'_{\rho\mathbf{k}} = \sum_{\rho_0} \int (\tfrac{1}{2}\varepsilon_0)^{\frac{1}{2}} i (v_{\substack{\mathbf{k}\mathbf{k}_0\\ \rho\rho_0}} a^*_{\rho_0\mathbf{k}_0} - v^*_{\substack{-\mathbf{k}\mathbf{k}_0\\ \rho\rho_0}} a_{\rho_0\mathbf{k}_0}) \mathrm{d}\mathbf{k}_0, \end{aligned} \tag{77}$$

wobei die hiermit eingeführten Transformationsfunktionen

$$u_{\substack{\mathbf{k}\mathbf{k}_0\\ \rho\rho_0}}, \qquad v_{\substack{\mathbf{k}\mathbf{k}_0\\ \rho\rho_0}}$$

wegen des Auftretens von $S_\rho S_{\rho'}$ auf der rechten Seite der Vertauschungsrelationen (66) ebenfalls noch die Operatoren S_ρ enthalten müssen und zwar aus Koviarianzgründen bezüglich des Isospinraumes in der Form

$$u_{\substack{\mathbf{k}\mathbf{k}_0\\ \rho\rho_0}} = A(\mathbf{k}, \mathbf{k}_0)\delta_{\rho\rho_0} + B(\mathbf{k}, \mathbf{k}_0) S_\rho S_{\rho_0} \tag{78}$$

und

$$v_{\substack{\mathbf{k}\mathbf{k}_0\\ \rho\rho_0}} = C(\mathbf{k}, \mathbf{k}_0)\delta_{\rho\rho_0} + D(\mathbf{k}, \mathbf{k}_0) S_\rho S_{\rho_0}. \tag{79}$$

Dabei sind die $A(\mathbf{k}, \mathbf{k}_0)$, $B(\mathbf{k}, \mathbf{k}_0)$, $C(\mathbf{k}, \mathbf{k}_0)$ und $D(\mathbf{k}, \mathbf{k}_0)$ zunächst unbestimmte reine c-Zahlfunktionen, die zur Erfüllung der Vertauschungsrelationen (66) bis (73) sowie der Beziehungen (72) und (73) für die $q'_{\rho\mathbf{k}}$, $p'_{\rho\mathbf{k}}$, S_ρ und $\mathring{\mathcal{T}}_{\rho\sigma}$ noch gewissen Bedingungen unterworfen werden müssen. Gehen wir zu diesem Zweck mit dem Ansatz (77) zunächst in die Vertauschungsrelationen (66) bis (68) ein, so ergibt sich, daß diese als Konsequenz der Vertauschungsrelationen für die $a^*_{\rho_0\mathbf{k}_0}$, $a_{\rho_0\mathbf{k}_0}$ und S_ρ (siehe Gln. (12), (13), (19), (52)) erfüllt sind, wenn die Transformationsfunktionen u und v den Bedingungen in

$$\sum_{\rho_0} \int v_{\substack{\mathbf{k}'\mathbf{k}_0\\ \rho'\rho_0}} u_{\substack{\mathbf{k}\mathbf{k}_0\\ \rho\rho_0}} \mathrm{d}\mathbf{k}_0 = \delta(\mathbf{k}'-\mathbf{k})\delta_{\rho'\rho} - v_{\mathbf{k}'} u_{\mathbf{k}} (\delta_{\rho'\rho} - S_{\rho'} S_\rho) \tag{80}$$

$$\text{a)}\quad \sum_{\rho_0}\int \frac{1}{\varepsilon_0}\, u^{*}_{\substack{-\mathbf{k}'\mathbf{k}_0\\ \rho'\rho_0}} u_{\substack{\mathbf{k}\mathbf{k}_0\\ \rho\rho_0}} \mathrm{d}\mathbf{k}_0,$$

$$\text{b)}\quad \sum_{\rho_0}\int \varepsilon_0 v^{*}_{\substack{-\mathbf{k}'\mathbf{k}_0\\ \rho'\rho_0}} v_{\substack{\mathbf{k}\mathbf{k}_0\\ \rho\rho_0}} \mathrm{d}\mathbf{k}_0 \qquad \text{(reell)}, \tag{81}$$

$$\text{a)}\quad u_{\substack{\mathbf{k}\mathbf{k}_0\\ \rho\rho_0}} = u_{\substack{-\mathbf{k}-\mathbf{k}_0\\ \rho\ \rho_0}},$$

$$\text{b)}\quad v_{\substack{\mathbf{k}\mathbf{k}_0\\ \rho\rho_0}} = v_{\substack{-\mathbf{k}-\mathbf{k}_0\\ \rho\ \rho_0}} \tag{82}$$

genügen, und zwar sorgt (80) für die Erfüllung von (66), und (81a, b) und (82a, b) für die Erfüllung von (67). Dann bekommen wir auf grund von (80) für die Funktionen $A(\mathbf{k}, \mathbf{k}_0)$, $B(\mathbf{k}, \mathbf{k}_0)$, $C(\mathbf{k}, \mathbf{k}_0)$ und $D(\mathbf{k}, \mathbf{k}_0)$ der Gln. (78) und (79)

$$\int C(\mathbf{k}', \mathbf{k}_0) A(\mathbf{k}, \mathbf{k}_0)\mathrm{d}\mathbf{k}_0 = \delta(\mathbf{k}'-\mathbf{k}) - v_{\mathbf{k}'} u_{\mathbf{k}},$$

$$\int C(\mathbf{k}',\mathbf{k}_0)B(\mathbf{k},\mathbf{k}_0)\mathrm{d}\mathbf{k}_0 + \int D(\mathbf{k}',\mathbf{k}_0)A(\mathbf{k},\mathbf{k}_0)\mathrm{d}\mathbf{k}_0 + \int D(\mathbf{k}',\mathbf{k}_0)B(\mathbf{k},\mathbf{k}_0)\mathrm{d}\mathbf{k}_0 = v_{\mathbf{k}'} u_{\mathbf{k}}. \tag{83}$$

Wir wollen aber der kürzeren Schreibweise wegen im Folgenden immer die für die u und v angeschriebenen Bedingungsgleichungen (80) bis (82) an Stelle derjenigen für die $A(\mathbf{k}, \mathbf{k}_0)$, $B(\mathbf{k}, \mathbf{k}_0)$, $C(\mathbf{k}, \mathbf{k}_0)$ und $D(\mathbf{k}, \mathbf{k}_0)$ bei unseren Darlegungen benutzen.

Mit dem Ansatz (77) und den Bedingungen (80) bis (82) haben wir somit die $q'_{\rho\mathbf{k}}$ und $p'_{\rho\mathbf{k}}$ durch die $a^{*}_{\rho_0\mathbf{k}_0}$, $a_{\rho_0\mathbf{k}_0}$ und S_ρ so ausgedrückt, daß die Vertauschungsrelationen (66) bis (68) für die $q'_{\rho\mathbf{k}}$, $p'_{\rho\mathbf{k}}$ und S_ρ als Konsequenz der Vertauschungsrelationen (12), (13), (19) und (52) für die $a^{*}_{\rho_0\mathbf{k}_0}$, $a_{\rho_0\mathbf{k}_0}$ und S_ρ befriedigt sind. Als nächsten Schritt wollen wir nun die Verifizierung der Vertauschungsrelationen (69) bis (71) für die Kommutatoren von $\mathring{\mathcal{T}}_{\rho\sigma}$ mit den $q'_{\rho\mathbf{k}}$ und $p'_{\rho\mathbf{k}}$ auf Grund von (76) und (77) durchführen. Dazu bilden wir mit dem Ausdruck (76) die Kommutatoren der $\mathring{\mathcal{T}}_{\rho\sigma}$ mit den $q'_{\rho'\mathbf{k}'}$ und $p'_{\rho'\mathbf{k}'}$ und erhalten, wenn wir die Abkürzung

$$\mathcal{I}'_{\rho\sigma} = \int (q'_{\rho\mathbf{k}} p'_{\sigma\mathbf{k}} - q'_{\sigma\mathbf{k}} p'_{\rho\mathbf{k}})\mathrm{d}\mathbf{k} \tag{84}$$

einführen,

$$\left[\mathring{\mathcal{T}}_{\rho\sigma}, \begin{matrix} q'_{\rho'\mathbf{k}'} \\ p'_{\rho'\mathbf{k}'} \end{matrix}\right] = \left[(\mathcal{I}^{\mathrm{f}}_{\rho\sigma} + \mathcal{T}^{\mathrm{c}}_{\rho\sigma}), \begin{matrix} q'_{\rho'\mathbf{k}'} \\ p'_{\rho'\mathbf{k}'} \end{matrix}\right] - \left[\mathcal{I}'_{\rho\sigma}, \begin{matrix} q'_{\rho'\mathbf{k}'} \\ p'_{\rho'\mathbf{k}'} \end{matrix}\right]. \tag{85}$$

Die Vertauschungseigenschaften von $\mathcal{I}'_{\rho\sigma}$ mit den $q'_{\rho\mathbf{k}}$ und $p'_{\rho\mathbf{k}}$ ergeben sich dann aus den schon soeben durch (77) mit den Bedingungen (80) bis (82)

verifizierten Vertauschungsrelationen (66) und (67) für die $q'_{\rho\mathbf{k}}$ und $p'_{\rho\mathbf{k}}$ untereinander zu,

$$i[\mathcal{I}'_{\rho\sigma}, q'_{\rho'\mathbf{k}'}] = \sum_{\rho''\sigma''} (\delta_{\rho\rho''}\delta_{\sigma\sigma''} - \delta_{\sigma\rho''}\delta_{\rho\sigma''}) \left\{ q'_{\rho''\mathbf{k}'}\delta_{\sigma''\rho''} - u_{\mathbf{k}''} \int v_{\mathbf{k}} q_{\rho''\mathbf{k}}\, \mathrm{d}\mathbf{k} \cdot (\delta_{\sigma''\rho''} - S_{\sigma''}S_{\rho''}) \right\}, \quad (86)$$

$$i[\mathcal{I}'_{\rho\sigma}, p'_{\rho'\mathbf{k}'}] = \sum_{\rho''\sigma''} (\delta_{\rho\rho''}\delta_{\sigma\sigma''} - \delta_{\sigma\rho'}\delta_{\rho\sigma''}) \left\{ p'_{\rho''\mathbf{k}'}\delta_{\sigma''\rho''} - v_{\mathbf{k}''} \int u_{\mathbf{k}} p_{\rho''\mathbf{k}}\, \mathrm{d}\mathbf{k} \cdot (\delta_{\sigma''\rho''} - S_{\sigma''}S_{\rho''}) \right\}. \quad (87)$$

Hingegen folgen die Vertauschungsrelationen von $\mathcal{I}^{\mathrm{f}}_{\rho\sigma} + \mathcal{T}^{\mathrm{e}}_{\rho\sigma}$ mit den $q'_{\rho\mathbf{k}}$ bzw. $p'_{\rho\mathbf{k}}$ aus dem Umstand, daß der Ansatz (77) für die Operatoren $q'_{\rho\mathbf{k}}$ und $p'_{\rho\mathbf{k}}$ gemäß (78) und (79) aus den Operatoren $a^*_{\rho_0\mathbf{k}_0}$, $a_{\rho_0\mathbf{k}_0}$ und S_ρ bezüglich des Isospinraumes in kovarianter Weise gebildet ist. Dadurch spielt nämlich der Operator $\mathcal{I}^{\mathrm{f}}_{\rho\sigma} + \mathcal{T}^{\mathrm{e}}_{\rho\sigma}$ — als Gesamtisospinoperator von freiem Mesonfeld + Eigenfeld — die Rolle des Drehoperators der $q'_{\rho\mathbf{k}}$ und $p'_{\rho\mathbf{k}}$ in Bezug auf den Isospinraum und es gilt

$$i[(\mathcal{I}^{\mathrm{f}}_{\rho\sigma} + \mathcal{T}^{\mathrm{e}}_{\rho\sigma}), q'_{\rho'\mathbf{k}'}] = \sum_{\rho''} (\delta_{\rho\rho''}\delta_{\sigma\rho'} - \delta_{\sigma\rho''}\delta_{\rho\rho'}) q'_{\rho''\mathbf{k}'}, \quad (88)$$

$$i[(\mathcal{I}^{\mathrm{f}}_{\rho\sigma} + \mathcal{T}^{\mathrm{e}}_{\rho\sigma}), p'_{\rho'\mathbf{k}'}] = \sum_{\rho''} (\delta_{\rho\rho''}\delta_{\sigma\rho'} - \delta_{\sigma\rho''}\delta_{\rho\rho'}) p'_{\rho''\mathbf{k}'}. \quad (89)$$

Die Vertauschungsrelationen für $\mathring{\mathcal{T}}_{\rho\sigma}$ mit den $q'_{\rho\mathbf{k}}$ und $p'_{\rho\mathbf{k}}$ erhalten wir dann gemäß (85), indem wir (86) und (87) von (88) und (89) subtrahieren. Somit ergibt sich

$$i[\mathring{\mathcal{T}}_{\rho\sigma}, q'_{\rho'\mathbf{k}'}] = u_{\mathbf{k}'} \left\{ \int v_{\mathbf{k}} q'_{\rho\mathbf{k}}\, \mathrm{d}\mathbf{k} (\delta_{\sigma\rho'} - S_\sigma S_{\rho'}) - \int v_{\mathbf{k}} q'_{\sigma\mathbf{k}}\, \mathrm{d}\mathbf{k} (\delta_{\rho\rho''} - S_\rho S_{\rho'}) \right\}, \quad (90)$$

$$i[\mathring{\mathcal{T}}_{\rho\sigma}, p'_{\rho'\mathbf{k}'}] = v_{\mathbf{k}'} \left\{ \int u_{\mathbf{k}} p'_{\rho\mathbf{k}}\, \mathrm{d}\mathbf{k} (\delta_{\sigma\rho'} - S_\sigma S_{\rho'}) - \int u_{\mathbf{k}} p'_{\sigma\mathbf{k}}\, \mathrm{d}\mathbf{k} (\delta_{\rho\rho''} - S_\rho S_{\rho'}) \right\}. \quad (91)$$

Aus (90) und (91) würden sich (69) und (70) ergeben, wenn auch (72) und (73) erfüllt wären. Zur Erfüllung von (72) und (73) müssen aber die Transformationen u und v des Ansatzes (77) noch den Forderungen

$$\sum_{\rho} (\delta_{\rho'\rho} - S_{\rho'}S_\rho) \int v_{\mathbf{k}} u_{\underset{\rho\rho_0}{\mathbf{k}\mathbf{k}_0}}\, \mathrm{d}\mathbf{k} = 0, \quad (92)$$

$$\sum_{\rho} (\delta_{\rho'\rho} - S_{\rho'}S_\rho) \int u_{\mathbf{k}} v_{\underset{\rho\rho_0}{\mathbf{k}\mathbf{k}_0}}\, \mathrm{d}\mathbf{k} = 0. \quad (93)$$

unterworfen werden, welche somit zu den Bedingungen (80) bis (82) noch hinzugefügt werden müssen, wenn die Vertauschungsrelationen (69) bis (71) für $\mathring{\mathcal{T}}_{\rho\sigma}$ mit den $q'_{\rho\mathbf{k}}$ und $p'_{\rho\mathbf{k}}$ durch den Ansatz (77) erfüllt sein sollen. Wir werden im Folgenden auf Seite 22 sehen, daß die Forderungen (92) und (93)

schon mit gestellt sind, wenn wir zu den Bedingungen (80) bis (82) noch diejenige Bedingungsgleichung hinzufügen, die zur Erfüllung der Umkehrbedingung notwendig ist.

Bevor wir uns jedoch dieser Frage zuwenden, wollen wir erst noch zeigen, daß auch die Vertauschungsrelationen für die $\mathring{\mathcal{T}}_{\rho\sigma}$, miteinander und mit den S_ρ, die den Gln. (18) und (20) entsprechen, auf Grund von (76) durch den Ansatz (77) efrüllt werden.

Für die Kommutatoren $\mathring{\mathcal{T}}_{\rho\sigma}$ mit den S_ρ folgt dies unmittelbar daraus, daß ja die S_ρ außer mit den $\mathcal{T}^{\mathrm{e}}_{\rho\sigma}$ mit allen anderen Termen der Gl. (76) kommutieren, wobei die Vertauschbarkeit der S_ρ mit den $\int (q'_{\rho\mathbf{k}} p'_{\sigma\mathbf{k}} - q'_{\sigma\mathbf{k}} p'_{\rho\mathbf{k}}) d\mathbf{k}$ in der $\mathcal{T}^{\mathrm{e}}_{\rho\sigma}$-Unabhängigkeit des Ansatzes (77) begründet liegt.

Was andererseits die Kommutatoren der $\mathring{\mathcal{T}}_{\rho\sigma}$ miteinander anbetrifft, so erhalten wir auf Grund von (76) mit der Abkürzung (84)

$$\begin{aligned}[\mathring{\mathcal{T}}_{\rho'\sigma'}, \mathring{\mathcal{T}}_{\rho\sigma}] &= [(\mathcal{I}^{\mathrm{f}}_{\rho'\sigma'} + \mathcal{T}^{\mathrm{e}}_{\rho'\sigma'}), (\mathcal{I}^{\mathrm{f}}_{\rho\sigma} + \mathcal{T}^{\mathrm{e}}_{\rho\sigma})] \\ &- [(\mathcal{I}^{\mathrm{f}}_{\rho'\sigma'} + \mathcal{T}^{\mathrm{e}}_{\rho'\sigma'}), \mathcal{I}'_{\rho\sigma}] - [\mathcal{I}'_{\rho'\sigma'}, (\mathcal{I}^{\mathrm{f}}_{\rho\sigma} + \mathcal{T}^{\mathrm{e}}_{\rho\sigma})] + [\mathcal{I}'_{\rho\sigma}, \mathcal{I}'_{\rho\sigma}].\end{aligned} \tag{94}$$

In den Kommutatoren $[(\mathcal{I}^{\mathrm{f}}_{\rho'\sigma'} + \mathcal{T}^{\mathrm{e}}_{\rho'\sigma'}), (\mathcal{I}^{\mathrm{f}}_{\rho\sigma} + \mathcal{T}^{\mathrm{e}}_{\rho\sigma})]$ und $[\mathcal{I}'_{\rho'\sigma'}, \mathcal{I}'_{\rho\sigma}]$ gehorchen die Operatoren $\mathcal{I}^{\mathrm{f}}_{\rho\sigma} + \mathcal{T}^{\mathrm{e}}_{\rho\sigma}$ und $\mathcal{I}'_{\rho\sigma}$ jeder für sich allein schon den der Gl. (18) entsprechenden Vertauschungsrelationen, und zwar ist dies für $\mathcal{I}^{\mathrm{f}}_{\rho\sigma} + \mathcal{T}^{\mathrm{e}}_{\rho\sigma}$ per definitionem der Fall, während es für $\mathcal{I}'_{\rho\sigma}$ daraus folgt, daß der zweite, S_ρ-abhängige Term auf der rechten Seite der Vertauschungsrelationen (66), der die Abweichung der $q'_{\rho\mathbf{k}}$ und $p'_{\rho\mathbf{k}}$ von der Kanonizität zum Ausdruck bringt, wegen seiner Symmetrieeigenschaften und wegen der Beziehungen (72) und (73) bei der Vertauschung der $\mathcal{I}'_{\rho\sigma}$ miteinander nicht zur Wirkung kommt, sodass sich also die $q'_{\rho\mathbf{k}}$ und $p'_{\rho\mathbf{k}}$ bezüglich der Vertauschungseigenschaften der $\mathcal{I}'_{\rho\sigma}$ miteinander wie kanonische Variable verhalten. Da andererseits, wie schon vor (88) hervorgehoben wurde, der Operator $\mathcal{I}^{\mathrm{f}}_{\rho\sigma} + \mathcal{T}^{\mathrm{e}}_{\rho\sigma}$ der Drehoperator der $q'_{\rho\mathbf{k}}$ und $p'_{\rho\mathbf{k}}$ in Bezug auf den Isospinraum ist, sodaß die Vertauschungsrelationen (88) und (89) gelten, folgt somit auch

$$[(\mathcal{I}^{\mathrm{f}}_{\rho'\sigma'} + \mathcal{T}^{\mathrm{e}}_{\rho'\sigma'}), \mathcal{I}'_{\rho\sigma}] = [\mathcal{I}'_{\rho'\sigma'}, \mathcal{I}'_{\rho\sigma}], \tag{95}$$

bzw. gemäß (76)

$$[\mathring{\mathcal{T}}_{\rho'\sigma'}, \mathcal{I}'_{\rho\sigma}] = 0, \tag{96}$$

wie wir es auch entsprechend (54), (74) und (84) zu erwarten haben. Dann wird aus (94)

$$[\mathring{\mathcal{T}}_{\rho'\sigma'}, \mathring{\mathcal{T}}_{\rho\sigma}] = [(\mathcal{I}^{\mathrm{f}}_{\rho'\sigma'} + \mathcal{T}^{\mathrm{e}}_{\rho'\sigma'}), (\mathcal{I}^{\mathrm{f}}_{\rho\sigma} + \mathcal{T}^{\mathrm{e}}_{\rho\sigma})] - [\mathcal{I}'_{\rho'\sigma'}, \mathcal{I}'_{\rho\sigma}] \tag{97}$$

und da, wie wir eben im Anschluß an (94) dargelegt haben, die $\mathcal{I}^{\mathrm{f}}_{\rho\sigma} + \mathcal{T}^{\mathrm{e}}_{\rho\sigma}$ und $\mathcal{I}'_{\rho\sigma}$ jeder für sich allein den Vertauschungsrelationen (18) gehorchen, haben wir damit gemäß (76) die Bestätigung der Vertauschungsrelationen (18) für die

$\mathring{\mathcal{T}}_{\rho\sigma}$ miteinander erhalten, wobei wir mit dem Ansatz (77) lediglich die Bedingung (80) bis (82) sowie (92) und (93) für die u und v benutzt haben.

2.2.3. *Die Umkehrbarkeit des gesamten Transformationsansatzes*

Gemäß den vorstehenden Ausführungen haben wir mit den Transformationsformeln (65), (76) und dem Ansatz (77) die ursprünglichen Mesonfeldoperatoren $q_{\rho\mathbf{k}}$ und $p_{\rho\mathbf{k}}$ durch die Operatoren $a^*_{\rho_0\mathbf{k}_0}$ und $a_{\rho_0\mathbf{k}_0}$ des freien Feldanteiles und durch die Operatoren S_ρ und $\mathcal{T}^{\mathrm{e}}_{\rho\sigma}$ des Eigenfeldanteiles so ausgedrückt, daß die kanonischen Vertauschungsrelationen (2) für die $q_{\rho\mathbf{k}}$ und $p_{\rho\mathbf{k}}$ als Konsequenz der Vertauschungsrelationen (12) bis (27) und (52) für die $a^*_{\rho_0\mathbf{k}_0}$, $a_{\rho_0\mathbf{k}_0}$, S_ρ und $\mathcal{T}^{\mathrm{e}}_{\rho\sigma}$ befriedigt sind, und auch die Isospinaufspaltungsbedingung (50) bzw. (51) erfüllt ist. Eine Zusammenfassung der gesamten Transformationsformeln geben wir am Schluß dieses Abschnittes.

Es bleibt nun noch zu untersuchen, ob die vorstehend hergeleitete Transformation auch umkehrbar ist, d.h. ob die Transformationsformeln nach den neuen Variablen $a^*_{\rho_0\mathbf{k}_0}$, $a_{\rho_0\mathbf{k}_0}$, S_ρ und $\mathcal{T}^{\mathrm{e}}_{\rho\sigma}$ auflösbar sind, und somit die $a^*_{\rho_0\mathbf{k}_0}$, $a_{\rho_0\mathbf{k}_0}$, S_ρ und $\mathcal{T}^{\mathrm{e}}_{\rho\sigma}$ durch die $q_{\rho\mathbf{k}}$ und $p_{\rho\mathbf{k}}$ ausgedrückt werden können. Wir zeigen, daß dies möglich ist, wenn wir zusätzlich zu den Bedingungen (80) bis (82) noch fordern

$$\sum_{\rho}\int u_{\substack{\mathbf{k}\mathbf{k}_0\\ \rho\rho_0}} v_{\substack{\mathbf{k}\mathbf{k}'_0\\ \rho\rho'_0}}\,\mathrm{d}\mathbf{k} = \delta(\mathbf{k}_0-\mathbf{k}'_0)\delta_{\rho_0\rho'_0}, \tag{98}$$

$$\sum_{\rho}\int u_{\substack{\mathbf{k}\mathbf{k}_0\\ \rho\rho_0}} v^*_{\substack{-\mathbf{k}\mathbf{k}'_0\\ \rho\rho'_0}}\,\mathrm{d}\mathbf{k} \propto \delta(k_0-k'_0). \tag{99}$$

Dazu ist zunächst festzustellen, daß sich dann die Bedingungen (92), (93) und (30) aus den Bedingungen (80) und (98) ableiten lassen. Die Anwendung der Operation

$$\sum_{\rho'}\int u_{\substack{\mathbf{k}'\mathbf{k}_0\\ \rho\rho_0}} \ldots \mathrm{d}\mathbf{k}'$$

auf (80) ergibt nämlich wegen (98) gerade (92), ebenso ergibt die Operation

$$\sum_{\rho}\int v_{\substack{\mathbf{k}\mathbf{k}'_0\\ \rho\rho'_0}} \ldots \mathrm{d}\mathbf{k}$$

auf (80) angewandt wegen (98) gerade (93) und die Operationen

$$\sum_{\rho}(\delta_{\rho''\rho}-S_{\rho''}S_\rho)\int v_{\mathbf{k}} \ldots \mathrm{d}\mathbf{k}, \qquad \text{bzw.} \sum_{\rho'}(\delta_{\rho''\rho'}-S_{\rho''}S_{\rho'})\int u_{\mathbf{k}'} \ldots \mathrm{d}\mathbf{k}'$$

auf (80) angewandt liefert wegen (92) bzw. (93) gerade (30).

Für die Auflösung der Transformation nach den neuen Variablen $a^*_{\rho_0\mathbf{k}_0}$, $a_{\rho_0\mathbf{k}_0}$, S_ρ und $\mathcal{T}^{\mathrm{e}}_{\rho\sigma}$ ist nun der Ansatz (77) wiederum der geeignete Ausgangspunkt.

Wenden wir dementsprechend die Operationen

$$\sum_{\rho}\int v_{\substack{\mathbf{k}\mathbf{k}_0\\ \rho\rho_0}}\ldots\mathrm{d}\mathbf{k} \quad \text{und} \quad \sum_{\rho}\int v^*_{\substack{-\mathbf{k}\mathbf{k}_0\\ \rho\rho_0}}\ldots\mathrm{d}\mathbf{k}$$

auf (77a) und die Operationen

$$\sum_{\rho}\int u^*_{\substack{-\mathbf{k}\mathbf{k}_0\\ \rho\rho_0}}\ldots\mathrm{d}\mathbf{k} \quad \text{und} \quad \sum_{\rho}\int u_{\substack{\mathbf{k}\mathbf{k}_0\\ \rho\rho_0}}\ldots\mathrm{d}\mathbf{k}$$

auf (77b) an, so erhalten wir durch Addition bzw. Subtraktion der so behandelten Gleichungen (77a) und (77b) bei Berücksichtigung von (98) und (99)

$$\begin{aligned}
&\text{a)}\quad a_{\rho_0\mathbf{k}_0} = (\tfrac{1}{2}\varepsilon_0)^{\frac{1}{2}}\sum_{\rho}\int v_{\substack{\mathbf{k}\mathbf{k}_0\\ \rho\rho_0}} q'_{\rho\mathbf{k}}\,\mathrm{d}\mathbf{k} + i(2\varepsilon_0)^{-\frac{1}{2}}\sum_{\rho}\int u^*_{\substack{-\mathbf{k}\mathbf{k}_0\\ \rho\rho_0}} p'_{\rho\mathbf{k}}\,\mathrm{d}\mathbf{k},\\
&\text{b)}\quad a^*_{\rho_0\mathbf{k}_0} = (\tfrac{1}{2}\varepsilon_0)^{\frac{1}{2}}\sum_{\rho}\int v^*_{\substack{-\mathbf{k}\mathbf{k}_0\\ \rho\rho_0}} q'_{\rho\mathbf{k}}\,\mathrm{d}\mathbf{k} - i(2\varepsilon_0)^{-\frac{1}{2}}\sum_{\rho}\int u_{\substack{\mathbf{k}\mathbf{k}_0\\ \rho\rho_0}} p'_{\rho\mathbf{k}}\,\mathrm{d}\mathbf{k}.
\end{aligned} \tag{100}$$

In (100) substituieren wir weiter auf Grund von (65)

$$\begin{aligned}
&\text{a)}\quad q'_{\rho\mathbf{k}} = q_{\rho\mathbf{k}} - u_{\mathbf{k}} S_{\rho},\\
&\text{b)}\quad p'_{\rho\mathbf{k}} = p_{\rho\mathbf{k}} + v_{\mathbf{k}}\frac{\sum_{\sigma}\langle S_{\sigma}\mathring{\mathscr{T}}_{\rho\sigma}\rangle}{1+\sum_{\rho'} S_{\rho'}\int v_{\mathbf{k}'} q'_{\rho'\mathbf{k}'}\,\mathrm{d}\mathbf{k}'}.
\end{aligned} \tag{101}$$

Den Beitrag des zweiten Termes von (101b) können wir bei der Substitution in die Gln. (100) in Fortfall bringen, wenn wir das symmetrisierte Produkt mit u bilden. Dann kommt nämlich (92) zur Wirkung und mit ihr (27) und (28), die ganz entsprechend auch für $\sum_{\sigma}\langle S_{\sigma}\mathring{\mathscr{T}}_{\rho\sigma}\rangle$ gelten. Somit erhalten wir

$$\begin{aligned}
&\text{a)}\quad a_{\rho_0\mathbf{k}_0} = (\tfrac{1}{2}\varepsilon_0)^{\frac{1}{2}}\sum_{\rho}\int v_{\substack{\mathbf{k}\mathbf{k}_0\\ \rho\rho_0}} q_{\rho\mathbf{k}}\,\mathrm{d}\mathbf{k} + i(2\varepsilon_0)^{-\frac{1}{2}}\sum_{\rho}\int \langle u^*_{\substack{-\mathbf{k}\mathbf{k}_0\\ \rho\rho_0}} p_{\rho\mathbf{k}}\rangle\,\mathrm{d}\mathbf{k} - (\tfrac{1}{2}\varepsilon_0)^{\frac{1}{2}}\sum_{\rho} S_{\rho}\int u_{\mathbf{k}} v_{\substack{\mathbf{k}\mathbf{k}_0\\ \rho\rho_0}}\,\mathrm{d}\mathbf{k},\\
&\text{b)}\quad a^*_{\rho_0\mathbf{k}_0} = (\tfrac{1}{2}\varepsilon_0)^{\frac{1}{2}}\sum_{\rho}\int v^*_{\substack{-\mathbf{k}\mathbf{k}_0\\ \rho\rho_0}} q_{\rho\mathbf{k}}\,\mathrm{d}\mathbf{k} - i(2\varepsilon_0)^{-\frac{1}{2}}\sum_{\rho}\int \langle u_{\substack{\mathbf{k}\mathbf{k}_0\\ \rho\rho_0}} p_{\rho\mathbf{k}}\rangle\,\mathrm{d}\mathbf{k} - (\tfrac{1}{2}\varepsilon_0)^{\frac{1}{2}}\sum_{\rho} S_{\rho}\int u_{\mathbf{k}} v^*_{\substack{\mathbf{k}\mathbf{k}_0\\ \rho\rho_0}}\,\mathrm{d}\mathbf{k},
\end{aligned} \tag{102}$$

wobei $\langle\rangle$ das symmetrisierte Produkt bedeutet.

Was nun die Umkehrung der Eigenfeldoperatoren anbelangt, so bekommen wir für S_{ρ} gemäß (61) und (55)

$$S_{\rho} = \frac{\int v_{\mathbf{k}} q_{\rho\mathbf{k}}\,\mathrm{d}\mathbf{k}}{\sqrt{\sum_{\rho'}\left|\int v'_{\mathbf{k}}\, q_{\rho'\mathbf{k}'}\,\mathrm{d}\mathbf{k}'\right|^2}} \tag{103}$$

und für die $\mathscr{T}^{\mathrm{e}}_{\rho\sigma}$ folgt aus der durch die Transformation erfüllten Isospinaufspaltungsbedingung (50)

$$\mathscr{T}^{\mathrm{e}}_{\rho\sigma} = \int (q_{\rho\mathbf{k}} p_{\sigma\mathbf{k}} - q_{\sigma\mathbf{k}} p_{\rho\mathbf{k}})\mathrm{d}\mathbf{k} - \mathscr{I}^{i}_{\rho\sigma}. \tag{104}$$

Um nun die Umkehrung (102a, b) für die Operatoren $a_{\rho_0 \mathbf{k}_0}$ und $a^*_{\rho_0 \mathbf{k}_0}$ des freien Feldanteiles vollständig zu machen und die $a_{\rho_0 \mathbf{k}_0}$ und $a^*_{\rho_0 \mathbf{k}_0}$ ausschließlich durch die $q_{\rho \mathbf{k}}$ und $p_{\rho \mathbf{k}}$ auszudrücken, müßten wir jetzt überall in (102a, b) den Eigenfeldoperator S_ρ gemäß (103) substituieren insbesondere auch in u und v (siehe (78) und (79)),

$$u^{\mathbf{k}\mathbf{k}_0}_{\rho\rho_0} = A(\mathbf{k}, \mathbf{k}_0)\delta_{\rho\rho_0} + B(\mathbf{k}, \mathbf{k}_0) \frac{\int v_{\mathbf{k}} q_{\rho\mathbf{k}} \mathrm{d}\mathbf{k} \cdot \int v_{\mathbf{k}''} q_{\rho_0 \mathbf{k}''} \mathrm{d}\mathbf{k}''}{\sum\limits_{\rho'} \left| \int v_{\mathbf{k}'} q_{\rho'\mathbf{k}'} \mathrm{d}\mathbf{k}' \right|^2}, \tag{105}$$

$$v^{\mathbf{k}\mathbf{k}_0}_{\rho\rho_0} = C(\mathbf{k}, \mathbf{k}_0)\delta_{\rho\rho_0} + D(\mathbf{k}, \mathbf{k}_0) \frac{\int v_{\mathbf{k}} q_{\rho\mathbf{k}} \mathrm{d}\mathbf{k} \cdot \int v_{\mathbf{k}''} q_{\rho_0 \mathbf{k}''} \mathrm{d}\mathbf{k}''}{\sum\limits_{\rho'} \left| \int v_{\mathbf{k}'} q_{\rho'\mathbf{k}'} \mathrm{d}\mathbf{k}' \right|^2}. \tag{106}$$

Auf die explizite Widergabe der so entstehenden Ausdrücke für $a_{\rho_0 \mathbf{k}_0}$ und $a^*_{\rho_0 \mathbf{k}_0}$ wollen wir hier aber verzichten, da wir sie in den folgenden Ausführungen zunächst nicht weiter benötigen. Ebenso wollen wir (104) nicht noch weiter auflösen. Wir hätten dabei in $\mathscr{I}^{\mathrm{f}}_{\rho\sigma}$, dem Isospinoperator des freien Feldanteiles Gl. (15), die $a_{\rho_0 \mathbf{k}_0}$ und $a^*_{\rho_0 \mathbf{k}_0}$ gemäß (102), (105) und (106) zu substituieren und $\mathscr{T}^{\mathrm{e}}_{\rho\sigma}$ liesse sich damit vollkommen durch die $q_{\rho\mathbf{k}}$ und $p_{\rho\mathbf{k}}$ ausdrücken, was wir aber hier nicht explizit wiedergeben wollen. Mit der Herleitung von (102), (103), (104) und (105) ist somit gezeigt, daß die $a^*_{\rho_0 \mathbf{k}_0}$, $a_{\rho_0 \mathbf{k}_0}$, S_ρ und $\mathscr{T}^{\mathrm{e}}_{\rho\sigma}$ sich vollständig durch die $q_{\rho\mathbf{k}}$ und $p_{\rho\mathbf{k}}$ ausdrücken lassen, wenn außer den Bedingungen (80) bis (82) auch noch die Bedingungen (98) und (99) gültig sind.

Wir wollen noch auf die besondere Rolle von (92) und (93) als Orthogonalitäts- und Vertauschbarkeitsrelationen zwischen dem freien Mesonfeld einerseits und dem Eigenfeld andererseits hinweisen. Versucht man nämlich (52) anhand der Umkehrformeln zu verifizieren, so stellt sich heraus, daß gerade (92) und (93) es sind, die die Vertauschbarkeit der Operatoren $a_{\rho_0 \mathbf{k}_0}$ und $a^*_{\rho_0 \mathbf{k}_0}$ des freien Mesonfeldes mit den Operatoren S_ρ und $\mathscr{T}^{\mathrm{e}}_{\rho\sigma}$ des Eigenfeldes garantieren.

2.2.4. *Zusammenfassung*

Mit der im vorangehenden Absatz durchgeführten Verifizierung der Umkehrbarkeit unserer Transformationsformeln haben wir die Aufstellung des einfachsten Transformationsansatzes zur Substitution der ursprünglichen kanonischen Mesonfeldvariablen $q_{\rho\mathbf{k}}$ und $p_{\rho\mathbf{k}}$ durch die Erzeugungs- und Vernichtungsoperatoren $a^*_{\rho_0 \mathbf{k}_0}$ und $a_{\rho_0 \mathbf{k}_0}$ des freien Feldanteiles einerseits und die Operatoren S_ρ und $\mathscr{T}^{\mathrm{e}}_{\rho\sigma}$ des Eigenfeldanteiles andererseits nun vollständig durchgeführt und wollen schließlich das Ergebnis zusammenfassend anschreiben. Dazu führen wir zuvor in die Transformationsformeln (65) entsprechend (76) noch die Abkürzung

$$-\tfrac{1}{2} \sum_\sigma (S_\sigma \mathring{\mathscr{T}}_{\rho\sigma} + \mathring{\mathscr{T}}_{\rho\sigma} S_\sigma) = p_\rho + A_\rho \tag{107}$$

ein, worin $\mathfrak{p}_\rho$ der aus den Eigenfeldoperatoren S_ρ und $\mathfrak{F}^{\mathrm{e}}_{\rho\sigma}$ gebildete Eigenfeldoperator (23) ist, und worin A_ρ gegeben ist durch

$$A_\rho = \sum_\sigma S_\sigma(\mathfrak{J}'_{\rho\sigma} - \mathfrak{J}^{\mathrm{f}}_{\rho\sigma}) \tag{108}$$

mit den Ausdrücken (84) für $\mathfrak{J}'_{\rho\sigma}$ und (15) für $\mathfrak{J}^{\mathrm{f}}_{\rho\sigma}$. Ganz entsprechend zu (27) und (28) gilt dann auch

$$\sum_\rho \langle S_\rho(\mathfrak{p}_\rho + A_\rho)\rangle = 0 \tag{109}$$

Unser vorstehend hergeleiteter einfachster Ansatz für die kanonische Aufspaltungstransformation lautet dann bei Zusammenfassung von (65), (76) und (77)

$$(\varkappa)\quad \begin{cases} \text{a)}\quad q_{\rho\mathbf{k}} = q'_{\rho\mathbf{k}} + u_{\mathbf{k}} S_\rho, \\ \text{b)}\quad \mathfrak{p}_{\rho\mathbf{k}} = \mathfrak{p}'_{\rho\mathbf{k}} + v_{\mathbf{k}} \dfrac{\mathfrak{p}_\rho + A_\rho}{1 + \sum\limits_{\rho'} S_{\rho'} \int v_{\mathbf{k}'} q'_{\rho'\mathbf{k}'}\,\mathrm{d}\mathbf{k}'}, \end{cases}$$

mit

$$(k)\quad \begin{cases} \text{a)}\quad q'_{\rho\mathbf{k}} = \sum\limits_{\rho_0} \int (2\varepsilon_0)^{-\frac{1}{2}} (u_{\substack{\mathbf{k}\mathbf{k}_0\\ \rho\rho_0}} a_{\rho_0\mathbf{k}_0} + u^*_{\substack{-\mathbf{k}\mathbf{k}_0\\ \rho\rho_0}} a^*_{\rho_0\mathbf{k}_0})\,\mathrm{d}\mathbf{k}_0, \\ \text{b)}\quad \mathfrak{p}'_{\rho\mathbf{k}} = \sum\limits_{\rho_0} \int (\tfrac{1}{2}\varepsilon_0)^{\frac{1}{2}} i (v_{\substack{\mathbf{k}\mathbf{k}_0\\ \rho\rho_0}} a^*_{\rho_0\mathbf{k}_0} - v^*_{\substack{-\mathbf{k}\mathbf{k}_0\\ \rho\rho_0}} a_{\rho_0\mathbf{k}_0})\,\mathrm{d}\mathbf{k}_0, \end{cases}$$

$$(\lambda)\quad A_\rho = \sum_\sigma S_\sigma \Big\{ \int (q'_{\rho\mathbf{k}} \mathfrak{p}'_{\sigma\mathbf{k}} - q'_{\sigma\mathbf{k}} \mathfrak{p}'_{\rho\mathbf{k}})\,\mathrm{d}\mathbf{k} - \frac{1}{i} \sum_{\rho_0,\sigma_0} \int (\delta_{\rho\rho_0}\delta_{\sigma\sigma_0} - \delta_{\sigma\rho_0}\delta_{\rho\sigma_0}) a^*_{\rho_0\mathbf{k}_0} a_{\rho_0\mathbf{k}_0}\,\mathrm{d}\mathbf{k}_0 \Big\}, \tag{110}$$

und

$$\mathfrak{p}_\rho = -\tfrac{1}{2} \sum_\rho (S_\sigma \mathfrak{F}^{\mathrm{e}}_{\rho\sigma} + \mathfrak{F}^{\mathrm{e}}_{\rho\sigma} S_\sigma), \tag{111}$$

wobei entsprechend der vorstehenden Herleitung die in Absatz 2.1.6 formulierten Aufspaltungsbedingungen (1), (2) und (3) erfüllt sind, wenn die Transformationsfunktionen

$$u_{\substack{\mathbf{k}\mathbf{k}_0\\ \rho\rho_0}},\ v_{\substack{\mathbf{k}\mathbf{k}_0\\ \rho\rho_0}},\ u_{\mathbf{k}} \text{ und } v_{\mathbf{k}}$$

den Bedingungsgleichungen

$$\sum_{\rho_0} \int v_{\substack{\mathbf{k}'\mathbf{k}_0\\ \rho'\rho_0}} u_{\substack{\mathbf{k}\mathbf{k}_0\\ \rho\rho_0}}\,\mathrm{d}\mathbf{k}_0 = \delta(\mathbf{k}'-\mathbf{k})\delta_{\rho'\rho} - v_{\mathbf{k}'} u_{\mathbf{k}} (\delta_{\rho'\rho} - S_{\rho'} S_\rho), \tag{112}$$

$$\sum_\rho \int u_{\substack{\mathbf{k}\mathbf{k}_0\\ \rho\rho_0}} v_{\substack{\mathbf{k}\mathbf{k}'_0\\ \rho\rho'_0}}\,\mathrm{d}\mathbf{k} = \delta(\mathbf{k}_0 - \mathbf{k}'_0)\delta_{\rho_0\rho'_0}, \tag{113}$$

$$\sum_\rho \int u_{\substack{\mathbf{k}\mathbf{k}_0\\ \rho\rho_0}} v^*_{\substack{-\mathbf{k}\mathbf{k}'_0\\ \rho\rho'_0}}\,\mathrm{d}\mathbf{k} \propto \delta(k_0 - k'_0), \tag{114}$$

$$\text{a. } \sum_{\rho_0}\int \frac{1}{\varepsilon_0} u^{*}_{\substack{-\mathbf{k}'\mathbf{k}_0\\ \rho'\rho_0}} u_{\substack{\mathbf{k}\mathbf{k}_0\\ \rho\rho_0}} \mathrm{d}\mathbf{k}_0, \qquad \text{b. } \sum_{\rho}\int \varepsilon_0 v^{*}_{\substack{-\mathbf{k}'\mathbf{k}_0\\ \rho'\rho_0}} v_{\substack{\mathbf{k}\mathbf{k}_0\\ \rho\rho_0}} \mathrm{d}\mathbf{k}_0 \quad \text{(reell)}, \tag{115}$$

$$\text{a) } u_{\substack{\mathbf{k}\mathbf{k}_0\\ \rho\rho_0}} = u_{\substack{-\mathbf{k}-\mathbf{k}_0\\ \rho\ \rho_0}}, \qquad \text{b) } v_{\substack{\mathbf{k}\mathbf{k}_0\\ \rho\rho_0}} = v_{\substack{-\mathbf{k}-\mathbf{k}_0\\ \rho\ \rho_0}} \tag{116}$$

gehorchen. Dabei sind Zähler und Nenner im zweiten Term von (110 κ, b) miteinander vertauschbar. Die Bedingung (4) von Absatz 2.1.6, die Bedingung der starken Kopplung, ist jedoch hiermit noch nicht gestellt, sodaß der Transformationsansatz (110 κ) bis (110 λ) mit den Bedingungsgleichungen (80) bis (82) noch von ziemlich allgemeinem Charakter ist und auch über die Methode der starken Kopplung hinaus noch von Bedeutung wäre. Seine weitere Einschränkung durch die Bedingung der starken Kopplung, und die Lösungen, die sich daraus ergeben, wollen wir im folgenden Abschnitt behandeln.

2.3. BEFRIEDIGUNG DER BEDINGUNG DER STARKEN KOPPLUNG

2.3.1. *Beseitigung der Wechselwirkung für* $g \to \infty$

Den Ansatz (110) wollen wir jetzt noch der Bedingung (4) von Absatz 2.1.6, der Bedingung der starken Kopplung, unterwerfen und werden dadurch weitere Gleichungen erhalten, die zusammen mit (112) bis (116) der Bestimmung der Transformationsfunktionen

$$u_{\substack{\mathbf{k}\mathbf{k}_0\\ \rho\rho_0}},\ v_{\substack{\mathbf{k}\mathbf{k}_0\\ \rho\rho_0}},\ u_{\mathbf{k}} \text{ und } v_{\mathbf{k}}$$

dienen können.

Dazu setzen wir (110) in (1) ein und erhalten mit den Bezeichnungen der Gleichungen (14) und (32) für den Operator der Wechselwirkungsenergie zwischen freiem Feldanteil und dem Compoundnukleon:

$$\begin{aligned} H^{\mathrm{W}} = {} & \tfrac{1}{2}\sum_{\rho}\int \{\dot{p}'^{*}_{\rho\mathbf{k}}\dot{p}'_{\rho\mathbf{k}} + \varepsilon^2 q'^{*}_{\rho\mathbf{k}} q'_{\rho\mathbf{k}}\}\,\mathrm{d}\mathbf{k} - H^{0\mathrm{f}} \\ & + \sum_{\rho}\left\langle \frac{\dot{p}_\rho + A_\rho}{1+\sum_{\rho'} S_{\rho'}\int v_{\mathbf{k}'} q'_{\rho'\mathbf{k}'}\,\mathrm{d}\mathbf{k}} \int v_{\mathbf{k}}\dot{p}'_{\rho\mathbf{k}}\,\mathrm{d}\mathbf{k}\right\rangle \\ & + \tfrac{1}{2}\int |v_{\mathbf{k}}|^2\,\mathrm{d}\mathbf{k}\sum_{\rho}\left(\frac{(\dot{p}_\rho + A_\rho)^2}{(1+\sum_{\rho'} S_{\rho'}\int v_{\mathbf{k}'} q'_{\rho'\mathbf{k}'}\,\mathrm{d}\mathbf{k}')^2} - \dot{p}_\rho{}^2\right) \\ & + \sum_{\rho}\int \left(S_\rho u_{\mathbf{k}}\varepsilon^2 + \frac{g}{2\pi}\left(\sum_{\rho'}\bar{\tau}_{\rho'} s_{\rho'\rho}\right) v(k)\right) q'_{\rho\mathbf{k}}\,\mathrm{d}\mathbf{k}. \end{aligned} \tag{117}$$

Für (117) haben wir (11) mit (9) zu befriedigen.

Beginnen wir mit der dritten Zeile von (117), in welcher entsprechend den

Abkürzungen (110 k) alle Anteile von H^{W} zusammengefaßt sind, die

$$u_{\substack{\mathbf{k}\mathbf{k}_0\\ \rho\rho_0}},\ u^*_{\substack{\mathbf{k}\mathbf{k}_0\\ \rho\rho_0}},\ a_{\rho_0\mathbf{k}_0},\ a^*_{\rho_0\mathbf{k}_0}$$

linear enthalten und frei sind von p_ρ †.

In der dritten Zeile von (117) sind die einzigen mit g in erster Ordnung multiplizierten Terme von H^{W} — als der höchsten in H^{W} überhaupt vorkommenden Ordnung von g — enthalten. Voraussetzung dafür, daß solche g in erster Ordnung enthaltenden Terme von H^{W} der Erfüllbarkeit von (11) mit (9) nicht im Wege stehen, ist zunächst, daß die Terme mit $\bar{\tau}_3$ und die $\bar{\tau}_\rho$-freien Terme nur in Form der Kombination $(1+\bar{\tau}_3)$ auftreten. Für die dritte Zeile von (117) wird dies, wie man sieht, gerade durch die Wahl (37) für $u_{\mathbf{k}}$ erreicht. Mit dieser ist aber, wie schon vor (38) erläutert wurde, auf grund der in (112) und (113) enthaltenen Bedingung (30) die $1/g$-Abhängigkeit von $v_{\mathbf{k}}$ notwendig verbunden, die ihrerseits die Erfüllung von (11) mit (9) für die zweite Zeile von (117) gewährleistet. Die dritte Zeile von (117) lautet dann mit (37) und (42)

$$H_3^{\mathrm{W}} = \frac{g}{2\pi}\sum_\rho \int \left((1+\bar{\tau}_3)S_\rho + \sum_{\rho'}^{\rho'\neq 3} \bar{\tau}_{\rho'} S_{\rho'\rho}\right) v(k) q'_{\rho\mathbf{k}}\,\mathrm{d}\mathbf{k}. \tag{119}$$

Die $(1+\bar{\tau}_3)$-Terme verschwinden nun in den $\bar{\tau}_3 = -1$ Eigenzuständen des Compoundnukleonoperators (44), (48) und können nur in den $\bar{\tau}_3 = +1$ Zuständen etwas liefern. Letztere rücken aber gemäß (44), (48) für $g \to \infty$ unendlich weit vom Grundzustand ab und können daher bei der auf endliche Anfangs- und Endenergieabstände beschränkten Bedingung der starken Kopplung (Gl. (11)) nur in den Zwischenzuständen der Reihe (9) eine Rolle spielen. Hier können sie dann aber nur in Verbindung mit Übergängen von den $\bar{\tau}_3 = -1$ Zuständen her vorkommen. Der aus (44), (48) ersichtliche Energiedifferenzanteil $2(g/2\pi)^2 b$ der $\bar{\tau}_3 = \pm 1$ Übergänge bewirkt aber durch sein Auftreten in den störungstheoretischen Nennern der Reihe (9) eine Verminderung der Ordnung in der Kopplungskonstanten um mindestens — 2 und damit die Erfüllung von (11) mit (9) für alle in H^{W} überhaupt vorkommenden $(1+\bar{\tau}_3)$-Terme wegen ihrer höchstens ersten Ordnung in g.

† Aus (112) und (113) folgt, daß die $u_{\substack{\mathbf{k}\mathbf{k}_0\\ \rho\rho_0}}$ und $v_{\substack{\mathbf{k}\mathbf{k}_0\\ \rho\rho_0}}$ den Operator p_ρ nicht enthalten können und außerdem von g unabhängig sein müssen, denn wäre z.B. $u_{\substack{\mathbf{k}\mathbf{k}_0\\ \rho\rho_0}}$ von g abhängig, so müßte $v_{\substack{\mathbf{k}\mathbf{k}_0\\ \rho\rho_0}}$ eine dazu entsprechend reziproke g-Abhängigkeit besitzen, um die g-Abhängigkeit der rechten Seiten der Gln. (112) und (113) erfüllen zu können. Dies würde aber dazu führen, daß entweder der Term mit $u^*_{\substack{\mathbf{k}\mathbf{k}_0\\ \rho\rho_0}}, u_{\substack{\mathbf{k}\mathbf{k}'_0\\ \rho\rho'_0}}$ oder der Term mit $v^*_{\substack{\mathbf{k}\mathbf{k}_0\\ \rho\rho_0}}, v_{\substack{\mathbf{k}\mathbf{k}'_0\\ \rho\rho'_0}}$ innerhalb des in $a_{\rho_0\mathbf{k}_0}, a^*_{\rho_0\mathbf{k}_0}$ quadratischen und bilinearen Anteiles von (117) für $g \to \infty$ beliebig anwachsen würde, sodaß der in $a_{\rho_0\mathbf{k}_0}, a^*_{\rho_0\mathbf{k}_0}$ quadratisch und bilineare Anteil der ersten Zeile von (117) im Grenzfall $g \to \infty$ nicht zum Verschwinden gebracht werden könnte.

Operatoren, die speziell nur diese Übergänge zwischen den $\bar{\tau}_3 = -1$ und $\bar{\tau}_3 = +1$ beschreiben, sind die $\bar{\tau}_\rho$ mit $\rho \neq 3$, und der letzte Term von (119) ist der damit behaftete H^{W}-Term. Die eben genannte Verminderung der Ordnung in der Kopplungskonstanten kann sich aber nur dann voll auswirken, wenn die H^{W}-Matrixelemente der Übergänge von $\bar{\tau}_3 = -1$ zu $\bar{\tau}_3 = +1$ kleiner als von erster Ordnung in g sind, wogegen der letzte Term von (119) zunächst verstößt. Er liefert zur störungstheoretischen Reihe (9) beim Übergang vom $\bar{\tau}_3 = -1$ in den $\bar{\tau}_3 = +1$ Zustand und zurück mit den g-proportionalen H^{W}-Matrixelementen im Zähler und dem $\bar{\tau}_3 = \pm 1$ Ernergiedifferenzanteil $2(g/2\pi)^2 b$ im Nenner für sich allein schon einen Beitrag der Ordnung g^0 und verstößt damit gegen (11).

Diesen g^0-Beitrag kann man jedoch mit dem g^0-Beitrag der bilinearen Terme der ersten Zeile von (117) zusammen durch die entsprechenden an die

$$u_{\substack{\mathbf{k}\mathbf{k}_0 \\ \rho\rho_0}} \text{ und } v_{\substack{\mathbf{k}\mathbf{k}_0 \\ \rho\rho_0}}$$

zu deren Bestimmung noch zu stellenden Bedingungen in eine für die Erfüllung der Bedingung der starken Kopplung geeignete Form bringen. Um dies durchführen zu können, üben wir die Transformation

$$U = \mathrm{e}^{-G}, \qquad \text{mit } G = -i\frac{2\pi}{bg}\sum_\rho \frac{\bar{\tau}_1 s_{2\rho} - \bar{\tau}_2 s_{1\rho}}{2}\int v(k) q'_{\rho\mathbf{k}}\,\mathrm{d}\mathbf{k} \tag{120}$$

aus, die angewandt auf die $\bar{\tau}_\rho$-Operatoren gemäß der Lieschen Reihe

$$U^{-1}\bar{\tau}_\rho U = \bar{\tau}_\rho + [G, \bar{\tau}_\rho] + \tfrac{1}{2}[G, [G, \bar{\tau}_\rho]] + \ldots \tag{121}$$

die Entwicklung nach der reziproken Kopplungskonstanten

$$\begin{aligned}
\bar{\tau}_3 \to \bar{\tau}_3 &- \left(\frac{2\pi}{g}\right)\frac{1}{b}\sum_{\rho'\rho}^{\rho' \neq 3} \bar{\tau}_{\rho'} s_{\rho'\rho}\int v(k) q'_{\rho\mathbf{k}}\,\mathrm{d}\mathbf{k} \\
&- \frac{\bar{\tau}_3}{2}\left(\frac{2\pi}{g}\right)^2 \sum_{\rho'}\Big(\sum_\rho (\delta_{\rho'\rho} - S_{\rho'} S_\rho)\int v(k) q'_{\rho\mathbf{k}}\,\mathrm{d}\mathbf{k}\Big)^2 \\
&+ \text{Terme von höherer Ordnung in } 1/g, \\
\bar{\tau}_1 \to \bar{\tau}_1 &+ \bar{\tau}_3 \frac{2\pi}{bg}\sum_\rho s_{1\rho}\int v(k) q'_{\rho\mathbf{k}}\,\mathrm{d}\mathbf{k} \\
&+ \text{Terme von höherer Ordnung in } 1/g, \\
\bar{\tau}_2 \to \bar{\tau}_2 &+ \bar{\tau}_3 \frac{2\pi}{bg}\sum_\rho s_{2\rho}\int v(k) q'_{\rho\mathbf{k}}\,\mathrm{d}\mathbf{k} \\
&+ \text{Terme von höherer Ordnung in } 1/g,
\end{aligned} \tag{122}$$

liefert. In Anwendung auf den nur $\bar{\tau}_3$ enthaltenden $H^{0\mathrm{C}}$-Anteil $H^{0\mathrm{C}}_{\bar{\tau}_3} = (g/2\pi)^2 b\bar{\tau}_3$

(siehe (44), (48)) ergibt sich daraus entsprechend

$$[G, H^{0C}_{\bar\tau_3}] = -\frac{g}{2\pi}\sum_{\rho',\rho}^{\rho'\neq 3}\bar\tau_{\rho'}s_{\rho'\rho}\int v(k)q'_{\rho\mathbf{k}}\,\mathrm{d}\mathbf{k}, \tag{123}$$

eine Kompensation des letzten Terms von (119) verbunden mit einem Hinzutreten von g^0-Termen und von Entwicklungstermen von negativer Ordnung in g.

Sämtliche dieser neu hinzukommenden g^0-Terme entstammen nur der Wirkung der Transformation U auf $H^{0C}_{\bar\tau_3}$ und H^W_3 als den Termen des Hamiltonoperators von der höchsten Ordnung in g, während U in ihrer Wirkung auf die übrigen Terme des Hamiltonoperators nur Terme von höchstens der Ordnung g^{-1} hinzutreten läßt, die somit die Bedingung der starken Kopplung (11) mit (9) ohnehin erfüllen. Letztere wird auch erfüllt von g^0-Termen mit $\bar\tau_\rho$ für $\rho\neq 3$, da sich bei diesen die Verminderung der Ordnung in g durch das Auftreten der $\bar\tau_3=\pm 1$ Energiedifferenz $2(g/2\pi)^2 b$ im störungstheoretischen Nenner bei der g^0-Abhängigkeit der Matrixelemente gemäß dem oben Gesagten nun voll auswirken kann.

Dann sind von den durch U hinzuerzeugten g^0-Termen nur noch die $\bar\tau_3$-Terme zu betrachten, die sich gemäß (120) bis (123) zu

$$\begin{aligned}\tfrac{1}{2}[G,[G,(H^{0C}_2)]]+[G,H^{W'}_3] &= \tfrac{1}{2}[G,H^{W'}_3]\\ &= \frac{\bar\tau_3}{2}\frac{1}{b}\sum_{\rho'}\left\{\sum_\rho(\delta_{\rho'\rho}-S_{\rho'}S_\rho)\int v(k)q'_{\rho\mathbf{k}}\,\mathrm{d}\mathbf{k}\right\}^2\end{aligned} \tag{124}$$

ergeben. Soll die rechte Seite von (124) zusammen mit den $\bar\tau_3$-freien g^0-Termen der ersten Zeile von (117) die Bedingung der starken Kopplung (11) mit (9) erfüllen, so kann dies ganz entsprechend den zu (119) gegebenen Erläuterungen ebenfalls nur innerhalb der Kombination $(1+\bar\tau_3)$ geschehen. Dann muß die erste Zeile von (117) der rechten Seite von (124) bis auf den Faktor $\bar\tau_3$ gleich sein, also

$$\tfrac{1}{2}\sum_\rho\int\{p'^*_{\rho\mathbf{k}}p'_{\rho\mathbf{k}}+\varepsilon^2 q'^*_{\rho\mathbf{k}}q'_{\rho\mathbf{k}}\}\mathrm{d}\mathbf{k}-H^{0f}=\frac{1}{2b}\sum_{\rho'}\left(\sum_\rho(\delta_{\rho'\rho}-S_{\rho'}S_\rho)\int v(k)q'_{\rho\mathbf{k}}\,\mathrm{d}\mathbf{k}\right)^2. \tag{125}$$

Die Forderung nach Erfüllung von (125) und damit von (11) mit (9) liefert nun gemäß (110 k) gerade die für die Bestimmung von v und u noch fehlenden Gleichungen, nämlich

$$\sum_\rho\int v_{\substack{\mathbf{kk}_0\\ \rho\rho_0}}v^*_{\substack{\mathbf{kk}'_0\\ \rho\rho'_0}}\mathrm{d}\mathbf{k}=\delta(\mathbf{k}_0-\mathbf{k}'_0)\delta_{\rho_0\rho'_0}, \tag{126}$$

$$\begin{aligned}\sum_\rho\int\varepsilon^2 u^*_{\substack{\mathbf{kk}_0\\ \rho\rho_0}}u_{\substack{\mathbf{kk}'_0\\ \rho\rho'_0}}\mathrm{d}\mathbf{k} &= \varepsilon_0{}^2\delta(\mathbf{k}_0-\mathbf{k}'_0)\delta_{\rho_0\rho'_0}\\ &\quad+\frac{1}{b}\sum_{\rho,\rho'}(\delta_{\rho\rho'}-S_\rho S_{\rho'})\int v(k)u^*_{\substack{\mathbf{kk}_0\\ \rho\rho_0}}\mathrm{d}\mathbf{k}\int v(k')\,u_{\substack{\mathbf{k}'\mathbf{k}'_0\\ \rho'\rho'_0}}\mathrm{d}\mathbf{k}'.\end{aligned} \tag{127}$$

Für die Terme mit $a^*_{\rho_0 \mathbf{k}_0}$, $a_{\rho'_0 \mathbf{k}'_0}$ in (125) ist dies entsprechend der Wirkungsweise der Gln. (126) und (127) gemäß (110 k) aus (125) unmittelbar ersichtlich, während man es den Termen mit $a^*_{\rho_0 \mathbf{k}_0}$, $a^*_{\rho'_0 - \mathbf{k}'_0}$ und $a_{\rho_0 - \mathbf{k}_0}$, $a_{\rho'_0 \mathbf{k}'_0}$ weniger leicht ansehen kann. Die dafür erforderlichen Beziehungen lassen sich aber, wie wir noch sehen werden, leicht aus den Gleichungen (126) und (127) ableiten, wenn man noch (112) bis (114) zu Hilfe nimmt. Den Beweis hierfür wollen wir nach Aufstellung des gesamten Gleichungssystems für die Transformationsfunktionen im Folgenden sogleich noch darlegen.

Das Ergebnis der vorstehenden Ausführungen ist also, daß (37), (38), (126) und (127) die im Anfang dieses Abschitts genannten weiteren Gleichungen für die

$$u_{\mathbf{k}},\ v_{\mathbf{k}},\ \underset{\rho\rho_0}{u_{\mathbf{k}\mathbf{k}_0}} \text{ und } \underset{\rho\rho_0}{v_{\mathbf{k}\mathbf{k}_0}}$$

sind, deren Hinzufügung zu (112) bis (116) notwendig und hinreichend ist, um die Bedingung der starken Kopplung (4) von Absatz 2.1.6 für den Ansatz (110) zu erfüllen.

2.3.2. *Gesamtes Integralgleichungssystem für die Transformationsfunktionen zur Befriedigung der Aufspaltungsbedingungen*

Das gesamte Integralgleichungssystem für die Transformationsfunktionen, das die Aufspaltungsbedingungen 1) bis 4) befriedigt, lautet damit

$$\text{a)}\quad \sum_{\rho} \int \underset{\rho\rho_0}{v_{\mathbf{k}\mathbf{k}_0}} \underset{\rho\rho'_0}{v^*_{\mathbf{k}\mathbf{k}'_0}} \mathrm{d}\mathbf{k} = \delta(\mathbf{k}_0 - \mathbf{k}'_0)\delta_{\rho_0\rho'_0},$$

$$\text{b)}\quad \sum_{\rho} \int \varepsilon^2 \underset{\rho\rho_0}{u^*_{\mathbf{k}\mathbf{k}_0}} \underset{\rho\rho'_0}{u_{\mathbf{k}\mathbf{k}'_0}} \mathrm{d}\mathbf{k} = \varepsilon_0{}^2 \delta(\mathbf{k}_0 - \mathbf{k}'_0)\delta_{\rho_0\rho'_0} + \frac{1}{b} \sum_{\rho',\rho} (\delta_{\rho'\rho} - S_{\rho'}S_{\rho}) \int v(k) \underset{\rho\rho_0}{u^*_{\mathbf{k}\mathbf{k}_0}} \mathrm{d}\mathbf{k} \int v(k') \underset{\rho'\rho'_0}{u_{\mathbf{k}'\mathbf{k}'_0}} \mathrm{d}\mathbf{k}',$$

$$\text{c)}\quad \sum_{\rho_0} \int \underset{\rho\rho_0}{v_{\mathbf{k}\mathbf{k}_0}} \underset{\rho'\rho_0}{u_{\mathbf{k}'\mathbf{k}_0}} \mathrm{d}\mathbf{k}_0 = \delta(\mathbf{k} - \mathbf{k}')\delta_{\rho\rho'} - \frac{1}{b} v^1(k) \frac{v(k')}{\varepsilon'^2} (\delta_{\rho\rho'} - S_{\rho}S_{\rho'}),$$

$$\text{d)}\quad \sum_{\rho} \int \underset{\rho\rho_0}{u_{\mathbf{k}\mathbf{k}_0}} \underset{\rho\rho'_0}{v_{\mathbf{k}\mathbf{k}'_0}} \mathrm{d}\mathbf{k} = \delta(\mathbf{k}_0 - \mathbf{k}'_0)\delta_{\rho_0\rho'_0},$$

$$\text{e)}\quad \sum_{\rho} \int \underset{\rho\rho_0}{u_{\mathbf{k}\mathbf{k}_0}} \underset{\rho\rho'_0}{v^*_{-\mathbf{k}\mathbf{k}'_0}} \mathrm{d}\mathbf{k} \propto \delta(k_0 - k'_0), \qquad (128)$$

$$\text{f)}\quad \sum_{\rho_0} \int \frac{1}{\varepsilon_0} \underset{\rho'\rho_0}{u^*_{-\mathbf{k}'\mathbf{k}_0}} \underset{\rho\rho_0}{u_{\mathbf{k}\mathbf{k}_0}} \mathrm{d}\mathbf{k}_0,$$

$$\text{g)}\quad \sum_{\rho_0} \int \varepsilon_0 \underset{\rho'\rho_0}{v^*_{-\mathbf{k}'\mathbf{k}_0}} \underset{\rho\rho_0}{v_{\mathbf{k}\mathbf{k}_0}} \mathrm{d}\mathbf{k}_0 \qquad \text{(reell)},$$

$$\text{h)}\quad \underset{\rho\rho_0}{u_{\mathbf{k}\mathbf{k}_0}} = \underset{\rho\ \rho_0}{u_{-\mathbf{k}-\mathbf{k}_0}},$$

$$\text{i)}\quad \underset{\rho\rho_0}{v_{\mathbf{k}\mathbf{k}_0}} = \underset{\rho\ \rho_0}{v_{-\mathbf{k}-\mathbf{k}_0}}.$$

Gln. (30) bzw. (40) oder (41) sind den Ausführungen von Absatz 2.2.3 entsprechend in (128 c und d) schon enthalten ebenso wie (92) und (93), die man gemäß (37) und (38) auch

$$\sum_{\rho}(\delta_{\rho'\rho}-S_{\rho'}S_{\rho})\int v^1(k)u_{\substack{\mathbf{kk}_0\\ \rho\rho_0}}\mathrm{d}\mathbf{k}=0, \tag{129}$$

$$\sum_{\rho}(\delta_{\rho'\rho}-S_{\rho'}S_{\rho})\int\frac{v(k)}{\varepsilon^2}v_{\substack{\mathbf{kk}_0\\ \rho\rho_0}}\mathrm{d}\mathbf{k}=0 \tag{130}$$

schreiben kann.

Die Beziehungen für die u und v die die Gültigkeit von (125) auch bezüglich der $a^*_{\rho_0\mathbf{k}_0}\,a^*_{\rho'_0-\mathbf{k}'_0}$ und $a_{\rho_0-\mathbf{k}_0}\,a_{\rho'_0\mathbf{k}'_0}$ Terme von (125) darlegen, bekommt man nun aus (128 a bis e) wie folgt:

Wenden wir die Operation

$$\sum_{\rho}\int v_{\substack{\mathbf{kk}'_0\\ \rho\rho'_0}}\ldots\mathrm{d}\mathbf{k}$$

auf das konjugiert Komplexe von (128 c) an, so erhalten wir unter Berücksichtigung von (128 a)

$$u^*_{\substack{\mathbf{kk}_0\\ \rho\rho_0}}=v_{\substack{\mathbf{kk}_0\\ \rho\rho_0}}-\frac{1}{b}\frac{v(k)}{\varepsilon^2}\sum_{\rho'}(\delta_{\rho\rho'}-S_{\rho}S_{\rho'})\int v^1(k')v_{\substack{\mathbf{k}'\mathbf{k}_0\\ \rho'\rho_0}}\mathrm{d}\mathbf{k}'. \tag{131}$$

Die Operation

$$\sum_{\rho'}\int v_{\substack{\mathbf{k}'\mathbf{k}'_0\\ \rho'\rho'_0}}\ldots\mathrm{d}\mathbf{k}'_0$$

auf (128 b) angewandt, ergibt ferner mit Rücksichtnahme auf (128 c)

$$\varepsilon^2 v_{\substack{\mathbf{kk}_0\\ \rho\rho_0}}=\varepsilon^2 u^*_{\substack{\mathbf{kk}_0\\ \rho\rho_0}}-\frac{1}{b}v(k)\sum_{\rho'}(\delta_{\rho\rho'}-S_{\rho}S_{\rho'})\int v(k')u^*_{\substack{\mathbf{k}'\mathbf{k}_0\\ \rho'\rho_0}}\mathrm{d}\mathbf{k}'. \tag{132}$$

Aus (131) wird weiterhin nach abermaliger Anwendung der Operation

$$\sum_{\rho}\int v_{\substack{\mathbf{kk}'_0\\ \rho\rho'_0}}\ldots\mathrm{d}\mathbf{k}$$

mit Benutzung von (130)

$$\sum_{\rho}\int v_{\substack{\mathbf{kk}'_0\\ \rho\rho'_0}}v_{\substack{\mathbf{kk}_0\\ \rho\rho_0}}\mathrm{d}\mathbf{k}=\sum_{\rho}\int v_{\substack{\mathbf{kk}'_0\\ \rho\rho'_0}}u^*_{\substack{\mathbf{kk}_0\\ \rho\rho_0}}\mathrm{d}\mathbf{k}. \tag{133}$$

Schließlich wenden wir auf (132) noch die Operation

$$\sum_{\rho}\int u^*_{\substack{\mathbf{kk}'_0\\ \rho\rho'_0}}\ldots\mathrm{d}\mathbf{k}$$

an und erhalten somit auf Grund von (129) und (133)

$$\sum_{\rho}\int \varepsilon^2 u^{*}_{\substack{\mathbf{k}\mathbf{k}_0\\ \rho\rho_0}} u^{*}_{\substack{\mathbf{k}\mathbf{k}'_0\\ \rho\rho'_0}}\,\mathrm{d}\mathbf{k} = {\varepsilon_0}^2 \sum_{\rho}\int v_{\substack{\mathbf{k}\mathbf{k}_0\\ \rho\rho_0}} v_{\substack{\mathbf{k}\mathbf{k}'_0\\ \rho\rho'_0}}\,\mathrm{d}\mathbf{k}$$

$$+\frac{1}{b}\sum_{\rho,\rho'}(\delta_{\rho\rho'}-S_\rho S_{\rho'})\int v(k)\,u^{*}_{\substack{\mathbf{k}\mathbf{k}_0\\ \rho\rho_0}}\mathrm{d}\mathbf{k}\int v(k')\,u^{*}_{\substack{\mathbf{k}'\mathbf{k}'_0\\ \rho'\rho'_0}}\mathrm{d}\mathbf{k}', \qquad (134)$$

welches gerade diejenige Beziehung ist, durch die die Terme mit $a^{*}_{\rho_0\mathbf{k}_0}\,a^{*}_{\rho'_0-\mathbf{k}'_0}$ zum Verschwinden gebracht werden, wenn man noch berücksichtigt, daß wegen (133) und (128 e)

$$\sum_{\rho}\int v_{\substack{\mathbf{k}\mathbf{k}_0\\ \rho\rho_0}} v_{\substack{\mathbf{k}\mathbf{k}'_0\\ \rho\rho'_0}}\,\mathrm{d}\mathbf{k} \propto \delta(k_0-k'_0). \qquad (135)$$

Das konjugiert Komplexe von (134) dient in entsprechender Weise dem Verschwinden der Terme mit $a_{\rho_0-\mathbf{k}_0}\,a_{\rho'_0\mathbf{k}'_0}$.

Damit ist der Beweis für die Erfüllung von (125) durch (126) und (127) bzw. (128 a und b) vollständig. Folgende Beziehungen sind noch wichtig:

Wenden wir die Operation

$$\sum_{\rho}^{\rho'\neq 3} s_{\rho'\rho}\int v(k)\ldots\mathrm{d}\mathbf{k}$$

und

$$\sum_{\rho}(\delta_{\rho'\rho}-S_{\rho'}S_\rho)\int v(k)\ldots\mathrm{d}\mathbf{k}$$

auf (131) an, so bekommen wir, wenn wir die Orthogonalitätsrelationen der S_ρ und $S_{\rho'\rho}$ (siehe (42) und (43)) und die Definition (39) von b berücksichtigen

$$\text{(a)}\ \sum_{\rho}^{\rho\neq 3} s_{\rho'\rho}\int v(k)\,u_{\substack{\mathbf{k}\mathbf{k}_0\\ \rho\rho_0}}\mathrm{d}\mathbf{k} = \sum_{\rho}^{\rho\neq 3} s_{\rho'\rho}\int (v(k)-v^1(k))\,v^{*}_{\substack{\mathbf{k}\mathbf{k}_0\\ \rho\rho_0}}\mathrm{d}\mathbf{k}, \qquad (136)$$

$$\text{(b)}\ \sum_{\rho}(\delta_{\rho'\rho}-S_{\rho'}S_\rho)\int v(k)\,u_{\substack{\mathbf{k}\mathbf{k}_0\\ \rho\rho_0}}\mathrm{d}\mathbf{k} = \sum_{\rho}(\delta_{\rho'\rho}-S_{\rho'}S_\rho)\int (v(k)-v^1(k))\,v^{*}_{\substack{\mathbf{k}\mathbf{k}_0\\ \rho\rho_0}}\mathrm{d}\mathbf{k},$$

und demnach

$$\sum_{\rho}^{\rho'\neq 3} s_{\rho'\rho}\int v(k)\,u_{\substack{\mathbf{k}\mathbf{k}_0\\ \rho\rho_0}}\mathrm{d}\mathbf{k}$$

$$= \sum_{\rho}(\delta_{\rho'\rho}-S_{\rho'}S_\rho)\int v(k)\,u_{\substack{\mathbf{k}\mathbf{k}_0\\ \rho\rho_0}}\mathrm{d}\mathbf{k} = 0 \qquad \text{für } v^1(k)=v(k). \qquad (137)$$

3.3. ZWISCHENFORMULIERUNG FÜR DEN NEU AUFGESPALTENEN HAMILTON-OPERATOR

Mit der Befriedigung der „Bedingung der starken Kopplung" 4) durch (37), (38) und (125) (letzteres auf Grund von (126), (127) und (128 a und b))

bekommt nun $H = H^{0f}+H^{0c}+\hat{H}^{W}$ ((14), (44), (117)) die Form

$$H = H^{0f}+\frac{1}{2b}\sum_{\rho'}\left(\sum(\delta_{\rho'\rho}-S_{\rho'}S_{\rho})\int v(k)q'_{\rho\mathbf{k}}\,\mathrm{d}\mathbf{k}\right)^2$$

$$+\frac{g}{2\pi}\sum_{\rho}(S_{\rho}+\sum_{\rho'}\bar{\tau}_{\rho'}s_{\rho'\rho})\int v(k)q'_{\rho\mathbf{k}}\,\mathrm{d}\mathbf{k}$$

$$+\frac{\sum_{\rho}\left\langle(p_{\rho}+A_{\rho})\int p'_{\rho\mathbf{k}}v^1(k)\mathrm{d}\mathbf{k}\right\rangle}{\frac{g}{2\pi}b+\sum_{\rho'}S_{\rho'}\int q'_{\rho\mathbf{k}'}v^1(k')\mathrm{d}\mathbf{k}'}$$

$$+\frac{\eta^2}{2}\frac{\sum_{\rho}(p_{\rho}+A_{\rho})^2}{\left(\frac{g}{2\pi}b+\sum_{\rho'}S_{\rho'}\int q'_{\rho\mathbf{k}}v^1(k')\mathrm{d}\mathbf{k}'\right)^2}+\left(\frac{g}{2\pi}\right)^2 b(\bar{\tau}_3+\tfrac{1}{2}),$$

in der es nur noch der τ-Transformation (122) bedarf, um die Erfüllung "der Bedingung der starken Kopplung" den Ausführungen von Abschnitt 3.1 entsprechend explizit in Erscheinung treten zu lassen. Die der τ-Transformation (122) entsprechende erzeugende Transformation U (siehe (120) und (122)) läßt, wie wir es in Abschnitt 3.1. gesehen haben, bei Anwendung auf den Hamiltonoperator außer der τ-Transformation sonst nur noch Terme in Hamiltonoperator hinzutreten, die eine Reihenentwicklung nach negativen Potenzen von g bilden und somit im Grenzfall $g \to \infty$ verschwinden. Für endliche g lassen sich diese Terme aus der Wirking von U auf den Hamiltonoperator (138) berechnen. Zuvor wollen wir jedoch im folgenden Teil die Lösungsmöglichkeiten des Gleichungssystems (128) näher diskutieren.

3.4. DIE LÖSUNGEN DES AUFSPALTUNGSPROBLEMS

2.4.1. *Herleitung der Lösungen*

Wie wir vorstehend gezeigt haben, ist nach Berücksichtigung von (37) und (38) das Gleichungssystem (128) hinreichend und notwendig, um die Aufspaltungsbedingungen (1) bis (4) für den Ansatz (110) zu befriedigen. Zur Diskussion seiner Lösungen läßt sich das Gleichungssystem (128) zunächst nach den u und v exakt auflösen. Dies geht aus dem System der beiden Integralgleichungen (131) und (121) hervor, die wir in der im Abschnitt 3.2 beschriebenen Weise aus dem Gleichungssystem (128) exakt abgeleitet hatten. Ihr Kern besteht jeweils aus einem Produkt, sodaß man sie durch Zurückführung auf ein lineares Gleichungssystem mit zwei Unbekannten exakt lösen kann.

Die Lösungen lauten

$$\left.\begin{aligned}
&\text{a)}\ v_{\substack{\mathbf{k}\mathbf{k}_0\\ \rho\rho_0}} = \delta(\mathbf{k}-\mathbf{k}_0)\delta_{\rho\rho_0}+\frac{1}{b}\,\frac{v(k)v_{0\mathbf{k}_0}}{\varepsilon^2-{\varepsilon_0}^2-i\alpha}\,(\delta_{\rho\rho_0}-S_\rho S_{\rho_0}),\\
&\text{b)}\ u_{\substack{\mathbf{k}\mathbf{k}_0\\ \rho\rho_0}} = \delta(\mathbf{k}-\mathbf{k}_0)\delta_{\rho\rho_0}+\frac{1}{b}\left[\frac{v(k)v^*_{0\mathbf{k}_0}}{\varepsilon^2-{\varepsilon_0}^2+i\alpha}-\frac{v(k)v'^*_{0\mathbf{k}_0}}{\varepsilon^2}\right](\delta_{\rho\rho_0}-S_\rho S_{\rho_0})\\
&\qquad = v^*_{\substack{\mathbf{k}\mathbf{k}_0\\ \rho\rho_0}}-\frac{1}{b}\,\frac{v(k)}{\varepsilon^2}\,v'^*_{0\mathbf{k}_0}(\delta_{\rho\rho_0}-S_\rho S_{\rho_0}),
\end{aligned}\right\}$$

worin

$$\left.\text{c)}\ v_{0\mathbf{k}_0} = \frac{v(k_0)}{1-A(k_0)}\right\}\quad(139)$$

und

$$\left.\begin{aligned}
&\text{d)}\ v'_{0\mathbf{k}_0} = \frac{v^1(k_0)(1-A(k_0))+v(k_0)B(k_0)}{1-A(k_0)}\\
&\qquad = v_{0\mathbf{k}_0}+\frac{v^1(k_0)((1-A(k_0))-v(k_0)(1-B(k_0))}{1-A(k_0)},
\end{aligned}\right\}$$

mit

$$\left.\text{e)}\ A(k_0)=\frac{1}{b}\int\frac{[v(k)]^2}{\varepsilon^2-{\varepsilon_0}^2-i\alpha}\,\mathrm{d}\mathbf{k},\quad B(k_0)=\frac{1}{b}\int\frac{v(k)v^1(k)}{\varepsilon^2-{\varepsilon_0}^2-i\alpha}\,\mathrm{d}\mathbf{k}.\right\}$$

Diese Lösungsausdrücke für die u und v sind aber gemäß (139) noch von der Fouriertransformierten $v(k)$ der Quellfunktion abhängig und hinzu kommt außerdem für u noch zusätzlich eine Abhängigkeit von der Funktion $v^1(k)$, wobei diese Abhängigkeiten recht kompliziert sind, wie man aus den Ausdrücken für $v_{0\mathbf{k}_0}$, $v'_{0\mathbf{k}_0}$, $A(k_0)$ und $B(k_0)$ erkennt.

Hinsichtlich $v^1(k)$ haben wir aber die schon im Absatz 2.1.5 besprochene Vieldeutigkeit und somit eine entsprechende Manigfaltigkeit für u, d.h. also auch für die gesamte Transformation. Im Spezialfall (46) ist gemäß (139 d und e) $v'_{0\mathbf{k}} = v_{0\mathbf{k}}$ und somit gemäß (139b)

$$u_{\substack{\mathbf{k}\mathbf{k}_0\\ \rho\rho_0}} = \frac{{\varepsilon_0}^2}{\varepsilon^2}\,v^*_{\substack{\mathbf{k}\mathbf{k}_0\\ \rho\rho_0}}. \tag{140}$$

Im Spezialfall (47) ist gemäß (139 d und e) $v'_{0\mathbf{k}_0} = 0$ und somit gemäß (139b)

$$u_{\substack{\mathbf{k}\mathbf{k}_0\\ \rho\rho_0}} = v^*_{\substack{\mathbf{k}\mathbf{k}_0\\ \rho\rho_0}}. \tag{141}$$

2.4.2 *Konsistenzbedingungen*

Wenden wir die Operation

$$\sum_{\rho'}(\delta_{\rho\rho'}-S_\rho S_{\rho'})\int\frac{v(k')}{\varepsilon'^2}\ldots\mathrm{d}\mathbf{k}'$$

auf (131) an, so erhalten wir bei Berücksichtigung von (130)

$$\sum_{\rho'}(\delta_{\rho\rho'}-S_\rho S_{\rho'})\int\frac{v(k')}{\varepsilon'^2}u^*_{\substack{\mathbf{k}'\mathbf{k}_0\\ \rho'\rho_0}}\mathrm{d}\mathbf{k}'=-\frac{W}{b}\sum_{\rho'}(\delta_{\rho\rho'}-S_\rho S_{\rho'})\int v^1(k')v_{\substack{\mathbf{k}'\mathbf{k}_0\\ \rho'\rho_0}}\mathrm{d}\mathbf{k}'. \quad (142)$$

Setzen wir dann (142) wiederum auf der rechten Seite von (131) ein, so können wir v vollständig durch u^* und $v(k)$ ausdrücken,

$$v_{\substack{\mathbf{k}\mathbf{k}_0\\ \rho\rho_0}}=u^*_{\substack{\mathbf{k}\mathbf{k}_0\\ \rho\rho_0}}-\frac{\dfrac{v(k)}{\varepsilon^2}}{W}\sum_{\rho'}(\delta_{\rho\rho'}-S_\rho S_\rho)\int\frac{v(k')}{\varepsilon'^2}u^*_{\substack{\mathbf{k}'\mathbf{k}_0\\ \rho'\rho_0}}\mathrm{d}\mathbf{k}'. \quad (143)$$

Bei Anwendung der Operation

$$\sum_{\rho_0}\int v^*_{\substack{\mathbf{k}'\mathbf{k}_0\\ \rho'\rho}}\ldots\mathrm{d}\mathbf{k}_0$$

auf (143) ergibt sich somit auf Grund von (128c)

$$\sum_{\rho_0}\int v^*_{\substack{\mathbf{k}'\mathbf{k}_0\\ \rho'\rho_0}}v_{\substack{\mathbf{k}\mathbf{k}_0\\ \rho\rho_0}}\mathrm{d}\mathbf{k}_0=\delta(\mathbf{k}'-\mathbf{k})\delta_{\rho'\rho}-\frac{\dfrac{v(k')}{\varepsilon'^2}\dfrac{v(k)}{\varepsilon^2}}{W}(\delta_{\rho\rho'}-S_\rho S_{\rho'}). \quad (144)$$

Weiterhin ergibt

$$\sum_{\rho_0}\int v^*_{\substack{\mathbf{k}'\mathbf{k}_0\\ \rho'\rho_0}}\ldots\mathrm{d}\mathbf{k}_0$$

auf (132) angewandt

$$\sum_{\rho'_0}\int v^*_{\substack{\mathbf{k}\mathbf{k}'_0\\ \rho\rho'_0}}\varepsilon_0'^2v_{\substack{\mathbf{k}'\mathbf{k}'_0\\ \rho'\rho'_0}}=\varepsilon^2\delta(\mathbf{k}-\mathbf{k}')\delta_{\rho\rho'}-\frac{1}{b}v(k)v(k')(\delta_{\rho\rho'}-S_\rho S_{\rho'}). \quad (145)$$

Gln. (144) und (145) folgen also notwendig aus dem Gleichungssystem (128). Während nun die Verifizierung von (128a, b) und (128 d-i) durch die Lösungsausdrücke (139) leicht nachgeprüft werden kann, ist dies bei (128c), (144) und (145) weniger einfach, da hier die Integration über den zweiten Index $\mathbf{k}_0$ geht, von dem die u und v gemäß (139 c-e) viel komplizierter abhängen als von dem ersten Index $\mathbf{k}$. Gln. (144) und (145) enthalten zudem nur v und $v(k)$ nicht aber u und $v^1(k)$. Die Größe v hängt aber gemäß (139a, c und e) selbst nur noch von $v(k)$ allein ab, sodaß (144) und (145) zunächst Integralgleichungen für die Fouriertransformierte $v(k)$ der Quellfunktion als eine Art Konsistenzbedingungen ergeben.

Dies sieht man schon beim Einsetzen von (139a) in (144) und (145). Dann wird die linke Seite von (144)

$$\sum_{\rho_0}\int v^*_{\substack{\mathbf{k}'\mathbf{k}_0\\ \rho'\rho_0}}v_{\substack{\mathbf{k}\mathbf{k}_0\\ \rho\rho_0}}\mathrm{d}\mathbf{k}_0=\delta(k-k')\delta_{\rho\rho'}+\frac{1}{b}\frac{v(k')v(k)}{\varepsilon'^2-\varepsilon^2+i\alpha}\left[\frac{v^*_{0\mathbf{k}}}{v(k)}-\frac{1}{b}\int\frac{|v_{0\mathbf{k}_0}|^2}{\varepsilon_0^2-\varepsilon^2+i\alpha}\mathrm{d}\mathbf{k}_0\right.$$
$$\left.-\left(\frac{v_{0\mathbf{k}'}}{v(k')}-\frac{1}{b}\int\frac{|v_{0\mathbf{k}_0}|^2}{\varepsilon_0-\varepsilon'^2-i\alpha}\mathrm{d}\mathbf{k}_0\right)\right](\delta_{\rho\rho'}-S_\rho S_{\rho'}), \quad (146)$$

und die linke Seite von (145)

$$\sum_{\rho'}\int v^{*}_{\mathbf{k}'\mathbf{k}_0\,\rho'\rho_0}\varepsilon_0{}^2 v_{\mathbf{k}\mathbf{k}_0\,\rho\rho_0}\,\mathrm{d}\mathbf{k}_0=\varepsilon^2\delta(\mathbf{k}'-\mathbf{k})\delta_{\rho'\rho}+\frac{1}{b}\,\frac{v(k')v(k)}{\varepsilon'^2-\varepsilon^2+i\alpha}$$
$$\times\left[\frac{v^{*}_{0\mathbf{k}}}{v(k)}\,\varepsilon^2-\frac{1}{b}\int\frac{|v_{0\mathbf{k}_0}|^2\varepsilon_0{}^2}{\varepsilon_0{}^2-\varepsilon^2+i\alpha}\,\mathrm{d}\mathbf{k}_0-\left(\frac{v_{0\mathbf{k}'}}{v(k')}\,\varepsilon'^2-\frac{1}{b}\int\frac{|v_{0\mathbf{k}_0}|^2\varepsilon_0{}^2}{\varepsilon_0{}^2-\varepsilon'^2-i\alpha}\,\mathrm{d}\mathbf{k}_0\right)\right]. \quad (147)$$

In den eckigen Klammern auf der rechten Seite von (146) und (147) steht jeweils die Differenz zwischen einer Funktion von k und ihrer konjugiert Komplexen aber von k'. Der Vergleich der rechten Seiten von (144) und (146) liefert dann

$$\int\frac{|v_{0\mathbf{k}_0}|^2}{\varepsilon_0{}^2-\varepsilon^2-i\alpha}\,\mathrm{d}\mathbf{k}_0=b\left(\frac{v_{0\mathbf{k}}}{v(k)}+\frac{1}{\varepsilon^2}\,\frac{b}{W}\right)+D, \quad (148)$$

und der rechten Seiten von (145) und (147)

$$\int\frac{|v_{0\mathbf{k}_0}|^2\varepsilon_0{}^2}{\varepsilon_0{}^2-\varepsilon^2-i\alpha}\,\mathrm{d}\mathbf{k}_0=b\varepsilon^2\left(\frac{v_{0\mathbf{k}}}{v(k)}-1\right)+\eta^2. \quad (149)$$

Hier sind D und η^2 noch hinzugefügte Konstanten, die sich bei der Differenzbildung auf den rechten Seiten von (146) und (147) herausheben. Das besagt aber nicht, daß hinsichtlich D und η^2 noch Freiheiten bestehen, denn bei der Herleitung von (148) und (149) aus (146) und (147) wurde der Zusammenhang (139c und e) von $v_{0\mathbf{k}}$ mit $v(k)$ noch nicht benutzt. Um dies nachzuholen, leiten wir aus (139a, c und e) die Beziehung

$$(\delta_{\rho_0\rho'_0}-S_{\rho_0}S_{\rho'_0})v^{*}_{0\mathbf{k}_0}=\sum_{\rho'}(\delta_{\rho_0\rho'}-S_{\rho_0}S_{\rho'})\int v(k')\,v^{*}_{\mathbf{k}'\mathbf{k}_0\,\rho'\rho_0}\,\mathrm{d}\mathbf{k}' \quad (150)$$

her und bilden ferner aus (139a)

$$\frac{v_{0\mathbf{k}_0}v(k)}{\varepsilon_0{}^2-\varepsilon^2+i\alpha}=b\left(\delta(\mathbf{k}_0-\mathbf{k})-\frac{\sum_{\rho'_0}(\delta_{\rho_0\rho'_0}-S_{\rho_0}S_{\rho'_0})v_{\mathbf{k}\mathbf{k}_0\,\rho\rho'_0}}{(\delta_{\rho\rho_0}-S_{\rho}S_{\rho_0})}\right). \quad (151)$$

Auf (151) wenden wir dann die Integraloperationen $\int\ldots v^{*}_{0\mathbf{k}_0}\mathrm{d}\mathbf{k}_0$ und $\int\ldots v^{*}_{0\mathbf{k}_0}\varepsilon_0{}^2\mathrm{d}\mathbf{k}_0$ an, wodurch sich

$$\int\frac{|v_{0\mathbf{k}_0}|^2}{\varepsilon_0-\varepsilon^2+i\alpha}\,\mathrm{d}\mathbf{k}_0=b\,\frac{v^{*}_{0\mathbf{k}}}{v(k)}-\frac{b}{v(k)}\,\frac{\sum_{\rho'_0}(\delta_{\rho_0\rho'_0}-S_{\rho_0}S_{\rho'_0})\int v_{\mathbf{k}\mathbf{k}_0\,\rho\rho'_0}v^{*}_{0\mathbf{k}_0}\,\mathrm{d}\mathbf{k}_0}{(\delta_{\rho\rho_0}-S_{\rho}S_{\rho_0})} \quad (152)$$

und

$$\int\frac{|v_{0\mathbf{k}_0}|^2\varepsilon_0{}^2}{\varepsilon_0{}^2-\varepsilon^2+i\alpha}\,\mathrm{d}\mathbf{k}_0=b\varepsilon^2\,\frac{v^{*}_{0\mathbf{k}}}{v(k)}-\frac{b}{v(k)}\,\frac{\sum_{\rho'_0}(\delta_{\rho_0\rho'_0}-S_{\rho_0}S_{\rho'_0})\int v_{\mathbf{k}\mathbf{k}_0\,\rho\rho'_0}v^{*}_{0\mathbf{k}_0}\varepsilon_0{}^2\mathrm{d}\mathbf{k}_0}{(\delta_{\rho\rho_0}-S_{\rho}S_{\rho_0})} \quad (153)$$

ergibt. Auf den rechten Seiten von (152) und (153) können wir nun (150) einsetzen und bekommen damit unter Verwendung von (144) und (145) die Gleichungen (148) und (149) mit

$$D = -b \tag{154}$$

und

$$\eta^2 = \int [v(k)]^2 \mathrm{d}\mathbf{k}. \tag{155}$$

Mit (154) können wir (148) dann

$$\int \frac{|v_{0\mathbf{k}_0}|^2}{\varepsilon_0{}^2 - \varepsilon^2 - i\alpha} \mathrm{d}\mathbf{k}_0 = b\left(\frac{v_{0\mathbf{k}}}{v(k)} - 1\right) + \frac{1}{\varepsilon^2}\frac{b^2}{W} \tag{156}$$

schreiben †. Mit der Umformung

$$\int \frac{|v_{0\mathbf{k}_0}|^2}{\varepsilon_0{}^2 - \varepsilon^2 - i\alpha} \mathrm{d}\mathbf{k}_0 = \frac{1}{\varepsilon^2}\left\{\int \frac{|v_{0\mathbf{k}_0}|^2 \varepsilon_0{}^2}{\varepsilon_0{}^2 - \varepsilon^2 - i\alpha} \mathrm{d}\mathbf{k}_0 - \int |v_{0\mathbf{k}_0}|^2 \mathrm{d}\mathbf{k}_0\right\} \tag{157}$$

können wir ferner (156) in die Form

$$\int \frac{|v_{0\mathbf{k}_0}|^2 \varepsilon_0{}^2}{\varepsilon_0{}^2 - \varepsilon^2 - i\alpha} \mathrm{d}\mathbf{k}_0 = b\,\varepsilon^2\left(\frac{v_{0\mathbf{k}}}{v(k)} - 1\right) + \int |v_{0\mathbf{k}_0}|^2 \mathrm{d}\mathbf{k}_0 + \frac{b^2}{W} \tag{158}$$

bringen und erhalten durch Vergleich mit (149) die weitere Beziehung

$$\int |v_{0\mathbf{k}_0}|^2 \mathrm{d}\mathbf{k}_0 = \eta^2 - \frac{b^2}{W}. \tag{159}$$

Außer diesen von (144) und (145) herrührenden Konsistenzbedingungen (156), (149) und (159), die nur $v(k)$ enthalten, erhält man aus (128c) noch eine solche, die auch $v^1(k)$ enthält. Sie ergibt sich durch Einsetzen von (128a und b) in die Differenz von (128c) und (144) zu

$$\int \frac{v^*_{0\mathbf{k}_0} v'_{0\mathbf{k}_0}}{\varepsilon_0{}^2 - \varepsilon^2 - i\alpha} \mathrm{d}\mathbf{k}_0 = \frac{b}{v(k)}\left\{v'_{0\mathbf{k}} - v^1(k) + \frac{b}{W}\frac{v(k)}{\varepsilon^2}\right\}. \tag{160}$$

Für (46) ist gemäß (139d und e) $v'_{0\mathbf{k}} = v_{0\mathbf{k}}$, sodaß sich (160) zu (156) und (128c) gemäß (140) zu (145) reduziert. Für (47) wird gemäß (139d und e) $v'_{0\mathbf{k}} = 0$, sodaß (160) auf beiden Seiten identisch Null wird und (128c) sich gemäß (141) zu (144) reduziert. Andere Fälle von $v^1(k)$ lassen sich nicht so leicht übersehen. Wir wollen auf sie hier nicht weiter eingehen.

† Die Interpretation von (156) als Grenzfall der Low-Gleichung für $g \to \infty$ haben wir in Ref. [21]) für die geladene skalare Theorie dargelegt.

2.4.3. *Beweis der Konsistenzbedingungen*

Der Beweis der Konsistenzbedingungen (156), (149) und (159) geht von der Beziehung

$$|v_{0k_0}|^2 = \frac{b}{i(2\pi)^2}\,\frac{v_{0k_0}-v^*_{0k_0}}{v(k_0)}\,\frac{1}{k_0} \tag{161}$$

aus, deren Gültigkeit sich durch direktes Ausrechnen aus (139c und e) bei Benutzung der Zerlegung

$$\frac{1}{\varepsilon''^2-\varepsilon^2\mp i\alpha} = \mathrm{P}\frac{1}{\varepsilon''^2-\varepsilon^2} \pm \frac{i\pi}{2\varepsilon}\,\delta(\varepsilon''-\varepsilon) \tag{162}$$

im Integralausdruck $A(k_0)$ von (139e) ergibt. Die damit aus (156), (149) und (159) entstehenden Ausdrücke

$$\frac{1}{2\pi i}\int_{\kappa^2}^{\infty}\frac{v_{0k_0}-v^*_{0k_0}}{bv(k_0)}\,\frac{\mathrm{d}\varepsilon_0{}^2}{\varepsilon_0{}^2-\varepsilon^2-i\alpha} = \frac{1}{b}\,\frac{v_{0k_0}}{v(k_0)} - \frac{1}{b} + \frac{1}{\varepsilon^2 W}, \tag{163}$$

$$\frac{1}{2\pi i}\int_{\kappa^2}^{\infty}\frac{v_{0k_0}-v^*_{0k_0}}{bv(k_0)}\,\frac{\varepsilon_0{}^2\mathrm{d}\varepsilon_0{}^2}{\varepsilon_0{}^2-\varepsilon^2-i\alpha} = \varepsilon^2\left(\frac{1v_{0k}}{bv(k)} - \frac{1}{b}\right) + \frac{\eta^2}{b^2}, \tag{164}$$

$$\frac{1}{2\pi i}\int_{\kappa^2}^{\infty}\frac{v_{0k_0}-v^*_{0k_0}}{bv(k_0)}\,\mathrm{d}\varepsilon_0{}^2 = \frac{1}{W} + \frac{\eta^2}{b^2}. \tag{165}$$

legen eine Verifizierung durch analytische Fortsetzung in die komplexe $\varepsilon_0{}^2$-Ebene nahe. Den analytischen Eigenschaften der Funktion $(1/b)(v_{0k_0}/v(k))$ entsprechend, die man gemäß (139c und e) auch in der Form

$$\frac{1}{b}\,\frac{v_{0k_0}}{v(k_0)} = \frac{1}{-\varepsilon_0{}^2\displaystyle\int\frac{[v(k')]^2}{\varepsilon'^2(\varepsilon'^2-\varepsilon_0{}^2-i\alpha)}\,\mathrm{d}\mathbf{k}'} \tag{166}$$

mit der auf Grund von (162) durchführbaren Zerlegung

$$\int\frac{[v(k')]^2}{\varepsilon'^2(\varepsilon'^2-\varepsilon_0{}^2-i\alpha)}\,\mathrm{d}\mathbf{k}' = \mathrm{P}\int\frac{[v(k')]^2}{\varepsilon'^2(\varepsilon'^2-\varepsilon_0{}^2)}\,\mathrm{d}\mathbf{k}' + i2\pi^2\,\frac{k_0[v(k_0)]^2}{\varepsilon_0{}^2}. \tag{167}$$

schreiben kann, haben wir wegen des Faktors $k_0 = \sqrt{\varepsilon_0{}^2-\kappa^2}$ im Imaginärteil dann einen Verzweigungspunkt bei $k_0 = 0$ bzw. $\varepsilon_0{}^2 = \kappa^2$. Legen wir dementsprechend einen Schnitt längs der positiven Achse von $\varepsilon_0{}^2 = \kappa^2$ bis $\varepsilon_0{}^2 = \infty$, so können wir die Integrale der linken Seiten von (163), (164) und (165) als Integrale längs der Ränder dieses Schnittes und zwar von ∞ bis κ^1 auf dem unteren und von κ^2 bis ∞ auf dem oberen Rand ausführen und zur Erlangung eines geschlossenen Integrationsweges C die Integration auf dem unendlichen

Kreis C_0 hinzuzählen und wieder subtrahieren. Das gibt für die linken Seiten von (163), (164) und (165):

$$\int_{\kappa^2}^{\infty} \frac{v_{0\mathbf{k}_0}-v^*_{0\mathbf{k}_0}}{bv(k_0)} \frac{\mathrm{d}\varepsilon_0^2}{\varepsilon_0^2-\varepsilon^2-i\alpha} = \underbrace{\int_C \frac{1v_{0\mathbf{k}_0}}{bv(k_0)} \frac{\mathrm{d}\varepsilon_0^2}{\varepsilon_0^2-\varepsilon^2-i\alpha}}_{2\pi i\left(\underbrace{\frac{1}{b}\frac{v_{0\mathbf{k}}}{v(k)}}_{\substack{\text{Residuum}\\ \text{bei } \varepsilon_0^2=\varepsilon^2}} + \underbrace{\frac{1}{\varepsilon^2}\frac{1}{W}}_{\substack{\text{Residuum}\\ \text{bei } \varepsilon_0^2=0}}\right)} - \underbrace{\int_{C_0} \frac{1v_{0\mathbf{k}_0}}{bv(k_0)} \frac{\mathrm{d}\varepsilon_0^2}{\varepsilon_0^2-\varepsilon^2-i\alpha}}_{\oint \frac{\mathrm{d}\varepsilon_0^2}{\varepsilon_0^2}=\frac{2\pi i}{b}}, \quad \frac{1}{b}\frac{v_{0\mathbf{k}_0}}{v(k_0)} \to \frac{1}{b} \text{ für } \varepsilon_0 \to \infty \tag{168}$$

$$\int_{\kappa^2}^{\infty} \frac{v_{0\mathbf{k}_0}-v^*_{0\mathbf{k}_0}}{bv(k_0)} \frac{\varepsilon_0^2\mathrm{d}\varepsilon_0^2}{\varepsilon_0^2-\varepsilon^2-i\alpha} = \underbrace{\int_C \frac{1v_{0\mathbf{k}_0}}{bv(k_0)} \frac{\varepsilon_0^2\mathrm{d}\varepsilon_0^2}{\varepsilon_0^2-\varepsilon^2-i\alpha}}_{2\pi i\ \underbrace{\varepsilon^2\frac{1}{b}\frac{v_{0\mathbf{k}}}{v(k)}}_{\substack{\text{Residuum}\\ \text{bei } \varepsilon_0=\varepsilon}}} - \underbrace{\int_{C_0} \frac{1v_{0\mathbf{k}_0}}{bv(k_0)} \frac{\varepsilon_0^2\mathrm{d}\varepsilon_0^2}{\varepsilon_0^2-\varepsilon^2-i\alpha}}_{\oint\left\{\frac{1}{b}+\frac{1}{\varepsilon_0^2}\left(\frac{\varepsilon^2}{b}-\frac{\eta^2}{b^2}\right)\right\}\mathrm{d}\varepsilon_0^2=2\pi i\left(\frac{\varepsilon^2}{b}-\frac{\eta^2}{b^2}\right)}, \tag{169}$$

und

$$\frac{1}{b^2}\int |v_{0\mathbf{k}_0}|^2\mathrm{d}\mathbf{k}_0 = \frac{1}{2\pi i}\int_{\kappa^2}^{\infty} \frac{v_{0\mathbf{k}_0}-v^*_{0\mathbf{k}_0}}{bv(k_0)}\mathrm{d}\varepsilon_0^2 = \underbrace{\frac{1}{2\pi i}\int_C \frac{v_{0\mathbf{k}_0}}{bv(k_0)}\mathrm{d}\varepsilon_0^2}_{-\frac{1}{W}} - \underbrace{\frac{1}{2\pi i}\int_{C_0} \frac{v_{0\mathbf{k}_0}}{bv(k_0)}\mathrm{d}\varepsilon_0^2}_{-\frac{\eta^2}{b^2}} = -\frac{1}{W}+\frac{\eta^2}{b^2}. \tag{170}$$

Die Ausführung der Integrationen auf den rechten Seiten wird durch Angabe der Werte für die zugehörigen aus (139c und e) und (166) folgenden Residuen unter den Integralen erklärt. Die Verifizierungen der rechten Seiten von (163), (164) und (165) sind daraus unmittelbar ersichtlich. Das vielleicht etwas schwerer erkennbare Zustandekommen der Residuen der Integration im Unendlichen bei (169) und (170) ergibt sich durch Entwicklung von $\varepsilon_0^2/(\varepsilon_0^2-\varepsilon^2)$ und von (139c) mit (139e) nach $1/\varepsilon_0^2$ mit der Bezeichnung (155) gemäß

$$\frac{1}{b}\frac{v_{0\mathbf{k}_0}}{v(k_0)} = \frac{1}{b+\frac{1}{\varepsilon_0^2}\int \frac{[v(k')]^2}{1-\frac{\varepsilon'^2}{\varepsilon_0^2}+i\alpha}\mathrm{d}\mathbf{k}'} \xrightarrow{\text{für } \varepsilon_0^2\to\infty} \frac{1}{b}-\frac{1}{\varepsilon_0^2}\frac{\eta^2}{b^2}+\ldots. \tag{171}$$

Im Grenzfall der Punktquelle bleibt (168) d.h. also (163) gültig entsprechend dem endlichen Grenzwert

$$\frac{1}{b}\frac{v_{0\mathbf{k}_0}}{v(k_0)} \to \frac{-1}{2\pi^2(\kappa+ik_0)} \quad \text{(im Grenzfall der Punktquelle)}, \tag{172}$$

wobei der Beitrag der Integration im Unendlichen, d.h. also der zweite Term auf der rechten Seite von (163) mit $1/b \to 0$ gemäß (39) verschwindet. Die Gültigkeit von (168) bzw. (163) kann man natürlich auch mit dem Grenzausdruck (172) selbst direkt beweisen, wobei das Verschwinden des Beitrages der Integration im Unendlichen aus dem $1/\varepsilon_0$-Verhalten des Grenzausdruckes (172) im Unendlichen direkt ersichtlich wird.

Bei (164) bzw. (169) und (165) bzw. (170) ist der Übergang zur Punktquelle zunächst nicht so ohne weiteres möglich, da der letzte Term von (164) bzw. (169) und (165) bzw. (170) dann linear divergiert. Dem entspricht, daß die zur Herleitung von (164) gemäß (169) dienende Entwicklung (171) nach $1/\varepsilon_0^2$ nur gilt, wenn der cut off klein gegen ε_0 bleibt. Man kann daraus die Vorschrift entnehmen, daß der Übergang zur Punktquelle bei solchen Beziehungen wie (164), (169), (165), (170) erst vorzunehmen ist, wenn ins Unendliche reichende Integrationen der Art, wie wir sie auf den linken Seiten von (149), (164), (159), (165) haben, vorher schon ausgeführt sind. Dann kann man (149) bzw. (164) und (159) bzw. (165) auch im Grenzfall der Punktquelle einen Sinn verleihen, indem man sie durch den im Grenzfall der Punktquelle divergierenden letzten Term dividiert. Setzt man somit abkürzungshalber

$$v^{\mathrm{r}}_{0\mathbf{k}_0} = \frac{b}{\eta^2}\, v_{0\mathbf{k}_0}, \tag{173}$$

so wird aus (149) bzw. (164) und aus (159) bzw. (165)

$$\int \frac{\eta^2}{b^2}\,\frac{|v^{\mathrm{r}}_{0\mathbf{k}_0}|^2\varepsilon_0^{\,2}}{\varepsilon_0^{\,2}-\varepsilon^2-i\alpha}\,\mathrm{d}\mathbf{k}_0 = \varepsilon^2\left(\frac{v^{\mathrm{r}}_{0\mathbf{k}_0}}{v(k_0)} - \frac{b}{\eta^2}\right) + 1 \tag{174}$$

und

$$\frac{1}{2\pi i}\int_{\kappa^2}^{\infty} \frac{v^{\mathrm{r}}_{0\mathbf{k}_0} - v^{\mathrm{r}*}_{0\mathbf{k}_0}}{v(k_0)}\,\frac{\varepsilon_0^{\,2}\,\mathrm{d}\varepsilon_0^{\,2}}{\varepsilon_0^{\,2}-\varepsilon^2-i\alpha} = \varepsilon^2\left(\frac{v^{\mathrm{r}}_{0\mathbf{k}_0}}{v(k_0)} - \frac{b}{\eta^2}\right) + 1, \tag{175}$$

bzw.

$$\int \frac{\eta^2}{b^2}\,|v_{0\mathbf{k}_0}|^2\,\mathrm{d}\mathbf{k}_0 = -\,\frac{1}{\displaystyle\int \frac{[v(k')]^4}{\varepsilon'^4}\,\mathrm{d}\mathbf{k}'}\,\frac{b}{\eta^2} + 1 \tag{176}$$

und

$$\frac{1}{2\pi i}\int_{\kappa^2}^{\infty} \frac{v^{\mathrm{r}}_{0\mathbf{k}_0} - v^{\mathrm{r}*}_{0\mathbf{k}_0}}{v(k_0)}\,\mathrm{d}\varepsilon_0^{\,2} = -\,\frac{1}{\displaystyle\int \frac{[v(k')]^4}{\varepsilon'^4}\,\mathrm{d}\mathbf{k}'}\,\frac{b}{\eta^2} + 1, \tag{177}$$

die gemäß dem eben Gesagten auch im Grenzfall der Punktquelle gelten, wenn man die Integrationen auf den linken Seiten vor diesem Grenzübergang ausführt. Andernfalls ergäbe sich ein Widerspruch, da gemäß (39), (155) und

(166) $v^{\mathrm{r}}_{0\mathbf{k}_0} \to 0$ beim Übergang zur Punktquelle, während auf den rechten Seiten von (174) bis (177) die 1 übrigbleibt. Solche Integrationen wie auf den linken Seiten von (149), (164), (159) und (177) können wie (160) zeigt, vor allem beim Spezialfall $v^1(k) = v(k)$ auftreten, wobei wir dann diese Vorschrift der Ausführungen der Integrationen vor dem Grenzübergang zur Punktquelle notwendig beachten müssen, falls wir diesen Grenzübergang ausführen wollen.

2.4.4. *Einsetzen einer speziellen Quellfunktion*

Nachdem wir somit durch den vorstehenden Beweis gezeigt haben, daß die Konsistenzbedingungen (156), (149) und (159) keine Einschränkung für die Quellfunktion bedeuten, wollen wir nun noch für die spezielle, verhältnismäßig leicht zu handhabende Wahl

$$v(k) = \frac{1}{1+\dfrac{k^2}{K^2}} \tag{178}$$

die Ausdrücke $v_{0\mathbf{k}_0}$ und $|v_{0\mathbf{k}_0}|^2$ angeben. Die Quellfunktion (178) erfüllt die Normierungsforderung (5) und fällt oberhalb des Abschneideimpulses K wie $1/k^2$ ab. Für $K \to \infty$ bekommen wir $v(k) = \text{const.} = 1$, d.h. im Ortsraum den Übergang zur δ-Funktion. Bei numerischen Rechnungen wird man K mindestens etwa von der Größenordnung der Comptonwellenlänge des Nukleons wählen. Die zugehörige Quellfunktion im Ortsraum ist

$$K(\mathbf{r}) = \frac{K^2}{4\pi}\frac{\mathrm{e}^{-Kr}}{r}, \tag{179}$$

deren räumliche Ausdehnung durch K^{-1} gegeben ist.

Mit dieser Wahl (178) für die Fouriertransformierte $v(k)$ der Quellfunktion lassen sich die für die Berechnung von $v_{0\mathbf{k}_0}$ gemäß (139c und e) erforderlichen Integrale b (39) und

$$\int \frac{[v(k'')]^2}{k''^2-k^2-i\alpha}\,\mathrm{d}\mathbf{k}''$$

sowie außerdem auch η^2 (155) exakt ausführen, und man erhält bei Beachtung der (162) entsprechenden Zerlegung

$$\begin{gathered}\eta^2 = \pi^2 K^3, \quad b = \pi^2 K \frac{1+\dfrac{\kappa^2}{K^2}-2\dfrac{\kappa}{K}}{\left(1-\dfrac{\kappa^2}{K^2}\right)^2}, \quad \mathrm{P}\int \frac{[v(k'')]^2}{k''^2-k^2}\,\mathrm{d}\mathbf{k}'' = \pi^2 K \frac{1-\dfrac{k^2}{K^2}}{\left(1+\dfrac{k^2}{K^2}\right)^2}, \\ b - \mathrm{P}\int \frac{[v(k'')]^2}{k''^2-k^2}\,\mathrm{d}\mathbf{k}'' = (2\pi^2)\left\{\frac{e^2}{2K}\frac{3-\dfrac{\kappa^2}{K^2}+\left(1+\dfrac{\kappa^2}{K^2}\right)\dfrac{k^2}{K^2}}{\left(1-\dfrac{\kappa^2}{K^2}\right)^2\left(1+\dfrac{k^2}{K^2}\right)^2} - \frac{\kappa}{\left(1-\dfrac{\kappa^2}{K^2}\right)^2}\right\}\end{gathered} \tag{180}$$

und somit gemäß (139c und e)

$$\frac{1}{b}\frac{v_{0\mathbf{k}}}{v(k)} = -\frac{v(k)}{2\pi^2\left\{\kappa[v(i\kappa)]^2+ik[v(k)]^2-\frac{\varepsilon^2}{2K}\left[3-\frac{\kappa^2}{K^2}+\left(1+\frac{\kappa^2}{K^2}\right)\frac{k^2}{K^2}\right][v(i\kappa)]^2[v(k)]^2\right\}}, \quad (181)$$

mit den bei (168), (169) und (170) angezeigten Grenzwerten für $\varepsilon \to \infty$ und (172) für den Fall der Punktquelle.

Daraus kann man bei Vernachlässigung von Termen der Größenordnung κ^2/K^2 gegen Terme der Größenordnung 1 einen genäherten Ausdruck für $|v_{0\mathbf{k}}|^2$ bekommen, der einigermassen leicht zu übersehen ist, und für den die bei späteren Rechnungen auszuführenden Integrationen noch einigermaßen durchführbar sind. Er lautet

$$\text{a)}\ |v_{0\mathbf{k}}|^2 = \frac{b^2\left(1-\frac{\kappa^2}{K^2}\right)^4}{(2\pi^2)^2\left(1-\frac{3}{2}\frac{\kappa}{K}\right)^2\left(1+\frac{k^2}{K'^2}\right)\varepsilon^2}, \quad \text{b)}\ K' = \frac{1-\frac{3}{2}\frac{\kappa}{K}}{\left(1-\frac{\kappa}{K}\right)^2}2K. \quad (182)$$

2.5. HAMILTONOPERATOR MIT FÜR $g \to \infty$ VERSCHWINDENDER WECHSELWIRKUNG ZWISCHEN FREIEM FELD UND COMPOUNDNUKLEON

Um einen neu aufgespaltenen Hamiltonoperator mit einem Wechselwirkungsterm zwischen freiem Feldanteil und Compoundnukleonanteil zu bekommen, der die Bedingung der starken Kopplung (4) explizit erfüllt, bedarf es gemäß den Ausführungen von Absatz (2.3.3) nur noch der Anwendung der Transformation U (120) auf den Ausdruck (138). Entsprechend der schon besprochenen, durch die Vieldeutigkeit von $v^1(k)$ hervorgerufenen, Vieldeutigkeit des gesamten Problems haben wir hier auch eine Vieldeutigkeit für die Transformation U und wollen uns wiederum auf die Fälle (46) und (47) beschränken. Im Fall (46) wird gemäß (120) und (138) $U = 1$ und es verschwinden gemäß (138) und (110 κ a) in der ersten Zeile von (138) der zweite Term und die $\rho' \neq 3$ Glieder im dritten Term, so daß man bekommt

$$[H^{\mathrm{W}}]_{v^1(k)=v(k)} = \frac{g}{2\pi}(1+\bar{\tau}_3)\sum_{\rho} S_\rho \int v(k) q'_{\rho\mathbf{k}}\,\mathrm{d}\mathbf{k}$$
$$+\frac{\sum_{\rho}\langle(p_\rho+A_\rho)\int v(k)p'_{\rho\mathbf{k}}\,\mathrm{d}\mathbf{k}\rangle}{\frac{g}{2\pi}b+\sum_{\rho'}S_{\rho'}\int v(k)\,q'_{\rho\mathbf{k}}\,\mathrm{d}\mathbf{k}}+\frac{\eta^2}{2}\left[\frac{\sum_{\rho}(p_\rho+A_\rho)^2}{\left(\frac{g}{2\pi}b+\sum_{\rho'}S_{\rho'}\int v(k)\,q'_{\rho\mathbf{k}}\,\mathrm{d}\mathbf{k}\right)^2}-\left(\frac{2\pi}{gb}\right)^2\sum_{\rho}p_\rho{}^2\right] \quad (183)$$

mit den Ausdrücken (14) und (44) für $H^{0\mathrm{f}}$ und $H^{0\mathrm{C}}$, wobei (155) an Stelle von (45).

Im Fall (47) verschwindet gemäß (110 κ, b) und (130) der erste Term der ersten Zeile von (138), der in $\dot{p}_\rho$ und $\dot{p}'_{\rho\mathbf{k}}$ linear ist. Dafür kommt aber die Transformation U (120) voll zur Geltung. Wir können dann aber im Unterschied zum Fall (46) und zum Fall (47) der geladenen skalaren Theorie (siehe Ref. [21])) keinen geschlossenen Ausdruck für H^{W} mehr anschreiben, sondern wollen ihn nur bis zu den Entwicklungstermen der Ordnung g^{-2} der Lie-schen Reihe angeben,

$$
\begin{aligned}
[H^{\mathrm{W}}]_{v^1(k)=\frac{b}{W}\frac{v(k)}{\varepsilon^2}} &= \frac{g}{2\pi}(1+\bar{\tau}_3)\sum_\rho S_\rho \int v(k) q'_{\rho\mathbf{k}}\,\mathrm{d}\mathbf{k} \\
&+ \frac{(1+\bar{\tau}_3)}{2b}\sum_{\rho'}\left(\sum_\rho (\delta_{\rho'\rho}-S_{\rho'}S_\rho)\int v(k) q'_{\rho\mathbf{k}}\,\mathrm{d}\mathbf{k}\right)^2 \\
&- \frac{1}{b}\sum_{\rho'\rho}^{\rho'\neq 3}\bar{\tau}_{\rho' S_{\rho'\rho}}\int v(k) q'_{\rho\mathbf{k}}\,\mathrm{d}\mathbf{k}\sum_\rho S_\rho\int v(k) q'_{\rho\mathbf{k}}\,\mathrm{d}\mathbf{k} \\
&- \frac{2\pi}{g}\left[\sum_\rho \frac{\bar{\tau}_1 S_{2\rho}-\bar{\tau}_2 S_{1\rho}}{2b}\int v(k)\dot{p}'_{\rho\mathbf{k}}\,\mathrm{d}\mathbf{k}\right. \qquad (184) \\
&\left.+ \frac{1}{2b^2}\sum_{\rho'}\left(\sum_\rho (\delta_{\rho'\rho}-S_{\rho'}S_\rho)\int v(k) q'_{\rho\mathbf{k}}\,\mathrm{d}\mathbf{k}\right)^2 \sum_{\rho',\rho}\bar{\tau}_{\rho' S_{\rho'\rho}}\int v(k) q'_{\rho\mathbf{k}}\,\mathrm{d}\mathbf{k}\right] \\
&+ \left(\frac{2\pi}{g}\right)^2\left[\frac{-\bar{\tau}_3}{4b^3}\left(\sum_\rho\left(\sum_{\rho'}(\delta_{\rho\rho'}-S_\rho S_{\rho'})\int v(k) q'_{\rho'\mathbf{k}}\,\mathrm{d}\mathbf{k}\right)^2\right)^2\right. \\
&\left.+ \frac{1}{2W}\sum_\rho\left\{\left(\frac{\dot{p}_\rho+A_\rho}{1+\dfrac{2\pi}{g\displaystyle\int\left(\frac{v(k')}{\varepsilon'^2}\right)^2\mathrm{d}\mathbf{k}'}\displaystyle\sum_{\rho'}S_{\rho'}\int\frac{v(k')}{\varepsilon^2}q'_{\rho\mathbf{k}}\,\mathrm{d}\mathbf{k}}\right)^2-\dot{p}_\rho{}^2\right\}\right]
\end{aligned}
$$

mit den Operatoren (14) und (48) für $H^{0\mathrm{f}}$ und $H^{0\mathrm{C}}$.

Denkt man sich in (183) und (184) nun noch für die $q'_{\rho\mathbf{k}}$ und $\dot{p}'_{\rho\mathbf{k}}$ die Ausdrücke (110 κ a, b) mit (139a), (140) bzw. (141) eingesetzt, so hat man H^{W} völlig durch die Operatoren $a^*_{\rho_0\mathbf{k}_0}$, $a_{\rho_0\mathbf{k}_0}$, S_ρ und $\dot{p}_\rho$ ausgedrückt, die in dem schon in Gl. (10) eingeführten, aus den Eigenzuständen θ_n von $H^{0\mathrm{f}}+H^{0\mathrm{C}}$ gebildeten Orthogonalsystem der starken Kopplung als Erzeugungs- und Vernichtungsoperatoren oder Operatoren mit Diagonalform wirken. Dafür sind dann die Beziehungen (150) und

$$
\sum_\rho S_\rho\int v(k) u_{\substack{\mathbf{k}\mathbf{k}_0\\ \rho\rho_0}}\,\mathrm{d}\mathbf{k} = S_{\rho_0} v(k_0) \qquad (185)
$$

wichtig, wobei (185) sich auf Grund der Orthogonalität von S_ρ und $(\delta_{\rho\rho'}-S_\rho S_{\rho'})$

aus (139b) ergibt. Der Ausdruck für A_ρ ergibt sich mit (110 λ), (110 κ a, b), (139a), (140) bzw. (141) im Fall (46) bei (183) zu

$$\begin{aligned} A_\rho = \frac{i}{2} \sum_{\rho_0, \sigma_0} \iint \Big\{ & \frac{1/b}{\varepsilon_0 - \varepsilon'_0 + i\alpha} \Big[\Big(\frac{\varepsilon'_0}{\varepsilon_0^3}\Big)^{\frac{1}{2}} v(k_0) v^*_{0\mathbf{k}'_0} S_{\rho_0} (\delta_{\rho\sigma_0} - S_\rho S_{\sigma_0}) \\ & + \Big(\frac{\varepsilon_0}{\varepsilon_0^3}\Big)^{\frac{1}{2}} v(k'_0) v_{0\mathbf{k}_0} (\delta_{\rho\rho_0} - S_\rho S_{\rho_0}) S_{\sigma_0} \Big] a^*_{\rho_0\mathbf{k}_0} a_{\sigma_0\mathbf{k}'_0} \\ & - \frac{1/b}{2(\varepsilon_0 + \varepsilon'_0)} \Big[\Big(\frac{\varepsilon'_0}{\varepsilon_0^3}\Big)^{\frac{1}{2}} v(k_0) v^*_{0\mathbf{k}'_0} S_{\rho_0} (\delta_{\rho\sigma_0} - S_\rho S_{\sigma_0}) \\ & + \Big(\frac{\varepsilon_0}{\varepsilon_0'^3}\Big)^{\frac{1}{2}} v(k'_0) v^*_{0\mathbf{k}_0} S_{\sigma_0} (\delta_{\rho\rho_0} - S_\rho S_{\rho_0}) \Big] a_{\rho_0\mathbf{k}_0} a_{\sigma_0\mathbf{k}'_0} \\ & - \frac{1/b}{2(\varepsilon_0 + \varepsilon'_0)} \Big[\Big(\frac{\varepsilon'_0}{\varepsilon_0^3}\Big)^{\frac{1}{2}} v(k_0) v_{0\mathbf{k}'_0} S_{\rho_0} (\delta_{\rho\sigma_0} - S_\rho S_{\sigma_0}) \\ & + \Big(\frac{\varepsilon_0}{\varepsilon_0'^3}\Big)^{\frac{1}{2}} v(k'_0) v_{0\mathbf{k}_0} S_{\sigma_0} (\delta_{\rho\rho_0} - S_\rho S_{\rho_0}) \Big] a^*_{\rho_0\mathbf{k}_0} a^*_{\sigma_0\mathbf{k}'_0} \Big\} \mathrm{d}\mathbf{k}_0 \mathrm{d}\mathbf{k}'_0 \end{aligned} \tag{186}$$

und im Fall (47) bei (184) zu

$$\begin{aligned} A_\rho = \frac{i}{2} \sum_{\rho_0, \sigma_0} \iint \Big\{ & \frac{1/b}{(\varepsilon_0 - \varepsilon'_0 + i\alpha)(\varepsilon_0 \varepsilon'_0)^{\frac{1}{2}}} [v(k_0) v^*_{0\mathbf{k}'_0} S_{\rho_0} (\delta_{\rho\sigma_0} - S_\rho S_{\sigma_0}) \\ & + v(k'_0) v_{0\mathbf{k}_0} (\delta_{\rho\rho_0} - S_\rho S_{\rho_0}) S_{\sigma_0}] a^*_{\rho_0\mathbf{k}_0} a_{\sigma_0\mathbf{k}'_0} \\ & - \frac{1/b}{2(\varepsilon_0 + \varepsilon'_0)(\varepsilon_0 \cdot \varepsilon'_0)^{\frac{1}{2}}} [v(k_0) v^*_{0\mathbf{k}'_0} S_{\rho_0} (\delta_{\rho\sigma_0} - S_\rho S_{\sigma_0}) \\ & + v(k'_0) v^*_{0\mathbf{k}_0} S_{\sigma_0} (\delta_{\rho\rho_0} - S_\rho S_{\rho_0})] a_{\rho_0\mathbf{k}_0} a_{\sigma_0\mathbf{k}'_0} \\ & - \frac{1/b}{2(\varepsilon_0 + \varepsilon'_0)(\varepsilon_0 \cdot \varepsilon'_0)^{\frac{1}{2}}} [v(k_0) v_{0\mathbf{k}'_0} S_{\rho_0} (\delta_{\rho\sigma_0} - S_\rho S_{\sigma_0}) \\ & + v(k'_0) v_{0\mathbf{k}_0} S_{\sigma_0} (\delta_{\rho\rho_0} - S_\rho S_{\rho_0})] a^*_{\rho_0\mathbf{k}_0} a^*_{\sigma_0\mathbf{k}_0} \Big\} \mathrm{d}\mathbf{k}_0 \mathrm{d}\mathbf{k}'_0. \end{aligned} \tag{187}$$

Damit können wir dann die in Gl. (10) eingeführten Koeffizienten $f_N(n)$ der dem Fall (46) oder (47) entsprechende Darstellung der starken Kopplung mittels eines entsprechenden Näherungsverfahrens der starken Kopplung berechnen.

Die Formulierungen (183) und (184) sind nur sinnvoll, wenn die entsprechenden Bedingungen der starken Kopplung erfüllt sind. Für den Fall (46), d.h. also auch für (183) lautet (36) mit den Ausdrücken (44) und (155) für H^{0C},

$$\Big(\frac{2\pi}{g}\Big)^2 \frac{\eta^2}{2b^2} \Delta\mathcal{F}^2 \ll 2 \Big(\frac{g}{2\pi}\Big)^2 b, \tag{188}$$

und für den Fall (47) d.h. für (184) lautet (36) mit dem Ausdruck (48) für H^{0c}

$$\left(\frac{2\pi}{g}\right)^2 \frac{\Delta\mathcal{T}^2}{2\int \frac{[v(k')]^2}{\varepsilon'^4}\,\mathrm{d}\mathbf{k}'} \ll 2\left(\frac{g}{2\pi}\right)^2 b. \tag{189}$$

Bei Benutzung der mit der Funktion (178) berechneten Werte (180) für η^2 und b ergibt (188):

$$g^4 \gg 4\left(1+\frac{\kappa}{K}\right)^4 \Delta\mathcal{T}^2 \tag{190}$$

und bei entsprechender Berechnung von

$$\int \frac{[v(k)]^2}{\varepsilon^4}\,\mathrm{d}k$$

mit (178) gibt (189)

$$g^4 \gg 4\left(1+\frac{\kappa}{K}\right)^5 \frac{\kappa}{K}\Delta\mathcal{T}^2, \tag{191}$$

wobei letzteres, wie schon am Ende von Absatz 2.1.5 bemerkt wurde, im Grenzfall der Punktquelle mit $\kappa/K \to 0$ für jedes g beliebig gut erfüllt ist.

Ferner darf der Nenner im zweiten und dritten Term von (183) und im letzten Term von (184) nicht verschwinden. Die Bedingung, die dazu erforderlich ist, lautet bei (183)

$$\frac{g}{2\pi} b \gg \sqrt{\int \frac{[v(k_0)]^2}{\varepsilon_0^2}\,\mathrm{d}\mathbf{k}_0} \tag{192}$$

und bei (184)

$$\frac{g}{2\pi}\int \frac{[v(k)]^2}{\varepsilon^4}\,\mathrm{d}\mathbf{k} \gg \sqrt{\int \frac{[v(k)]^2}{\varepsilon^5}\,\mathrm{d}\mathbf{k}}, \tag{193}$$

wobei die Abschätzung mittels des Vakuumerwartungswertes von

$$\left(\sum_{\rho'} S_\rho \int v(k) q'_{\rho\mathbf{k}}\,\mathrm{d}\mathbf{k}\right)^2 \quad \text{bzw.} \quad \left(\sum_{\rho} S_\rho \int \frac{v(k')}{\varepsilon^2}\, q'_{\rho\mathbf{k}}\,\mathrm{d}\mathbf{k}\right)^2$$

durchgeführt ist. Durch Einsetzen von (178) wird aus (192)

$$g \gg 2\sqrt{\frac{2}{\pi}} \tag{194}$$

und aus (193) wird bei Vernachlässigung von Termen der Ordnung κ/K in den ohnehin schwach cut-off-abhängigen Integralen

$$g \gg \frac{4}{\sqrt{6}}\sqrt{\frac{2}{\pi}} \approx 1.57\sqrt{\frac{2}{\pi}} \tag{195}$$

was von (194) nur wenig verschieden ist. (194) ist durch (190) schon mit erfüllt, während man dies bei (195) und (191) besonders in Anbetracht ihrer unterschiedlichen cut-off-Abhängigkeit nicht sagen kann.

Die Güte der durch Abbrechen der Reihenentwicklung von U (120) erzielten Annäherung, wie wir sie bei der Herleitung von (184) benutzt haben, wird durch die Bedingung

$$\frac{g}{2\pi} b \gg \sqrt{\int \frac{|v_{0k_0}|^2}{\varepsilon} \mathrm{d}\mathbf{k}} \tag{196}$$

gekennzeichnet, für die sich mit (182) bei Vernachlässigung von Termen der Größenordnung κ/K

$$g \gg \sqrt{\ln 4 \frac{K}{\kappa}} \sqrt{\frac{2}{\pi}} \tag{197}$$

ergibt.

Hauptmerkmal von (184) ist, daß $\not{p}_\rho$ darin erst von der Ordnung g^{-2} an abwärts enthalten ist und zwar in der Ordnung g^{-2} nur linear, sodaß wegen der Orthogonalitätsbeziehungen des $S_{\rho'\rho}$ und der T-Abhängigkeit ihrer Beträge und ihrer Skalarprodukte mit $\not{p}_\rho$ die Eigenwertkorrekturen zum Isobarenspektrum bis zur Ordnung g^{-2} herab T-unabhängig sind und sich bei der Bildung der Isobarenanregungsenergien herausheben. Letztere werden somit bis zur Ordnung g^{-2} herab durch (48) wiedergegeben und bekommen von H^{W} herrührende Eigenwertkorrekturen erst von der Ordnung g^{-4} an abwärts, wie wir es schon am Ende von Absatz 2.1.5 und in Ref. [21]) für die geladene skalare Theorie ausgeführt haben. Aus diesem Grunde haben wir den Fall (47) zu dem (48) und (184) gehören in Ref. [21]) zur Entwicklung der Methode der starken Kopplung beim Chew-Low-Formalismus benutzt. Der Fall (46) mit (183) und (44) (wobei (155) statt (45)) würde dazu weniger geeignet sein, da der erste, $\not{p}_\rho$ in der Ordnung g^{-1} linear enthaltende Term der zweiten Zeile von (183) noch Eigenwertkorrekturen der Ordnung g^{-2} zum Isobarenspektrum liefert, und (44) (wobei (155) statt (45)) erst mit diesem zusammen das (48) entsprechende vollständige Spektrum der Ordnung g^{-2} ergibt. Andererseits könnte aber (183) wegen seiner größeren Einfachkeit für eine Dämpfungsrechnung zur Behandlung der π-Meson-Nukleon-Resonanzstreuung besser geeignet sein. (Wir wollen diese Frage noch im Folgenden erörtern).

3. Das Näherungsverfahren der starken Kopplung

3.1. GLEICHUNGSSYSTEM DER STARKEN KOPPLUNG

Auf Grund der Neuaufspaltung des Hamiltonoperators, die die Bedingung der starken Kopplung (4) erfüllt, und die wir durch die im Vorstehenden entwickelte Feldaufspaltungstransformation (110) mit (37), (38), (46) bzw. (47), den Lösungen (139), (140) bzw. (141) des Gleichungssystems (128) und

den Wechselwirkungstermen (183) und (184) konstruiert haben, läßt sich nun das Näherungsverfahren der starken Kopplung entwickeln. Die störungstheoretische Entwicklung haben wir schon mit Gl. (9) formal angeschrieben. Sie ergibt sich mit den Bezeichnungen von Absatz 2.1.2 durch Einsetzen der Darstellung der starken Kopplung (10) und der Neuaufspaltung (8) in die Eigenwertgleichung

$$H\chi_N = E_N\chi_N. \tag{198}$$

Daraus folgt zunächst für $f_N(n)$ das Gleichungssystem

$$(E_N - E_n^0)f_N(n) = \sum_{n'} (n|H^W|n')f_N(n'), \tag{199}$$

das dann in die störungstheoretische Reihe (11) entwickelt werden kann.

Wie wir vorstehend gesehen haben (siehe (183) und (184)), kann hierin H^W auf Grund der Feldaufspaltungstransformation völlig durch die Compoundnukleonoperatoren $S_{\rho'\rho}$, $\mathfrak{p}_\rho$, $\bar{\tau}_\rho$ und die Erzeugungs- und Vernichtungsoperatoren $a^*_{\rho\mathbf{k}}$ und $a_{\rho\mathbf{k}}$ der freien Mesonen ausgedrückt werden, deren Wirkung auf die Eigenzustände θ_n des wechselwirkungsfreien Anteils $H^{0f}+H^{0C}$ der Neuaufspaltung wir kennen. θ_n ist dabei eine abgekürzte Schreibweise für einen Zustand

$$\theta_{\substack{\mathbf{k}_{01}\dots\mathbf{k}_{0n},\,T_n \\ \rho_{01}\cdots\rho_{0n}}}$$

mit n Mesonen der Impulse $\mathbf{k}_{01}\dots\mathbf{k}_{0n}$ und Ladungskonfigurationen $\rho_{01}\dots\rho_{0n}$ und einem Compoundnukleonzustand der Quantenzahlen T_n, worin die Isospinbetrags- und Ladungsquantenzahlen sowie die $\bar{\tau}_1{}^C$-Quantenzahlen des Compoundnukleons (siehe Absatz 2.1.5) zusammengefasst sein mögen. Die Mesonen befinden sich in diesen Zuständen nicht als ebene Wellen, sondern als zu den Compoundnukleonzuständen für $g \to \infty$ orthogonale Streuwellen, wie es durch die Transformationsfunktionen (139a, b) sowie durch (129) und (130) zum Ausdruck gebracht wird. Das von den Zuständen

$$\theta_{\substack{\mathbf{k}_{01}\dots\mathbf{k}_{0n},\,T_n \\ \rho_{01}\cdots\rho_{0n}}}$$

aufgespannte Orthonormalsystem kann durch fortgesetzte Anwendung der Operatoren $a^*_{\rho_0\mathbf{k}_0}$, $\mathcal{T}_{23}\pm i\mathcal{T}_{31}$, $S_1\pm iS_2$, und $\bar{\tau}_{23}\pm i\bar{\tau}_{31}$ (siehe Absätze 2.1.3 bis 2.1.5 und Gln. (102) bis (106)) auf den Mesonvakuum-Ein-Nukleon-Zustand θ_{0T_0} gemäß der Methode von Becker und Leibfried [22]) aufgebaut werden, wobei θ_{0T_0} derjenige Zustand ist, für den

$$a_{\rho_0\mathbf{k}_0}\theta_{0T_0} = 0. \tag{200}$$

Damit lassen sich aus solchen Ausdrücken für H^W, wie wir sie für die beiden vorstehend behandelten Spezialfälle mit (183) und (184) angeschrieben haben, die für das vorstehende Gleichungssystem benötigten H^W-Matrixelemente entnehmen.

3.2. BERECHNUNG DER *S*-MATRIX

3.2.1. *Aufspaltung in nullte Näherung und Näherungsanteil für endliche g*

Eine Entwicklung der *S*-Matrix nach negativen Potenzen der Kopplungskonstanten haben wir schon in Ref. [21]) für die geladene skalare Theorie dargelegt. Es geschah dies dort in einer Formulierung, die dem (47) mit (141) und (184) entsprechenden Spezialfall am besten angepaßt ist, bei dem die nullte Näherung schon in der (122) entsprechenden τ-Transformation mit enthalten ist. Wir wollen hier eine Formulierung geben, die auch für den Spezialfall (46) mit (140) und (183) geeignet ist, bei dem mit (138) die τ-Transformation (122) entfällt. Als Ausgangspunkt wählen wir in der der *S*-Matrix

$$S_{N\mathbf{k}} = \delta_{N\mathbf{k}} - 2\pi i \delta(E_N - E_{\mathbf{k}}) T_{\mathbf{k}}(N) \tag{201}$$

einen Ausdruck für $T_{\mathbf{k}}(N)$, der sich unmittelbar aus dem in Ref. [21b]) wiedergegebenen Ausdruck (24) ergibt, und in dem die auf dem Modell der festen Quellen basierende, zum Wickschen Ausdruck führende Umformung noch nicht vorgenommen ist. Er lautet

$$T_{\mathbf{k}}(N) = (E_N - E_{\mathbf{k}})(\chi_N^-, \hat{a}^*_{\rho\mathbf{k}} \chi_{0\tau_S}), \tag{202}$$

worin

$$\Phi_{\rho\mathbf{k}\tau_S} = \hat{a}^*_{\rho\mathbf{k}} \chi_{0\tau_S} \tag{203}$$

nach Wick [30]) den einlaufenden asymptotischen Zustand bedeutet, bestehend aus dem physikalischen Nukleonzustand $\chi_{0\tau_S}$ und dem einlaufenden Meson, welches im dem hier benutzten Modell, wegen des dabei fehlenden Unterschiedes zwischen nacktem und angezogenem Meson durch die Anwendung des aus den ursprünglichen Mesonfeldvariablen (3) gebildeten von Absatz 2.1.3 gemäß (102) verschiedenen Erzeugungsoperators

$$\hat{a}^*_{\rho\mathbf{k}} = (\tfrac{1}{2}\varepsilon)^{\frac{1}{2}} q_{\rho\mathbf{k}} - (2\varepsilon)^{-\frac{1}{2}} i p_{\rho\mathbf{k}} \tag{204}$$

auf $\chi_{0\tau_S}$ richtig beschrieben wird (Näheres dazu Wick [30]), Eckstein [31]), Brenig und Haag [32]), Lehmann, Symanzik und Zimmermann [33])). χ_N^- bedeutet dabei einen Streueigenzustand des Gesamthamiltonoperators mit einlaufendem Kugelwellenanteil und auslaufenden ebenen Wellenanteil, während $\Phi_{\rho\mathbf{k}\tau_S}$ der einlaufende ebene Wellenanteil eines entsprechenden Streueigenzustandes $\chi_{\mathbf{k}}^+$ ist, und E_N und $E_{\mathbf{k}}$ die entsprechenden Eigenwerte des Gesamthamiltonoperators sind. Ist ε die einlaufende Mesonenergie und E_S die Proton-Neutron-Selbstenergie, so ist

$$E_{\mathbf{k}} = \varepsilon + E_S, \qquad \text{mit } \varepsilon = \sqrt{k^2 + \kappa^2}. \tag{205}$$

Hier ist E_N die Energie des Endzustandes, in dem auch mehrere Mesonen und bei genügend starker Kopplung auch angeregte stabile Isobaren vorhanden

sein können. Eine zu (205) analoge Aufteilung in Mesonenenergie und Compoundnukleonenergie führen wir auch für E_N ein gemäß

$$E_N = \varepsilon_N + \varepsilon_{T_N}, \qquad \text{mit } \varepsilon_N = \sqrt{k^2+\kappa^2}. \tag{206}$$

Der differentielle Wirkungsquerschnitt für das Raumwinkelelement $d\Omega_N$ lautet dann †

$$\mathrm{d}\sigma = \mathrm{d}\Omega_N (2\pi)^4 \frac{\varepsilon}{k} \sum_N \int \delta(E_N - E_{\mathbf{k}}) |T_{\mathbf{k}}(N)|^2 k_N^2 \mathrm{d}\mathbf{k}_N. \tag{207}$$

Einsetzen der Darstellung der starken Kopplung (10) in (202) ergibt nun

$$T_{\mathbf{k}}(N) = (E_N - E_{\mathbf{k}}) \sum_{n',n} (\theta_{n'}^-, \hat{a}_{\rho\mathbf{k}}^* \theta_n^-) f_N^{-*}(n') f_{0T_S}(n). \tag{208}$$

Die Matrixelemente $(\theta_{n'}^-, \hat{a}_{\rho\mathbf{k}}^* \theta_n^-)$ lassen sich aber unmittelbar aus der Feldaufspaltungstransformation entnehmen, da mittels dieser ja die $q_{\rho\mathbf{k}}$ und $p_{\rho\mathbf{k}}$ und damit gemäß (204) auch die $\hat{a}_{\rho\mathbf{k}}^*$ durch die Compoundnukleonoperatoren $S_{\rho'\rho}$, p_ρ, $\bar{\tau}_\rho$ und die Erzeugungs- und Vernichtungsoperatoren $a_{\rho\mathbf{k}}^*$ und $a_{\rho\mathbf{k}}$ der freien Mesonen ausgedrückt werden, deren Wirkung auf die θ_n^- wir kennen. So ergibt sich aus (110) und (204)

$$\begin{aligned}
\hat{a}_{\rho\mathbf{k}}^* &= \sum_{\rho_0} \int \left\{ w_{\substack{\mathbf{k}_0\mathbf{k}\\ \rho_0\rho}} a_{\rho_0\mathbf{k}_0}^* + \chi_{\substack{\mathbf{k}_0\mathbf{k}\\ \rho_0\rho}} a_{\rho_0\mathbf{k}_0} \right\} \mathrm{d}\mathbf{k}_0 + w_{\mathbf{k}} S_\rho + \chi_{\mathbf{k}} \frac{p_\rho + A_\rho}{1+q}, \\
w_{\substack{\mathbf{k}_0\mathbf{k}\\ \rho_0\rho}} &= \tfrac{1}{2} \left[\left(\frac{\varepsilon}{\varepsilon_0}\right)^{\frac{1}{2}} u_{\substack{\mathbf{k}\mathbf{k}_0\\ \rho_0\rho}}^* + \left(\frac{\varepsilon_0}{\varepsilon}\right)^{\frac{1}{2}} v_{\substack{\mathbf{k}\mathbf{k}_0\\ \rho_0\rho}} \right], \\
\chi_{\substack{\mathbf{k}_0\mathbf{k}\\ \rho_0\rho}} &= \tfrac{1}{2} \left[\left(\frac{\varepsilon}{\varepsilon_0}\right)^{\frac{1}{2}} u_{\substack{-\mathbf{k}\mathbf{k}_0\\ \rho_0\rho}} - \left(\frac{\varepsilon_0}{\varepsilon}\right)^{\frac{1}{2}} v_{\substack{-\mathbf{k}\mathbf{k}_0\\ \rho_0\rho}}^* \right], \\
w_{\mathbf{k}} &= \left(\frac{\varepsilon}{2}\right)^{\frac{1}{2}} u_{\mathbf{k}}, \qquad \chi_{\mathbf{k}} = \frac{v_{\mathbf{k}}}{i(2\varepsilon)^{\frac{1}{2}}}.
\end{aligned} \tag{209}$$

Beim Einsetzen von (209) in (208) interessieren entsprechend dem S-Matrix-Ausdruck (201) nur die Beiträge, die im Limes $E \to E_{\mathbf{k}}$ übrigbleiben, d.h. eine dem Faktor $(E_N - E_{\mathbf{k}})$ entsprechende Singularität besitzen. Dies ist nur bei w der Fall. Daher bekommt man

$$\begin{aligned}
\lim_{E_N \to E_{\mathbf{k}}} T_{\mathbf{k}}(N) &= (E_N - E_{\mathbf{k}}) \sum_{n',n,\rho_0} \int (\theta_{n'}^-, w_{\substack{\mathbf{k}_0\mathbf{k}\\ \rho_0\rho}} a_{\rho_0\mathbf{k}_0}^* \theta_n^-) f_N^{-*}(n') f_{0T_S}(n) \mathrm{d}\mathbf{k}_0 \\
&= (E_N - E_{\mathbf{k}}) \sum_{\rho_0,T',T} \int (T' | w_{\substack{\mathbf{k}_0\mathbf{k}\\ \rho_0\rho}} | T) \sum_n \sqrt{n+1}\, f_N^{-*}(n, {}^{\mathbf{k}_0}_{\rho_0})_{T'} f_{0T_S}(n) \mathrm{d}\mathbf{k}_0.
\end{aligned} \tag{210}$$

† Siehe z.B. Ref. [34]), Gl. (137). Die dort auftretende Matrix $\bar{R}$ ist durch hier verwendete Matrix $2\pi T_{\mathbf{k}}(N)$ zu ersetzen.

Wegen der in w noch enthaltenen Compoundnukleonoperatoren $S_{\rho 0} S_\rho$ haben wir in der zweiten Zeile die Summationen über die Compoundnukleonzustände und die freien Mesonzustände gesondert angeschrieben.

Entsprechend der Bedingung der starken Kopplung (siehe insbesondere (11)) haben $f_{0T_S}(n)_T$ und $f_N^-(n, {}^{\mathbf{k}_0}_{\rho_0})_T$, die Form

$$\begin{aligned} f_{0T_S}(n)_T &= \delta_{0\,\left|\,{}^{n}_{T_S}\right.\,T} + \text{Terme von der Ordnung } g^{-1} \text{ an abwärts,} \\ f_N^-(n, {}^{\mathbf{k}_0}_{\rho_0})_{T'} &= \delta_{N\left|\,{}^{n,\mathbf{k}_0}_{\rho_0 T'}\right.} + \text{Terme von der Ordnung } g^{-1} \text{ an abwärts,} \end{aligned} \tag{211}$$

sodaß in der nullten Näherung nur der Term mit $n = 0$

$$\lim_{E_N \to E_{\mathbf{k}}} T_{\mathbf{k}}(N)_0 = \lim_{E_N \to E_{\mathbf{k}}} (E_N - E_{\mathbf{k}})(T_N | w_{\substack{\mathbf{k}_N \mathbf{k} \\ \rho_N \rho}} | T_S) = h^0 \left(\begin{matrix} \mathbf{k}_N \\ \rho_N \\ T_N \end{matrix} \middle| \begin{matrix} \mathbf{k} \\ \rho \\ T_S \end{matrix} \right) \tag{212}$$

in der Summation von (210) übrigbleibt, und man somit in der nullten Näherung nur Ein-Meson-Streuung ohne Mesonerzeugungsprozesse bekommt, die im Grenzfall $g \to \infty$ verschwinden in Übereinstimmung mit den in Ref. [21]) erhaltenen Resultaten. Einsetzen von (9) in (210) ergibt die Entwicklung der S-Matrix in die störungstheoretische Reihe der starken Kopplung, aus der man die Entwicklung nach der reziproken Kopplungskonstanten

$$S = S_0 + \frac{1}{g} S_1 + \frac{1}{g^2} S_2 + \ldots \tag{213}$$

mit

$$S_{0N\mathbf{k}} = \delta_{N\mathbf{k}} - 2\pi i \delta(E_N - E_{\mathbf{k}}) T_{\mathbf{k}}(N)_0 \tag{214}$$

bekommt, wobei $T_{\mathbf{k}}(\mathrm{N})_0$ durch (212) gegeben ist (siehe auch Gln. (222), (223) und (232)).

Berechnen wir über die Störungstheorie der starken Kopplung hinaus für endliche g die Ein-Meson-Streuung, so dürfte der Term mit $n = 0$ in (210) den Hauptbeitrag ergeben und die Terme mit $n > 0$ nur Korrekturen von höherer Ordnung in g^{-1} liefern. Bleiben wir somit also auch für endliche g für die Ein-Meson-Streuung in der Ein-Meson-Näherung, so erhalten wir

$$\lim_{E_N \to E_{\mathbf{k}}} T_{\mathbf{k}}(N)_1 = \lim_{E_N \to E_{\mathbf{k}}} \sum_{\rho_0, T'} \int (T' | w_{\substack{\mathbf{k}_0 \mathbf{k} \\ \rho_0 \rho}} | T_S) f_N^{-*}(\mathbf{k}_0)_{\rho_0 T'}, \, \mathrm{d}\mathbf{k}_0. \tag{215}$$

Gemäß der üblichen Beschreibungsweise für einen Ein-Teilchen-Streuvorgang im Impulsraum muß $f_N^{-*}(\mathbf{k}_0)_{\rho_0, T'}$ die allgemeine Form haben

$$f_N(\mathbf{k}_0)_{\rho_0, T'} = \delta_{N\left|\,{}^{\mathbf{k}_0}_{\rho_0}\right.\,T'} - \frac{h\left(N \middle| \begin{matrix} \mathbf{k}_0 \\ \rho_0 \\ T' \end{matrix}\right)}{E_N - E_0 - \varepsilon_{T'} + i\alpha} \tag{216}$$

mit der Energie $\varepsilon_{T'}$ des betreffenden Compoundnukleonzustandes. Ganz entsprechend gilt auch für $(T'|w_{\substack{\mathbf{k}_0\mathbf{k}\\ \rho_0\rho}}|T_S)$

$$(T'|w_{\substack{\mathbf{k}_0\mathbf{k}\\ \rho_0\rho}}|T_S) = \delta_{\substack{\mathbf{k}_0|\mathbf{k}\\ \rho_0|\rho\\ T'|T_S}} - \frac{h^0\begin{pmatrix}\mathbf{k}_0|\mathbf{k}\\ \rho_0|\rho\\ T'|T_S\end{pmatrix}}{\varepsilon_0-\varepsilon+i\alpha}, \tag{217}$$

wie es sich aus (209) und (139) bzw. (140) oder (141) ergibt. An Hand der Gleichungen (209) und (139) bzw. (140) oder (141) können wir dann auch

$$h^0\begin{pmatrix}\mathbf{k}_0|\mathbf{k}\\ \rho_0|\rho\\ T'|T_S\end{pmatrix}$$

aus den Transformationsfunktionen u und v entnehmen, worauf wir aber im folgenden gleich noch zurückkommen wollen. Setzen wir nun (217) und (216) in den Ausdruck (215) für die Streuamplitude ein, so erhalten wir

$$\sum_{\rho_0,T'}\int (T'|w_{\substack{\mathbf{k}_0\mathbf{k}\\ \rho_0\rho}}|T_S)f_N^{-*}(\mathbf{k}_0)_{T'}\,\mathrm{d}\mathbf{k}_0$$

$$= \delta_{N\left|\begin{smallmatrix}\mathbf{k}_0\\ \rho_0\\ T'\end{smallmatrix}\right.} - \left\{\frac{h^0\left(N\left|\begin{smallmatrix}\mathbf{k}\\ \rho\\ T_S\end{smallmatrix}\right.\right)}{\varepsilon_N-\varepsilon+i\alpha} + \frac{h\left(N\left|\begin{smallmatrix}\mathbf{k}\\ \rho\\ T_S\end{smallmatrix}\right.\right)}{E_N-E_{\mathbf{k}}+i\alpha}\right\} - \sum_{\rho_0,T'}\int \frac{h^0\begin{pmatrix}\mathbf{k}_0|\mathbf{k}\\ \rho_0|\rho\\ T'|T_S\end{pmatrix} h\left(\begin{smallmatrix}\mathbf{k}_0\\ \rho_0\\ T'\end{smallmatrix}\middle|N\right)}{(\varepsilon_0-\varepsilon-i\alpha)(\varepsilon_0+\varepsilon_{T'}-E_N-i\alpha)}\,\mathrm{d}\mathbf{k}_0. \tag{218}$$

Der letzte Term enthält keine Singularität und trägt somit zur Streuung nichts bei. Dabei haben wir für E_N und $E_{\mathbf{k}}$ die (205) und (206) entsprechende Aufteilung in Mesonenergie und Compoundnukleonenergie berücksichtigt.

Beim Einsetzen von (218) in (215) liefern wiederum nur die Terme von (218) mit der dem Faktor (E_N-E_n) in (215) entsprechenden Singularität einen Beitrag. Das sind der zweite und der dritte Term in (218). Der Beitrag des zweiten Terms ist mit (212) identisch und ergibt sich nur, wenn gleichzeitig mit $E_N = E_{\mathbf{k}}$ auch $\varepsilon_N = \varepsilon$ ist. D.h., es kann keine Anregung von Compoundnukleonzuständen durch den zweiten, von der Feldaufspaltungstransformation herrührenden, der nullten Näherung entsprechende Term beschrieben werden außer im Grenzfall $g \to \infty$, in dem die Energieseparation der Compoundnukleonzustände auf Null zusammenschrumpft (siehe (44), (48) und (49)). Der dritte Term von Gl. (218), der von der Darstellung der starken Kopplung herrührt, mittels des Näherungsverfahrens für starke Kopplung zu berechnen ist und gemäß (11) und (211) für $g \to \infty$ verschwindet, kann hingegen auch eine Anregung von Compoundnukleonzuständen beschreiben, falls die Kopplung für die stabile Existenz solcher Zustände stark genug ist. Denn, da hier die Differenz $E_N-E_{\mathbf{k}}$ selbst den Nenner bildet, wird das Verschwinden mit $(E_N-E_{\mathbf{k}})$ auch für $\varepsilon_N \neq \varepsilon$ und $E_T \neq E_S$ kompensiert. Falls die Kopplung nicht die für die Stabilität der Compoundnukleonzustände hinreichende Stärke

hat, findet ein anschließender Zerfall des Isobars statt, d.h. wir bekommen eine Mesonerzeugung auf dem Umweg über eine Anregung mit anschließendem Zerfall eines Isobars, wie es in dem phänomenologischen Isobarenmodell von Lindenbaum und Sternheimer[35]) angenommen ist. Die Begründung eines solchen Mesonerzeugungsmodells mittels der Methode der starken Kopplung soll aber einer späteren Untersuchung vorbehalten bleiben (siehe hierzu die Ausführungen in Ref. [21]), über die Ein-Meson-Näherung der starken Kopplung des Chew-Low-Formalismus, die einer Mehr-Meson-Näherung des gewöhnlichen Chew-Low-Formalismus entspricht).

Einsetzen von (218) in (215) ergibt also für die Streuamplitude bei Streuung ohne Isobarenanregung

$$\lim_{E_N \to E_{\mathbf{k}}} T_{\mathbf{k}}(N) = -\left\{h^0\left(\begin{matrix}\mathbf{k}_N \\ \rho_N \\ T_N\end{matrix}\middle|\begin{matrix}\mathbf{k} \\ \rho \\ T_S\end{matrix}\right) + h\left(\begin{matrix}\mathbf{k}_N \\ \rho_N \\ T_N\end{matrix}\middle|\begin{matrix}\mathbf{k} \\ \rho \\ T_S\end{matrix}\right)\right\}, \quad \text{mit } \varepsilon_N = \varepsilon,\ \varepsilon_{T_N} = E_S, \tag{219}$$

und bei Streuung mit Isobarenanregung

(a) Im Grenzfall $g \to \infty$

$$\lim_{E_N \to E_{\mathbf{k}}} T_{\mathbf{k}}(N)_0 = -h^0\left(\begin{matrix}\mathbf{k}_N \\ \rho_N \\ T_N\end{matrix}\middle|\begin{matrix}\mathbf{k} \\ \rho \\ T_S\end{matrix}\right), \quad \begin{matrix}\text{mit } \varepsilon_N = \varepsilon, \quad \varepsilon_{T_N} = E_S, \\ \text{aber } T_N{}^2 \neq T_S{}^2.\end{matrix} \tag{220}$$

(b) Für endliche g

$$\lim_{E_N \to E_{\mathbf{k}}} T_{\mathbf{k}}(N) = -h\left(\begin{matrix}\mathbf{k}_N \\ \rho_N \\ T_N\end{matrix}\middle|\begin{matrix}\mathbf{k} \\ \rho \\ T_S\end{matrix}\right) \quad \text{mit } \varepsilon_N = E_N - \varepsilon_T \neq \varepsilon,\ \varepsilon_{T_N} \neq E_S. \tag{221}$$

Wir haben also gemäß (219) bis (221) eine Aufspaltung der Streuamplitude (202) in zwei Anteile erhalten:

1) den Anteil

$$h^0\left(N\middle|\begin{matrix}\mathbf{k} \\ \rho \\ T_S\end{matrix}\right)$$

Gln. (212) und (217), der durch die kanonische Aufspaltungstransformation gegeben ist, die nullte Näherung darstellt und im Grenzfall $g \to \infty$ allein übrigbleibt.

2) den Anteil

$$h\left(N\middle|\begin{matrix}\mathbf{k} \\ \rho \\ T_S\end{matrix}\right)$$

(siehe Gl. (216)), der durch das Näherungsverfahren für starke Kopplung zu berechnen ist und im Grenzfall $g \to \infty$ verschwindet.

3.2.2. *Diskussion der nullten Näherung*

Der Anteil

$$h^0\left(\begin{matrix}\mathbf{k}_N \\ \rho_N \\ T_N\end{matrix}\middle|\begin{matrix}\mathbf{k} \\ \rho \\ T_S\end{matrix}\right)$$

der Streuamplitude $T_{\mathbf{k}}(N)$, der die nullte Näherung zu unserem Näherungsverfahren der starken Kopplung darstellt, ergibt sich aus der kanonischen Aufspaltungstransformation gemäß (212), (217) und (209) zu

$$h^0\left(\begin{matrix}\mathbf{k}_N\\ \rho_N\\ T_N\end{matrix}\middle|\begin{matrix}\mathbf{k}\\ \rho\\ T_S\end{matrix}\right)=-(\varepsilon_N-\varepsilon)(T_S^N|w_{\substack{\mathbf{k}_N\mathbf{k}\\ \rho_N\rho}}|T_S)=-(\varepsilon_N-\varepsilon)\tfrac{1}{2}\left(T_N\left|\left[\left(\frac{\varepsilon}{\varepsilon_N}\right)^{\frac{1}{2}}u^*_{\substack{\mathbf{k}\mathbf{k}_0\\ \rho_N\rho}}+\left(\frac{\varepsilon_N}{\varepsilon}\right)^{\frac{1}{2}}v_{\substack{\mathbf{k}\mathbf{k}_N\\ \rho_N\rho}}\right]\right|T_S\right). \tag{222}$$

Anhand von (139), speziell (140) und (141) und von (222) sieht man, daß

$$h^0\left(\begin{matrix}\mathbf{k}_N\\ \rho_N\\ T_N\end{matrix}\middle|\begin{matrix}\mathbf{k}\\ \rho\\ T_S\end{matrix}\right)$$

für $\varepsilon_N\to\varepsilon$, d.h. also auf der Energieschale, für jedes zu einem bestimmten $v(k)$ gewählte $v^1(k)$, d.h. für jeden Vertreter aus der Schar der kanonischen Aufspaltungstransformationen denselben Wert annimmt, nämlich

$$h^0\left(\begin{matrix}\mathbf{k}_N\\ \rho_N\\ T_N\end{matrix}\middle|\begin{matrix}\mathbf{k}\\ \rho\\ T_S\end{matrix}\right)=\frac{v(k)}{2\varepsilon}\,\frac{v_{0\mathbf{k}}}{b}\,(\delta_{\rho_N\rho}\delta_{T_NT_S}-(T_N|S_{\rho_N}S_\rho|T_S)), \tag{223}$$

sodaß sich im Grenzfall $g\to\infty$ für jedes $v^1(k)$ derselbe Streuquerschnitt ergibt.

In (223) müssen wir dann das Matrixelement $(T_N|S_{\rho_N}S_\rho|T_S)$ berechnen.

Die hierfür benötigte Matrixdarstellung der Operatoren S_ρ ergibt sich aus ihren Vertauschungseigenschaften miteinander und mit den $\mathscr{T}_{\rho\sigma}$ (siehe (19) und (20)) und entspricht im Übrigen auch der Matrixdarstellung des elektrischen Dipolmomentoperators in der Quantenmechanik der Atomhülle. Matrixdarstellungen derartiger Operatoren sind in der Literatur hinreichend behandelt (z.B. von Born und Jordan [36]), Pauli [37]) und Fierz [38])). Dabei folgt aus den Vertauschungseigenschaften der S_ρ, daß ihre Matrixelemente nur für Übergänge mit $\Delta T_{12}=0,\pm1$ und $\Delta T=0,\pm1$ von Null verschieden sind, und zwar hat S_ρ gemäß seiner Vertauschbarkeit mit $\mathscr{T}_{12}$ nur Matrixelemente mit $\Delta T_{12}=0$, während in S_1 und S_2 nur Matrixelemente mit $\Delta T_{12}=\pm1$ vorkommen. Es ergibt sich

$$S_\rho=|A_{TT}(T|d_\rho|T)+A_{TT-1}(T|b_\rho|T-1)+(T-1|b_\rho{}^*|T)A_{T-1T}, \tag{224}$$

mit

$$\begin{aligned}
&(T|d_\rho|T)=\mathscr{T}_\rho, && (T,T_{12}|b_1+ib_2|T-1,T_{12}-1)=-\sqrt{(T+T_{12})(T+T_{12}-1)},\\
&A_{TT}=\frac{1}{2T(T+1)}, && (T,T_{12}|b_1-ib_2|T-1,T_{12}+1)=\sqrt{(T-T_{12})(T-T_{12}-1)},\\
&A_{TT-1}=\frac{1}{2T}, && (T,T_{12}|b_3|T-1,T_{12})=\sqrt{(T-T_{12})(T+T_{12})}.
\end{aligned} \tag{225}$$

Speziell mit den tiefsten Zuständen beginnend bekommen wir

$$S_\rho = \begin{vmatrix} \frac{2}{3}(\frac{1}{2}|d_\rho|\frac{1}{2}) + \frac{1}{3}\{(\frac{3}{2}|b_\rho|\frac{1}{2}) + (\frac{1}{2}|b_\rho{}^*|\frac{3}{2})\} \\ \frac{2}{15}(\frac{3}{2}|d_\rho|\frac{3}{2}) + \frac{1}{5}\{(\frac{5}{2}|b_\rho|\frac{3}{2}) + (\frac{3}{2}|b_\rho{}^*|\frac{5}{2})\} \\ \cdots\cdots\cdots\cdots\cdots \\ \cdots\cdots\cdots\cdots\cdots \end{vmatrix}, \tag{226}$$

mit

$$(\tfrac{1}{2}|d_\rho|\tfrac{1}{2}) = \left\{\begin{pmatrix} 0 & \frac{1}{2} \\ \frac{1}{2} & 0 \end{pmatrix}; \begin{pmatrix} 0 & -\frac{1}{2}i \\ \frac{1}{2}i & 0 \end{pmatrix}; \begin{pmatrix} \frac{1}{2} & 0 \\ 0 & -\frac{1}{2} \end{pmatrix}\right\},$$

$$(\tfrac{3}{2}|d_\rho|\tfrac{3}{2}) = \left\{\begin{pmatrix} 0 & \frac{1}{2}\sqrt{3} & 0 & 0 \\ \frac{1}{2}\sqrt{3} & 0 & 1 & 0 \\ 0 & 1 & 0 & \frac{1}{2}\sqrt{3} \\ 0 & 0 & \frac{1}{2}\sqrt{3} & 0 \end{pmatrix}; i\begin{pmatrix} 0 & -\frac{1}{2}\sqrt{3} & 0 & 0 \\ \frac{1}{2}\sqrt{3} & 0 & -1 & 0 \\ 0 & 1 & 0 & -\frac{1}{2}\sqrt{3} \\ 0 & 0 & \frac{1}{2}\sqrt{3} & 0 \end{pmatrix}; \begin{pmatrix} \frac{3}{2} & 0 & 0 & 0 \\ 0 & \frac{1}{2} & 0 & 0 \\ 0 & 0 & -\frac{1}{2} & 0 \\ 0 & 0 & 0 & -\frac{3}{2} \end{pmatrix}\right\},$$

$$(\tfrac{3}{2}|b_\rho|\tfrac{1}{2}) = \left\{\frac{1}{2}\begin{pmatrix} -\sqrt{6} & 0 \\ 0 & -\sqrt{2} \\ \sqrt{2} & 0 \\ 0 & \sqrt{6} \end{pmatrix}; \frac{1}{2}i\begin{pmatrix} \sqrt{6} & 0 \\ 0 & \sqrt{2} \\ \sqrt{2} & 0 \\ 0 & \sqrt{6} \end{pmatrix}; \begin{pmatrix} 0 & 0 \\ \sqrt{2} & 0 \\ 0 & \sqrt{2} \\ 0 & 0 \end{pmatrix}\right\}, \tag{227}$$

$$(\tfrac{1}{2}|b_\rho{}^*|\tfrac{3}{2}) = \left\{\frac{1}{2}\begin{pmatrix} -\sqrt{6} & 0 & \sqrt{2} & 0 \\ 0 & -\sqrt{2} & 0 & \sqrt{6} \end{pmatrix}; -\frac{1}{2}i\begin{pmatrix} \sqrt{6} & 0 & \sqrt{2} & 0 \\ 0 & \sqrt{2} & 0 & \sqrt{6} \end{pmatrix}; \begin{pmatrix} 0 & \sqrt{2} & 0 & 0 \\ 0 & 0 & \sqrt{2} & 0 \end{pmatrix}\right\}.$$

Für Streuung ohne Isobarenanregung mit dem Nukleongrundzustand sowohl im einlaufenden als auch im auslaufenden Zustand folgt nun mit $(\frac{1}{2}|b^*_{\rho'} b_\rho|\frac{1}{2}) = -(\frac{1}{2}|b_\rho{}^* b_{\rho'}|\frac{1}{2})$ gemäß Fierz [38]) die Beziehung

$$(\tfrac{1}{2}|b_\rho{}^* b_{\rho'}|\tfrac{1}{2}) = -2i(\tfrac{1}{2}|d_{\rho'}|\tfrac{1}{2}), \qquad (\rho \neq \rho' \neq \rho'' \text{ zyklisch}), \tag{228}$$

und mit $(\frac{1}{2}|d_\rho d_{\rho'}|\frac{1}{2}) = \frac{1}{2}i(\frac{1}{2}|d_{\rho'}|\frac{1}{2})$, $(\rho \neq \rho' \neq \rho''$ zyklisch) folgt daraus eine Kompensation der Ladungsaustauschbeiträge zum Matrixelement $(\frac{1}{2}|S_{\rho_N} S_\rho|\frac{1}{2})$, sodaß man bekommt

$$(\tfrac{1}{2}|S_{\rho_N} S_\rho|\tfrac{1}{2}) = \tfrac{4}{9}(\tfrac{1}{2}|d_{\rho_N}|\tfrac{1}{2})(\tfrac{1}{2}|d_\rho|\tfrac{1}{2}) + \tfrac{1}{9}(\tfrac{1}{2}|b^*_{\rho_N}|\tfrac{3}{2})(\tfrac{3}{2}|b_\rho|\tfrac{1}{2}) = \tfrac{1}{3}\delta_{\rho_N \rho}. \tag{229}$$

Übergänge mit Ladungsaustausch resultieren in dem Produktoperator $S_{\rho_N} S_\rho$ erst bei gleichzeitiger Anregung eines Compoundnukleonzustandes im auslaufenden Zustand, z.B. bei Anregung des Isobars mit $T = \frac{3}{2}$ mit den Matrixelementen

$$\tfrac{2}{9}(\tfrac{3}{2}|b_{\rho_N}|\tfrac{1}{2})(\tfrac{1}{2}|d_\rho|\tfrac{1}{2}) + \tfrac{2}{45}(\tfrac{3}{2}|d_{\rho_N}|\tfrac{3}{2})(\tfrac{3}{2}|b_\rho|\tfrac{1}{2}) \tag{230}$$

und bei Anregung von $T = \frac{5}{2}$ mit den Matrixelementen

$$\tfrac{1}{15}(\tfrac{5}{2}|b_{\rho_N}|\tfrac{3}{2})(\tfrac{3}{2}|b_\rho|\tfrac{1}{2}). \tag{231}$$

Entsprechend den Darlegungen nach Gl. (218) kommt dies aber erst im Grenzfall $g \to \infty$ in der so definierten nullten Näherung vor. Für enliche g haben wir in der nullten Näherung nur die Matrixelemente (229) in (223) und daher mit

$$(\delta_{\rho_N \rho}\delta_{T_N T} - (\tfrac{1}{2}|S_{\rho_N} S_{\rho}|\tfrac{1}{2})) = \tfrac{2}{3}\delta_{\rho_N \rho}\delta_{T_N T} \tag{232}$$

und mit der wegen der Isotropie des Kopplungsterms nur isotropen Winkelverteilung (nur S-Streuung) gemäß (207) den Wirkungsquerschnitt:

$$\sigma_0 \begin{pmatrix} \mathbf{k} & \mathbf{k} \\ \rho_N & \rho \\ T_N & T_S \end{pmatrix} = 4\pi(2\pi)^4 \varepsilon^2 \left| h^0 \begin{pmatrix} \mathbf{k} & \mathbf{k} \\ \rho_N & \rho \\ T_N & T_S \end{pmatrix} \right|^2 = \frac{16\pi}{9}\left(\frac{2\pi^2}{b}\right)^2 [v_{0\mathbf{k}_N}|^2 [v(k_N)]^2 \delta_{\rho_N \rho}\delta_{T_N T_S}. \tag{233}$$

Mit der schon in Absatz 2.4.3 erörterten Wahl (178) für $v(k)$ ergaben sich gemäss (180) für $v_{0\mathbf{k}}$ und $|v_{0\mathbf{k}}|^2$ die Ausdrücke (181) und (182). Wählen wir hingegen für $v(k)$ die Stufenfunktion

$$v(k) = \begin{cases} 1 \text{ für } 0 \leqq k \leqq A, \\ 0 \text{ für } k > A, \end{cases} \tag{234}$$

so bekommen wir gemäß (139c und e)

$$\frac{v_{0\mathbf{k}_0}}{b} = \frac{v(k_0)}{2\pi k \ln \dfrac{A+k_0}{A-k_0} - 4\pi\kappa \operatorname{arctg} \dfrac{A}{\kappa} + i2\pi^2 k_0 [v_1(k_0)]^2}, \tag{235}$$

und für $k_0 < A$ bei Entwicklung des Logarithmus bis zum ersten Gliede

$$\frac{v_{0\mathbf{k}_0}}{b} \approx \frac{v(k_0)}{\dfrac{4\pi\varepsilon_0{}^2}{A} - 2\pi^2\kappa - i2\pi^2 k_0} \tag{236}$$

und somit

$$\left(\frac{2\pi^2}{b}\right)^2 |v_{0\mathbf{k}_0}|^2 = \frac{[v(k_0)]^2}{\left(1 - \dfrac{2}{\pi}\dfrac{\kappa}{A}\right)^2 \left\{1 + \dfrac{k^2}{\left(\dfrac{\pi}{2} A - 1\right)^2}\right\} \varepsilon_0{}^2}. \tag{237}$$

Dies ist die gleiche Energieabhängigkeit des Nenners, die in (182) für jedes k galt. Für den Fall der Gaussfunktion

$$v(k) = \mathrm{e}^{-\left(\frac{ka}{\sqrt{2}}\right)^2} \tag{238}$$

bekommt man diese Energieabhängigkeit sogar exakt und nicht nur für $\kappa^2/K^2 \ll 1$ wie bei (182). Somit scheint $v_{0\mathbf{k}_0}/b$ für einigermaßen glattes $v(k)$, d.h. für einen im Ortsraum einigermaßen stark lokalisierten Funktionstyp nicht sehr stark von der speziellen Wahl der Funktion abzuhängen. Dieses

Verhalten läßt sich bei Übergang in den Ortsraum gut veranschaulichen. Nach Fouriertransformation innerhalb von (139c und e) wird dann

$$\frac{1}{b}\frac{v_{0\mathbf{k}_0}}{v(k_0)} = \left\{\frac{(2\pi)^3}{4\pi}\iint K(\mathbf{r})\frac{e^{-\varkappa|\mathbf{r}-\mathbf{r}'|}-e^{ik_0|\mathbf{r}-\mathbf{r}'|}}{|\mathbf{r}-\mathbf{r}'|}K(\mathbf{r}')\,d\mathbf{r}\,d\mathbf{r}'\right\}^{-1}. \tag{239}$$

(239) zeigt, wie die Eigenfeldfunktion

$$\int K(\mathbf{r}')\frac{e^{-\varkappa|\mathbf{r}-\mathbf{r}'|}}{|\mathbf{r}-\mathbf{r}'|}\,d\mathbf{r}'$$

und die auslaufende Kugelwellenfunktion

$$\int K(\mathbf{r}')\frac{e^{ik_0|\mathbf{r}-\mathbf{r}'|}}{|\mathbf{r}-\mathbf{r}'|}\,d\mathbf{r}'$$

in die Streuamplitude der nullten Näherung eingehen. Die Entwicklung der Exponentialfunktionen $e^{-\varkappa|\mathbf{r}-\mathbf{r}'|}$ und $e^{ik_0|\mathbf{r}-\mathbf{r}'|}$ in (239) bis zum dritten Glied ergibt unmittelbar den Nenner von (236), wenn darin für den Fall einer beliebigen Wahl der Quellfunktion an Stelle von $1/A$

$$\frac{1}{A'} = \frac{\pi}{4}\iint K(\mathbf{r})|\mathbf{r}-\mathbf{r}'|K(\mathbf{r}')\,d\mathbf{r}\,d\mathbf{r}' \tag{240}$$

gesetzt wird. Die übrigen Glieder der Entwicklung der Exponentialfunktionen in (239) gehen mit immer höheren Potenzen von $|\mathbf{r}-\mathbf{r}'|$ und dürften somit für hinreichend stark lokalisierte Quellfunktionen $K(\mathbf{r})$ zu vernachlässigen sein. Unter dieser Voraussetzung erhalten wir für den Wirkungsquerschnitt gemäß (233), (237) und (240) für beliebige, hinreichend stark lokalisierte Quellfunktionen

$$\sigma_0\left(\begin{matrix}\mathbf{k} & \mathbf{k}\\ \rho_N & \rho\\ T_N & T_S\end{matrix}\right) = \frac{16\pi}{g}\,\frac{[v(k)]^4}{\left(1-\frac{2}{\pi}\frac{\varkappa}{A'}\right)^2\left\{1+\frac{k^2}{\left(\frac{\pi}{2}A'-1\right)^2}\right\}\varepsilon^2}\,\delta_{\rho_N\rho}\delta_{T_NT_S}. \tag{241}$$

Im Grenzfall der Punktquelle ($1/A' \to 0$) wird daraus †

$$\sigma_0\left(\begin{matrix}\mathbf{k} & \mathbf{k}\\ \rho_N & \rho\\ T_N & T_S\end{matrix}\right) \to \frac{16\pi}{g}\frac{1}{\varepsilon^2}\,\delta_{\rho_N\rho}\delta_{T_NT_S}. \tag{242}$$

Im Grenzfall der Punktquelle bekommt man also in dem hier benutzten Modell der symmetrischen skalaren Theorie für den Streuanteil der nullten Näherung

† (242) und (243) sind im Einklang mit den von Wentzel [1]) mit Hilfe des Gitterraumes erzielten Ergebnisse. Der endlichen Zellengröße des Gitterraumes entspricht hier die endliche Ausdehnung der Quellfunktion, und dem Grenzfall verschwindender Zellengröße der Grenzfall der Punktquelle.

einen endlichen Grenzwert. Ferner erhält man für endliche ausgedehnte, aber stark lokalisierte Quellfunktionen im Grenzfall großer Energieen $k_0 \gg A'$ gemäß (241)

$$\sigma_0 \left(\begin{matrix} \mathfrak{k} \\ \rho_N \\ T_N \end{matrix} \middle| \begin{matrix} \mathfrak{k} \\ \rho \\ T_S \end{matrix} \right) \to \frac{4\pi^3}{g} \frac{A'^2}{\varepsilon^4} \delta_{\rho_N \rho} \delta_{T_N T_S}. \tag{243}$$

Wegen der Kugelsymmetrie des Kopplungstermes in (1) haben wir es natürlich hier und in den nachstehenden Ausführungen immer nur mit S-Streuung zu tun.

3.3. DÄMPFUNGSRECHNUNG AN DER RESONANZSTELLE

3.3.1. *Näherung an der Resonanzstelle*

Der zweite Anteil

$$h \left(N \middle| \begin{matrix} \mathfrak{k} \\ \rho \\ T_S \end{matrix} \right)$$

der Streuamplitude $T_{\mathfrak{k}}(N)$ (siehe (219)—(221)) ist gemäß seiner durch (216) gegebenen Definition aus dem Gleichungssystem (199) zu berechnen. Von besonderem Interesse ist dabei eine Annäherung des Gleichungssystems (199) für die Berechnung einer aus der Möglichkeit der Isobarenanregung sich etwa ergebenden π-Meson-Nukleonresonanzstreuung, entsprechend den experimentell gefundenen, theoretisch aber erst teils unvollkommen teils noch gar nicht berechneten Resonanzen der π-Meson-Nukleon-Streuung. Entsprechend den Dämpfungsrechnungen von Dirac [39]) und Heitler [40]) brauchen dann in der unmittelbaren Umgebung des Resonanzmaximums nur die Übergänge zwischen dem Ein-Meson-Zustand

$$\theta_{\substack{\mathfrak{k}_0 \\ \rho_0}, T}$$

mit dem Darstellungskoeffizienten

$$f_N \left(\begin{matrix} \mathfrak{k}_0 \\ \rho_0 \end{matrix} \right)_T$$

und dem Isobarenzustand θ_{0I} (Mesonvakuum mit Isobar der Quantenzahl I) mit dem Darstellungskoeffizienten $f_N(0)_I$ berücksichtigt zu werden, sodaß sich das Gleichungssystems (199) reduziert zu

$$\begin{aligned} (\varepsilon_0 + \varepsilon_T{}^0 + \Delta\varepsilon_T(\varepsilon_0, E_N) - E_N) f_N \left(\begin{matrix} \mathfrak{k}_0 \\ \rho_0 \end{matrix} \right)_T &= -\left(\begin{matrix} \mathfrak{k}_0 \\ \rho_0 \end{matrix}, T | H^{\mathrm{W}} | 0, I \right) f_N(0)_I, \\ (E_N - \varepsilon_I{}^0) f_N(0)_I &= \sum_{\rho_0, T} \int (0, I | H^{\mathrm{W}} | \begin{matrix} \mathfrak{k}_0 \\ \rho_0 \end{matrix}, T) f_N \left(\begin{matrix} \mathfrak{k}_0 \\ \rho_0 \end{matrix} \right)_T. \end{aligned} \tag{244}$$

Mit $\Delta\varepsilon_T(\varepsilon_0, E_N)$ sei dabei der Selbstenergiebeitrag bezeichnet, der durch die Übergänge vom Ein-Meson in den Zwei-Mesonzustand und wieder zurück zustande kommt, bei denen ein- und dasselbe Meson emittiert und auch wieder

reabsorbiert wird, also

$$\begin{aligned}\Delta\varepsilon_T(\varepsilon_0, E_N) &= \sum_{\rho'_0, T'} \int \frac{(\begin{smallmatrix}\mathbf{k}_0, \\ \rho_0,\end{smallmatrix} T|H^W|\begin{smallmatrix}\mathbf{k}_0, \mathbf{k}'_0 \\ \rho_0, \rho'_0\end{smallmatrix}, T')(\begin{smallmatrix}\mathbf{k}_0, \mathbf{k}'_0 \\ \rho_0, \rho'_0\end{smallmatrix}, T'|H^W|\begin{smallmatrix}\mathbf{k}_0, \\ \rho_0,\end{smallmatrix} T)}{E_N-(\varepsilon_0+\varepsilon'_0+\varepsilon^0_{T'})}\,\mathrm{d}\mathbf{k}'_0 \\ &= \sum_{\rho'_0, T'} \int \frac{(0T|H^W|\begin{smallmatrix}\mathbf{k}'_0, \\ \rho'_0,\end{smallmatrix} T')(\begin{smallmatrix}\mathbf{k}'_0, \\ \rho'_0,\end{smallmatrix} T'|H^W|0T)}{E_N-(\varepsilon_0+\varepsilon'_0+\varepsilon^0_{T'})}\,\mathrm{d}\mathbf{k}'_0.\end{aligned} \tag{245}$$

Die Berücksichtigung dieses Selbstenergieterms erscheint insbesondere bei Verwendung von (183) als wesentlich, da dann $\Delta\varepsilon_T(\varepsilon_0, E_N)$ vom zweiten Term in (183) herrührend noch T-abhängige Beiträge der Ordnung $1/g^2$ zu den $1/g^2$-Beiträgen des zugehörigen $\varepsilon_T{}^0$-Spektrums der Gl. (44) mit (46) hinzuliefert, während dies bei den entsprechenden Termen von (184) mit (48) erst von der Ordnung g^{-4} an abwärts der Fall ist, wie schon vor (48) betont wurde. (184) ist daher auch besser geeignet für die Untersuchung der Chew-Low-Näherung der starken Kopplung [21]) und des von Nickle und Serber behandelten Renormierungsproblems [20]).

Zur Verifizierung von (216) auf Grund von (244) müssen wir zunächst unter Berücksichtigung der ε_0- und E_N-Abhängigkeit von $\Delta\varepsilon_T(\varepsilon_0, E_N)$ die Nullstellen von

$$(\varepsilon_0+\varepsilon_T+\Delta\varepsilon_T(\varepsilon_0, E_N)-E_N) = \mathcal{N}_T \tag{246}$$

aufsuchen. Dabei schreiben wir für E_N gemäß (206)

$$E_N = \varepsilon_N+\varepsilon_{\frac{1}{2}}{}^0+\Delta\varepsilon_{\frac{1}{2}}, \tag{247}$$

wobei wir für den hier zu betrachtenden Fall der instabilen Isobaren berücksichtigt haben, daß im auslaufenden Anteil des Streueigenzustandes χ_N^- das Compoundnukleon sich asymptotisch nur im Grundzustand, d.h. im Proton-Neutron-Zustand mit dem Isospinbetrag $|T_S| = \frac{1}{2}$ befinden kann. Mit (247) wird dann aus (245)

$$\Delta\varepsilon_T\{(\varepsilon_0-\varepsilon_N)\} = -\sum_{\rho'_0, T'} \int \frac{|(0, T|H^W|\begin{smallmatrix}\mathbf{k}'_0, \\ \rho'_0,\end{smallmatrix} T')|^2}{\varepsilon'_0+\varepsilon^0_{T'}-(\varepsilon_{\frac{1}{2}}{}^0+\Delta\varepsilon_{\frac{1}{2}})+(\varepsilon_0-\varepsilon_N)}\,\mathrm{d}\mathbf{k}'_0 \tag{248}$$

und aus (246)

$$\mathcal{N}_T = \varepsilon_T{}^0+\Delta\varepsilon_T\{(\varepsilon_0-\varepsilon_N)\}-(\varepsilon_{\frac{1}{2}}{}^0+\Delta\varepsilon_{\frac{1}{2}})+(\varepsilon_0-\varepsilon_N). \tag{249}$$

Der Selbstenergiebeitrag $\Delta\varepsilon_{\frac{1}{2}}$ zum Compoundnukleongrundzustand ist dann dadurch gegeben, daß $\mathcal{N}_{\frac{1}{2}} = 0$ für $\varepsilon_0 = \varepsilon_N$ sein muß. Daraus folgt:

$$\Delta\varepsilon_{\frac{1}{2}} = \Delta\varepsilon_{\frac{1}{2}}\{(\varepsilon_0-\varepsilon_N)\}_{\varepsilon_0=\varepsilon_N} = -\sum_{\rho'_0, T'} \int \frac{|(0, \frac{1}{2}|H^W|\begin{smallmatrix}\mathbf{k}'_0, \\ \rho'_0,\end{smallmatrix} T')|^2}{\varepsilon'_0+\varepsilon^0_{T'}-(\varepsilon_{\frac{1}{2}}+\Delta\varepsilon_{\frac{1}{2}})}\,\mathrm{d}\mathbf{k}_0. \tag{250}$$

Bei Entwicklung von $\Delta\varepsilon_T\{(\varepsilon_0-\varepsilon_N)\}$ nach Potenzen von $(\varepsilon_0-\varepsilon_N)$ gemäß

$$\Delta\varepsilon_T\{(\varepsilon_0-\varepsilon_N)\} = \Delta\varepsilon_T+a_T{}^{(1)}(\varepsilon_0-\varepsilon_N)+\ldots. \tag{251}$$

wird aus (249) in der in $(\varepsilon_0-\varepsilon_N)$ linearen Näherung von (251)

$$\mathcal{N}_T = (1+a_T^{(1)})\left\{\varepsilon_0-\left[\varepsilon_N-\frac{(\varepsilon_T{}^0+\Delta\varepsilon_T)-(\varepsilon_{\frac{1}{2}}{}^0+\Delta\varepsilon_{\frac{1}{2}})}{1+a_T^{(1)}}\right]\right\} \tag{252}$$

und für die Nullstellen von $\mathcal{N}_T$ folgt somit

$$(\varepsilon_0)_{\mathcal{N}_{T=0}} = \varepsilon_N-\frac{\varepsilon_T{}^0+\Delta\varepsilon_T-(\varepsilon_{\frac{1}{2}}{}^0+\Delta\varepsilon_{\frac{1}{2}})}{1+a_T^{(1)}} \equiv E_T. \tag{253}$$

$f_N\binom{\mathbf{k}_0}{\rho_0}_T$ wird dann, nach Division der ersten Gleichung von (244) durch den Näherungsausdruck (252) von $\mathcal{N}_T$ (246)

$$f_N\binom{\mathbf{k}_0}{\rho_0}_T = \delta(\mathbf{k}_0-\mathbf{k}_{E_T})\delta_{\substack{\rho_0\,\rho_N\\ T\,T_S}}-\frac{\binom{\mathbf{k}_0}{\rho_0},\,T|H^{\mathrm{W}}|0,\,I)\,f_N(0)_I}{(1+a_T^{(1)})(\varepsilon_0-E_T-i\alpha)} \tag{254}$$

mit $k_{E_T}=\sqrt{E_T{}^2-\kappa^2}$. Wie in (202), (203) und den folgenden Ausführungen, zeigt der Index T_S hier wieder den physikalischen Proton-Neutron-Zustand mit dem Isospinbetrag $\frac{1}{2}$ an, sodaß $E_{T_S}=\varepsilon_N$. Sonst ist $E_T<\varepsilon_N$ entsprechend der Verminderung der Mesonenergie um die Anregungsenergie des Isobars T.

Einsetzen von (254) in die zweite Gleichung von (244) gibt nach Berücksichtigung von (247)

$$f_N(0)_I = \frac{(0,\,I|H^{\mathrm{W}}|{}^{\mathbf{k}_N}_{\rho_N},\,T_S)}{\varepsilon_N-(\varepsilon_I{}^0+\Delta'\varepsilon_I-(\varepsilon_{\frac{1}{2}}{}^0+\Delta\varepsilon_{\frac{1}{2}}))}, \tag{255}$$

mit

$$\Delta'\varepsilon_I = -\sum_{\rho_0,\,T}\int\frac{|(0,\,I|H^{\mathrm{W}}|{}^{\mathbf{k}_0}_{\rho_0},\,T|)^2}{(1+a_T^{(1)})(\varepsilon_0-E_T-i\alpha)}\,\mathrm{d}\mathbf{k}_0. \tag{256}$$

Bei Berücksichtigung der weiteren Terme der Entwicklung (251) wäre in (256) $a_T^{(1)}$ zu ersetzen durch $a_T^{(1)}+a_T^{(2)}(\varepsilon_0-\varepsilon)+a_T^{(3)}(\varepsilon_0-\varepsilon)^2+\ldots$. Zur Abschätzung der Güte der mit der alleinigen Berücksichtigung des $a_T^{(1)}$-Termes gemachten Näherung wäre dann nachzusehen, inwieweit

$$a_T^{(2)}(\varepsilon_0-\varepsilon)+a_T^{(3)}(\varepsilon_0-\varepsilon)^2+\ldots \ll a_T^{(1)}, \tag{257}$$

wobei als Maß für $(\varepsilon_0-\varepsilon)$ etwa der Abschneideimpuls K (siehe (178)) einzusetzen wäre.

Der zweite Anteil

$$h\left(\begin{matrix}\mathbf{k}_N\\ \rho_N\\ T_{S_N}\end{matrix}\middle|\begin{matrix}\mathbf{k}\\ \rho\\ T_S\end{matrix}\right)$$

der Streuamplitude $T_{\mathbf{k}}(N)$ (siehe (219)) wird nun mit (254) und (255) entsprechend (216) und (218)

$$h\left(\begin{matrix}\mathbf{k}_N\\ \rho_N\\ T_{S_N}\end{matrix}\middle|\begin{matrix}\mathbf{k}\\ \rho\\ T_S\end{matrix}\right) = -\frac{(\binom{\mathbf{k}_N}{\rho_N},\,T_{S_N}|H^{\mathrm{W}}|0,\,I)(0,\,I|H^{\mathrm{W}}|{}^{\mathbf{k}}_{\rho},\,T_S)}{\varepsilon_N-(\varepsilon_I{}^0+\Delta'\varepsilon_I-(\varepsilon_{\frac{1}{2}}+\Delta\varepsilon_{\frac{1}{2}}))}, \tag{258}$$

wobei N bei T_{S_N} nur eine mögliche Änderung der Ladung ohne Änderung des Isospinbetrags anzeigen soll.
(258) hat die Gestalt einer Formel für Resonanzstreuung. Eine Resonanzstreuung kann aber nur auftreten, wenn

$$\varepsilon_I + \mathrm{Re}\, \Delta'\varepsilon_I - (\varepsilon_{\frac{1}{2}} + \Delta\varepsilon_{\frac{1}{2}}) > \kappa. \tag{259}$$

Dann ergibt die linke Seite von (259) die Resonanzenergie (siehe (271)) und die Resonanzbreite ist durch $\mathrm{Im}\, \Delta'\varepsilon_I$ gegeben. Ein solcher Imaginärteil von $\Delta'\varepsilon_I$ folgt daraus, daß der Nenner im Integranden von (256) entsprechend (253) immer wenigstens die Nullstelle $\varepsilon_0 = \varepsilon$ für $|T| = \frac{1}{2}$ besitzt. Dann bekommt man den Imaginärteil von $\Delta'\varepsilon_I$ auf Grund der Zerlegung des Integrals (256) in Hauptwertanteil und δ-Funktionsanteil gemäß

$$\frac{1}{\varepsilon_0 - E_T - i\alpha} = \mathrm{P}\,\frac{1}{\varepsilon_0 - E_T} + i\pi\delta(\varepsilon_0 - E_T). \tag{260}$$

Zur Nachprüfung von (259) und zur dementsprechenden Berechnung von Resonanzenergie- und Breite müssen wir im Folgenden zu numerischen Berechnungen von $\Delta'\varepsilon_I$ mit den entsprechenden H^{W}-Matrixelementen der aus der Neuaufspaltung des Hamiltonoperators folgenden H^{W}-Ausdrücke (183) oder (184) übergehen.

3.3.2. *Matrixelemente*

Wir diskutieren hier nur kurz die Berechnung von $\Delta'\varepsilon_I$ und die daraus folgenden Ergebnisse für die Resonanzenergie- und Breite auf der Basis von (183). Berechnungen von $\Delta'\varepsilon_I$ auf der Basis von (184) sollen in einer folgenden Arbeit behandelt werden, eventuell gleich in Anwendung auf den physikalisch wichtigereren Fall der symmetrischen pseudoskalaren Theorie.

Zu den in (244) auftretenden H^{W}-Matrixelementen tragen nur diejenigen Terme von H^{W} bei, in denen die Operatoren $a_{\rho_0\mathbf{k}_0}$ und $a^*_{\rho_0\mathbf{k}_0}$ der freien Mesonen in ungerader Anzahl miteinander multipliziert vorkommen. Wir wollen hier nur die Beiträge der Ordnung g^{-1} berücksichtigen. Diese kommen bei (183) nur vom zweiten Term (siehe die Bemerkungen nach (245)), und zwar erhält man einen in $a_{\rho_0\mathbf{k}_0}$ und $a^*_{\rho_0\mathbf{k}_0}$ linearen Term, der bei der Berücksichtigung von (23), (24) und (160) lautet:

$$\hat{H}^{\mathrm{W}}_{(1)} = -\frac{2\pi}{gb}\sum_{\rho_0,\sigma}\langle S_\sigma \mathscr{T}_{\rho_0\sigma}\rangle \int\left(\frac{\varepsilon_0}{i}\right)^{\frac{1}{2}} i(v_{0\mathbf{k}_0}a^*_{\rho_0\mathbf{k}_0} - v^*_{0\mathbf{k}_0}a_{\rho_0\mathbf{k}_0})\,\mathrm{d}\mathbf{k}_0 \tag{261}$$

und einen Term von dritter Ordnung in $a^*_{\rho_0\mathbf{k}_0}$ und $a_{\rho_0\mathbf{k}_0}$

$$H^{\mathrm{W}}_{(3)} = \frac{2\pi}{gb}\sum_{\rho_0}\left\langle A_{\rho_0}\int\left(\frac{\varepsilon_0}{2}\right)^{\frac{1}{2}} i(v_{0\mathbf{k}_0}a^*_{\rho_0\mathbf{k}_0} - v^*_{0\mathbf{k}_0}a_{\rho_0\mathbf{k}_0})\,\mathrm{d}\mathbf{k}_0\right\rangle \tag{262}$$

mit dem Ausdruck (186) für A_ρ. Der erste Term von (183) trägt entsprechend den Bemerkungen nach (119) nur in Verbindung mit den Übergängen zu den höheren Niveaus mit $\bar{\tau}_3 = +1$ etwas bei, die wir aber gemäß (188) hier nicht berücksichtigen wollen. Daher haben wir auch die $\tau_{3\rho}$-Terme fortgelassen, die auf Grund von (23) und (34) in (261) sonst noch auftreten müßten.

Aus (261) folgt für das in (244) einzusetzende Matrixelement von $H^{\mathrm{W}}_{(1)}$

$$(I0|\hat{H}^{\mathrm{W}}_{(1)}|^{\mathbf{k}_0}_{\rho_0}, T) = i\frac{2\pi}{gb}\left(\frac{\varepsilon'_0}{2}\right)^{\frac{1}{2}} v^*_{0\mathbf{k}'_0} \sum_\sigma \langle S_\sigma \mathscr{T}_{\rho_0\sigma}\rangle|^T_I . \tag{263}$$

Es unterscheidet sich $H^{\mathrm{W}}_{(3)}$ von $H^{\mathrm{W}}_{(1)}$ lediglich durch das Auftreten von A_ρ Gl. (186) an Stelle von $-\sum_\sigma\langle S_\sigma \mathscr{T}_{\rho\sigma}\rangle$. Mit (186) erhält man nach einigen Umformungen für das in (244) einzusetzende $H^{\mathrm{W}}_{(3)}$-Matrixelement

$$(I0|\hat{H}^{\mathrm{W}}_{(3)}|^{\mathbf{k}_0}_{\rho_0}, T) = \frac{2\pi}{gb}\frac{1}{\sqrt{2}b}\int \frac{|v_{0\mathbf{k}'_0}|^2\varepsilon'_0}{\varepsilon'_0-\varepsilon_0{}^2}\,\mathrm{d}\mathbf{k}'_0\,\frac{v(k_0)}{\varepsilon_0{}^{\frac{1}{2}}}\,(I|S_{\rho_0}|T). \tag{264}$$

Damit ergibt sich das gesamte Matrixelement zu

$$(I0|\hat{H}^{\mathrm{W}}|^{\mathbf{k}_0}_{\rho_0}, T) = \frac{2\pi}{gb}\left\{i\left(\frac{\varepsilon_0}{2}\right)^{\frac{1}{2}} v^*_{0\mathbf{k}_0}(I|\sum_\sigma\langle S_\sigma \mathscr{T}_{\rho_0\sigma}\rangle|T) + \frac{1}{\sqrt{2}b}\int \frac{|v_{0\mathbf{k}'_0}|^2\varepsilon'_0}{\varepsilon'_0{}^2-\varepsilon_0{}^2+i\alpha}\,\mathrm{d}\mathbf{k}'_0\,\frac{v(k_0)}{\varepsilon_0{}^{\frac{1}{2}}}\,(I|S_{\rho_0}|T)\right\}. \tag{265}$$

Aus den Kommutatoren (20) ergibt sich ferner

$$\sum_\sigma\langle S_\sigma \mathscr{T}_{\rho\sigma}\rangle = \frac{i}{2}\,[S_{\rho_0}, \mathscr{T}^2]. \tag{266}$$

Mit (266) können wir die Matrixelemente von $\sum_\sigma\langle S_\sigma \mathscr{T}_{\rho\sigma}\rangle$ durch die Matrixelemente von S_ρ ((224)—(227)) und die Eigenwerte von $\mathscr{T}^2$ ausdrücken:

$$(I|\sum_\sigma\langle S_\rho \mathscr{T}_{\rho\sigma}\rangle|T) = \frac{i}{2}\,(I|[S_\rho, \mathscr{T}^2]|T) = \frac{i}{2}\,(I|S_\rho|T)(I(I+1)-T(T+1)). \tag{267}$$

Der in $\Delta'\varepsilon_I$ (256) sowie in $\Delta\varepsilon_T$ (248) und $\Delta\varepsilon_{\frac{1}{2}}$ (250) benötigte Absolutbetrag von (265) wird damit

$$|(I0|\hat{H}^{\mathrm{W}}|^{\mathbf{k}_0}_{\rho_0}, T)|^2 = \left(\frac{2\pi}{gb}\right)^2\left\{\frac{\varepsilon_0}{2}\,|v_{0\mathbf{k}_0}|^2\left|\left(I\left|\frac{[S_{\rho_0}, \mathscr{T}^2]}{2}\right|T\right)\right|^2\right.$$

$$-\frac{1}{4b}\left[v_{0\mathbf{k}'_0}\left(\int\frac{|v_{0\mathbf{k}'_0}|^2\varepsilon'_0}{\varepsilon'_0{}^2-\varepsilon_0{}^2+i\alpha}\,\mathrm{d}\mathbf{k}'_0\right)+v^*_{0\mathbf{k}'_0}\left(\int\frac{|v_{0\mathbf{k}'_0}|^2\varepsilon'_0}{\varepsilon'_0{}^2-\varepsilon_0-i\alpha}\,\mathrm{d}\mathbf{k}'_0\right)\right](I|[S_{\rho_0}, \mathscr{T}^2]|T)(T|S_{\rho_0}|I)$$

$$\left.+\frac{1}{2b^2}\left|\int\frac{|v_{0\mathbf{k}'_0}|^2\varepsilon'_0}{\varepsilon'_0{}^2-\varepsilon_0{}^2+i\alpha}\,\mathrm{d}\mathbf{k}'_0\right|^2\frac{[v(k_0)]^2}{\varepsilon_0}\,|(I|S_{\rho_0}|T)|^2\right\}. \tag{268}$$

3.3.3. *Numerische Rechnungen*

Die Ausdrücke (248), (250) und (256) für $\Delta\varepsilon_T$, $\Delta\varepsilon_{\frac{1}{2}}$ und $\Delta'\varepsilon_I$ bestehen aus Integralen der Form

$$\int \frac{|(0, I|H^{\mathrm{W}}|^{\mathbf{k}_0}_{\rho_0}, T)|^2}{\varepsilon_0 + B_T} \mathrm{d}\mathbf{k}_0, \tag{269}$$

worin mit $B_{T'}$ die von ε'_0 unabhängigen Summanden bezeichnet sind. Diese lauten:
für $\Delta\varepsilon_T$ (248) und mit $\varepsilon_0 = \varepsilon$ für $\Delta\varepsilon_{\frac{1}{2}}$ (250):

$$B\{(\varepsilon_0 - \varepsilon_N)\}_{T'} = \varepsilon^0_{T'} - (\varepsilon_{\frac{1}{2}}{}^0 + \Delta\varepsilon_{\frac{1}{2}}) + (\varepsilon_0 - \varepsilon_N)$$
$$= \bar{B}_{T'} + (\varepsilon_0 - \varepsilon_N - \Delta\varepsilon_{\frac{1}{2}}), \quad \text{mit } \bar{B}_{T'} = \varepsilon^0_{T'} - \varepsilon_{\frac{1}{2}}{}^0, \tag{270a}$$

für $\Delta'\varepsilon_I$ (256):

$$B'\{\varepsilon_N\}_{T'} = -E_{T'} = \bar{B}'_{T'} - \varepsilon_N, \quad \text{mit } \bar{B}'_{T'} = \frac{(\varepsilon^0_{T'} + \Delta\varepsilon_{T'}) - (\varepsilon_{\frac{1}{2}}{}^0 + \Delta\varepsilon_{\frac{1}{2}})}{1 + a_{T'}}. \tag{270b}$$

Durch die Einführung der Bezeichungen $\bar{B}_{T'}$ und $\bar{B}'_{T'}$ sind in (270a, b) noch die $B_{T'}$ und $B'_{T'}$ in T'-abhängige und T'-unabhängige Glieder unterteilt.

Mit dem Ausdruck (268) für das Absolutquadrat des Matrixelementes haben wir auf Grund der vorstehenden Formeln numerische Berechnungen von $\Delta\varepsilon_T$, $\Delta\varepsilon_{\frac{1}{2}}$ und $\Delta'\varepsilon_I$ auf der Basis der Entwicklung (251) sowie einer entsprechenden Entwicklung von $\Delta'\varepsilon_I$ nach ε durchgeführt. Dabei haben wir die Wahl (178) für die Fouriertransformierte der Quellfunktion mit den dazugehörigen Ausdrücken (181) und (182) für $v_{0\mathbf{k}}$ und $|v_{0\mathbf{k}}|^2$ zugrundegelegt. Die Ergebnisse für eine der Nukleonmasse entsprechende Wahl des cut-off K und einen Wertebereich der Kopplungskonstanten, für den die Näherungsbedingungen der starken Kopplung (188)—(197) sowie (236) gut erfüllt sind, haben wir in der Tabelle 1 wiedergegeben.

Die in den Zeilen 4 und 5 wiedergegebenen $\bar{B}_T$-Werte entsprechen bei der hier zugrundegelegten Verwendung von (183) als Basis der Rechnung dem Eigenwertspektrum von (44) mit (46). Zeile 3 enthält die Werte für die $\bar{\tau}_3$-Energiedifferenz. Der Vergleich der Zeilen 4, 5, 10, 13, 16 und 18 mit Zeile 3 zeigt die gute Erfüllung von (36) bzw. (188) bzw. der entsprechenden Bedingung für alle hier berechneten oder in die Rechnung eingehenden Werte der Isobarenenergiedifferenzen. Weiterhin zeigen die Zeilen 7, 8, 9, 11, 12 und 14 eine gute Erfüllung von (257) und die Zeilen 15, 17, 19 und 21 eine gute Erfüllung der entsprechenden Bedingung für die Entwicklung von $\Delta'\varepsilon_I$ nach ε in dem größten Teil des betrachteten Wertebereiches der Kopplungskonstanten. Die günstigsten Werte der Rechnung liegen etwa bei $g^2 = 36$ mit dem (259) erfüllenden Resonanzenergiewert

$$E_{R_{\frac{3}{2}}} = \frac{\varepsilon_{\frac{3}{2}}{}^0 - \varepsilon_{\frac{1}{2}}{}^0 + \mathrm{Re}\,\Delta'\varepsilon_{\frac{3}{2}} - \Delta\varepsilon_{\frac{1}{2}}}{1 + a'_{\frac{3}{2}}} = 2.04\kappa \tag{271}$$

TABELLE 1

Ergebnisse der Berechnung der Resonanzenergie $E_{R_{\frac{1}{2}}}$ und und Breite $\frac{1}{2}\Gamma_{\frac{1}{2}}$

1	g^2	27	30	33	36	39	42	48
2	$\left(\frac{g}{2\pi}\right)^2$	0.684	0.761	0.836	0.911	0.988	1.063	1.215
3	$2\left(\frac{g}{2\pi}\right)^2 \frac{b}{\kappa}$	68.6	76.2	83.9	91.5	99.1	106.8	121.8
4	$\frac{B_{\frac{1}{2}}}{\kappa}$	3.703	3.328	3.029	2.789	2.563	2.383	2.084
5	$\frac{\bar{B}_{\frac{1}{2}}}{\kappa}$	9.874	8.875	8.078	7.413	6.836	6.353	5.559
6	$\frac{\Delta\varepsilon_{\frac{1}{2}}}{\kappa}$	−4.586	−3.807	−3.337	−3.003	−2.742	−2.540	−2.230
7	$1+a_{\frac{1}{2}}^{(1)}$	0.366	0.597	0.729	0.817	0.880	0.925	0.987
8	$(a_{\frac{1}{2}}^{(2)}K+a_{\frac{1}{2}}^{(3)}K^2)$	0.036	0.109	0.148	0.170	0.184	0.191	0.196
9	$1+a_{\frac{1}{2}}^{(1)}$	0.832	0.789	0.786	0.800	0.822	0.846	0.893
10	$\frac{B'_{\frac{1}{2}}}{\kappa}$	4.664	3.379	2.703	2.277	1.975	1.756	1.443
11	$(a_{\frac{1}{2}}^{(2)}K+a_{\frac{1}{2}}^{(3)}K^2)$	−0.478	−0.294	−0.177	−0.095	−0.036	0.007	0.064
12	$1+a_{\frac{1}{2}}^{(1)}$	3.600	2.506	1.990	1.529	1.295	1.153	1.006
13	$\frac{\bar{B}'_{\frac{1}{2}}}{\kappa}$	6.721	5.759	5.123	4.650	1.975	3.963	3.458
14	$(a_{\frac{1}{2}}^{(2)}K+a_{\frac{1}{2}}^{(3)}K^2)$	−1.330	−0.966	−0.717	−0.536	−0.399	−0.298	−0.155
15	$1+a_{\frac{1}{2}}^{(1)}$	1.100	1.113	1.140	1.169	1.198	1.221	1.253
16	$\frac{E_{R_{\frac{1}{2}}}}{\kappa}$	3.965	3.543	2.746	2.042	1.471	1.057	0.868
17	$a_{\frac{1}{2}}^{(2)'}E_{R_{\frac{1}{2}}}+a_{\frac{1}{2}}^{(3)'}E_{R_{\frac{1}{2}}}^2$	−0.255	−0.080	−0.014	+0.012	0.020	0.020	0.029
18	$\frac{\frac{1}{2}\Gamma_{\frac{1}{2}}}{E_{R_{\frac{1}{2}}}}$	0.702	0.411	0.342	0.299	0.244	0.106	
19	$1+a_{\frac{1}{2}}^{(1)}$	1.471	1.433	1.440	1.433	1.416	1.396	1.360
20	$\frac{E_{R_{\frac{1}{2}}}}{\kappa}$	−0.451	−0.565	−0.637	−0.630	−0.585	−0.530	−0.420
21	$a_{\frac{1}{2}}^{(2)'}E_{R_{\frac{1}{2}}}+a_{\frac{1}{2}}^{(3)'}E_{R_{\frac{1}{2}}}^2$	−0.023	−0.034	−0.039	−0.037	−0.032	−0.027	−0.019

und der Resonanzbreite

$$\frac{\Gamma_{\frac{1}{2}}}{2} = 0.61\kappa. \tag{272}$$

Die Größe $E_{R_{\frac{1}{2}}}$ ergibt wegen seiner viel zu kleinen und negativen Werte keine Resonanzenergie. Die ziemlich großen negativen $\Delta\varepsilon_{\frac{1}{2}}/\kappa$-Werte (Zeile 6) tragen wesentlich dazu bei, daß bei den in Frage kommenden nicht zu großen ε-Werten der Nenner von (248) im Unterschied zu dem von (256) keine Nullstellen besitzt und somit $\Delta\varepsilon_T$ im Unterschied zu $\Delta'\varepsilon_I$, wie es sein muß, reell ist.

3.3.4. $(1/g^2)$-*Beiträge zur Resonanzenergie*

Wie schon im Anschluß an (245) bemerkt wurde, liefert bei der den vorstehenden Rechnungen zugrunde gelegten Aufspaltung (183), welcher als Isobarenspektrum der nullten Näherung das Eigenwertspektrum von (44) mit (46) zugrunde gelegt ist, die Selbstenergiekorrektur $\Delta\varepsilon_T$ bzw. $\Delta'\varepsilon_I$ zu den $1/g^2$-Beiträgen von (44) mit (46) noch Beiträge der Ordnung $1/g^2$-hinzu, mit denen zusammen sich erst die vollständige $1/g^2$-Näherung des Isobarenspektrums ergibt. Diese $1/g^2$-Beiträge von $\Delta\varepsilon_T$ bzw. $\Delta'\varepsilon_I$ rühren nur von dem ersten Term in (268) her, während die anderen beiden Terme in (268) T-abhängige Beiträge gemäß (21) und (27) erst in Verbindung mit den T-abhängigen Nennern in (245) und (256) (siehe (269) und (270)), d.h. also erst von Ordnung g^{-4} an abwärts liefern. Der T-abhängige $1/g^2$-Beitrag von $\Delta\varepsilon_T$ bzw. $\Delta'\varepsilon_I$ wird also bei Berücksichtigung (267), (266) und den in Absatz 2.1.4 wiedergegebenen Vertauschungseigenschaften der S_ρ und $\mathcal{T}_{\rho\sigma}$-Operatoren

$$(\Delta\varepsilon_T)_{\frac{1}{g^2}} = -\tfrac{1}{2}\left(\frac{2\pi}{gb}\right)^2 \int |v_{0\mathbf{k}}|^2 \mathrm{d}\mathbf{k} \cdot T(T+1). \tag{273}$$

(273) ergibt aber auf Grund von (159) mit den Eigenwerten von (44) mit (46) zusammen gerade das Eigenwertspektrum von (48) bis zur Ordnung $1/g^2$, welches entsprechend den Bemerkungen vor (48) und im Anschluß an (245) das vollständige Isobarenspektrum bis zur Näherung $1/g^2$ ist. Seine numerische Auswertung bei Benutzung von (178) mit dem gleichen K-Wert wie bei der vorstehend besprochenen Rechnung liefert für die niedrigste Anregungsstufe bei $g^2 = 36$:

$$(\varepsilon_{\frac{3}{2}} - \varepsilon_{\frac{1}{2}})_{\frac{1}{g^2}} = 0.25\kappa \tag{274}$$

d.h. also nur $\frac{1}{8}$ des Wertes (271). Die in der Tabelle wiedergegebenen Werte für $E_{R_{\frac{3}{2}}}$ rühren also ebenso wie die ungefähr gleich großen Werte von $\bar{B}'_{\frac{3}{2}}$ nur zu einem Bruchteil ($\frac{1}{8}$ für $g^2 = 36$) vom $1/g^2$-Beitrag her, sondern den Hauptanteil bilden die von der Ordnung g^{-4} an abwärts gehenden Beiträge, die auf Grund der T-abhängigen Anteile der Nenner in (245) und (256) (siehe (269) und (270)) auch vom zweiten und dritten Term in (268) herrührend zustande kommen. Zu den Ordnungen von g^{-4} an abwärts liefern aber auch die weiteren

Terme von (183), insbesondere auch die von den höheren Entwicklungsgliedern der Nenner in (183) herrührenden Terme noch Beiträge, die wir hier fortgelassen haben, und die noch berücksichtigt werden müßten. Dies kann wohl besser in dem (184) entsprechenden Aufspaltungsfall geschehen, wie es Nickle und Serber [20]) bei der Berechnung der g^{-4}-Korrektur zum Isobarenspektrum für die geladene skalare Theorie getan haben. Das Studium des Chew-Low-Formalismus scheint aber andererseits zu zeigen [21]), daß bei einem so schwach cut-off-abhängigen Modell, wie es die skalare Theorie darstellt, gar keine Instabilität der Isobaren zu bekommen ist, sondern daß dazu erst eine so starke cut-off-Abhängigkeit nötig ist, wie sie die pseudoskalare Theorie aufweist.

Das würde bedeuten, daß die Erfüllung von (259) durch die meisten E_{R_l}-Werte der Tabelle nur durch die Unvollkommenheit unserer Näherung zustande kommt. Allerdings sind die genannten Untersuchungen [21]) zu dieser Frage am Chew-Low-Formalismus bei der schwach cut-off-abhängigen skalaren Theorie nur im geladenen Fall und nur für den im geladenen skalaren Fall möglichen Grenzfall der Punktquelle durchgeführt und müßten erst auf den vorstehend behandelten Fall der symmetrischen, skalaren Theorie mit endlichem cut-off ausgedehnt werden, um über diese Frage entgültiges sagen zu können.

Die Behandlung des Chew-Low-Formalismus bei den stärkeren cut-off-abhängigen Theorieen zeigt andererseits [26, 41]), daß bei diesen Theorieen die Resonanzenergie eher durch $1/g^2$-Beiträge allein wiedergegeben wird, als bei der hier behandelten skalaren Theorie. So wäre eine $1/g^2$-Näherung bei einer starken cut-off-abhängigen Theorie sinnvoller und das vorstehende Näherungsverfahren somit noch besser anwendbar.

Die zuletzt dargelegte Rechnung soll hauptsächlich zeigen, wie eine Berechnung der Resonanzenergie- und Breite durch die in der vorliegenden Arbeit entwickelte, die Bedingung 4) Absatz 2.1.6 erfüllende Aufteilung des Hamiltonoperators, die die Compoundnukleon- und freien Mesonfeldanteile durchgehend als voneinander getrennte Teilsysteme behandelt, prinzipiell ermöglicht wird. Damit ist eine methodische Vorlage für eine entsprechende Rechnung an dem komplizierteren, aber physikalisch wesentlicheren und für das Näherungsverfahren wegen seiner stärkeren cut-off-Abhängigkeit offenbar auch günstigen Modell der symmetrischen pseudoskalaren Theorie gegeben.

Mein Dank gilt Herrn Professor Dr. W. Heisenberg und der Feldtheoretischen Arbeitsgrupppe des Max-Planck-Institutes für Physik, für die Aufnahme im Institut und für anregende Diskussionen. Ganz besonders möchte ich den Herren Prof. Dr. R. Haag, Prof. Dr. H. Lehmann, Prof. Dr. G. Lüders, Prof. Dr. K. Symanzik und Dr. W. Zimmermann für ihr Interesse und die mir gewährten Aussprachen danken.

Literatur

1) G. Wentzel, Helv. Phys. Acta **13** (1940) 169, **14** (1941) 633
2) G. Wentzel, Helv. Phys. Acta **26** (1943) 222, 551
3) R. Oppenheimer u. J. Schwinger, Phys. Rev. **60** (1941) 150
4) W. Pauli u. S. M. Dancoff, Phys. Rev. **62** (1942) 85
5) W. Heisenberg, Zeitschrift f. Physik **113** (1939) 61;
S. Tomonaga, Prog. Theor. Phys. **1** (1946) 83
6) R. Serber u. S. M. Dancoff, Phys. Rev. **63** (1943) 143
7) W. Pauli u. S. Kusaka, Phys. Rev. **63** (1943) 400;
M. Fierz u. G. Wentzel, Helv. Phys. Acta **17** (1944) 215;
F. Coester, Helv. Phys. Acta **17** (1944) 35;
G. Wentzel, Helv. Phys. Acta **17** (1944) 251;
K. Bleuler, Helv. Phys. Acta **17** (1944) 405, **18** (1945) 317;
K. W. Chun, preprint (1960)
8) A. Houriet, Helv. Phys. Acta **18** (1945) 473
9) S. Tomonaga, Prog. Theor. Phys. **1** (1946) 109
10) G. Wentzel, Rev. Mod. Phys. **19** (1947) 1
11) W. Pauli, Meson Theory of Nuclear Forces (Interscience, New York, 1948) (Zusammenfassende Darstellung)
12) T. Miyazima, T. Tati u. S. Tomonaga, Prog. Theor. Phys. **3** (1948) 26
13) A. N. Kaufman, Phys. Rev. **92** (1953) 468
14) B. T. Geilikman, JETP USSR **29** (1955) 417, Soviet Phys. JETP **2** (1956) 509
15) V. N. Baier u. S. I. Pekar, Soviet Phys. JETP **3** (1956/57) 340;
S. I. Pekar, Soviet Phys. JETP **3** (1956/57) 205
16) J. Hamilton, Phys. Rev. **97** (1955) 1390;
S. F. Edwards, Proc. Roy. Soc. Lond. A **243** (1957/58) 458
17) A. Pais u. R. Serber, Phys. Rev. **105** (1957) 1636
18) A. Pais u. R. Serber, Phys. Rev. **113** (1959) 955
19) L. Landovitz u. B. Margolis, Phys. Rev. Letters **1** (1958) 206, **2** (1959) 318, Ann. Physics **7** (1959) 52
20) H. Nickle u. R. Serber, Phys. Rev. **119** (1960) 449
21) H. Jahn, Zeitschrift f. Physik **156** (1959) 633; Forschr. d. Phys. **7** (1959) 452
22) M. Gell-Mann u. M. L. Goldberger, Phys. Rev. **87** (1952) 218;
G. Wentzel, Phys. Rev. **92** (1953) 173, Lectures on strong coupling mesons theory, Rochester, Spring 1954;
H. Miyazawa, Phys. Rev. **99** (1955) 944, **97** (1955) 1399;
A. Pais u. R. Serber, Phys. Rev. **105** (1957) 1636
23) M. A. Ruderman u. S. Gasiorowics, Nuovo Cim. **8** (1958) 861
24) C. J. Goebel, Phys. Rev. **109** (1958) 1846
25) G. F. Chew u. F. E. Low, Phys. Rev. **101** (1956) 1579
26) T. D. Lee u. R. Serber, mitgeteilt in Castillejo, Dalitz u. Dyson, Phys. Rev. **101** (1956) 453 und in Ref. [25]) (siehe auch Ref. [24, 21b]))
27) F. E. Low, Phys. Rev. **97** (1955) 1392
28) F. Hund, Zeitschrift f. Phys. **36** (1926) 657, **42** (1927) 93;
W. Weizel, Zeitschrift f. Phys. **54** (1929) 321, **56** (1929), 727 **31** (1930) 880
29) R. Becker u. G. Leibfried, Zeitschrift f. Phys. **125** (1949) 347
30) G. C. Wick, Rev. Mod. Phys. **27** (1955) 339
31) H. Eckstein, Nuovo Cim. **4** (1956) 1017
32) W. Brenig u. R. Haag, Fortschritte d. Phys. **7** (1959) 183

33) H. Lehmann, K. Symanzik u. W. Zimmermann, Nuovo Cim. **1** (1955) 205
34) W. Pauli, ausgewählte Kapitel aus der Feldquantisierung, Zürich (1950/51)
35) S. J. Lindenbaum u. R. M. Sternheimer, Phys. Rev. **106** (1957) 1107, **105** (1957) 1874, **109** (1958) 1227
36) M. Born, u. P. Jordan, Elementare Quantenmechanik (Springer Verlag, Berlin, 1930)
37) W. Pauli, Handbuch der Physik **24**/1, 2. Auflage (1933), Seite 182
38) M. Fierz, Helv. Phys. Acta **17** (1944) 181
39) P. A. M. Dirac, The Principles of Quantum Mechanics (Oxford University Press, Oxford, 1954)
40) W. Heitler, Quantum Theory of Radiation (Oxford University Press, Oxford, 1954)
41) H. Jahn, siehe vervielfältigtes Vortragsmanuskript über „Die Näherungen der starken Kopplung in der Mesonentheorie", Oberwolfach (1959)
42) H. Jahn, preprint März 1961, erscheint demnächst in Phys. Rev.

2.F:2.L

Nuclear Physics **26** (1961) 420—433; © *North-Holland Publishing Co., Amsterdam*

Not to be reproduced by photoprint or microfilm without written permission from the publisher

EXCITATION OF THE GIANT DIPOLE RESONANCE BY INELASTIC PROTON SCATTTERING ON CARBON

E. A. SANDERSON

Department of Mathematical Physics, University of Birmingham

Received 28 February 1961

Abstract: The inelastic scattering of 185 MeV protons leaving the C^{12} nucleus in a "giant resonance" final state is studied using the method of distorted waves. The distortion of the scattered proton is calculated in the semi-classical approximation using an optical potential with a theoretical root-mean-square radius equal to 3.04 fm. The impulse approximation is employed. Coulomb corrections are also included. Comparison of the results with experiment is discussed in some detail, with a view to the interpretation of the observed resonances.

1. Introduction

Recent measurements of inelastic proton scattering on carbon at 185 MeV by Tyrén and Maris [1]) reveal two very similar giant resonances centred at about 22 MeV and 19 MeV excitation energy. Calculations based on the particle-hole interaction theory [2]) predict most of the electric dipole strength to lie at 22.5 MeV with a strong magnetic quadrupole resonance 2 or 3 MeV below this. The angular dependence of the observed resonances supports these predictions.

In this paper we present calculations of the differential cross-section for the reaction

$$p+C^{12} \rightarrow p'+(C^{12})^*,$$

leaving C^{12} in 1^- and 2^- states of ≈ 20 MeV excitation energy, using the direct interaction theory.

In the last few years direct interaction theory, as developed by Butler [3]) and others, has been used extensively to calculate scattering of particles by nuclei. The so-called "cut-off Born approximation", which the Butler technique employs at low energies has met with success in predicting angular distributions for the scattered particles but, in general, the absolute magnitudes of cross-sections have not been reproduced too well. Even full-scale distorted wave calculations [4–6]), in which the wave functions of incident and scattered particles are calculated in complex wells, have met with only limited success in predicting absolute cross-sections. At high energies one would expect the situation to be different. Here the impulse approximation should describe the elementary collision quite well, removing one of the greatest uncertainties of the calcula-

tions at lower energies. Furthermore, the distortions are relatively easy to take into account at the higher energies, as we shall show.

Our model, then, consists of the incident proton being scattered inelastically by one of the nucleons in the nucleus, while its interaction with the other $(A-1)$ nucleons is represented by the effect of a central distorting potential which partially absorbs the scattered proton both before and after its collision. The distortion is calculated within the framework of the semi-classical approximation (see for example refs. [7,8])). Some justification for this approach is given in papers by Squires [9]) and McCauley and Brown [10]). The approximation involved is that the deflection of the incident particle by the optical potential is neglected. We also employ small-angle approximations making use of the fact that dipole scattering occurs predominantly through small angles.

We assume most of the strength of the level considered, 1^- or 2^-, to lie in the region of energies considered, and therefore employ closure, which removes the necessity for knowing the final state wave function of the nucleus.

By using the short range approximation for nuclear forces we are able to obtain the Fourier transform $V(q)$, of the nucleon-nucleon potential as a multiplicative factor in the scattering amplitude. Employing the impulse approximation [11]), we then replace $V(q)$ by a t-matrix [12,13]). However, since the transition is from a nuclear ground state of total isobaric spin $T = 0$ to an excited state with $T = 1$ we must, in fact, replace $V(q)$ by only the vector part (in isobaric spin space) of the t-matrix. This point is discussed in sect. 5.

Finally, Coulomb scattering corrections are applied, although these turn out to be relatively unimportant.

Comparison with the experimental results of Tyrén and Maris [1]) is made.

2. Distorted Wave Formalism

The initial system consists of an incident proton and a ground state carbon nucleus. The final system is an out-going proton and an excited carbon nucleus. Thus, in distorted wave Born approximation the transition amplitude T_{0f}, is given by

$$T_{0f} = \int \psi_f^*(\mathbf{r}_1, \mathbf{r}_2, \ldots \mathbf{r}_A)\chi_{out}(\mathbf{k}', \mathbf{r}) \sum_{j=1}^{A} V(|\mathbf{r}-\mathbf{r}_j|)\chi_{in}(\mathbf{k}, \mathbf{r})\psi_0(\mathbf{r}_1, \mathbf{r}_2, \ldots \mathbf{r}_A)\mathrm{d}\mathbf{r} \prod_{i=1}^{A} \mathrm{d}\mathbf{r}_i, \tag{2.1}$$

where ψ_0, ψ_f are the initial and final wave functions of the nucleus, respectively, while χ_{in}, χ_{out} are the distorted wave functions of the proton, incident with momentum $\hbar\mathbf{k}$ and scattered with momentum $\hbar\mathbf{k}'$. The operator $V(|\mathbf{r}-\mathbf{r}_j|)$ is the interaction potential of the projectile proton with the jth nucleon in the nucleus.

Using a central optical potential $\hat{V}(r)$ and the semi-classical approximation,

we have

$$\chi_{\rm in}(\mathbf{k}', \mathbf{r}) = e^{i\mathbf{k}\cdot\mathbf{r}} \exp\left[-i\frac{E}{k}\int_{-\infty}^{z_0} \hat{V}(r)dz\right],$$

$$\chi^*_{\rm out}(\mathbf{k}', \mathbf{r}) = e^{-i\mathbf{k}'\cdot\mathbf{r}} \exp\left[-i\frac{E}{k'}\int_{z_0}^{\infty} \hat{V}(r)dz'\right],$$

where $E = (k^2+M^2)^{\frac{1}{2}}$ is the relativistic proton energy ($\hbar = c = 1$), M is the proton mass and the directions $\hat{Z}$ and $\hat{Z}'$ are defined so that $\hat{Z} \parallel k$ and $Z' \parallel k'$. We have neglected here the deflection of the path of the proton by the optical potential. (See for example Glauber [14]). Since the loss in energy of the scattered proton is about 10 % only of its original energy $k' \approx k$; and since the scattering takes place mainly through small angles, $\mathbf{k}'$ is almost parallel to $\mathbf{k}$, i.e. $\hat{\mathbf{Z}} \approx \hat{\mathbf{Z}}'$ (see fig. 1) and hence we have

$$\chi_{\rm in}(\mathbf{k}, \mathbf{r})\chi^*_{\rm out}(\mathbf{k}', \mathbf{r}) \approx e^{i\mathbf{q}\cdot\mathbf{r}}\Gamma(b), \tag{2.2}$$

where $\mathbf{q} \equiv \mathbf{k} - \mathbf{k}'$ is the momentum transfer, and

$$\Gamma(b) \equiv \exp\left[-i\frac{E}{K}\int_{-\infty}^{\infty} \hat{V}(r)dz\right], \tag{2.3}$$

where b is the impact parameter of the projectile.

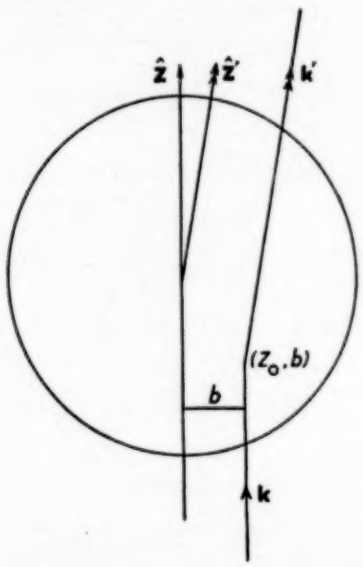

Fig. 1. Schematic representation of scattering through small angles.

Then from (2.1), (2.2) and (2.3) we have

$$T_{0f} = \sum_{j=1}^{A}\int \psi_f^*\psi_0 V(|\mathbf{r}-\mathbf{r}_j|)e^{i\mathbf{q}\cdot\mathbf{r}}\Gamma(b)d\mathbf{r}\prod_{i=1}^{A} d\mathbf{r}_i. \tag{2.4}$$

We now assume that $\Gamma(b)$ varies very little over distances of the order of the nucleon-nucleon interaction range. This enables us to replace $\Gamma(b)$ by $\Gamma(b_j)$

in (2.4). The error resulting from this approximation is roughly estimated from the form (3.3) of $\Gamma(b)$ and is found to be sufficiently small for our purposes,† certainly not greater than 10 %.

Putting $e^{iq\cdot r}$ as $e^{iq\cdot(r-r_j)}\cdot e^{iq\cdot r_j}$ we can now rewrite (2.4) in the form

$$T_{0t}=\sum_{j=1}^{A}V_j(q)\int\psi_t^*(\mathbf{r}_1,\ldots,\mathbf{r}_j,\ldots,\mathbf{r}_A)e^{iq\cdot r_j}\Gamma(b_j)\psi_0(\mathbf{r}_1,\ldots,\mathbf{r}_j,\ldots\mathbf{r}_A)\prod_{i=1}^{A}d\mathbf{r}_i, \tag{2.5}$$

where

$$V_j(q)\equiv\int d(\mathbf{r}-\mathbf{r}_j)e^{iq\cdot(r-r_j)}V(|\mathbf{r}-\mathbf{r}_j|) \tag{2.6}$$

is the Fourier transform of the potential. This still depends on the index j through the spin of the jth nucleon.

We now expand $e^{iq\cdot r_j}$ (in eq. (2.5)) in terms of spherical Bessel functions $j_l(qr_j)$ and Legendre polynomials $P_l(\hat{\mathbf{q}}\cdot\hat{\mathbf{r}}_j)$, where $\wedge$ denotes a unit vector

$$e^{iq\cdot r_j}=\sum_{l=0}^{\infty}i^l(2l+1)j_l(qr_j)P_l(\hat{\mathbf{q}}\cdot\hat{\mathbf{r}}_j). \tag{2.7}$$

Keeping only the term ($l=1$) in the expansion (2.7) and using the closure relation to obtain the transition probability, we find from eq. (2.5)

$$T_{00}\equiv\sum_f T_{0t}T_{0t}^*=\sum_f|\langle\psi_t|\sum_j 3ij_1P_1\Gamma V_j|\psi_0\rangle|^2=\langle\psi_0||\sum_j 3ij_1P_1\Gamma V_j|^2|\psi_0\rangle, \tag{2.8}$$

where the summation $\sum_f$ is taken over all final states obtained by the operator $j_1P_1\Gamma$ acting on the ground state.

Since $\Gamma(b)$ is an even function of $r\sin\theta$ (in spherical polar coordinates), the operator $j_1(qr)P_1(\hat{\mathbf{q}}\cdot\hat{\mathbf{r}})\Gamma(r^2\sin^2\theta)$ can give rise to the excitation of octupole and higher odd multipole states besides the required electric dipole and magnetic quadrupole transitions. However, on expanding

$$\Gamma(r^2\sin^2\theta)=\sum_{k=0}^{\infty}c_{2k}(r^2)Y_{2k}(\cos\theta),$$

we find that for the important range of values of r^2, the coefficients $c_2(r^2)$, $c_4(r^2)\ldots$ are sufficiently small compared with $c_0(r^2)$ to make T_{00} as given by (2.8) a good approximation to the required transition probability. Numerical integration indicates that the error we make by incorrectly including these other terms in the differential cross section is about 5 %. Using this approximation reduces the numerical work by an order of magnitude. However, this approximation is probably not justified for heavier nuclei for which these higher odd multipole transitions may well become important.

† By exploiting the fact that the scattering angles considered here are small, we can arrive at essentially the same result as is obtained above by assuming that the product $\psi_t^*(\mathbf{r}_j)\psi_0(\mathbf{r}_j)$ varies slowly with $\mathbf{r}_j$, and replacing $\psi_t^*(\mathbf{r}_j)\psi_0(\mathbf{r}_j)$ by $\psi_t^*(\mathbf{r})\psi_0(\mathbf{r})$ in (2.4) and then performing the integration over $\mathbf{r}_j$ for fixed $\mathbf{r}$. Since both Γ and $\psi_t^*\psi_0$ vary slowly and we need the fulfilment of only one of these conditions, the above approximation should be quite good.

Of course, we also here neglect electric dipole and magnetic quadrupole transitions which could result from the terms $j_3 P_3 \Gamma$, $j_5 P_5 \Gamma \ldots$ but for small q, $j_3(qr)$, $j_5(qr) \ldots$ are small compared with $j_1\ (qr)$, for values of r extending right out to the nuclear radius, and ignoring these terms is quite consistent with our small angle approximation.

For $\psi_0(\mathbf{r}_1, \mathbf{r}_2 \ldots \mathbf{r}_A)$ we use a 12×12 Slater determinant of harmonic oscillator wave functions $\phi_k\ (r)$ (including spin and isobaric spin dependence) for neutrons and protons in $1s_{\frac{1}{2}}$ and $1p_{\frac{3}{2}}$ states i.e. in j-j coupling. Hence we have

$$T_{00} = \sum_{k=1}^{A} \langle \phi_k(1) | |A(1)|^2 | \phi_k(1) \rangle + 2 \sum_{k<l} [\langle \phi_k(1)\phi_l(2) | \mathrm{Re}(A^*(1)A(2)) | \phi_k(1)\phi_l(2) \rangle$$
$$- \langle \phi_k(1)\phi_l(2) | \mathrm{Re}(A^*(1)A(2)) | \phi_l(1)\phi_k(2) \rangle], \quad (2.9)$$

where

$$A(j) \equiv 3 j_1(qr_j) P_1(\hat{\mathbf{q}} \cdot \hat{\mathbf{r}}_j) \Gamma(b_j) V_j(q) \qquad (j = 1,2). \quad (2.10)$$

Because of the spin dependence of $V_j(q)$, the operator $P_1 V_j$ can give rise to 0^-, 1^- and 2^- excitations. The explicit separation of the 1^- and 2^- parts of $P_1 V_j$ is carried out in sect. 4. In the following, we assume that $A(j)$ denotes only the required part of the operator (2.10).

The first term of the double sum in eq. (2.9) is identically zero for all values of k and l since it is the product of two Dirac brackets each of which represents the matrix element of an odd parity operator between identical states. Thus,

$$\langle \phi_k(1)\phi_l(2) | A(1)A(2) | \phi_k(1)\phi_l(2) \rangle = \langle \phi_k | A | \phi_k \rangle \langle \phi_l | A | \phi_l \rangle \equiv 0,$$

so the transition probability can be written in the form

$$M = S + P - E, \quad (2.11)$$

where

$$S \equiv \sum_{s=1}^{4} \langle \phi_s | |A|^2 | \phi_s \rangle, \quad \text{i.e. the sum over the four } s_{\frac{1}{2}}\text{-nucleon states,}$$

$$P \equiv \sum_{p=1}^{8} \langle \phi_p | |A|^2 | \phi_p \rangle, \quad \text{i.e. the sum over the eight } p_{\frac{3}{2}}\text{-nucleon states,} \quad (2.12)$$

$$E \equiv 2 \sum_{k<l=1}^{12} |\langle \phi_k | A | \phi_l \rangle|^2, \quad \text{i.e. the exchange contribution.}$$

Fig. 2 shows the graphs of P, S and E against a dimensionless parameter $\eta \equiv q^2/4\alpha$ for the dipole transition. For comparison, the same quantities P', S' and E' are shown in Born approximation (i.e. $\Gamma(b) = 1$). The parameter α is the one occurring in the exponential part of the harmonic oscillator wave functions ($\exp[-\frac{1}{2}\alpha r^2]$). The value used for α is 0.234 fm^{-2} corresponding to a theoretical root mean square radius equal to 3.04 fm as given by Kerman, McManus and Thaler [13]).

The necessity for a theoretical radius somewhat larger than the experimental value arises out of our approximation which neglects the range of the nucleon-nucleon interaction. The adjustment in the radius to some degree compensates for this error.

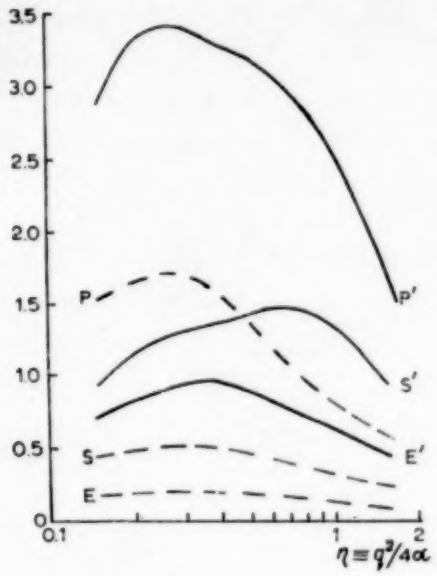

Fig. 2. Comparison of the various contributions to the electric dipole differential cross-section in the distorted wave calculation and in Born approximation. Curves S and P are the direct terms from $s_{\frac{1}{2}}$ states and $p_{\frac{3}{2}}$ states, respectively, and curve E the exchange terms in the distorted wave calculation. Curves S^1 and P^1 and E^1 are the corresponding quantities in Born approximation.

McManus and Thaler [15]) give more theoretical detail about this point.

3. Distortion

First of all we note that the real part of the distorting potential $V(r)$ affects only the phase of the operator $A(j)$ given by eq. (2.10). Since $|A|^2$ only occurs in the terms S and P, these are unaltered by a change in the phase of A. The exchange term E is therefore the only one depending on the real part of the optical potential $\hat{V}(r)$. Putting in approximate numerical values indicates that the phase of A varies only very slowly with impact parameter b so that the effect of a real part in the optical potential is probably negligible. We therefore assume

$$\hat{V}(r) = -iW(r).$$

For light nuclei such as carbon, it is permissible to use a Gaussian form (3.1) for the distorting potential $W(r)$, the advantage being great simplification in the mathematical manipulation. This assumption would not be good for heavier nuclei in which the nucleon distribution as determined by electron scattering [16])

does not conform to Gaussian shape. Thus we take

$$W(r) = W_0 e^{-\beta r^2}, \tag{3.1}$$

where $W_0 = 32$ MeV and $\beta = 0.162$ fm^{-2}. The value of W_0 is estimated from expressions for the absorption coefficient in terms of n-p and p-p total cross-sections. The value of β is chosen to fit a root mean square radius of 3.04 fm for the optical potential. Squires [9]) making similar calculations, has $W_0 = 60$ MeV and $\beta = 0.26$ fm^{-2}. This is because Squires fits his parameters to a root mean square radius of 2.40 fm, which is the experimental value.

Simple algebra leads to

$$\Gamma(b) \approx \exp\left[-\tfrac{1}{2}A\bar{\sigma}\frac{\beta}{\pi}e^{-\beta b^2}\right],$$

where $\bar{\sigma}$ is the mean proton-nucleon total cross-section at 180 MeV. Hence, we have

$$\Gamma(b) = \exp[-1.16\, e^{-0.162b^2}]. \tag{3.2}$$

Following Squires [9]) we approximate (3.2) by

$$\Gamma(b) \approx 1 - 0.734\, e^{-0.125b^2} \tag{3.3}$$

for algebraic convenience. The approximation (3.3) has the added advantage that we can separate off the effect of the distortion given by the second term of (3.3), and hence compare our results with those given in Born approximation (see fig. 2).

4. Transition to the Impulse Approximation

By using the short range approximation we are able to remove the Fourier transform $V_j(q)$ of the proton-nucleon interaction potential, defined by (2.6), from the spatial integrals in all following expressions for the transition matrix element. We now use the impulse approximation [11]) to replace $V_j(q)$ phenomenologically in terms of the free proton-nucleon scattering amplitude in the two-body centre-of-mass system. In other words, we identify $V_j(q)$ with the nucleon-nucleon scattering t-matrix $\langle k'|t|k\rangle$,

$$V_j(q) \to t_j. \tag{4.1}$$

Here we are making the usual 'off-energy shell approximation'. This is discussed in some detail by Kerman, McManus and Thaler [13]), whose notation we adopt in writing

$$t_j = A + B\sigma_{\hat{\mathbf{n}}}\sigma_{\hat{\mathbf{n}}}(j) + C(\sigma_{\hat{\mathbf{n}}} + \sigma_{\hat{\mathbf{n}}}(j)) + E\sigma_{\hat{\mathbf{q}}}\sigma_{\hat{\mathbf{q}}}(j) + F\sigma_{\hat{\mathbf{p}}}\sigma_{\hat{\mathbf{p}}}(j),$$

where

$$\hat{\mathbf{q}} \equiv \mathbf{q}/|\mathbf{q}|, \quad \hat{\mathbf{n}} \equiv \mathbf{n}/|\mathbf{n}|, \quad \mathbf{n} \equiv \mathbf{k}\times\mathbf{k}' \text{ and } \hat{\mathbf{p}} \equiv \hat{\mathbf{q}}\times\hat{\mathbf{n}}. \tag{4.2}$$

The quantity $\boldsymbol{\sigma}$ operates on the spin wave function of the projectile and $\boldsymbol{\sigma}(j)$ operates on the spin wave function of the jth nucleon in the nucleus.

We note that the Legendre polynomial P_1, as an operator, changes the orbital angular momentum by unity and also reverses the sign of the parity of the system upon which it acts, whereas $\boldsymbol{\sigma}(j)$ can change the spin by unity but does not alter the parity. Consequently, the operator $P_1(\hat{\mathbf{q}}\cdot\hat{\mathbf{r}}_j)\cdot t_j$, which within the impulse approximation and the approximation discussed following eq. (2.8) describes the angular momentum behaviour of $A(j)$ (given by (2.10)), can excite 0^-, 1^- and 2^- states when acting on the 0^+ ground state of the carbon nucleus.

To isolate the electric dipole and magnetic quadrupole parts of this operator, we note that $P_1(\hat{\mathbf{q}}\cdot\hat{\mathbf{r}}) = \hat{\mathbf{q}}\cdot\hat{\mathbf{r}}$ and that we can expand

$$(\hat{\mathbf{q}}\cdot\hat{\mathbf{r}})(\boldsymbol{\sigma}\cdot\hat{\mathbf{n}}) = \tfrac{1}{3}(\hat{\mathbf{q}}\cdot\hat{\mathbf{n}})(\hat{\mathbf{r}}\cdot\boldsymbol{\sigma})+\tfrac{1}{2}(\hat{\mathbf{q}}\times\hat{\mathbf{n}})\cdot(\hat{\mathbf{r}}\times\boldsymbol{\sigma})$$
$$+\tfrac{1}{4}[\hat{q}_\alpha\hat{n}_\beta+\hat{q}_\beta\hat{n}_\alpha-\tfrac{2}{3}\delta_{\alpha\beta}(\hat{\mathbf{q}}\cdot\hat{\mathbf{n}})][\hat{r}_\alpha\sigma_\beta+\hat{r}_\beta\sigma_\alpha-\tfrac{2}{3}\delta_{\alpha\beta}(\hat{\mathbf{r}}\cdot\boldsymbol{\sigma})]. \quad (4.3)$$

The three terms on the right hand side of (4.3) behave as tensors of order 0, 1 and 2 it is the second (vector) term which gives rise to 1^- excitations and the third to 2^- excitations.

Thus defining the x direction as that of the momentum transfer $\mathbf{q}$ and using (2.10), (4.1), (4.2) and (4.3), we find that the required 1^- and 2^- operators are

$$\text{for } 1^-\text{: } A(j) = \frac{3}{r_j}j_1(qr_j)\Gamma(b_j)[Ax_j+B\sigma_y\tfrac{1}{2}(x_j\sigma_y(j)-y_j\sigma_x(j))+Cx_j\sigma_y$$
$$+C\tfrac{1}{2}(x_j\sigma_y(j)-y_j\sigma_x(j))+F\sigma_z\tfrac{1}{2}(x_j\sigma_z(j)-z_j\sigma_x(j))], \quad (4.4)$$

$$\text{for } 2^-\text{: } A(j) = \frac{3}{r_j}j_1(qr_j)\Gamma(b_j)[B\sigma_y\tfrac{1}{2}(x_j\sigma_y(j)+y_j\sigma_x(j))+C\tfrac{1}{2}(x_j\sigma_y(j)+y_j\sigma_x(j))$$
$$+E\sigma_x\tfrac{1}{3}(2x_j\sigma_x(j)-y_j\sigma_y(j)-z_j\sigma_z(j))+F\sigma_z\tfrac{1}{2}(x_j\sigma_z(j)+z_j\sigma_x(j))].$$

5. Isobaric Spin Considerations

So far we have ignored the fact that the carbon nucleus is excited from a state of total isobaric spin $T = 0$ to one of total isobaric spin $T = 1$. Such an isobaric spin excitation can come only from the vector part (in isobaric spin space) of the interaction potential. We can allow for the isobaric spin dependence of the interaction in making the t-matrix correction given in sect. 4. There, we effectively replaced the Fourier transform $V(q)$ of the interaction potential by the scattering amplitudes $A(q)$, $B(q)$, $C(q)$ $E(q)$, and $F(q)$. Now in isobaric spin space each of A, B, C, E and F can be written

$$F = F^{\text{S}}+F^{\text{V}}\boldsymbol{\tau}\cdot\boldsymbol{\tau}(j), \quad (5.1)$$

where F^{S} is the scalar part of the scattering amplitude, F^{V} the vector part of the scattering amplitude and $\boldsymbol{\tau}$, $\boldsymbol{\tau}(j)$ are the isobaric spin vectors of the projectile

and the struck nucleon, respectively. For the correct isobaric spin treatment we therefore substitute A^V, B^V, C^V and F^V into (4.4). In terms of $\langle 0|F|0\rangle$ and $\langle 1|F|1\rangle$, the amplitudes for nucleon-nucleon scattering in isobaric spin states $T = 0$ and $T = 1$, respectively, F is given by

$$F = \tfrac{1}{4}[3\langle 1|F|1\rangle + \langle 0|F|0\rangle] + \tfrac{1}{4}[\langle 1|F|1\rangle - \langle 0|F|0\rangle]\ \boldsymbol{\tau}\cdot\boldsymbol{\tau}(j).$$

Hence we obtain $F^V(q)$ from

$$F^V(q) = \tfrac{1}{4}[\langle 1|F|1\rangle - \langle 0|F|0\rangle]. \tag{5.2}$$

The amplitudes A, B, C, E and F for both $T = 0$ and $T = 1$ scattering states, as calculated from a Gammel-Thaler potential, are tabulated by Kerman, McManus and Thaler [13]). (Actually the amplitudes given for 156 MeV are used.)

Thus, we finally have, corresponding to the expressions (4.4),

$$\begin{aligned}
\text{for } 1^-\text{: } A(j) = {} & \frac{3}{r_j} j_1(qr_j)\Gamma(b_j)\{x_j[A^V + C^V\sigma_y] + \tfrac{1}{2}[x_j\sigma_y(j) - y_j\sigma_x(j)][C^V + B^V\sigma_y] \\
& + \tfrac{1}{2}F^V\sigma_z[x_j\sigma_z(j) - z_j\sigma_x(j)]\}. \\
\text{for } 2^-\text{: } A(j) = {} & \frac{3}{r_j} j_1(qr_j)\Gamma(b_j)\{\tfrac{1}{2}[x_j\sigma_y(j) + y_j\sigma_x(j)][C^V + B^V\sigma_y] \\
& + \tfrac{1}{2}[x_j\sigma_z(j) + z_j\sigma_x(j)]F^V\sigma_z + \tfrac{1}{3}[2x_j\sigma_x(j) - y_j\sigma_y(j) - z_j\sigma_z(j)]E^V\sigma_x\},
\end{aligned} \tag{5.3}$$

where A^V, B^V, C^V, E^V and F^V are given by expression corresponding to (5.2).

The factor $\boldsymbol{\tau}\cdot\boldsymbol{\tau}(j)$ occurring in (5.1) reduces to unity in the square of the matrix element. The isobaric spin dependent part of the wave function of the scattered proton projects out the third component of $\boldsymbol{\tau}$, so that (cf. (2.8))

$$M = \langle \psi_0 || \sum_j A^V(j)\tau_3(j)|^2|\psi_0\rangle.$$

But $\tau_3(k)\,\tau_3(l) = 1$ when i and j both denote protons or both neutrons.

The possibility of the one representing a proton and the other a neutron does not arise since in that case $\langle \phi_k|\phi_l\rangle = 0$, from the orthogonality of the isobaric spin wave functions of proton and neutron states.

Hence the required proton-carbon differential cross-section is given by

$$\frac{d\sigma}{d\Omega} = 4\left(\frac{A}{A+1}\right)^2 \frac{k'}{k} M, \tag{5.4}$$

where M is calculated explicitly by means of eqs. (2.11), (2.12) and (5.3). The factors in front of M in (5.4) are the usual kinematical factors.

6. Coulomb Scattering Corrections

In the scattering amplitudes A, B, C, E and F given by Kerman, McManus and Thaler [13]) no allowance is made for Coulomb interaction which can occur

in proton-proton scattering (i.e. pure $T = 1$ state scattering). The Coulomb scattering amplitude M_C is given by

$$M_C = \tfrac{1}{4}\frac{m}{\pi} V_C(q) e^{i\varepsilon},$$

where $V_C(q) = 4\pi e^2/q^2$ is the Fourier transform of the Coulomb potential.

For scattering angles $\Theta > 10°$ in the two body centre-of-mass system, the phase ε is equal to π to within less than 2 % error. Since we do not consider values of Θ less than 10° (see below), we may assume the Coulomb amplitude to be real and negative. Hence the vector part of the Coulomb amplitude is given by

$$M_C^V = -\tfrac{1}{4} m \frac{e^2}{q^2}. \tag{6.1}$$

Strictly this amplitude should be symmetrised with respect to angle (see for example Stapp [17])), but the effect of doing so is negligible to the accuracy required. So finally the amplitude $A^V(q)$, which is the only one affected by the unsymmetrical Coulomb amplitude is corrected for Coulomb interaction by adding to it the quantity M_C^V given by (6.1).

However, since we are dealing with an inelastic collision $k' < k$ and consequently the momentum transfer **q** is not transverse at very small angles and does not go to zero as the scattering angle goes to zero. The latter fact means that the smallest scattering angles considered correspond to angles Θ in the proton-nucleon centre-of-mass system, of at least 15° and the Coulomb correction for $\Theta \geqq 15°$ is almost negligible, certainly less than 5 %. The non-transverse nature of **q** at very small angles is of little consequence since we expect most of the small angle scattering to come from the edge of the nucleus so that the distortion is relatively unimportant at such angles and the calculation effectively reduces to Born approximation in which the direction of **q** has no special significance.

7. Comparison of Results with Experiment

The experimental results of Tyrén and Maris [1]) are published in the form of graphs of the differential cross-section per unit solid angle per unit energy $d^2\sigma/d\Omega dE$ against the excitation energy E_{exc} of the nucleus for various angles of scattering θ in the laboratory system; whereas our calculations give the differential cross-section per unit solid angle

$$\frac{d\sigma}{d\Omega} = \int \frac{d^2\sigma}{d\Omega dE}\, dE.$$

Consequently it is necessary to integrate the curves given by Tyrén and Maris

over the energy range of the dipole resonance. This is accomplished by fitting Lorentzian resonance forms (eq. (7.1)) to the experimental curves, and at the same time allowing for some random background counts. We have

$$\left(\frac{\mathrm{d}^2\sigma}{\mathrm{d}\Omega \mathrm{d}E}\right)_{\mathrm{expt}} = \frac{W^2\sigma_{\mathrm{R}}}{(E-E_0)^2+W^2} + B, \tag{7.1}$$

where σ_{R} is the height of the peak (not including the background), W is the half width of the peak at half height, E_0 is the value of the energy corresponding to σ_{R} and B is the estimated background.

The parameter E_0 is determined immediately by the position of the resonance peak and then σ_{R}, W and B are adjusted so that the Lorentzian shape fits the experimental curve. Then we get

$$\frac{\mathrm{d}\sigma}{\mathrm{d}\Omega} = \int \frac{W^2\sigma_{\mathrm{R}}}{(E-E_0)^2+W^2}\,\mathrm{d}E = \pi\sigma_{\mathrm{R}}W.$$

This method of integration over energy is rather insensitive to the value of W. Also the experimental curves of Tyrén and Maris [1]) have a possible error of ± 15 % so the experimental points shown in fig. 3 have errors which probably lie between 20 % and 25 %.

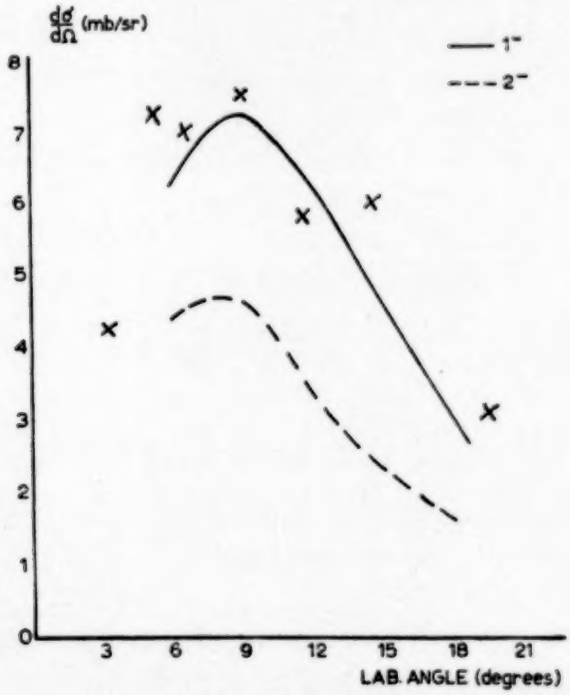

Fig. 3. The angular distributions of the giant dipole and magnetic quadrupole resonances excited in C^{12} by inelastic proton scattering. The curves show the differential cross-sections calculated using distorted waves. The crosses denote the experimental points obtained from the 19 MeV peak of Tyrén and Maris [1]); the corresponding values for the 22 MeV peak are not distinguishably different within the estimated error of 20—25 %.

8. Conclusion

We see from fig. 3 that the experimental points lie close to the dipole theoretical curve†. However, we have used closure (see eq. (2.8)) in our calculation, so the extent to which fig. 3 indicates good agreement between theory and experiment depends on just how much of the dipole sum is present in this resonance.

Particle-hole calculations [18]) indicate that about $\frac{2}{3}$ of the dipole sum occurs at 22.5 MeV excitation in carbon. However, the dominance of the spin dependent terms F and B (see (4.2)) in the nucleon-nucleon t-matrix can give rise to comparatively large inelastic proton scattering cross-sections for the spin-flip transitions $(p_{\frac{1}{2}}^{-1}, d_{\frac{1}{2}})$ and $(s_{\frac{1}{2}}^{-1}, p_{\frac{1}{2}}^{-1})$, which carry only small proportions of the dipole strength in the electromagnetic calculations. Consequently, the above-mentioned number gives no more than an indication for the interpretation of our results.

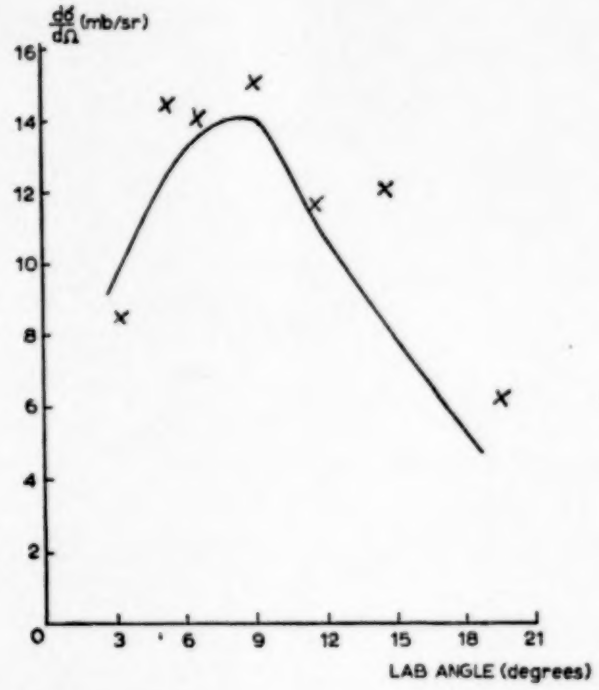

Fig. 4. The differential cross-section for the summed scattering from $T = 1$; 0^-, 1^- and 2^- levels. The crosses denote the experimental values of the summed cross-section for the 19 and 22.5 MeV peaks of Tyrén and Maris [1]).

We must also take into account the fact that the observed resonance is almost certainly not entirely due to dipole excitation. In particular, particle-hole calculations by N. Gilbert [2]), predict a $T = 1$, 2^- level at 22.9 MeV which carries 20—25 % of the M2 strength at small angles. It seems likely that a $T = 0$, 2^- level exists in this vicinity also. Thus, the agreement in absolute

† See the *Note added in proof* at the end of this paper

value between theory and experiment in fig. 3 is somewhat spurious, part of the experimental cross section coming from 2^- states.

In fact, in the early stages of the work, both the 19 and 22.5 MeV levels found by Tyrén and Maris were thought to be 1^- levels because of the similar angular distributions they gave. The 19 MeV level does not show up in γ-ray absorption, nor does it in the (p, γ) reaction. Furthermore, if we considered both the 19 and 22.5 MeV levels to be 1^- ones, their summed cross-section would be about twice the theoretical summed cross section for 1^- contributions shown in fig. 3. It turned out to be rather easy to make a sum-rule calculation of the summed scattering from $T = 1$, 0^-, 1^- and 2^- levels at small angles; for example looking at eq. (4.3), we employ for this simply the term on the left-hand side, rather than picking out a specific term on the right-hand side. The theoretical values of this summed scattering from all three levels are shown in fig. 4, together with the sum of experimental cross-sections for 19 and 22.5 MeV levels. The agreement is good and suggests strongly the interpretation of the 19 MeV level as 2^-. Particle-hole calculations by N. Gilbert show a $T = 1$, 2^- level at 19.2 MeV, carrying ≈ 70 % of the total 2^- strength. Of course, from the angular distribution, the level might also be 0^-. However, these levels are not excited with as large probability.

Several interesting points emerge from the above. Firstly, the angular distributions from excitation of 0^-, 1^- and 2^- excitations are similar at small angles. This is not true at large angles, because the 2^- state can be excited by a combination of $P_3(\mathbf{q} \cdot \mathbf{r})$ and the t-matrix, whereas the 0^- and 1^- states cannot. Therefore, one would expect the cross-section for 2^- excitation to persist at large angles, whereas that for 1^- excitation would not. Secondly, the inelastic scattering of protons at the energies we consider excites magnetic transitions about as strongly as electric ones. Thirdly, there seem to be a wealth of states, all fairly strongly excited, in the 20 MeV range in C^{12}, so that one cannot attribute the entire cross-section to the giant dipole 1^- level. It is likely that a similar situation exists also in O^{16} and other elements investigated by Tyrén and Maris.

The question is very interesting as to whether a giant 2^- state occurs in all nuclei as does the 1^- one. The particle-hole considerations of Brown *et al*[19]) indicate that it should. However, in heavy nuclei, it may lie almost on top of the 1^- levels, and not be discernible experimentally. For example in 0^{16}, a $T = 1$, 2^- level carrying 50 % of the total 2^- strength is predicted [20]) at 20.3 MeV. This would not be distinguished experimentally from the 1^- one at 22 MeV. The calculations of Evans indicate, however, the concentration of strength in the highest 2^- levels is not so complete as in the case of the 1^- excitations.

It is clear that further calculations, similar to those described in this paper, but using explicit wave functions for each excited state instead of employing the closure relation, would be useful and these are being carried out at present.

In considerations of heavier nuclei, it is also clear that it would be useful to have experimental results with improved resolutions, since the levels are closer together here.

I would like to express my thanks to Professor G. E. Brown for suggesting this problem and for many helpful discussions. The idea of using closure in this problem came from the work of Madame P. Benoist and Mademoiselle N. Gilbert, to whom I am grateful.

I acknowledge, with thanks, a Research Studentship from the Department of Scientific and Industrial Research.

Note added in proof: In plotting the experimental cross sections, it was not noticed that the data published in the first paper of Tyrén and Maris [1]) were preliminary, and that their later work (second paper of ref. [1])) showed these to be too high by a factor that we would estimate to be 1.5 to 2. Therefore, the experimental points shown in figs. 3 en 4 should be reduced by such a factor. Further, there is no indication of a dip in the experimental data at small angles, since the point at 3° came from the later work, and should not be lowered.

Later, more detailed theoretical work, using the explicit nuclear states determined by Gilbert and Brown (to be published) has shown that the calculated cross sections at 19 and 22 MeV are $\approx \frac{2}{3}$ of those obtained for the 1^- levels using closure.

References

1) H. Tyrén and Th. A. J. Maris, Nuclear Physics **3** (1957) 52; **4** (1957) 637, 662
2) N. Gilbert, to be published
3) S. T. Butler, Phys. Rev. **106** (1957) 272
4) C. A. Levinson and M. K. Banerjee, Ann. Phys. **2** (1957) 471, 499; **3** (1958) 67
5) W. Tobocman and M. H. Kalos, Phys. Rev. **97** (1955) 132
6) W. Tobocman, Phys. Rev. **115** (1959) 98; **94** (1954) 1655
7) L. I. Schiff, Phys. Rev. **103** (1956) 443
8) I. I. Shapiro, thesis, Harvard University (1955)
9) E. J. Squires, Nuclear Physics **6** (1958) 504
10) G. P. McCauley and G. E. Brown, Proc. Roy. Soc. **71** (1958) 893, appendix
11) G. Chew, Phys. Rev. **80** (1950) 196
12) N. Austern, S. T. Butler and H. McManus, Phys. Rev. **92** (1953) 350
13) A. K. Kerman, H. McManus and R. M. Thaler, Ann. Phys. **8** (1959) 551
14) R. J. Glauber, Lectures in theoretical physics **1** (1958) 315
15) H. McManus and R. M. Thaler, Phys. Rev. **110** (1958) 590
16) B. Hahn, D. G. Ravenhall and R. Hofstadter, Phys. Rev. **101** (1956) 1131
17) H. Stapp *et al.*, Phys. Rev. **105** (1957) 302
18) N. Gilbert and Werner, private communications (1960)
19) G. E. Brown, J. A. Evans and D. J. Thouless, Nuclear Physics **24** (1961) 1
20) J. A. Evans, private communication

2.D

Nuclear Physics **26** (1961) 434—445; © *North-Holland Publishing Co., Amsterdam*

Not to be reproduced by photoprint or microfilm without written permission from the publisher

ANALYSIS OF RECENT MEASUREMENT OF NUCLEAR LEVEL DENSITY PARAMETERS

D. W. LANG

Department of Theoretical Physics, Australian National University, Canberra, A.C.T.

Received 24 March 1961

Abstract: Data from experiments leading to values of the nuclear logarithmic level density derivatives are analysed and shown to be reasonably self consistent. A modified form of the curve drawn by Newton for the value of the single particle level density parameter a is found to be in accord with the data. Attention is drawn to the effect of restriction of the allowed angular momentum of the emitted particles on the value found for the temperature in an evaporative process.

1. Introduction

Since the experimental evidence about the statistical theory of nuclear reactions was analysed [1]) many accurate low energy measurements have become available. It was shown in the previous analysis that high energy cascade processes were consistent with a Fermi gas model of the nucleus. At lower energies the log of the level density on the Fermi gas model is no longer dominated by the term containing the square root of the excitation energy. In this paper, it is shown that the data available are still consistent with a Fermi gas model with appropriate corrections for condensation effects in the low energy spectrum.

2. Level Densities in a Fermi Gas

In terms of a thermodynamic temperature t, the Fermi gas equation of state for a gas of N neutrons and Z protons is [1])

$$U = \tfrac{1}{6}\pi^2 g t^2 - t, \tag{2.1}$$

where g is the sum of the single particle level densities for neutrons and protons in the given potential well and U is the excitation energy of the nucleus measured from the Fermi level.

Treatments of residual interactions between particles in the potential well have resulted in the development of the concept of a condensation energy, which must be supplied to the nucleus before it may be considered as a Fermi gas and must therefore be subtracted from the excitation energy before substitution in eg. (2.1), which is then valid for excitation energies greater than

2 or 3 times the condensation energy. Thus the odd-proton effect is often [2, 3]) treated by assuming that the ground state of an odd nucleus is uncondensed, that the ground state of an odd mass nucleus has a pairing energy $\frac{1}{2}\Delta$ and that of an even nucleus has a pairing energy Δ. According to Stolovy and Harvey [4]) the value of Δ is given for the atomic mass A greater than 40 by

$$\Delta = 3.36(1-A/400). \tag{2.2}$$

Treatment of the lower nuclear levels as analogous to the superconducting state of a metal [5]) suggests that the ground state of a nucleus may be even farther below the Fermi level, but a model [6]) in which the odd-proton effect is treated by assuming a definite pairing between nucleon states would require the Fermi level to coincide with the ground state of an even nucleus and an apparent further negative condensation energy to make eq. (2.1) apply at higher energies.

In a simple Fermi gas, the density of states is

$$\omega(U,N,Z) = \tfrac{1}{12}\left(\frac{6}{g}\right)^{\frac{1}{4}} (U+t)^{-5/4} \exp\{2(\tfrac{1}{6}\pi^2 gU)^{\frac{1}{2}}\}. \tag{2.3}$$

The factor $\frac{1}{6}\pi^2 g$ is often replaced by the single symbol a.

This leads to the definition of the logarithmic derivative of the level density τ, commonly called the "nuclear temperature":

$$\frac{1}{\tau} = \frac{\mathrm{d}}{\mathrm{d}U}\log\omega, \tag{2.4}$$

so that a can be derived from measurements of U and τ through

$$a \approx \frac{U}{\tau^2} + \frac{2.5}{\tau}. \tag{2.5}$$

For levels of a given value of J and of both parities, the density is

$$\Omega(U,N,Z,J) = \frac{2J+1}{\pi^{\frac{1}{2}}(2c\tau)^{\frac{3}{2}}} \exp\{-(J+\tfrac{1}{2})^2/2c\tau\}\,\omega(U,N,Z), \tag{2.6}$$

where $c\hbar^2$ can be shown [7, 8]) to be equal to the (rigid body) moment of inertia for a Fermi-Thomas model of a nucleus. Also in simple models [6]), we have

$$c = \overline{m^2}\,g, \tag{2.7}$$

where $\overline{m^2}$ is the mean square of the magnetic quantum number m. Jensen and Luttinger [9]) have shown that the sequence of states in the shell model implies

$$\overline{m^2} \approx 0.146\,A^{\frac{5}{3}}, \tag{2.8}$$

with about 10 % fluctuation due to shell effects.

At low excitation energies the nuclear moment of inertia is smaller than the rigid body value and this has been shown to follow from either a superconducting state of the nucleus [10]) or from the pairing energy model of Lang and Le Couteur [6]).

A value of τ for levels of given J, τ_J, is obtained from the logarithmic derivative of Ω in eq. (2.6). Expression (2.5) then becomes

$$a \approx \frac{U}{\tau_J{}^2} + \frac{2r_J}{\tau_J}, \tag{2.9}$$

where r_J is 2 if there is no energy dependence of c, but because of the energy dependence is actually greater.

The difference between (2.5) and (2.9) may be important in low energy evaporation processes or in level density counts. If in an evaporation process, particles may leave the nucleus without any restriction in the angular momentum carried, eq. (2.5) gives the correct form linking the observed temperature and the excitation energy of the Fermi gas. If only particles of zero angular momentum may be emitted, eq. (2.9) is correct. In most nuclear reactions there are restrictions on the emitted angular momentum but not quite so stringent as to justify the use of eq. (2.9).

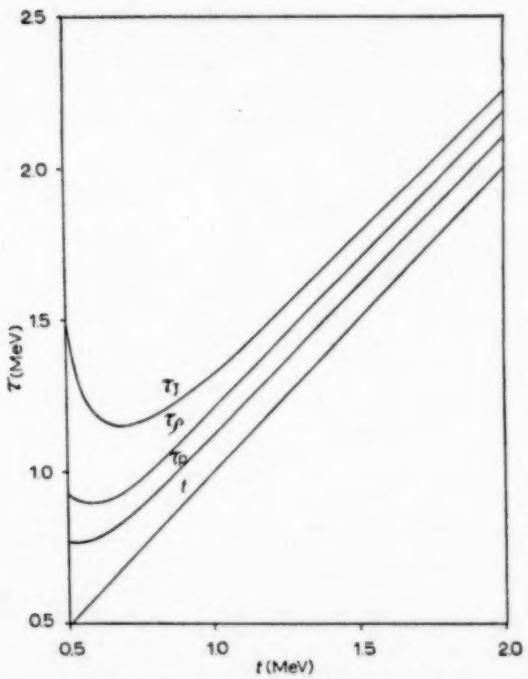

Fig. 1. Plots of the various values of the apparent logarithmic density derivative τ against the thermodynamic temperature t for a nucleus with a single particle level density $g = 5$ MeV^{-1}, using the pairing energy model of Lang and Le Couteur [6]), a pairing energy of $\Delta = 2.80$ MeV and a mean square projection value if the angular momentum of levels near the Fermi level $\overline{m^2} = 2.223$. Values of τ_p depend on all levels and the multiplicity of their projected value of their spins according to expression (2.5); τ_J depends on levels with a single value of J, in this case $J = \frac{1}{2}$, as given by expression (2.9); τ_ρ depends on all levels with $J \leqq 4\frac{1}{2}$ without considering different spin projections as separate states.

In counts of individual levels, if all levels are observed, the value of the temperature τ_ρ is derived from the equation

$$\omega_\rho(U, N, Z) = \frac{1}{2(\pi c t)^{\frac{1}{2}}}\omega(U, N, Z). \tag{2.10}$$

Then it follows that

$$a \approx \frac{U}{\tau_\rho{}^2} + \frac{2r_\rho}{\tau_\rho}, \tag{2.11}$$

where the value of r_ρ is larger than $\frac{3}{2}$ owing to the energy dependence of c.

The difference between these logarithmic derivatives, normally called temperatures, and the thermodynamic temperature t is illustrated in fig. 1.

3. Inelastic Scattering of Neutrons

Pulsed beams of monochromatic neutrons and time of flight methods have made possible accurate measurements of low energy neutron spectra resulting from inelastic scattering.

If a compound nucleus process is involved, the number $N(E)\,\mathrm{d}E$ of neutrons emitted by an energy range E to $E+\mathrm{d}E$ is given by [11])

$$N(E)\mathrm{d}E = \text{const. } E\sigma_c(E)\omega(U)\mathrm{d}E, \tag{3.1}$$

where $U+E$ is equal to the bombarding energy U_0, $\sigma_c(E)$ is the capture cross section for neutrons of energy E and $\omega(U)$ is the level density at energy U. Over a small range of U the variation of $\omega\ (U)$ can be approximated as exponential, if insufficient data are available to use a more exact form for $\omega(U)$. The usual experimental result is a value of τ derived from a plot of $\log\{N(E)/E\sigma_c(E)\}$ against E.

The value of τ should be measured near the range of energies for which the spectrum is most accurately determined, i.e. those a round the average energy of the emitted neutrons 2τ. Then the value of the excitation energy U appropriate to the measured value of τ is

$$U = U_0 - 2\tau. \tag{3.2}$$

From the previous section the values of τ and U should be connected by the equation

$$U = a\tau^2 - 2r\tau + \Delta_p, \tag{3.3}$$

where Δ_p is a condensation energy, taken here equal to the value from Stolovy and Harvey [4]). The orbital angular momentum carried away by neutrons at these energies is usually less than 3, according to the work of Beyster *et al* [12]). The value of r is taken in consequence as 2.

In table 1 values of τ and U are given from listed references. Using the given value of Δ_p, values have been derived for a.

TABLE 1

Analysis of single spectra for inelastic scattering of neutrons

Element	Ref.	U_0 (MeV)	τ (MeV)	Δ_p (MeV)	a (MeV)$^{-1}$ ±22%
$_{13}Al^{27}$	[13])	7.0	0.96±0.15	1.56	7.9
$_{23}V^{51}$	[13])	7.0	0.90±0.09	1.47	9.0
$_{21}Mn^{55}$	[13])	7.0	1.00±0.10	1.45	7.5
$_{33}As^{75}$	[13])	7.0	0.67±0.06	1.36	15.6
$_{34}Se^{80}$	[13])	7.0	0.62±0.05	2.68	14.7
$_{38}Sr^{88}$	[13])	7.0	0.80±0.08	2.62	9.3
$_{42}Mo^{96}$	[14])	4.10	0.48±0.04	2.54	10.7
$_{47}Ag^{107, 109}$	[15])	6.34	0.59	1.23	18.2
$_{80}Hg^{200}$	[14])	4.10	0.55±0.04	1.68	10.3
$_{82}Pb^{206}$	[13])	7.0	0.92±0.09	1.62	8.3

In table 2 nucleides are given for which several values of τ have been measured. The references are given and measured temperatures are listed under the appropriate value of U_0. Also included is the value Δ_p assigned to the pairing

TABLE 2

Temperatures τ (in MeV) from (n, n') experiments

Target nucleus	Refs.	U_0 (MeV) / Δ_p (MeV)	2.44	3.40	4.00	4.10	5.0	6.0	6.34	7.00
$_{26}Fe^{56}$	[13, 16])	2.88					0.85			0.95, 0.74
$_{29}Cu^{63}$	[13])	1.41					0.72			0.79
$_{41}Nb^{93}$	[13])	1.29			0.33		0.48	0.49		0.59
$_{48}Cd^{112}$	[16])	2.43	0.45				0.62			0.73
$_{49}In^{115}$	[13])	1.20			0.40		0.48	0.52		0.56
$_{50}Sn^{118}$	[16])	2.37	0.52				0.64			0.77
$_{51}Sb^{121, 123}$	[13, 14])	1.17			0.40	0.44				0.58
$_{53}I^{127}$	[13])	1.14			0.41					0.60
$_{57}La^{139}$	[13])	1.10			0.65		0.69			0.68
$_{58}Ce^{140}$	[13])	2.18					0.60			0.60
$_{73}Ta^{181}$	[13, 15, 16])	0.92	0.37, 0.32	0.39			0.50		0.50	0.49, 0.52
$_{74}W^{184}$	[13, 15, 16])	1.82	0.38, 0.36	0.36			0.55		0.44	0.50, 0.57
$_{79}Au^{197}$	[13, 15])	0.85	0.30	0.45	0.47				0.65	0.60
$_{81}Te^{205}$	[13])	0.82			0.76		0.81	0.80		0.78
$_{83}Bi^{209}$	[13])	0.80					0.68			1.05

energy term in (3.3). If the eq. (3.3) is accurate, a plot of $U_0-\Delta_p+2\tau$ against τ^2 should be a straight line passing through the origin. Such plots are shown figs. 2, 3 and 4. These are consistent with straight lines through the origin in most cases, but often indicate that a better straight line could be drawn to

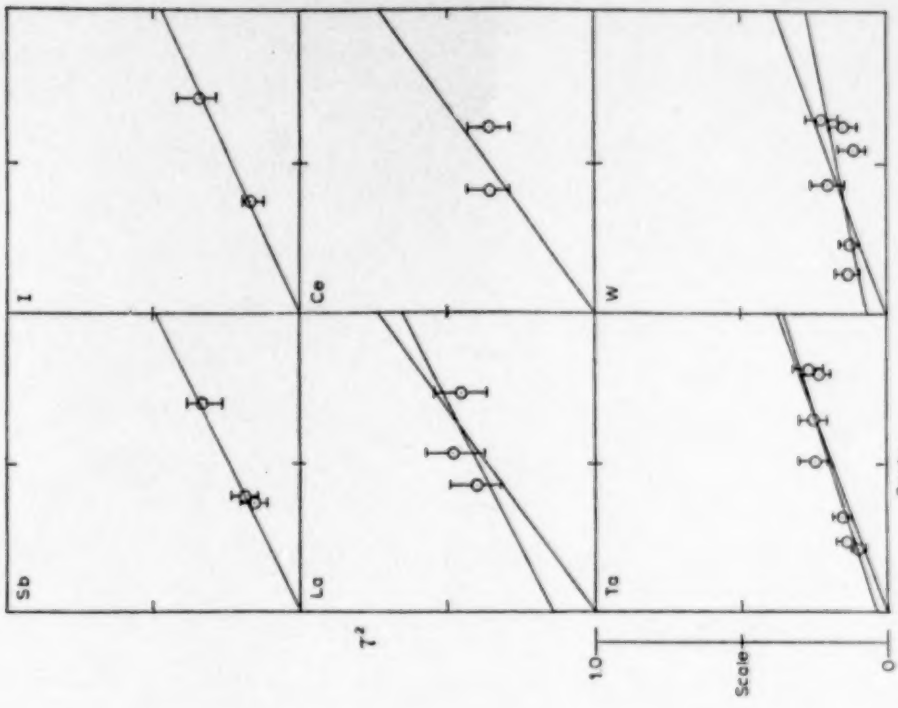

Fig. 3. Plots for antimony, iodine, lanthanum, cerium, tantalum and wolfram of the data for inelastic scattering of neutrons. The data are plotted in the form $U_0-\Delta_p+2T$ against T^2.

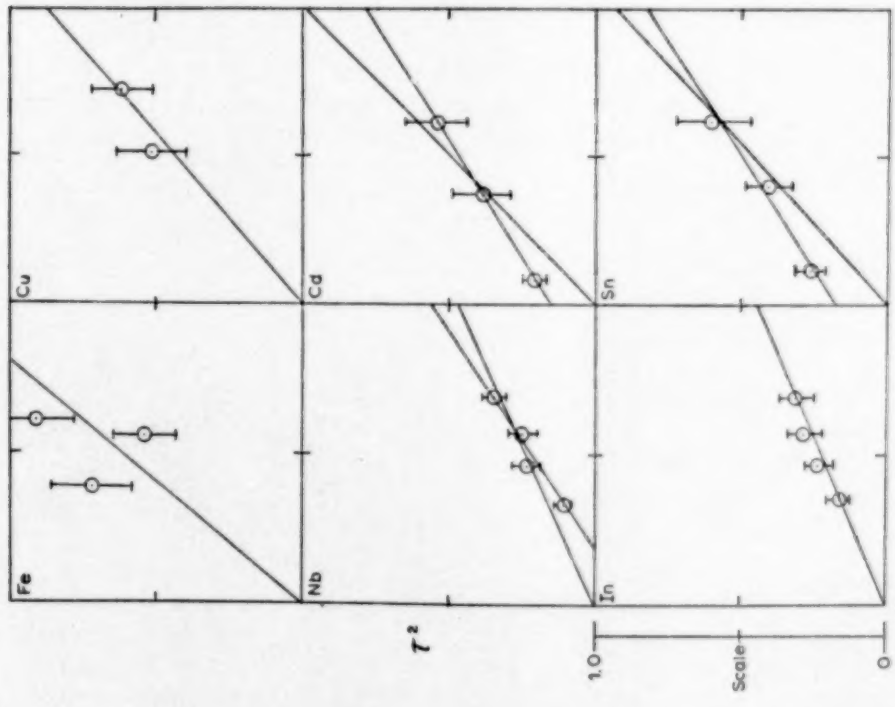

Fig. 2. Plots for iron, copper, niobium, cadmium, indium and tin of the data for inelastic scattering of neutrons. The data are plotted in the form $U_0-\Delta_p+2T$ against T^2.

pass through the points only, and not the origin. This indicates an addition to the value for the condensation of pairing energy.

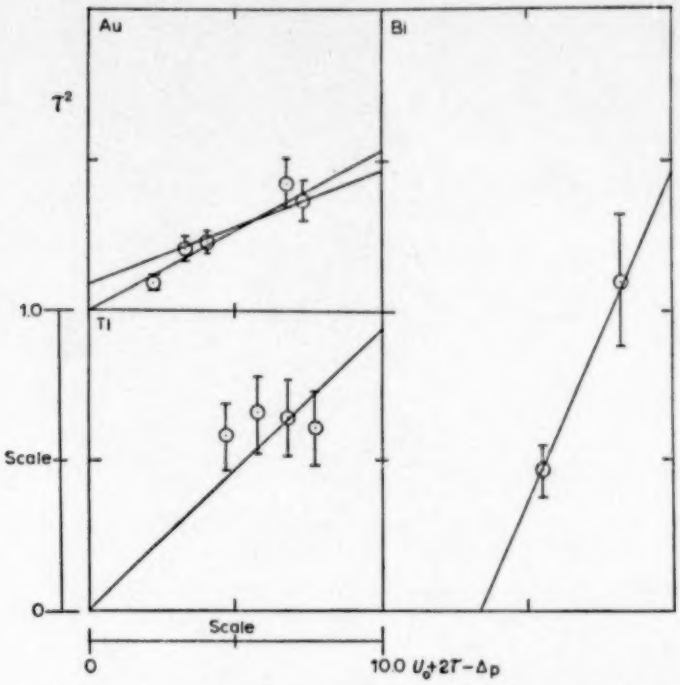

Fig. 4. Plots for gold, thallium and bismuth of the data for inelastic scattering of neutrons. The data are plotted in the form $U_0-\Delta_p+2\tau$ against τ^2.

In table 3 the values derived for a, assuming that the plots all pass through the origin, are listed. Where applicable the values of a_n for a line of different

TABLE 3

Parameters a, a_n, a_0, a_1 and a_∞ (in MeV^{-1}) from inelastic (n, n′) experiments over a range of initial energies

Target nucleus	(n, n′) data			Cameron [18]) (theoretical)		
	a	a_n	Δ_n(MeV)	a_0	a_1	a_∞
$_{26}Fe^{56}$	8.5±2.5			1.34	3.80	3.56
$_{29}Cu^{63}$	11.2	20.3	−5.4	5.34	5.73	4.42
$_{41}Nb^{93}$	21.2	14.4	+1.9	5.92	5.57	7.10
$_{48}Cd^{112}$	10.2	15.5	−2.3	13.24	9.57	8.00
$_{49}In^{115}$	22.2±2.6			10.72	9.49	7.78
$_{50}Sn^{118}$	10.7	15.7	−2.9	10.97	9.05	8.47
$_{51}Sb^{121, 123}$	21.0±3.0			6.40	9.03	7.51
$_{53}I^{127}$	16.4	14.4	+0.7	11.64	7.84	8.17
$_{57}La^{139}$	13.6	19.2	−2.6	5.89	7.13	9.70
$_{58}Ce^{140}$	13.8±2.0			6.05	7.47	9.43
$_{73}Ta^{181}$	26.5	30.2	−1.0	12.84	12.80	12.85
$_{74}W^{184}$	26.8	46.5	−3.3	14.42	12.89	13.57
$_{79}Au^{197}$	19.0	26.0	−2.0	18.23	11.09	15.20
$_{81}Te^{205}$	10.7	14.0	−2.3	9.07	6.75	13.87
$_{83}Bi^{209}$	9.7	4.4	+3.3	2.74	5.84	14.37

slope and the consequent value of the extra condensation energy Δ_n are also listed. For comparision, values derived by Cameron [17]) for a, using level densities at the neutron binding energy, are included: a_0 is the value for which the thermodynamic temperature t is zero; a_1 that for which $t = 1$ MeV; a_∞ that for which $t \to \infty$. It is noted that these values are too small.

The values of a are plotted in fig. 6.

4. Charged Particle Data

Data from heavy ion reactions have been previously analysed [1]) and, more recently [18]), the (p, α) data of Fulmer and Goodman [19]). These data are summarized in table 4 and are plotted in fig. 6.

Fulbright, Lassen and Poulsen [22]) used inelastic alpha scattering to measure alpha emission from compound nuclei. The data from nickel, copper and zinc were interpreted by means of a constant temperature approximation, i.e. $\omega(U) = \exp U/\tau$ and by $\omega(U) = K \exp(2\sqrt{aU})$. (The factor 2 was apparently omitted from this equation by a misprint in the original paper.) The constant temperature approximation was preferred but the theoretical form $\omega(U) = U^{-2} \exp(2\sqrt{aU})$, equivalent to (2.6), is still better. The appropriate values of a are 10.5, 9.4 and 11.5 MeV^{-1} for nickel, copper and zinc. These data are also included in table 4 and fig. 6.

TABLE 4

Alpha particle and heavy ion reactions

Elements	a MeV^{-1}	Reaction	Ref.
F^{19}	1.1±0.2	heavy ion	[29])
Ne^{21}	1.4±0.2	heavy ion	[20])
Ne^{22}	2.6±0.8	heavy ion	[20])
A^{37}	4.1±0.3	heavy ion	[21])
K^{40}	5.0±0.2	heavy ion	[21])
Co^{55}	10.6±1.2	(p, α)	[18, 19])
Ni^{58}	10.5±1.5	(α, α′)	[22])
Cu^{63}	9.4±1.5	(α, α′)	[22])
Zn^{64}	11.5±1.5	(α, α′)	[22])
Ru^{100}	16.0±5.0	(p, α)	[18, 19])

Allan [23, 24]) has measured proton spectra of fourteen nucleides following 14 MeV neutron bombardment. Similar measurements have been made by Glover and Weigold [25]) and by Glover and Purser [26]). Results are given in table 5 and are plotted in fig. 6. In (n, p) experiments it is necessary to distinguish the (n, p) process being studied from components of deuteron emission, direct interactions and (n, np) processes. The work of Colli, Facchini and

Micheletti [27]), Colli, Pignanelli, Rytz and Zurmuhle [28]) and of Storey, Jack and Ward [29]) has not had these distinctions made and cannot be readily used.

TABLE 5

Data from (n, p) reactions

Residual nucleus	a MeV^{-1}	Refs.
Na^{24}	3.4±0.6	[24])
Mg^{27}	4.1±1.0	[25])
Mg^{27}	4.8±0.9	[24])
Al^{28}	3.9±0.7	[24])
Sc^{46}	6.8±1.1	[24])
V^{50}	9.7±1.8	[24])
V^{52}	7.2±1.3	[24])
Mn^{54}	9.7±1.8	[24])
Mn^{56}	7.2±1.3	[24])
Co^{58}	6.9±1.0	[26])
Co^{58}	10.1±1.9	[24])
Co^{60}	8.0±1.5	[24])
Ni^{63}	10.1±1.9	[24])
Ni^{63}	8.5±1.0	[23])
Cu^{64}	9.7±1.8	[24])
Cu^{66}	8.0±1.5	[24])
Cu^{67}	9.7±1.8	[24])

5. Level Density Counts

The level densities observed at the neutron binding energy show some shell structure, which Newton [3]) represented by replacing the equation

$$g = KA \qquad (K \text{ unknown constant}) \tag{5.1}$$

used in simple treatments connecting the single particle level density g and the atomic mass number A, by the equation

$$g = K(\overline{j_n}+\overline{j_p}+1)A^{\frac{2}{3}}, \tag{5.2}$$

where $\overline{j_n}$ and $\overline{j_p}$ are means of j values for neutrons and protons, respectively, close to the Fermi level in the nucleus studied; tables were given for these quantities. Newton also assumed that the level density is proportional to the Fermi gas form with an unknown constant of proportionality. This constant and the constant K in eq. (5.2) were evaluated together by a least squares fit to the measured level densities at the neutron binding energy. Thus the value of K was required to fit the variation of level densities with variation of excitation energy while the other constant, which by (2.3) and (2.6) determines the value c of the moment of inertia of the nucleus, was required to set the absolute value of the level density. The excitation energy used was always the binding

energy of the last neutron. Variations of this quantity may be associated with extra condensation energies in the ground state, which are not reflected in higher level densities. It is thus not surprising that the value found for K was too low to allow (5.2) to fit other experimental data, and to compensate the other constant corresponded to a value of the moment of inertia, being in all cases only about one fifth the rigid body value.

The form chosen by Newton [3]) is a convenient means of displaying the shell structure of the quantity g. A fit to the level density counts treating K as adjustable, using Newton's semi-empirical values of $\overline{j_n}$ and $\overline{j_z}$, but taking c from (2.7) and (2.8), was therefore arranged.
This gave

$$g = 0.0455\ (\overline{j_n}+\overline{j_p}+1)A^{\frac{2}{3}}, \tag{5.3}$$

i.e.

$$a = 0.0748\ (\overline{j_n}+\overline{j_p}+1)A^{\frac{2}{3}}, \tag{5.4}$$

which is about 20 % higher than Newton's value. The values of a found from the analysis of the neutron binding energy counts are compared in fig. 5 with the curves obtained from (5.4) and derived from the work of Miss Ross [30]), respectively. Inspection of fig. 5 shows that the general trend of both curves is in good agreement with experiment. The structure exhibited by the data is usually intermediate between the curves. Ericson [31]) has analysed actual level

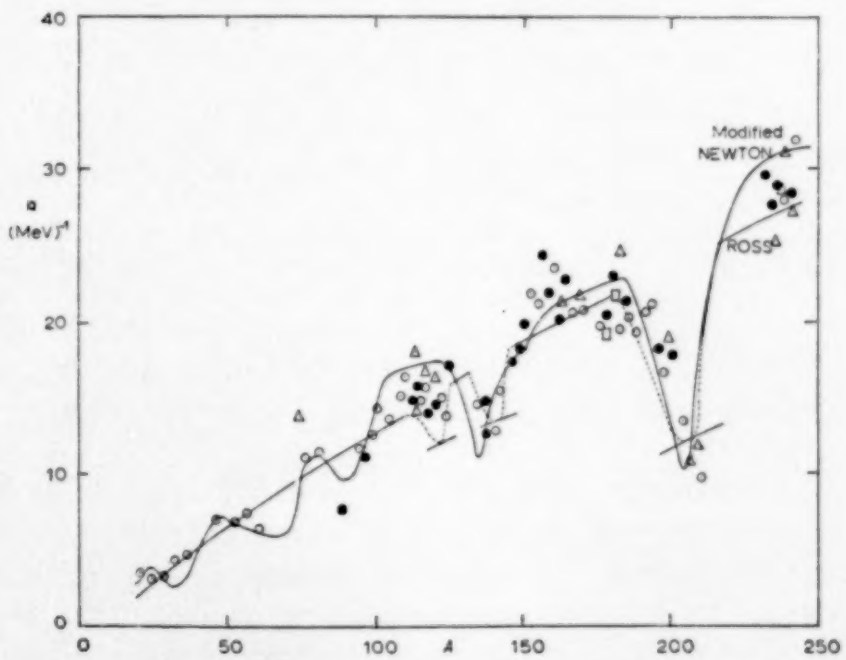

Fig. 5. The value of the level density parameter a derived from level spacings at the neutron binding energy plotted against the atomic mass number A. The compound nuclei are distinguished as □ odd-proton, △ odd-neutron ● even and ○ odd. These are compared with curves for a modified from the work of Newton [3]) and derived from the work of Miss Ross [30]), respectively.

densities found using the M.I.T. Van de Graaff. Some doubt [32]) has however, been cast on the detection of all levels in such experiments.

6. Conclusions

Fig. 6 is a plot of data on the value of the level density parameter a against atomic mass number A for the nucleus involved. Values of a from sects. 3 and 4 are plotted, also five points derived in a previous paper [1]) from the high energy cascades measured by Gross [33]) and two points derived by Terrell [34]) from the spectra of neutrons emitted in the fission process. The curves from the work of

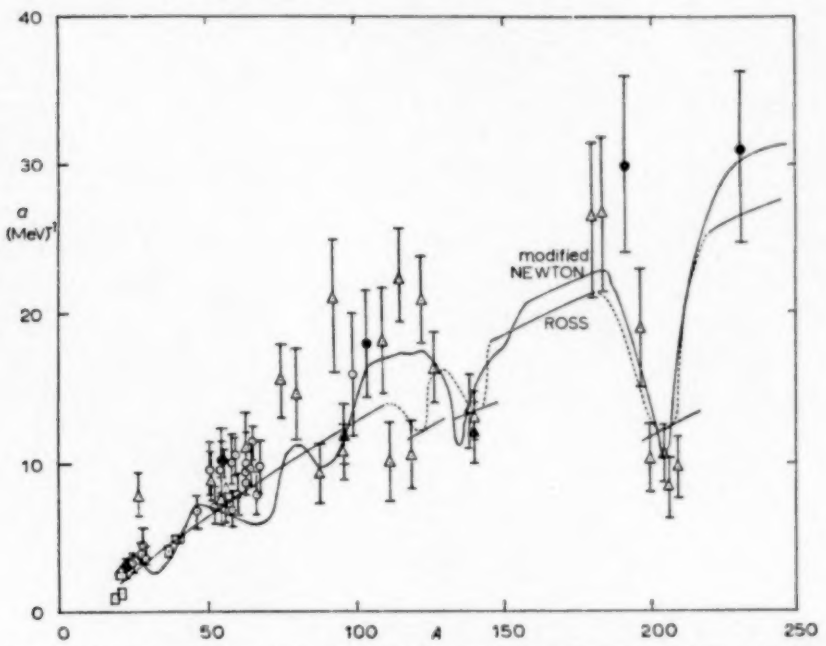

Fig. 6. Experimental data on the value of the level density parameter a plotted against the atomic mass number A. For comparison the theoretical curves modified from Newton's results and derived from Miss Ross' results respectively, are included. The experimental data are distinguished as ● high energy nuetron cascades, △ neutron inelastic scattering, □ heavy ion reactions, ⊙ other charged particle data and ▲ fission neutron spectra.

Miss Ross [30]), as modified in sect. 5 from work by Newton [3]), are replotted from fig. 5. The experimental level density data at the neutron binding energy are not replotted.

It is seen that the experimental data, while scattered, nevertheless do show a general trend, and it is significant that different types of data show the same trend. At present, predictions of the level density are best made using the values of the level density parameter a modified as above from the work of Newton. It would be of great interest to have further cascade experiments carried out at any energy up to those used by Gross [33]), using target nuclei just above closed shells to test whether the shell effects shown in fig. 5 and 6, which depend only on low energy data, persist to higher excitations. It is already

possible to predict almost within the limits of experimental error the variation of level density in a particular nucleus. It may be concluded that the level densities of most nuclei in excited states, other than closed shell nuclei are, well described by the Fermi gas model.

Thanks are due to Dr. D. B. Thomson of Los Alamos, Dr. R. I. Ewing of Rice Institute and Dr. R. N. Glover, Mr. K. H. Purser and Mr. E. C. Weigold of the Australian National University, all of whom generously supplied data used in this paper prior to publication.

References

1) K. J. Le Couteur and D. W. Lang, Nuclear Physics **13** (1959) 32
2) H. Hurwitz and H. A. Bethe, Phys. Rev. **81** (1951) 952
3) T. D. Newton, Can. J. Phys. **34** (1956) 804
4) A. Stolovy, J. A. Harvey, Phys. Rev. **108** (1957) 353
5) D. W. Lang, Ph. D. thesis, Australian National University 1960 (unpublished)
6) D. W. Lang and K. J. Le Couteur, Nuclear Physics **14** (1959) 21
7) H. A. Bethe, Rev. Mod. Phys. **9** (1937) 69
8) C. Bloch, Phys. Rev. **93** (1954) 1094
9) J. D. H. Jensen and J. M. Luttinger, Phys. Rev. **86** (1952) 907
10) S. T. Balyaev, Mat. Fys. Medd. Dan. Vid. Selsk. **31** no. 11 (1959)
11) V. F. Weisskopf, Phys. Rev. **52** (1937) 295
12) J. R. Beyster, R. E. Schrandt, M. Walt and E. W. Salmi, LA2099
13) D. B. Thomson, Ph. D. thesis, Los Alamos **1960** (private communication)
14) L. D. Vincent, R. N. Little Jr., J. L. Morgan and J. T. Prud'homme, Bull Am. Phys. Soc.**5** (1960) 103 (G-6)
15) L. Cranberg and J. S. Levin, ORNL 2309 (1956) 84 (Gatlinburg Conference)
16) R. I. Ewing, Ph. D. Thesis, Rice Institute (private communication)
17) A. G. W. Cameron, Can. J. Phys. **36** (1958) 1040)
18) D. W. Lang, Phys. Rev. **123** (1961)
19) C. B. Fulmer and C. D. Goodman, Phys. Rev. **117** (1960) 1339
20) C. D. Goodman and J. L. Need, Phys. Rev. **110** (1958) 676
21) A. Zucker, Nuclear Physics **6** (1958) 420
22) H. W. Fulbright, H. O. Lassen and N. O. R. Poulsen, Mat. Fys. Medd. Dan. Vid. Selsk. **31**, no. 10 (1959)
23) D. L. Allan, Nuclear Physics **6** (1958) 464
24) D. L. Allan, Nuclear Physics **24** (1961) 274
25) R. N. Glover and E. C. Weigold, Nuclear Physics
26) R. N. Glover and K. H. Purser, Nuclear Physics **24** (1961) 431
27) L. Colli, V. Facchini, and S. Micheletti, Nuovo Cim **5** (1957) 502
28) L. Colli, M. Pignanelli, A. Rytz and R. Zurmuhle, Nuovo Cim. **9** (1958) 280
29) R. S. Storey, W. Jack and A. Ward, Proc. Phys. Soc. **75** (1960) 526
30) A. A. Ross, Phys. Rev. **108** (1957) 110
31) T. Ericson, Nuclear Physics **11** (1959) 481
32) J. B. French and B. J. Raz, Phys. Rev. **104** (1956) 1411
33) E. Gross, UCRL **3330**, UCRL **3337**
34) J. Terrell, Phys. Rev. **113** (1959) 327

1.E.3

Nuclear Physics **26** (1961) 446—451; © *North-Holland Publishing Co., Amsterdam*

Not to be reproduced by photoprint or microfilm without written permission from the publisher

THE MAGNETIC MOMENT OF THE SECOND EXCITED STATE OF F^{19}

R. M. FREEMAN

Cavendish Laboratory, Cambridge

Received 27 March 1961

Abstract: The magnetic moment of the second excited state of F^{19} has been determined by a direct measurement of the Larmor precession frequency after the state has been excited in the reaction F^{19} (p, p′) F^{19*}. A value of $+3.69\pm0.04$ n.m. was obtained where the error mainly arose from statistics. Systematic errors were believed to be small by compa rison.

1. Introduction

A number of previous measurements of the magnetic moment of the second excited state of F^{19} have been made [1–5]). In these measurements the manner in which the angular correlation of the 200 keV gamma radiation from this level was attenuated by an externally applied magnetic field yielded an estimate of $g\tau$, where g is the gyromagnetic ratio and τ is the lifetime of the state. The accuracy with which the magnetic moment could be determined was partly dependent on the accuracy with which the lifetime of the state was known. Angular correlations are also attenuated by the electric quadrupole moment of the state interacting with electric field gradients, though this was shown to be a small effect in some of the measurements. In the present experiment the rate of rotation of the angular distribution was measured in an externally applied magnetic field by observing the decay of F^{19*} (200 keV) as a function of time. To a counter, detecting gamma rays emitted into a small solid angle and set in a plane through the source perpendicular to the magnetic field, the excited state will appear to decay as $f(\theta+\omega t)e^{-t/\tau}$, where $f(\theta)$ is the angular distribution of the gamma radiation and $\omega/2\pi$ the Larmor precession frequency of the excited nuclei. Electric quadrupole effects influence the accuracy of the results only indirectly by attenuating the angular distribution. Though a value of the lifetime of the state was used to remove the exponential part from the curves, the results were virtually independent of any error in it. Moreover the resulting curves, having more structure than those obtained by the other method, can be more accurately fitted to a theoretical function.

2. Experimental Procedure

In the actual experiment a fluorine target about 50 keV thick to 873 keV protons was bombarded by a pulsed beam of protons from the 1.4 MV Cock-

croft-Walton generator at the Cavendish Laboratory, Cambridge. The maximum range of the recoiling fluorine nuclei was calculated to be less than half the target thickness by using the results of cloud chamber experiments [6]). As the resonance under study was narrow it was possible to prevent the nuclei from recoiling out of the target material by keeping the bombarding energy of the protons close to the resonant energy. The level was excited by inelastic proton scattering at the 873 keV resonance, a resonance chosen for its large cross-section rather rather than the anisotropy of the gamma ray distribution. The proton pulses were separated by intervals of 250 ns, i e. about 3 halflives of the 200 keV level in F^{19}.

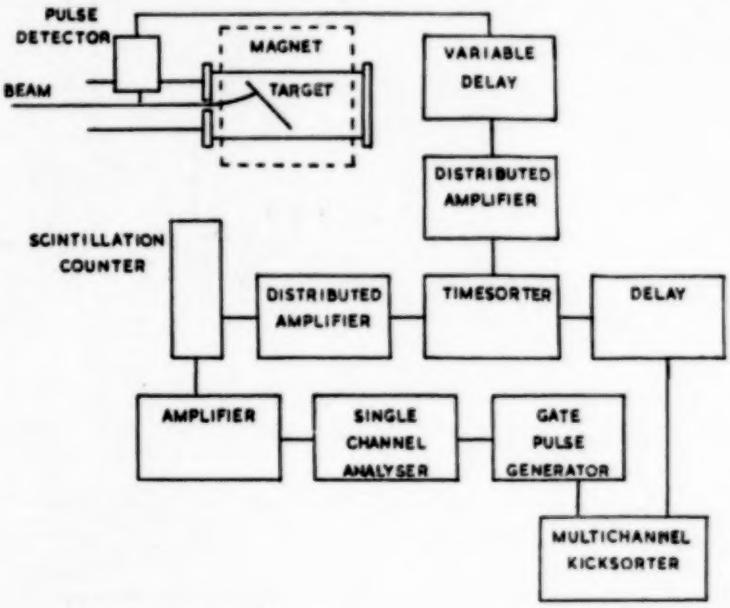

Fig. 1. Block diagram of experiment.

A block diagram of the experiment is shown in fig. 1. The proton pulses were detected some distance before they reached the target by a method described by James and Johnson [7]) in which secondary electrons ejected from a wire intersecting the beam were detected by a scintillation counter. The gamma radiation was detected in a 1.3 cm $\times$ 0.64 cm NaI(Tl) crystal situated about 10 cm from the target at an angle of about 90° to the beam direction and in a plane through the centre of the magnet's gap. The crystal was coupled via a 20 cm light pipe to a magnetically shielded 6810 photomultiplier. Fast pulses from the pulse detector and the gamma ray counter were amplified and brought together in a time-to-pulse height converter (timesorter) designed by James [8]). Pulses from the timesorter were displayed on a multi-channel kick-sorter gated by proportional pulses in the photopeak of the 200 keV radiation. The time resolution measured by the full width at half height of the peak formed by prompt gamma radiation was 9 ns.

Experiments on the 873 keV resonance [9]) have been consistent with a reaction in which p-wave protons were captured into a 2^- state of ^{20}Ne and re-emitted with $j = \frac{3}{2}$ or $\frac{1}{2}$. The resulting 200 keV ($\frac{5}{2}^+$) state decays by an E2 gamma transition to the ground state ($\frac{1}{2}^+$). From the above parameters the gamma rays should be distribubed about the beam direction according to $(1+A\cos^2\theta)$, where A can range from 0.23 for $j = \frac{3}{2}$ to 0.75 for $j = \frac{1}{2}$. Experimentally the measured value of A is less than 0.23 and depends on the nature of the fluorine target. This can be explained by internal effects attenuating the anisotropy which, considering the relatively long lifetime of the state, are not unexpected [10, 11]).

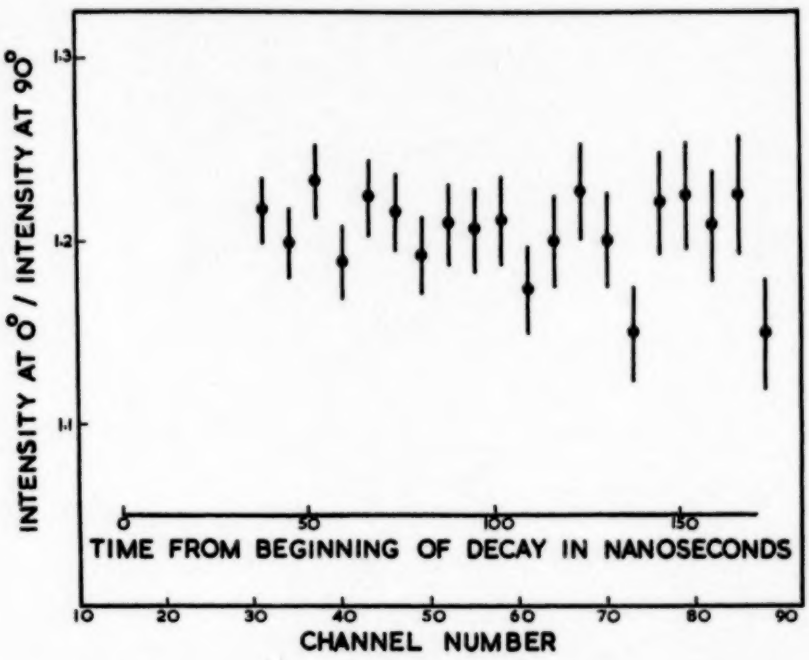

Fig. 2. Variation of anisotropy of 200 keV gamma radiation with time for NaF target.

The anisotropy was measured roughly for targets of several fluorine compounds by timesorting the 200 keV gamma radiation as in the magnetic moment experiments but without a magnetic field. This enabled radiation from the isomeric 200 keV level to be separated from pulses formed by Compton scattering of higher energy prompt gamma radiation in the crystal. At the same time it allowed any changes in the anisotropy with time to be followed. The ratio of the intensity of the 200 keV gamma radiation at 0° and at 90° was measured for targets of LiF, NaF and CaF_2, each about 50 keV thick to 873 keV protons. For NaF the ratio was approximately constant at 1.2 as shown in fig. 2. Because of the size and width of the peak formed at the beginning of the decay curve by prompt gamma radiation, no estimate of the ratio was made until about 40 ns had elapsed from the formation of the excited state. Results were similar for LiF and CaF_2 though the ratio had dropped to between 1.10

and 1.15 for both targets. In the case of CaF_2 there was some evidence at 30 ns from the beginning of the decay that the ratio was falling from a higher value. This could not be explained by the presence of the prompt gamma radiation as this tended to decrease rather than increase the apparent anisotropy. For all three targets it appeared that the ratio had dropped to a constant from some unperturbed value in less than 40 ns. Christy [10]) has estimated this value to be about 1.3 by comparing the gamma ray distribution with the distribution of inelastically scattered protons for several resonances. To understand such behaviour the strength and symmetry of the magnetic and electric fields at the position of the fluorine nuclei after recoil would have to be known [11, 12]). NaF was used as the target in all subsequent experiments.

3. Experimental Results

Fig. 3 shows the timesorted spectrum from one determination of the magnetic moment. The full line corresponds to a function of the form $(1+A\cos^2\omega t)e^{-t/\tau}$

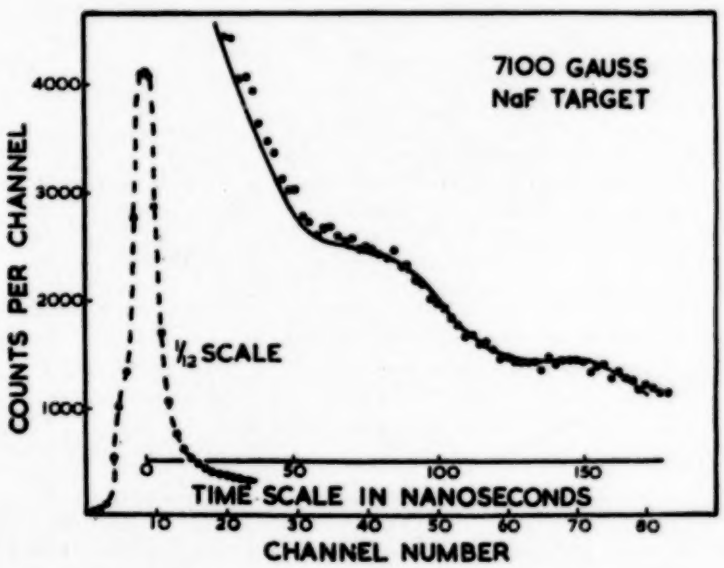

Fig. 3. A spectrum from the timesorter in one of the determinations of the magnetic moment.

corrected for non-linear effects in the timesorter, where $\omega/2\pi$ is the Larmor precession frequency, τ the lifetime of the state and to give the best fit A has been put equal to 0.185. The observed value of A is decreased by the finite time resolution of the apparatus. The fit is not perfect though this did not affect the accuracy with which the precession frequency could be determined and probably arose from not having completely compensated for non-linearity. The magnetic field was measured and monitored throughout the experiments by proton resonance measurements. The timesorter was calibrated by a series of cables whose resonant frequencies were subsequently determined. Departures

from linearity in the timesorter were measured by arranging the counter to detect gamma rays from a radioactive source instead of from the target. The resulting pulses, being random in time, should produce a flat spectrum. The deviation of the spectrum from a constant value was used to correct the curves for the determination of the magnetic moment. The range over which the rotation of the nuclei could be observed was extended by using the prompt peak as a marker for the beginning of the decay. From the position of the gamma ray counter, and from a calculation of the bending of the beam in the magnetic field before striking the target, it was possible to find the angle corresponding to the beginning of the decay, and in this way to follow the rotation of the nuclei for more than 400°. The precession frequencies could be estimated to an accuracy of about 3 %. A small correction, never much greater than 1 %, was applied as some of the nuclei excited by one proton pulse would not have decayed before the arrival of the next pulse. In table 1 the Larmor precession frequencies for five determinations have been listed with the proton resonant frequencies measured in the magnet and the corresponding value calculated for the gyromagnetic ratio of the state. The proton resonant frequencies have been corrected for the change in field between the target position and the point where the magnetic field was measured.

TABLE 1

Larmor precession frequencies

Proton resonant frequency (MHz)	Larmor Precession frequency (MHz)	Gyromagnetic ratio
32.08	8.15	+ 1.42
30.97	8.07	+ 1.45
30.23	8.08	+ 1.49
29.33	7.92	+ 1.51
28.62	7.71	+ 1.50

An average of the five determination gives $+1.475 \pm 0.015$ as the gyromagnetic ratio. The error quoted is only the standard deviation of the mean and is consistent with the estimated statistical error for each determination. Systematic errors were believed to be small by comparison. The proton resonant frequencies and the time scale were known to better than $\frac{1}{2}$ %.

As the state has a spin of $\frac{5}{2}$ the magnetic moment is $+3.69 \pm 0.04$ n.m. This value is more accurate than those previously recorded and lies within their experimental errors. It agrees well with several theoretical calculations. Paul [13]) predicted a value of 3.7 n.m. in a collective model calculation while Rakavy [14]) in another collective model interpretation of the F^{19} nucleus predicted 3.8 n.m. Redlich [15]) using a deformed nucleus model calculated the magnetic moment to be 3.68 comparing this with the value 3.74 he calculated from the shell model.

The author is grateful to Mr. D. D. Stewart for running the set. He is also indebted to the Royal Commissioners for the Exhibition of 1851 for an overseas scholarship.

References

1) W. R. Phillips and G. A. Jones, Phil Mag. **1** (1956) 576
2) K. Sugimoto and A. Mizobucki, Phys. Rev. **103** (1956) 739
3) P. Lehmann, A. Leveque and R. Pick, Phys. Rev. **104** (1956) 411
4) P. B. Treacy, Nuclear Physics **2** (1956) 239
5) M. Martin, R. Szostak and P. Marmier, Helv. Phys. Acta **31** (1958) 481
6) P. M. S. Blackett and D. S. Lees, Proc. Roy. Soc. **134** (1932) 658
7) A. N. James and C. M. P. Johnson Nuclear Instruments **10** (1961) 68
8) A. N. James, Ph. D. Thesis (1960), University of Cambridge
9) R. W. Peterson, C. A. Barnes, W. A. Fowler and C. C. Lauritsen, Phys. Rev. **94** (1954) 1075
10) R. F. Christy, Phys. Rev. **94** (1954) 1077
11) P. B. Treacy, Aust. J. Phys. **10** (1957) 373
12) A. Abragam and R. V. Pound, Phys. Rev. **92** (1953) 943
13) E. B. Paul, Phil. Mag. **2** (1957) 311
14) G. Rakavy, Nuclear Physics **4** (1957) 375
15) M. G. Redlich, Phys. Rev. **110** (1958) 468

8.B

Nuclear Physics **26** (1961) 452—456; © *North-Holland Publishing Co., Amsterdam*

Not to be reproduced by photoprint or microfilm without written permission from the publisher

THE NEW PARTICLES AND THE BARYON MASS SPECTRUM

A. I. SOLOMON †

Laboratoire de Physique Théorique et Hautes Energies, Orsay (S. et O.), France

Received 28 March 1961

Abstract: This paper considers the effects of the new strange particles which complete the Gell-Mann—Nishijima scheme on the mass levels the baryons from the point of view of pertur bation theory. It is shown that the observed baryon mass spectrum ordering may be obtained by a suitable choice of parities.

1. Introduction

The point of view adopted is the following. We consider the baryons as forming a mass degenerate system without their strong interactions, and we may then write expressions for their masses after these interactions have been switched on. By assuming global symmetry and an even (Σ, Λ) parity, we may write results true to all orders in the pion coupling constant for the known baryons; due to the asymmetry between the Λ and Σ interactions introduced by the new particles we may assume equality of K-coupling constants and still get a $\Sigma-\Lambda$ mass difference, unlike Katsumori [1]) or Tanaka [2]). Lichtenberg [3]) also showed that it was possible to obtain a $\Sigma-\Lambda$ mass difference by considering only two new particles; here we work within the framework of the Gell-Mann—Nishijima strangeness scheme and must therefore take into account three new mesons and two new baryons. All these particles are as yet unobserved, though there have been some indications of the strangeness-2 mesons [4]).

The particles to be considered are therefore the following:

baryons ($B = 1$)	N	($S = 0$, $T = \frac{1}{2}$),
	Λ	($S = -1$, $T = 0$),
	Σ	($S = -1$, $T = 1$),
	Ξ	($S = -2$, $T = \frac{1}{2}$),
	X^+	($S = +1$, $T = 0$),
	X^-	($S = -3$, $T = 0$),
mesons ($B = 0$)	ρ	($S = 0$, $T = 0$),
	π	($S = 0$, $T = 1$),
	K	($S = 1$, $T = \frac{1}{2}$),
	$\bar{K}$	($S = -1$, $T = \frac{1}{2}$), with $\bar{K} \equiv \begin{bmatrix} -\bar{K}^0 \\ K^- \end{bmatrix}$,
	ω^+	($S = 2$, $T = 0$),
	ω^-	($S = -2$, $T = 0$).

† On leave of absence from Peterhouse, Cambridge.

The general interaction Hamiltonian formed by Yukawa invariants consistent with this scheme is

$$\begin{aligned}H_{\text{int}} = {} & g_{1\pi}\overline{\mathrm{N}}\boldsymbol{\tau}\cdot\boldsymbol{\pi}\mathrm{N}+g_{2\pi}\Lambda\boldsymbol{\Sigma}\cdot\boldsymbol{\pi}+ig_{3\pi}\boldsymbol{\Sigma}\times\boldsymbol{\Sigma}\cdot\boldsymbol{\pi}+g_{4\pi}\bar{\Xi}\boldsymbol{\tau}\cdot\Xi\boldsymbol{\pi}\\ & +g_{1\mathrm{K}}\overline{\mathrm{N}}\Lambda\mathrm{K}+g_{2\mathrm{K}}\overline{\mathrm{N}}\boldsymbol{\tau}\cdot\boldsymbol{\Sigma}\mathrm{K}+g_{3\mathrm{K}}\bar{\Xi}\Lambda\overline{\mathrm{K}}+g_{4\mathrm{K}}\bar{\Xi}\boldsymbol{\tau}\cdot\boldsymbol{\Sigma}\overline{\mathrm{K}}+g_{5\mathrm{K}}\overline{\mathrm{N}}\mathrm{X}^{+}\overline{\mathrm{K}}+g_{6\mathrm{K}}\bar{\Xi}\mathrm{X}^{-}\mathrm{K}\\ & +g_{1\omega}\overline{\mathrm{N}}\omega^{+}\Xi+g_{2\omega}\bar{\Xi}\omega^{-}\mathrm{N}+g_{3\omega}\overline{\mathrm{X}}^{+}\Lambda\omega^{+}+g_{4\omega}\overline{\mathrm{X}}^{-}\Lambda\omega^{-}\\ & +g_{1\rho}\overline{\mathrm{N}}\mathrm{N}\rho+g_{2\rho}\bar{\Lambda}\Lambda\rho+g_{3\rho}\bar{\boldsymbol{\Sigma}}\cdot\boldsymbol{\Sigma}\rho+g_{4\rho}\bar{\Xi}\Xi\rho+g_{5\rho}\overline{\mathrm{X}}^{+}\mathrm{X}^{+}\rho+g_{6\rho}\overline{\mathrm{X}}^{-}\mathrm{X}^{-}\rho, \qquad (1)\end{aligned}$$

where we have omitted factors such as γ_5 and the hermitian conjugate terms. For the sake of comparison we give the three-dimensional form of the Salam-Polkinghorne [5, 6]) Hamiltonian which introduces in addition to the particles already noted a third X baryon X^0 ($S=-1$, $T=0$) and a third ω-meson ω^0 ($S=0$, $T=0$):

$$\begin{aligned}H_{\text{int}} = {} & g_{1\pi}[\overline{\mathrm{N}}\boldsymbol{\tau}\cdot\boldsymbol{\pi}\mathrm{N}+\bar{\Xi}\boldsymbol{\tau}\cdot\boldsymbol{\pi}\Xi]+g_{2\pi}\Lambda\boldsymbol{\Sigma}\cdot\boldsymbol{\pi}+ig_{3\pi}\bar{\boldsymbol{\Sigma}}\times\boldsymbol{\Sigma}\cdot\boldsymbol{\pi}\\ & +g_{1\mathrm{K}}[\overline{\mathrm{N}}\Lambda\mathrm{K}+\bar{\Xi}\Lambda\overline{\mathrm{K}}]+g_{2\mathrm{K}}[\overline{\mathrm{N}}\boldsymbol{\tau}\cdot\boldsymbol{\Sigma}\mathrm{K}+\bar{\Xi}\boldsymbol{\tau}\cdot\boldsymbol{\Sigma}\overline{\mathrm{K}}]\\ & +g'_{3\mathrm{K}}[\overline{\mathrm{N}}\mathrm{X}^0\mathrm{K}+\sqrt{2}\,\overline{\mathrm{N}}\mathrm{X}^{+}\overline{\mathrm{K}}-\bar{\Xi}\mathrm{X}^0\overline{\mathrm{K}}+\sqrt{2}\,\bar{\Xi}\mathrm{X}^{-}\mathrm{K}]\\ & +g_{1\omega}[\overline{\mathrm{N}}\omega^0\mathrm{N}+\sqrt{2}\,\overline{\mathrm{N}}\omega^{+}\Xi-\bar{\Xi}\omega^0\Xi+\sqrt{2}\,\bar{\Xi}\omega^{-}\mathrm{N}] \qquad (2)\\ & +g'_{2\omega}[\overline{\mathrm{X}}^{+}\mathrm{X}^0\omega^{+}-\overline{\mathrm{X}}^{+}\mathrm{X}^{+}\omega^0+\overline{\mathrm{X}}^{-}\mathrm{X}^{-}\omega^0-\overline{\mathrm{X}}^{-}\mathrm{X}^0\omega^{-}+\overline{\mathrm{X}}^0\mathrm{X}^{+}\omega^{-}-\overline{\mathrm{X}}^0\mathrm{X}^{-}\omega^{+}]\\ & +g_{3\omega}[\overline{\mathrm{X}}^{+}\Lambda\omega^{+}+\overline{\mathrm{X}}^0\Lambda\omega^0+\overline{\mathrm{X}}^{-}\Lambda\omega^{-}]+g_{1\rho}[\overline{\mathrm{N}}\mathrm{N}\rho+\bar{\Xi}\Xi\rho]+g_{2\rho}\bar{\Lambda}\Lambda\rho+g_{3\rho}\bar{\boldsymbol{\Sigma}}\cdot\boldsymbol{\Sigma}\rho\\ & +g_{4\rho}[\overline{\mathrm{X}}^{+}\mathrm{X}^{+}\rho+\overline{\mathrm{X}}^0\mathrm{X}^0\rho+\overline{\mathrm{X}}^{-}\mathrm{X}^{-}\rho].\end{aligned}$$

In spite of the inclusion of two extra particles, this more highly symmetrical scheme contains 7 fewer constants. However, it is clear from this Hamiltonian that we shall be unable to explain the Ξ—N mass difference if we assume complete invariance in the four dimensional space, for the method to be adopted in the first scheme, namely allowing the X-particles to have different parities, cannot be applied here. For another method see ref. [6]).

2. Calculation of the Self-Masses

Using Hamiltonian (1) we may now write down expressions for the self-masses in lowest order perturbation theory. We consider all the mesons to be pseudoscalar, and use the notation of Katsumori [1]), viz. $F(\mathrm{B_1B_2M})$ stands for the contribution to the self-mass of the baryon $\mathrm{B_1}$ from the interaction $\mathrm{B_1}\rightarrow\mathrm{B_2}+\mathrm{M}$. We get

$$\begin{aligned}\Delta M_{\mathrm{N}} = {} & 3g_{1\pi}^2F(\mathrm{NN}\pi)+3g_{2\mathrm{K}}^2F(\mathrm{N}\Sigma\mathrm{K})+g_{1\mathrm{K}}^2F(\mathrm{N}\Lambda\mathrm{K})+g_{5\mathrm{K}}^2F(\mathrm{NX}^{+}\overline{\mathrm{K}})\\ & +g_{1\omega}^2F(\mathrm{N}\Xi\omega^{+})+g_{1\rho}^2F(\mathrm{NN}\rho),\\ \Delta M_{\Lambda} = {} & 3g_{2\pi}^2F(\Lambda\Sigma\pi)+2g_{1\mathrm{K}}^2F(\Lambda\mathrm{N}\overline{\mathrm{K}})+2g_{3\mathrm{K}}^2F(\Lambda\Xi\mathrm{K})+g_{3\omega}^2F(\Lambda\mathrm{X}^{-}\omega^{+})\\ & +g_{4\omega}^2F(\Lambda\mathrm{X}^{+}\omega^{-})+g_{2\rho}^2F(\Lambda\Lambda\rho),\end{aligned}$$

$$\Delta M_\Sigma = 2g_{3\pi}^2 F(\Sigma\Sigma\pi)+g_{2\pi}^2 F(\Sigma\Lambda\pi)+2g_{2K}^2 F(\Sigma N\overline{K})+2g_{4K}^2 F(\Sigma\Xi K)+g_{3\rho}^2 F(\Sigma\Sigma\rho),$$

$$\Delta M_\Xi = 3g_{4\pi}^2 F(\Xi\Xi\pi)+3g_{4K}^2 F(\Xi\Sigma\overline{K})+g_{3K}^2 F(\Xi\Lambda\overline{K})+g_{6K}^2 F(\Xi X^- K) + g_{2\omega}^2 F(\Xi N\omega^-)+g_{4\rho}^2 F(\Xi\Xi\rho), \quad (3)$$

$$\Delta M_{X^+} = 2g_{5K}^2 F(X^+ NK)+g_{3\omega}^2 F(X^+\Lambda\omega^+)+g_{5\rho}^2 F(X^+X^+\rho),$$

$$\Delta M_{X^-} = 2g_{6K}^2 F(X^-\Xi\overline{K})+g_{4\omega}^2 F(X^-\Lambda\omega^-)+g_{6\rho}^2 F(X^-X^-\rho).$$

In order to evaluate these expressions we must know the relative parities of the baryons. The parities of the N and Λ are taken conventionally as positive, and the assumption of an even (Σ, Λ) parity is made. This leaves three parities to be determined.

We now introduce the following symmetries:

Global Symmetry	(equality of π-coupling constants),
Cosmic Symmetry	(equality of K-coupling constants),
Galactic Symmetry	(equality of ω-coupling constants),
Universal Symmetry	(equality of ρ-coupling constants).

The remaining parities are now fixed by noting that the contribution from a scalar self-energy is negative, while that from a pseudoscalar is positive, and so a positive Ξ—N mass difference implies the following parities:

$$P_\Xi = +, \qquad P_{X^-} = +, \qquad P_{X^+} = -.$$

The use of Global Symmetry now enables us to consider the calculations as having been made to all orders in the π-coupling constant, and the same is true for the ρ-coupling constant and those K-terms not involving the new particles, the lowest order calculation being made only for those interactions which split the masses (viewpoint I).

Thus, including the π and ρ terms, and the 'old' K terms, in a modified bare mass M, we may write down the masses of the known baryons as follows:

$$\begin{aligned} &M_N = M+g_K^2 F_K(-)+g_\omega^2 F_\omega(+), \qquad M_\Lambda = M+g_\omega^2[F_\omega(-)+F_\omega(+)], \\ &M_\Sigma = M, \qquad M_\Xi = M+g_K^2 F_K(+)+g_\omega^2 F_\omega(+), \end{aligned} \quad (4)$$

where $F_B(+)$ [$F_B(-)$] stands for the contribution from a pseudoscalar [scalar] interaction involving the boson B. In the limit as $\Lambda \to \infty$ these expressions are independent of B:

$$F_B(+) \sim \frac{M}{4\pi}\log\frac{\Lambda}{M}, \qquad F_B(-) \sim \frac{-3M}{4\pi}\log\frac{\Lambda}{M},$$

where Λ is some cut-off.

By elimination of the coupling constants we may immediately derive the

expression for infinite cut-off

$$\frac{5M_N+6M_\Xi}{2M_\Lambda+9M_\Sigma}=1. \tag{5}$$

Experimentally †, this value is found to be 0.97.

Secondly, one derives a quantity dependent on the coupling constants (but the cut-off is again infinite

$$\frac{M_\Xi-M_N}{M_\Sigma-M_\Lambda}=\frac{2g_K^2}{g_\omega^2}. \tag{6}$$

We may estimate this expression by using a remark of Lichtenberg [3]) that $M_\pi g_\pi = M_K g_K = M_\omega g_\omega$ seems to hold for the π- and K-coupling constants at any rate, and a value for M_ω of 750 MeV [6]). The result is 4.56 (experimentally 4.88).

The baryon mass spectrum can now be calculated from two points of view. *Viewpoint I.* The baryon masses consist of a bare mass M_0 (which may be partly gravitational in origin) plus the contributions from the strong interactions. The stated mass relations (4) thus enable one to calculate the baryon mass differences to all orders in the π, ρ, and 'old' K coupling constants, and to lowest order in the 'new' K and ω couplings, provided we put in a cut-off.
Viewpoint II. The baryon masses come from their strong interactions, or equivalently, we may neglect M_0. We may then calculate the baryon mass differences to lowest order only in all the coupling constants, but without resort to a cut-off. For example, in equation (4) M is replaced by

$$(3g_\pi^2+4g_K^2+g_\rho^2)F(+) \quad \text{and} \quad M_N/M_\Sigma = 1-(3g_K^2-g_\omega^2)/(3g_\pi^2+4g_K^2+g_\rho^2), \text{ etc.}$$

This last viewpoint involves an estimate of g_ρ. However, the value of g_ρ, if near that of g_K or less, hardly affects the result as the main contribution comes from the pion terms.

The results of applying each of these points of view are shown in table 1.

TABLE 1

Calculated masses

Particle	Experimental mass (MeV)	Viewpoint I Cut-off: $1.6M_\Sigma$ [a])	Viewpoint II Cut-off: ∞
N	939	937	1 120
Λ	1 115	1 116	1 168
Σ	1 192	1 192 [b])	1 192 [b])
Ξ	1 315	1 268	1 232

[a]) Calculated by the Feynman technique b) Conventional assignment

† The masses used in this paper are those given in ref. [7]).

3. The New Baryons

The masses of the new baryons cannot be satisfactorily discussed from either point of view, but we may include here the result

$$M_{X^-} - M_{X^+} = 2[(M_\Xi - M_N) + (M_\Sigma - M_\Lambda)] \approx 906 \text{ MeV} \qquad (7)$$

for infinite cut-off, independent of the two coupling constants g_K^2 and g_ω^2.

If $M_{X^+} > 1436$ MeV, then $X^+ \to N + K$ is a strong decay, and so the X^+ will be very unstable and only appear possibly as a resonance in N–K scattering.

Then relation (7) implies $M_{X^-} > 2340$ MeV, and so the X^- will also have the strong decay $X^- \to \Xi + \overline{K}$, and will consequently be also very unstable.

4. Conclusion

We have shown that, within the framework of the Gell-Mann-Nishijima strangeness scheme, it is possible to explain the ordering of the baryons within the known baryon mass spectrum by a suitable assignment of parities, under a most symmetrical coupling constant scheme where there is only one coupling constant associated with each meson.

We have considered two points of view. The first treats the contributions from the known interactions exactly to all orders in the coupling constants, although only the lowest order expressions are given, and regards the new particles as producing perturbations which give rise to the mass differences and can be calculated in lowest order using a cut-off. The second point of view calculates the mass differences to lowest order only, but does not involve a cut-off.

It will be noted that this scheme always reproduces the correct ordering, independent of cut-off, provided only $g_K^2 > g_\omega^2$.

This picture fails to give any indication as to how the new baryons introduced by the scheme obtain their assumed relatively large masses.

The author wishes to thank the electors to the Robert Gardiner Memorial Fund, and the Dodds Fund, Peterhouse, for maintenance grants, and Dr. M. Lévy for hospitality extended to him during his stay at Orsay where this work was carried out. He is also indebted to Dr. B. d'Espagnat for much helpful criticism.

References

1) H. Katsumori, Prog. Theor. Phys. **19** (1958) 342
2) K. Tanaka, Phys. Rev. **119** (1960) 1436
3) D. B. Lichtenberg, Phys. Rev. Lett. **4** (1960) 143
4) W. Kan-Chang, Proc. of the Kiev Conference (1959);
H. Ting Chang, JETP **11** (1960) 1172
T. Yamanouchi and M. F. Kaplon, Phys. Rev. Lett. **3** (1959) 283
5) A. Salam and J. C. Polkinghorne, Nuovo Cim. **2** (1955) 685
6) J. C. Polkinghorne, Nuovo Cim. **6** (1957) 864
7) Report of the Rochester Conference, 1960

1.E.1:
3.A

Nuclear Physics **26** (1961) 457—462; © *North-Holland Publishing Co., Amsterdam*
Not to be reproduced by photoprint or microfilm without written permission from the publisher

GAMMA-RAY SPECTRUM OF Te^{131}

J. M. FERGUSON and F. M. TOMNOVEC
U.S. Naval Radiological Defense Laboratory, San Francisco 24, California

Received 13 March 1961

Abstract: The gamma-ray spectrum of 25 min Te^{131} was investigated with scintillation spectrometers. Gamma rays with energies of 0.145, 0.445, 0.604, 0.940, 0.985 and 1.13 MeV were found, and their relative abundances were measured. The 0.445 and 0.985 MeV gammas are in coincidence with the 0.145 MeV gamma ray. A decay scheme is proposed with I^{131} levels at 0.145, 0.604, 0.940 and 1.13 MeV.

1. Introduction

The gamma-ray spectrum of 25 min Te^{131} was studied using NaI(Tl) crystals, multichannel analyzers and a slow-fast coincidence unit.

Some of the results of other workers are given in table 1. Te^{131} decays by

TABLE 1

Previous measurements of beta and gamma energies and abundances

	Hebb[1])		Mallman [2])		Ergen [3])	
	Energy (MeV)	Abundance	Energy (MeV)	Abundance (Relative)	Energy	Abundance
β_1	1.35	15%				
β_2	1.69	25%				
β_3	2.14	60%				
γ_1	0.147		0.145	100		
γ_2	0.446		0.450	24		
γ_3			0.595	6		
γ_4	0.77					
γ_5			0.950	4		
γ_6			1.14	8		
γ_7					> 2.23	22%

negaton emission to the excited levels of I^{131}. The gamma-ray energies have been measured by Hebb [1]) and Mallman *et al.* [2]). Also, Ergen has reported relatively strong high-energy gamma rays (> 2.2 MeV) which are not reported by other workers [3]). Mallman *et al.* have measured relative abundances as well as energies of the gamma rays.

2. Experimental Technique and Results

2.1. SAMPLE IRRADIATION

Te^{131} was produced by slow-neutron irradiation of natural tellurium. The neutrons came from proton bombardment of beryllium at the University of California Crocker cyclotron. Each sample consisted of 2 g tellurium metal powder in a gelatin capsule; each was irradiated for 20 min.

2.2. SINGLES SPECTRUM

A 10.16 cm diameter, 10.16 cm high NaI(Tl) crystal was used to obtain the singles gamma-ray spectrum. The pulse-height spectrum from the crystal was recorded with a 100-channel analyzer. The crystal was surrounded by a 15.24 cm lead shield. The source was placed outside the shield and the gamma rays entered the crystal through a 1.27 cm diameter aperture in the shield.

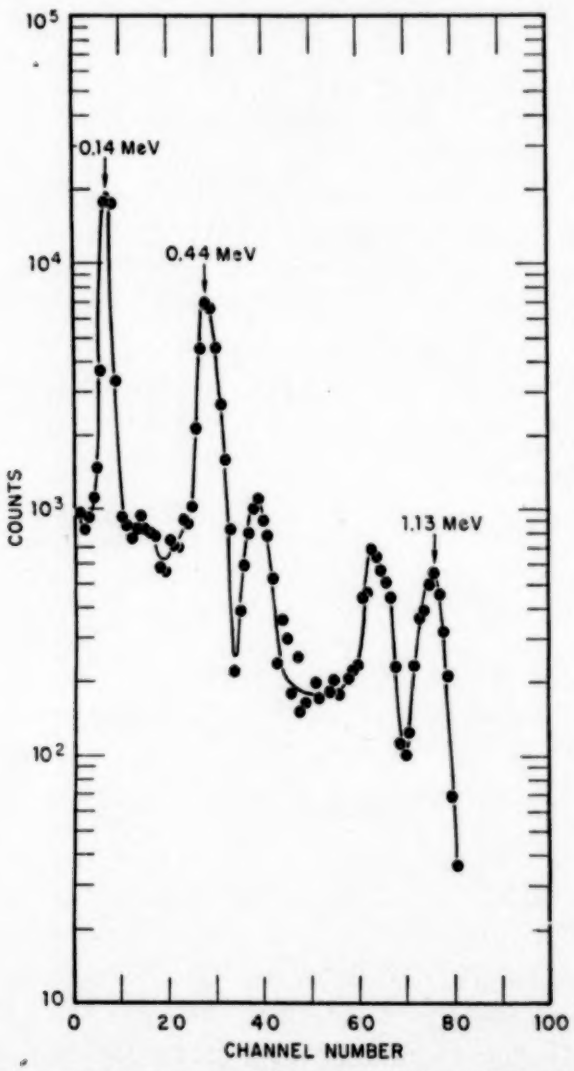

Fig. 1. Te^{131} singles gamma-ray spectrum with background subtracted. The crystal views the source through a 15.24 cm long, 1.27 cm diameter collimator. There is a small contribution to the 0.44 MeV peak from Te^{129}.

This equipment is in a mobile-laboratory trailer which was located next to the cyclotron building during the experiment. The counting was begun a few minutes after the irradiations. Later runs were used to subtract out the background and longer-lived acitivities.

The singles spectrum is shown in fig. 1. Five full-energy peaks from Te^{131} gamma rays are evident. The 0.95 MeV peak is a composition peak. There is a contribution to the 0.44 MeV peak from Te^{129}. No gamma rays above 1.13 MeV were observed; any such gamma rays must have abundances below 1 % to escape detection. Also, we did not observe the 0.77 MeV gamma ray reported by Hebb. If it is present it must have an abundance of less than 1 %.

The pulse-height spectra of single-energy gamma rays for this apparatus have been measured for a wide variety of energies. The pulse-height of the spectrum for each Te^{131} gamma ray was calculated from the known shapes for single-energy gamma rays. The contribution from each gamma ray was then subtracted from the spectrum, starting with the highest energy gamma ray. The relative abundances of the gamma rays were then obtained from the area of the full-energy peaks and the known efficiency of the crystal. The large size of the source made it necessary to apply a self-absorption correction. The correction factor was calculated to be 0.50 for the 0.145 gamma ray. This is the largest source of error in the determination of abundances.

TABLE 2

Gamma ray energies and abundances

E_γ (MeV)	Abundance (gammas/dis)	Standard deviation for abundances
0.145±0.005	0.67	±0.13
0.445±0.01	0.14	±0.03
0.604±0.01	0.060	±0.012
0.940±0.01	0.028	±0.006
0.985±0.01	0.037	±0.007
1.13 ±0.01	0.051	±0.010

The singles results are listed in table 2. The abundances of the gamma rays are expressed in terms of gammas per disintegration. Actually only the relative abundances were measured. The absolute abundances were inferred from decay scheme considerations (see sect. 3).

2.3. COINCIDENCE SPECTRA

The coincidence spectrometer consists of two 10.16 × 10.16 cm NaI (Tl) crystals, a slow-fast coincidence unit with the associated amplifiers, a differential discriminator and a 256-channel analyzer. The fast coincidence unit has a resolving time of 4×10^{-8} sec. Pulses of a certain height from the first crystal are selected by the differential discriminator and fed to the coincidence unit. The

coincidence unit requires a fast coincidence between the pulses from the two crystals and a pulse from the differential discriminator. The output of the coincidence unit then triggers the 256-channel analyzer to accept a pulse from the second crystal.

The crystals are mounted 12.7 cm apart with the source in between. Each crystal has a lead collimator 5.08 cm long, with an aperture tapered from 1.52 cm in diameter at the source end to 2.54 cm in diameter at the crystal end.

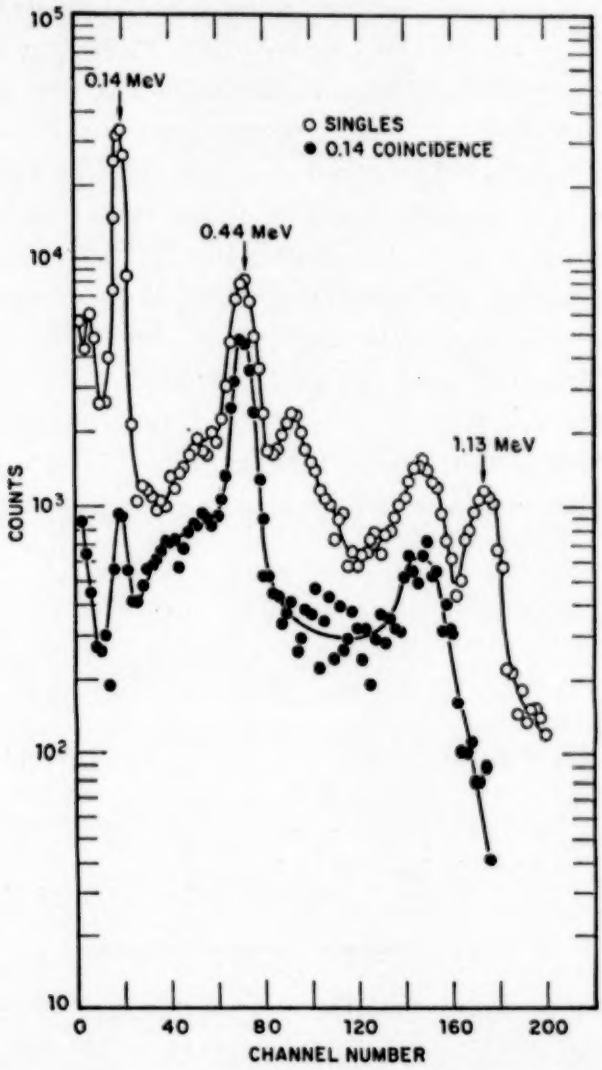

Fig. 2. The open circles represent the Te^{131} singles spectrum. Other activities have been subtracted out on the basis of later runs. The solid circles represent the pulse-height spectrum in coincidence with the 0.14 MeV gamma ray. The coincidence counts have been multiplied by 10 to bring the curves closer together.

Since the coincidence equipment is not mobile, the samples to be coincidence counted were brought back to NRDL. Hence there was a half-hour delay between irradiation and counting, and the ratio of Te^{127} and Te^{129} to Te^{131} was higher than in the samples counted in singles. Also there was time for I^{131} to grow in. However, the effects of these other activities were subtracted out

on the basis of later runs. The Te^{131} singles spectrum taken with the coincidence apparatus is shown in fig. 2. Also shown is the spectrum in coincidence with pulses in the 0.14 MeV region from the other crystal. It is clear that the 0.44 MeV gamma and one or both of the 0.9 MeV gammas are in coincidence with the 0.14 MeV gamma. The 0.14 peak in the coincidence spectrum is due to Compton events in the discriminator crystal. A fit of the singles spectrum to the coincidence data around 0.9 MeV indicates that the 0.985 MeV gamma ray is in coincidence with the 0.145 MeV gamma ray, but the 0.940 MeV gamma ray is not.

The gamma-ray spectrum in coincidence with the 0.604 MeV gamma ray was also taken, but no coincidences were found. The results of the coincidence studies are summarized in table 3.

TABLE 3

Coincidence data

Energy (MeV)	0.14	0.44	0.60	0.94	0.98	1.13
0.14	(No)		No			
0.44	Yes		No			
0.60	No		No			
0.94	(No)		No			
0.98	Yes		No			
1.13	No		No			

(Observed coincidences are indicated by *yes*. Coincidences which we looked for but did not observe are indicated by *no*, The result for the 0.14—0.94 coincidences are in parentheses because this result is not as certain as the others.

3. Discussion

The above data can be combined with those of other workers to establish a complete decay scheme. The character of the Te^{131} ground level is known to be $\frac{3}{2}+$ from the Te^{131m}—Te^{131} isomeric transition and shell model considerations [4,5]). The ground level of I^{131} has been measured [6]) to be $\frac{7}{2}+$. Hence the beta transition to the I^{131} ground level should be second forbidden and negligible.

Hebb [1]) has measured the beta ray spectrum (see table 1). On the basis of energies and intensities, the 2.14 MeV beta transition must go to a I^{131} level at 0.145 MeV. The 1.69 beta goes to a level at 0.604 MeV; the 0.44 MeV and 0.59 MeV gammas are transitions from this level to the 0.145 MeV level and ground level, respectively. Our gamma-ray data indicate I^{131} levels at 0.940 and 1.13 MeV. This would indicate that the 1.35 MeV beta group reported by Hebb actually corresponds to two groups with energies of 1.15 and 1.34 MeV. In view of the difficulty of resolving weak inner beta groups, the two sets of data are not inconsistent.

We thus obtain the decay scheme of fig. 3. We may combine this information with the data on gamma-ray relative abundances to obtain absolute

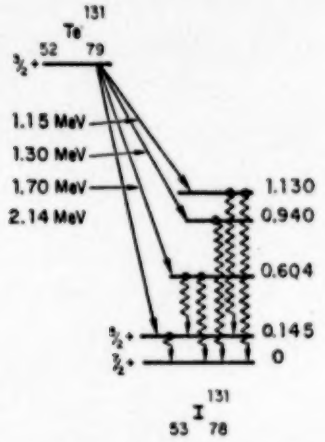

Fig. 3. Proposed Te^{131} decay scheme. The Te^{131} character assignment is based on the work of Alväger and Oelsner [4]) and Goldhaber and Hill [5]). The character of the I^{131} ground level is taken from the work of Lipworth and Garvin [6]) and the character of the first excited level is based on the log *ft* value and the values of Bedesen *et al.* for the conversion coefficient [7]). The beta-ray energies are based on Hebb's work and the energy level assignments are from this work.

abundances. To do this we must take into account the internal conversion coefficient of the 0.145 MeV gamma ray. Bedesen *et al.* [7]) have measured the K-shell coefficient to be 0.26. On the basis of Rose's tabulation of conversion coefficients [8]) we take the ratio K/L+M+ . . . of K-shell conversion to other conversion to be 3.8. Internal conversion is considered negligible for the other gammas. Now by simply requiring the number of transitions to the ground level to be 100 % we obtain the absolute abundances given in table 2.

References

1) E. Hebb, Phys. Rev. **97** (1955) 987
2) C. A. Mallmann, A. H. W. Aten, Jr., D. R. Bess and C. M. deMcMillan, Phys. Rev. **7** (1955) 99
3) W. K. Ergen, Aircraft nuclear propulsion-59 (Oak Ridge, 1951)
4) A. Alvager and G. Oelsner, Ark. Fys. **12** (1957) 319
5) M. Goldhaber and R. D. Hill, Rev. Mod. Phys. **25**, (1953) 469
6) E. P. Lipworth and H. L. Garvin, Bull. Am. Phys. Soc. **2** (1957) 316
7) A. Bedesen, K. P. Mitrofanov, A. A. Sorokin and V. S. Shpinel, JETP(USSR) **37** (1959) 314
8) M. E. Rose, Internal conversion coefficients (Interscience Publishers, New York, 1958)

1.B: 2.L

Nuclear Physics **26** (1961) 463—468; © *North-Holland Publishing Co., Amsterdam*

Not to be reproduced by photoprint or microfilm without written permission from the publisher

PHASE SHIFT CALCULATIONS ON α-α SCATTERING

E. W. SCHMID and K. WILDERMUTH

Florida State University, Tallahassee, Florida

and

Oak Ridge National Laboratory †

Received 4 April 1961

Abstract: The α—α scattering phase shifts are calculated with two nucleon forces which describe the low energy two-nucleon scattering data. The obtained results are discussed.

Starting from the nucleon-nucleon forces, the α—α interaction has been previously investigated within the framework of Wheeler's resonating group theory [1–5]). A. C. Butcher and J. M. McNamee [1]) have calculated the scattering phase shifts, but they employed a force which does not describe the two-nucleon S-wave scattering data. Furthermore their conclusion about the force mixture ($\frac{2}{3}$ Serber + $\frac{1}{3}$ Rosenfeld mixture) seems to contradict that arrived at from another analyses [6]).

Therefore we have re-examined this problem in order to determine if it is not possible to derive the α—α scattering phase shifts starting from two-nucleon interaction forces which describe the deuteron and the two nucleon low-energy scattering data as well as possible. This point of view was stimulated by the following considerations:

1) Due to the indistinguishability of the nucleons the resonating group (cluster) description can be considered as a generalization of the shell model and is not in contradiction with it [7]).

2) The hard core part of the nucleon-nucleon forces is not important for the interaction between the two α-particle clusters, and therefore we have only to take it into account in the intrinsic motion of the clusters [8]).

3) The radius of the α-particle clusters stays essentially the same during the compound nucleus formation. Also the polarization of the α-particles can be neglected [8]). Therefore the saturation character of the nuclear forces can be taken into account to a good approximation by choosing the α-particle cluster radii equal to the experimental radius of the free α-particles.

4) Owing to the spherical symmetry of the α-particles the spin orbit and tensor forces will not contribute to the α—α scattering in a first approximation. These forces would bring in an ambiguity since they cannot be determined with good accuracy from the low energy two-nucleon data.

† Work partially supported by the Office of Naval Research.

The two-nucleon potential assumed is of the form

$$V_{ik} = -V_0 \exp(-\beta \mathbf{r}_{ik}^2)[w - m\tfrac{1}{4}(1+\boldsymbol{\sigma}_i\boldsymbol{\sigma}_k)(1+\boldsymbol{\tau}_i\boldsymbol{\tau}_k) + b\tfrac{1}{2}(1+\boldsymbol{\sigma}_i\boldsymbol{\sigma}_k) - h\tfrac{1}{2}(1+\boldsymbol{\tau}_i\boldsymbol{\tau}_k)]. \quad (1)$$

Previous calculations of the ground state and the first two excited states of Be [8]) using a Yukawa potential did not show a remarkable difference from the calculation with a Gaussian potential. Therefore it can be expected that the shape of the potential is not important as long as the two-nucleon scattering data are described with equal accuracy.

The parameters of our potential (1) are chosen to be

$$\begin{aligned} V_0 &= 72.98 \text{ MeV}, & \beta &= 0.46\times 10^{-26} \text{ cm}^{-2} \\ w+m-b-h &= 0.63, & w+m+b+h &= 1. \end{aligned} \quad (1a)$$

This potential yields a n—p singlet effective range r_{0s}, triplet effective range r_{0t}, n—p singlet scattering length a_s and deuteron binding energy E_d, in close agreement with experiment, as shown by table 1.

TABLE 1

n—p parameters

	r_{0s} (fm)	r_{0t} (fm)	a_s (fm)	E_d (MeV)
calculated	2.41	1.701	−22	2.226
experimental [9])	2.40±0.23	1.704±0.028	−23.69±	2.226±0.002

The S-wave phase shifts of p—p scattering calculated with the above force constants are shown in fig. 1.

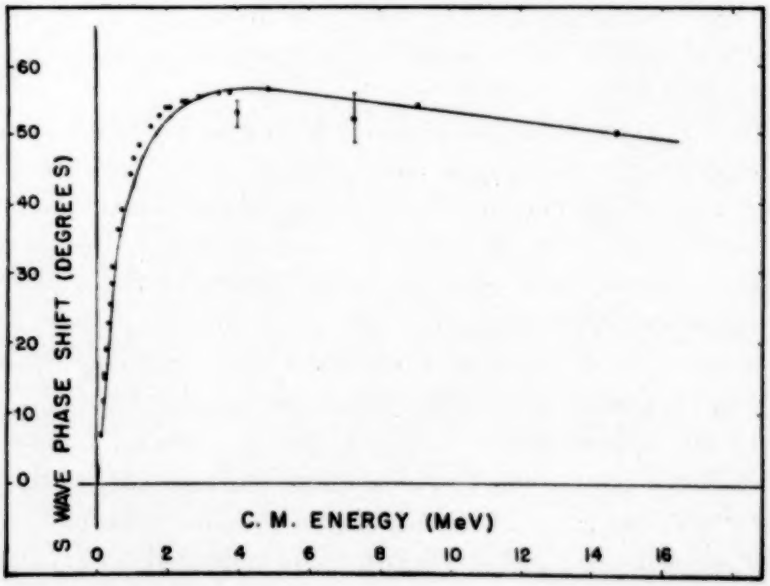

Fig. 1. Proton-proton scattering, S-wave phase shifts; experimental points from ref. [9]).

The main part of our force mixture consists of a Serber mixture ($w = m$, $h = h$), which describes the symmetry of the two-nucleon scattering phase shifts around 90° in the centre-of-mass system. The small deviation from this symmetry in the low energy region ($\leqq 50$ MeV c.m.) we describe in a first approximation by an admixture of a small portion of Rosenfeld force (m = 2b, h = 2w), which gives, for instance, the negative sign of the observed P-wave phase shifts for the low energy p—p scattering [9]). However these experimental data are not accurate enough to determine the portion of Rosenfeld force exactly. They only can tell that it is somewhere less than 10 %. We will later choose it to be 6 %.

To obtain the integro-differential equation for the α—α scattering, the Ritz variational principle was employed. As a trial wave function for the system we used

$$\psi_l = A\varphi(\alpha_1)\varphi(\alpha_2)\chi_l(\mathbf{R}_{\alpha_1}-\mathbf{R}_{\alpha_2}),$$

where $\varphi(\alpha_1)$ and $\varphi(\alpha_2)$ (which also contain spin and isobaric spin variables) describe the internal motion of the two α-particle clusters, $\chi_l(\mathbf{R}_{\alpha_1}-\mathbf{R}_{\alpha_2})$ describes the relative motion ($\mathbf{R}_{\alpha_1}$, $\mathbf{R}_{\alpha_2}$ are centre-of-mass co-ordinates) and A denotes complete antisymmetrization of the wave function [7]). The space part of the internal motion $\varphi(\alpha_1)\,\varphi(\alpha_2)$ was assumed to be

$$\exp\left[-\tfrac{1}{2}a\sum_{i=1}^{4}(\mathbf{r}_i-\mathbf{R}_{\alpha_1})^2-\tfrac{1}{2}(a)\sum_{i=5}^{8}(\mathbf{r}_i-\mathbf{R}_{\alpha_2})^2\right]$$

with $a = 0.535\times10^{-26}$ cm^{-2} corresponding to a cluster radius of 1.45 fm. This radius follows from the *rms* radius 1.61 fm of the α-particle [10]) if one takes into account the finite charge distribution of the proton, which has been reported to be 0.72 fm for an assumed Gaussian charge distribution [10]).

For $\chi_l(\mathbf{R}_{\alpha_1}-\mathbf{R}_{\alpha_2})$, an integro-differential equation was obtained in the usual way [7]) by variation of $\chi_l(\mathbf{R}_{\alpha_1}-\mathbf{R}_{\alpha_2})$ in the expression

$$\delta\int(\psi^*H\psi-\lambda\psi^*\psi)\mathrm{d}\tau = 0.$$

It has the form

$$\left[\frac{\hbar^2}{4M}\left(\frac{\mathrm{d}^2}{\mathrm{d}r^2}-\frac{l(l+1)}{r^2}\right)+E-V(r)\right]f_l(r) = \int_0^\infty k_l(r,r')f_l(r')\mathrm{d}r', \qquad (2)$$

where $f_l(r)$ is the radial part of $\chi_l(\mathbf{R}_{\alpha_1}-\mathbf{R}_{\alpha_2})$. The left side describes the direct interaction of the two α-clusters; the right side contains all exchange interactions and is a rather complicated function. Eq. (2) is in agreement with that derived by van der Spuy [2]). The exchange part of the Coulomb interaction is neglected because of the long range of the Coulomb forces †.

† The values of the kernel function k_l (r, r') calculated by van der Spuy have been useful in checking our computer programmes.

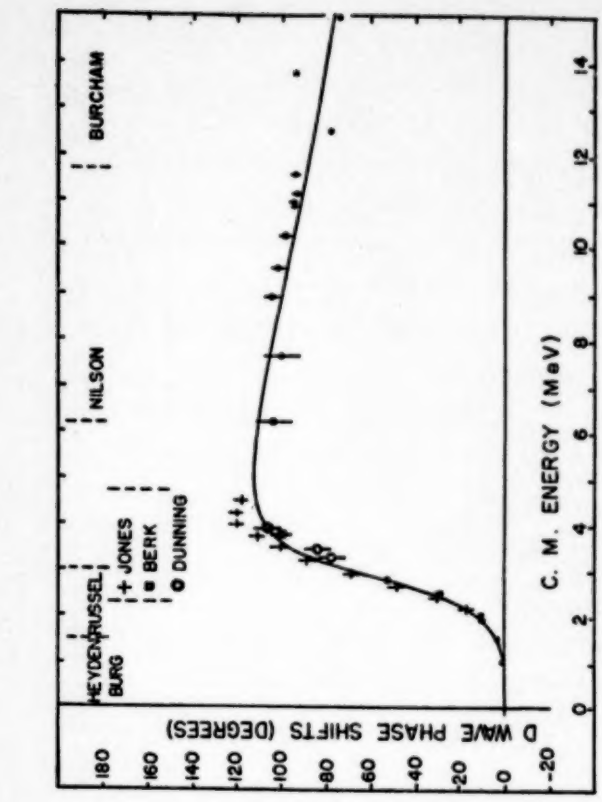
D WAVE PHASE SHIFTS (DEGREES)
C. M. ENERGY (MeV)
HEYDENBURG
RUSSEL
JONES
BERK
DUNNING
NILSON
BURCHAM

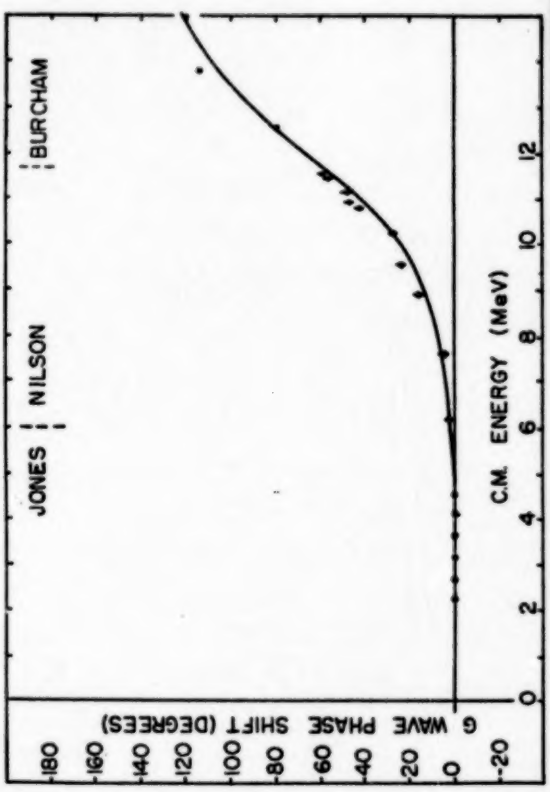
G WAVE PHASE SHIFT (DEGREES)
C.M. ENERGY (MeV)
JONES
NILSON
BURCHAM

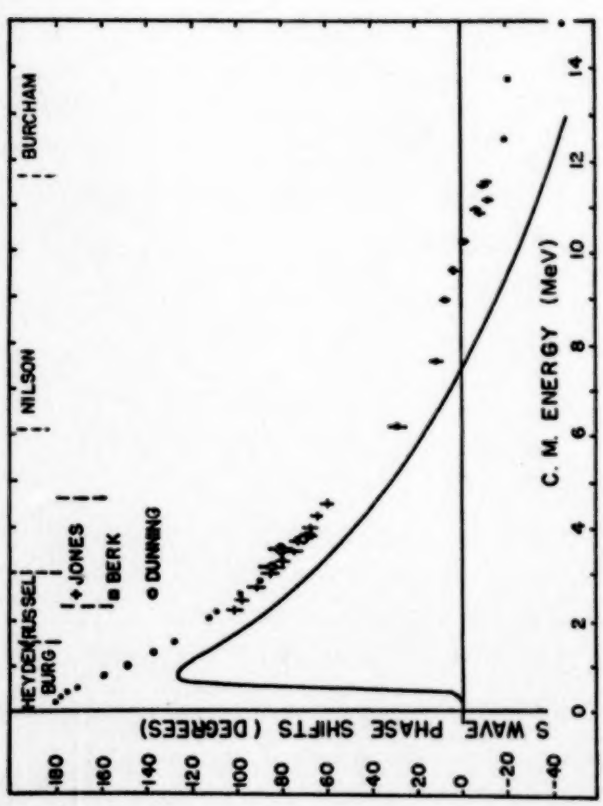
S WAVE PHASE SHIFTS (DEGREES)
C. M. ENERGY (MeV)
HEYDENBURG
RUSSEL
JONES
BERK
DUNNING
NILSON
BURCHAM

Eq. (2) was solved on an IBM 7090 computer using the above given parameters and different percentages of Rosenfeld force. To obtain $f_l(r)$, the method of Robertson [11]) was used in the region $0 \leqq r \leqq 4.5$ fm, and a method given by Fox and Goodwin [12]) in the region $r > 4.5$ fm. The solution $f_l(r)$ was matched to Coulomb functions at a distance r which was large enough to fulfil the requirements of a simple calculation method for Coulomb functions given by Fröberg [13]).

The agreement of the obtained phase shifts with the experimental data of several authors [14–20]) was fairly good for the portions of Rosenfeld force between 0 and 10 %. The best agreement was obtained for 94 % Serber force and 6 % Rosenfeld force; no further attempt to fit the parameters was made. Fig. 2 shows the S, D and G wave phase shift curves for this force mixture together with the experimental values [14–20]). The agreement for the $l = 2$ and $l = 4$ phase shifts is very good. For $l = 0$ the resonance energy is about 0.4 MeV too high. For the right resonance energy of around 95 keV this curve would rise up to almost 180° and would then also fit the experimental points very well †.

These results indicate that it is possible to derive the α—α scattering phase shifts to a good approximation by forces which describe the low energy two-nucleon scattering data ($E_{\text{c.m}} < 50$ MeV.) The form and character of these forces are very probably not important, as the before-mentioned calculations of ref. [8]) indicate. Furthermore, it follows from our considerations that it should also be possible to describe other scattering problems (α-triton scattering and so on) with these kinds of forces. However, as already mentioned, the ambiguity of the tensor and spin orbit forces enters in here. The other clusters are not as tightly bound as the α-particle cluster ††. Therefore the results very probably will not be as good as in the α—α scattering case, especially if one does not take into account the possible internal excitation of the clusters.

We wish to thank R. Herndon for his help in fitting the two-nucleon forces and Dr. Y. C. Tang for helpful discussions. We also would like to thank Mrs. N. M. Dismuke and Mr. D. K. Cavin for their kind assistance in carrying out the calculations.

† One can obtain this, for instance, by increasing the potential depth V_0 of (1a) by a small amount.

†† This means that the probability that the clusters get internally excited during the scattering process increases.

References

1) A. C. Butcher and J. M. McNamee, Proc. Phys. Soc. **74** (1959) 529
2) E. van der Spuy, Nuclear Physics **11** (1959) 615
3) R. H. Haefner, Revs. Mod. Phys. **23** (1951) 228
4) A. Herzenberg, Nuclear Physics **3** (1957) 1, 314
5) Hans Wittern, Naturwissenschaften **46** (1959) 443

6) S. Hochberg, H. S. W. Massey, H. H. Robertson and L. H. Underhill, Proc. Phys. Soc. **68** (1955) 746
7) K. Wildermuth and Th. Kanellopoulus, Nuclear Physics **7** (1958) 150; **9** (1958) 449, CERN Report 59–23 (1959);
J. K. Perring and T. H. R. Skyrme, Proc. Phys. Soc. **69** (1956) 600;
D. M. Brink, Nuclear Physics **4** (1957) 215
8) L. D. Pearlstein, Y. C. Tang and K. Wildermuth, Nuclear Physics **18** (1960) 23
9) L. Hulthén and M. Sugawara in S. Flügge, Handbuch d. Physik, XXXIX, 1 (Springer-Verlag Berlin, 1957)
10) R. Hofstadter, Ann. Rev. Nuclear Sci. **7** (1957) 231
11) H. H. Robertson, Proc. Cambridge Phil. Soc. **52** (1956) 538
12) L. Fox and E. T. Goodwin, Proc. Cambridge Phil. Soc. **45** (1949) 373
13) C. E. Fröberg, Revs. Mod. Phys **27** (1955) 399
14) N. P. Heydenburg and G. M. Temmer, Phys. Rev. **104** (1956) 123
15) C. W. Reich, J. L. Russell and G. C. Phillips, Phys. Rev. **104** (1956) 135
16) R. Nilson, W. K. Jentschke, G. R. Briggs, R. O. Kerman and J. N. Snyder, Phys. Rev. **109** (1958) 850
17) C. M. Jones, G. C. Phillips and P. D. Miller, Phys. Rev. **117** (1960) 525
18) N. Berk, F. E. Steigert and G. L. Salinger, Phys. Rev. **117** (1960) 531
19) J. R. Dunning, A. M. Smith and F. E. Steigert, Phys. Rev. **121** (1961) 580
20) W. E. Burcham *et al.* See ref. 1).

7.A

Nuclear Physics **26** (1961) 469—479; © *North-Holland Publishing Co., Amsterdam*

Not to be reproduced by photoprint or microfilm without written permission from the publisher

CHANGE OF VARIABLES IN QUANTUM FIELD THEORIES

J. S. R. CHISHOLM

Department of Mathematics, University College, Cardiff, Wales

Received 23 January 1961

Abstract: It is shown that any local or almost local change of variables in quantum field theories which leaves the free field part of the Lagrangian unchanged does not alter the S-matrix. The relation of this result to Haag's theorem is discussed.

1. Introduction

In classical mechanics it is well known that the system of Lagrange equations for a dynamical system is invariant under any reasonable change of variables with non-zero Jacobian determinant; the Lagrange equations ensure that the action integral is minimum along the track, and this property is independent of the variables used to describe the dynamical system. This paper deals with the corresponding theorem for quantum field theories. There is not a complete analogy between the theorems in classical mechanics and quantum field theory, for this reason: if we make a change of variables for a classical system, the new variables are observably different from the original variables; this is not always true for changes of quantum field variables, since observables are not in fact observable during an interaction. Let us consider, for example, a spinor field $\psi(x)$ and a neutral scalar or pseudoscalar field $\phi(x)$ in interaction. If we neglect renormalisation for the present, the Lagrangian density will be

$$\mathscr{L} = \mathscr{L}_f + \mathscr{L}_m + \mathscr{L}_1, \tag{1.1}$$

where

$$\mathscr{L}_f = \bar{\psi}(\gamma_\mu \partial_\mu + M)\psi, \tag{1.2}$$

$$\mathscr{L}_m = \tfrac{1}{2}[(\partial_\mu \phi)^2 + m^2\phi^2]; \tag{1.3}$$

at present we assume that the interaction Lagrangian $\mathscr{L}_1$ is purely local, and that it consists of a sum of terms each containing at least three field variables or their derivatives. Consider now a change of variables of the form

$$\psi(x) = [1 + H_1(\zeta, \chi)]\zeta(x), \tag{1.4a}$$

$$\phi(x) = [1 + H_2(\zeta, \chi)]\chi(x), \tag{1.4b}$$

and their conjugate equations, H_1 and H_2 being sums of terms consisting of at least one field operator. It is clear that the quadratic part of the Lagrangian

is $L_f(\zeta) + L_m(\chi)$. Thus, provided that ζ and χ have the correct symmetry and transformation properties, they have equal claim with ψ and ϕ to represent the physical fields; these group restrictions are easily imposed by ensuring that H_1 and H_2 are scalar and Hermitian when ζ and χ have the required symmetry properties. If the functions H_1 and H_2 in (1.4) are infinite series, we assume that they are convergent for all finite ζ and χ.

When the substitutions (1.4) are made, the interaction Lagrangian in terms of the variables ζ and χ may look very different from the original $\mathscr{L}_1$. We are therefore faced with the question: which of all possible pairs of variables (ζ, χ) with the correct free field Lagrangian represent the real physical field? The only reasonable answer to this question is that all pairs (ζ, χ) are equivalent. This means that the S-matrix calculated using the variables (ζ, χ) must be identically equal to that using variables (ϕ, ψ); in sects 2 and 3 a proof of this invariance property is given with certain simplifying assumptions:

(a) To each field variable there corresponds only one type of particle, bound states or composite particles not being considered. This restriction does not seem to be essential.

(b) The changes of variable (1.4) are purely local. Physical considerations suggest that "almost local" changes of variable will also leave the S-matrix invariant, and the proof of this result is indicated in sect 4.1.

(c) The renormalisation difficulty is ignored in the proof of the theorem, but is discussed in sect. 4.2. We see then that the theorem is not true as it stands for unrenormalised fields.

In addition, we make the basic assumption of the asymptotic condition in the form:

(d) The fields ϕ, ψ, ζ, χ satisfy the appropriate free field equations in the limits $x_0 \to \pm\infty$.

2. The Asymptotic Product Theorem

The essential mathematical result of this paper is a theorem concerning the product of three or more functions $A(x)$, $B(x)$, $C(x)\ldots$ of spacetime coordinates $x \equiv (\mathbf{x}, x_0)$, each of which obeys a Klein-Gordon equation as $x_0 \to \pm\infty$. The theorem states that the space integral

$$\int \mathrm{d}\mathbf{x}[A(x)\, B(x)\, C(x)\ldots] \to 0 \qquad \text{as} \qquad x_0 \to \pm\infty, \tag{2.1}$$

there being at least three functions in the integrand. Coester and Kummel [1]) have given a proof of this theorem for a product of three functions, two of which obey a free field equation; our proof is basically the same as that of Coester and Kummel, but a fuller study of the analytic conditions is given.

It is assumed that the integrand in (2.1) is well defined and that the integral converges; these are assumptions which in fact fail when $A(x)$, $B(x)\ldots$ are

unrenormalised field operators for physically important fields. This difficulty is discussed in sect. 4.2. Since we are considering fields representing only two types of particle, we shall establish (2.1) on the assumption that $A(x)$, $B(x)$ ... each satisfy asymptotically a Klein-Gordon equation with mass m or M; the assumption of only two masses is not essential to the proof.

Let us assume that $\{f_\alpha(x)\}$ and $\{g_\gamma(x)\}$ are complete orthonormal sets of positive frequency solutions of the equations

$$(\Box^2-m^2)\, f_\alpha(x) = 0, \tag{2.2a}$$

$$(\Box^2-M^2) g_\gamma(x) = 0. \tag{2.2b}$$

If, for example, we assume that $A(x)$ and $B(x)$ satisfy (2.2a) asymptotically, and that $C(x)$ satisfies (2.2b), we can expand these functions as Haag expansions:

$$A(x) = \sum_\alpha [A^\alpha(x_0) f_\alpha(\mathbf{x}, x_0) + A^{\alpha *}(x_0) f_\alpha^*(\mathbf{x}, x_0)], \tag{2.3a}$$

$$B(x) = \sum_\beta [B^\beta(x_0) f_\beta(\mathbf{x}, x_0) + B^{\beta *}(x_0) f_\beta^*(\mathbf{x}, x_0)], \tag{2.3b}$$

$$C(x) = \sum_\gamma [C^\gamma(x_0) g_\gamma(\mathbf{x}, x_0) + C^{\gamma *}(x_0) g_\gamma^*(\mathbf{x}, x_0)]. \tag{2.3c}$$

The asymptotic condition (d) ensures that $A^\alpha(x_0)$, $A^{\alpha *}(x_0)$ ... become constants A^α_{in}, $A^{\alpha *}_{\text{in}}$ ... as $x_0 \to -\infty$, and are also constant when $x_0 \to +\infty$. Hence as $x_0 \to -\infty$, the integral (2.1) becomes

$$\sum_{\alpha, \beta, \gamma} A^{\alpha(*)}_{\text{in}} B^{\beta(*)}_{\text{in}} C^{\gamma(*)}_{\text{in}} I_{\alpha\beta\gamma \ldots}(x_0), \tag{2.4}$$

where

$$I_{\alpha\beta\gamma \ldots}(x_0) = \int \mathrm{d}\mathbf{x} f_\alpha^{(*)}(\mathbf{x}, x_0) f_\beta^{(*)}(\mathbf{x}, x_0) g_\gamma^{(*)}(\mathbf{x}, x_0) \ldots; \tag{2.5}$$

the asterisks in brackets indicate that the wave packets f_α ... may have either positive or negative frequencies. The integrals (2.5) have good convergence properties, since the functions f_α ... are normalisable. If we perform three-dimensional Fourier analysis of the orthonormal functions, for example

$$f_\alpha(\mathbf{x}, x_0) = \int \mathrm{d}\mathbf{p}_\alpha \exp [iE_\alpha x_0 - i\mathbf{p}_\alpha \cdot \mathbf{x}] F_\alpha(\mathbf{p}_\alpha), \tag{2.6}$$

where $E_\alpha = (\mathbf{p}^2+m^2)^{\frac{1}{2}}$, the integral (2.5) becomes a multiple of

$$\int \mathrm{d}\mathbf{p}_\alpha \mathrm{d}\mathbf{p}_\beta \mathrm{d}\mathbf{p}_\gamma F_\alpha^*(\mathbf{p}_\alpha) F_\beta^*(\mathbf{p}_\beta) G_\gamma^*(\mathbf{p}_\gamma) \ldots \times \delta(\pm\mathbf{p}_\alpha \pm \mathbf{p}_\beta \pm \mathbf{p}_\gamma \pm \ldots) \exp [ix_0(\pm E_\alpha \pm E_\beta \pm E_\gamma \pm \ldots)]. \tag{2.7}$$

For definiteness, let us consider an integrand containing F_α and F_β^*. If we write $\pm\mathbf{p}_\gamma \pm \mathbf{p}_\delta \pm \ldots = 2\mathbf{P}$, we can use $\mathbf{P}$ as a variable of integration instead

of $\mathbf{p}_\gamma$, for instance. Writing further $\pm E_\gamma \pm E_\delta \pm = E$, the integration to be performed over the variables $\mathbf{p}_\alpha$, $\mathbf{p}_\beta$ and $\mathbf{P}$ becomes a multiple of

$$\int d\mathbf{p}_\alpha d\mathbf{p}_\beta d\mathbf{P} F_\alpha(\mathbf{p}_\alpha) F_\beta^*(\mathbf{p}_\beta) \delta(\mathbf{p}_\alpha - \mathbf{p}_\beta + 2\mathbf{P}) \exp[ix_0(E_\alpha - E_\beta + E)]$$
$$= \int d\mathbf{p}_\alpha d\mathbf{P} F_\alpha(\mathbf{p}_\alpha) F_\beta^*(\mathbf{p}_\alpha + 2\mathbf{P}) \ldots \exp[ix_0(E_\alpha - E_\beta + E)]. \quad (2.8)$$

where $E = [(\mathbf{p}_\alpha + 2\mathbf{P})^2 + m^2]^{\frac{1}{2}}$. The integral (2.8) has a more symmetric appearance if we introduce the variable

$$\mathbf{q} = \mathbf{p}_\alpha + \mathbf{P};$$

then becomes

$$\int d\mathbf{q} d\mathbf{P} F_\alpha(\mathbf{q} - \mathbf{P}) F_\beta^*(\mathbf{q} + \mathbf{P}) \ldots \exp[ix_0(G + E)], \quad (2.9)$$

where

$$G = [(\mathbf{q} - \mathbf{P})^2 + m^2]^{\frac{1}{2}} - [(\mathbf{q} + \mathbf{P})^2 + m^2]^{\frac{1}{2}}, \quad (2.10)$$

E being independent of $\mathbf{q}$. If now we choose new variables G and $\alpha_r (r = 1,2)$ instead of $\mathbf{q}$, the integral becomes

$$\int dG d\alpha_1 d\alpha_2 d\mathbf{P} F_\alpha(\mathbf{q} - P) F_\beta^*(\mathbf{q} + \mathbf{P}) \exp[ix_0(G + E)] \frac{\partial(\mathbf{q})}{\partial(G, \alpha_r)}. \quad (2.11)$$

Provided the integrand in (2.11) is bounded, the integral over G tends to zero as $|x_0| \to \infty$, by the Riemann-Lebesgue theorem. More precisely, if the integrand as a function of $\mathbf{q}$ is bounded in modulus by M, the integral is $O(M/x_0)$. Since F_α, $F_\beta^* \ldots$ are normalised, they can be assumed bounded. Thus, provided $\partial(\mathbf{q})/\partial(G, \alpha_r)$ is bounded as a function of $\mathbf{q}$, we have shown that the integral over $\mathbf{q}$ vanishes as $|x_0| \to \infty$. This condition fails when

$$\frac{\partial G}{\partial \mathbf{q}} \equiv \frac{\mathbf{q} - \mathbf{P}}{[(\mathbf{q} - \mathbf{P})^2 + m^2]^{\frac{1}{2}}} - \frac{\mathbf{q} + \mathbf{P}}{[(\mathbf{q} + \mathbf{P})^2 + m^2]^{\frac{1}{2}}} \approx 0. \quad (2.12)$$

This can easily be seen to happen when $q \equiv |\mathbf{q}| \to \infty$ or when $P \equiv |\mathbf{P}| \approx 0$. It is shown in the appendix† that if $q \leqq (m/\varepsilon)$ and $P \geqq m\varepsilon^2$, then $|\partial G/\partial \mathbf{q}| \geqq O(\varepsilon^6)$; in fig. 1, this region in the positive quadrant of the (P, q) plane is shaded. Because F_α, $F_\beta \ldots$ are normalised and the integrals we are calculating are assumed convergent, the contribution to (2.9) from the region $q \geqq (m/\varepsilon)$ will tend to zero as $\varepsilon \to 0$. The contribution to (2.9) from the rectangle $0 \leqq P \leqq m\varepsilon^2$, $0 \leqq q \leqq (m/\varepsilon)$ will also tend to zero since the integrand is finite and the area of integration tends to zero. Finally, in the shaded region, the integral (2.9) can be transformed to the form (2.11), the integrand being no greater than $O(\varepsilon^{-6})$ in this region. Hence the integral over this region is $O(1/x_0\varepsilon^6)$ by the Riemann-Lebesgue theorem. Thus, provided we let $\varepsilon \to 0$

† The proof in the appendix is due to G. M. Dixon and is shorter than the proof originally formulated by the author.

as $|x_0| \to \infty$ in such a way that $|x_0\varepsilon^6| \to \infty$, the whole integral (2.9) will tend to zero. Therefore, the integrals $I_{\alpha\beta\gamma\ldots}$ defined by (2.5) tend to zero as $|x_0| \to \infty$, and provided that the summation (2.4) has suitable convergence properties, eq. (2.1) is established. It should be noted that the vanishing of $I_{\alpha\beta\gamma\ldots}$ as

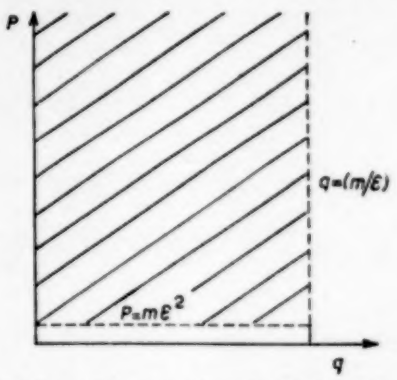

Fig. 1. The positive quadrant of the (P, q) plane.
The region $q \leqq m/\varepsilon$ and $P = m\varepsilon^2$ is shaded.

$|x_0| \to \infty$ is intuitively obvious when the functions f_α, $f_\beta \ldots$ do not all correspond to the same wave packet; asymptotically some of these wave packets, representing freely travelling particles, will have different mean momenta and will become widely separated in space as $|x_0| \to \infty$. It is not obvious that an integral (2.5) of the form $\mathrm{I}_{\alpha\alpha\alpha\ldots}$ is zero asymptotically.

The theorem (2.1) fails when the integrand in (2.7) contains only two functions F_α and F_β^*, since the momentum $\mathbf{P}$ does not enter. The integration over $\mathbf{q}$ is, in effect on the line $P = 0$ in fig. 1, where the Riemann-Lebesgue theorem does not apply. This failure is expected, since the normalisation integral is of this form with $\alpha = \beta$.

When the integrand (2.7) contains $F_\alpha F_\beta$ or $F_\alpha^* F_\beta^*$ so that the exponential contains the sum $(E_\alpha + E_\beta)$ rather than $(E_\alpha - E_\beta)$, eq. (2.10) is replaced by

$$G = [(\mathbf{q}+\mathbf{P})^2+m^2]^{\frac{1}{2}}+[(\mathbf{q}-\mathbf{P})^2+m^2)]^{\frac{1}{2}}.$$

The regions where $|\partial G/\partial \mathbf{q}|$ is small are now $\mathbf{q} \approx 0$ and $P \to \infty$. Hence the proof applies provided we inter change the roles of q and P. The assumption of equal masses in the energies E_α, E_β is not essential, and G. M. Dixon [2]) has established eq. (2.1) for a convergent product of functions which satisfy Klein-Gordon equations with arbitrary masses.

3. The Invariance of the S-Matrix

The two rival meson field operators ϕ and χ are related by eq. (1.4b). The field $\phi(x)$ can be expanded in terms of Hilbert space components

$$\phi(x) = \sum_\alpha [f_\alpha(x)\phi^\alpha(x_0)+f_\alpha^*(x)\phi^{\alpha*}(x_0)], \tag{3.1}$$

the complete set $\{f_\alpha(x)\}$ obeying the orthonormality condition

$$i\int d\mathbf{x} f_\alpha(\mathbf{x}, x_0) \overleftrightarrow{\frac{\partial}{\partial x_0}} f_\beta^*(\mathbf{x}, x_0) = \delta_{\alpha\beta}. \tag{3.2}$$

Then it follows that

$$\phi^\alpha(x_0) = i\int \mathrm{d}\mathbf{x}\phi(x) \overleftrightarrow{\frac{\partial}{\partial x_0}} f_\alpha^*(x_0). \tag{3.3}$$

As $x_0 \to -\infty$, eq. (3.1) takes the asymptotic form

$$\phi_{\mathrm{in}}(x) = \sum_\alpha [f_\alpha(x)\phi_{\mathrm{in}}^\alpha + f_\alpha^*(x)\phi_{\mathrm{in}}^{\alpha *}], \tag{3.4}$$

the operators $\phi_{\mathrm{in}}^\alpha$, $\phi_{\mathrm{in}}^{\alpha *}$ being given by the limit of (3.3):

$$\phi_{\mathrm{in}}^\alpha = \lim_{x_0 \to -\infty} i\int \mathrm{d}\mathbf{x}\phi(x) \overleftrightarrow{\frac{\partial}{\partial x_0}} f_\alpha^*(x_0). \tag{3.5}$$

Let us now substitute for $\phi(x)$ from eq. (1.4b). We find

$$\phi_{\mathrm{in}}^\alpha = \chi_{\mathrm{in}}^\alpha + \lim_{x_0 \to -\infty} i\int \mathrm{d}\mathbf{x} H_2(\zeta, \chi) \overleftrightarrow{\frac{\partial}{\partial x_0}} \chi(x) f_\alpha(x), \tag{3.6}$$

where $\chi_{\mathrm{in}}^\alpha$ is the asymptotic component of the field $\chi(x)$, defined by an equation analogous to (3.5). By hypothesis, $H_2(\zeta, \chi)$ consists of terms containing at least one operator $\zeta(x)$ or $\chi(x)$ and each component of these operators obeys a Klein-Gordon equation asymptotically. Hence the second term in (3.6) consists entirely of terms which vanish by (2.1) when the limit $x_0 \to -\infty$ is taken. Thus (3.6) becomes simply

$$\phi_{\mathrm{in}}^\alpha = \chi_{\mathrm{in}}^\alpha. \tag{3.7}$$

In exactly the same way it can be shown that all the creation and annihilation operators of the incoming and outgoing asymptotic fields are invariant under the changes of variable (1.4).

The asymptotic vacuum $|0\rangle_{\mathrm{in}}$ in terms of the fields ψ and ϕ has two basic properties:

(a) When operated on by any annihilation operator, the result is zero; for example, one has

$$\phi_{\mathrm{in}}^\alpha|0\rangle_{\mathrm{in}} = 0.$$

(b) It is an eigenstate of the normally ordered four-momentum $:P^\mu:$, with eigenvalue zero; that is,

$$:P^\mu:|0\rangle_{\mathrm{in}} = 0.$$

From (3.7) it is obvious that property (a) is invariant under the changes of field variable (1.4). For classical fields P^μ is defined by considering the variation in the action when the coordinated x_μ vary by amounts δx_μ:

$$\delta \int \mathscr{L} \mathrm{d}x = P^\mu \delta x_\mu. \tag{3.8}$$

For a Lagrangian density which is a function of several fields ϕ_r and their derivatives $\partial \phi_r / \partial x^\mu \equiv \phi_{r\mu}$, we have

$$P^\mu = \int \mathrm{d}\mathbf{x}\, T^{\mu 0}, \tag{3.9}$$

where

$$T^{\mu\nu} = \frac{\partial \mathscr{L}}{\partial \phi_{r\mu}} \phi_r{}^\nu - \delta^{\mu\nu} \mathscr{L}. \tag{3.10}$$

The important point to note is that terms in $\mathscr{L}$ which contain n field operators give rise to terms in P^μ also containing n field operators. In particular, the quadratic terms in $\mathscr{L}$ give rise to the free field contributions to P^μ. Interaction terms, containing at least three operators, give contributions to P^μ which are of the form (2.1) and vanish asymptotically. Thus P^μ is asymptotically the sum of the free field four-momenta, an assumption which is often made as part of the asymptotic conditions.

From the definition (3.8) it is clear that P^μ is classically independent of the choice of field variables ϕ_r. For a quantum field the Lagrangian must be taken as the ordered product $:\mathscr{L}:$ in order to give $:P^\mu:$ as the four momentum. It is clear that any change of variable of type (1.4) leaves the ordering of the quadratic terms in $:\mathscr{L}:$ unchanged, so that the ordering in $:P^\mu:$ is asymptotically unchanged. Hence property (b) of the vacuum is also preserved asymptotically, so that the asymptotic vacua are invariant under changes of variable (1.4). We note that the vacuum at finite times is not generally invariant; the presence of unobservable "virtual particles" prevents a unique definition of the vacuum.

The possible initial states of the quantum field are found by operating on $|0\rangle_{\mathrm{in}}$ with a number of creation operators such as ϕ_{in}^{x*}; hence these states, and likewise the final states, are invariant under changes of variable (1.4). The S-matrix elements are the inner products of initial and final state vectors, and are therefore also invariant. This completes the proof that the S-matrix is invariant under changes of variable of the type (1.4).

4. Discussion

In this section we shall deal with three main topics (a): the scope of the theorem proved in sect. 3, (b) the failure of the theorem for unrenormalised fields, and (c) the relation of the theorem to Haag's theorem.

4.1. THE SCOPE OF THE THEOREM

We have assumed that the functions H_1 and H_2 in (1.4) are scalar and Hermitian, but an examination of the proof shows that these properties are nowhere used. We can in fact make changes of variable (1.4) which violate the basic symmetry properties of fields at finite times, since we are assured that the asymptotic fields have the correct properties. The choice of field variables at finite times is a purely mathematical one; if the new variables lack any symmetry, the Lagrangian will then possess a compensating lack of symmetry when expressed in terms of these variables. The possibility of violating apparent relativistic invariance makes it reasonable to consider extending the theorem to almost local changes of variable, the functions H_1 and H_2 in (1.4) being replaced by integral operators which average products of several field quantities taking values over small space-like regions. The integrals which have to be proved zero asymptotically are then of the type

$$\iiint \mathrm{d}\mathbf{x}\,\mathrm{d}\mathbf{x}'\,\mathrm{d}\mathbf{x}''A(\mathbf{x}, x_0)B(\mathbf{x}', x_0)C(\mathbf{x}'', x_0)H(\mathbf{x}-\mathbf{x}')K(\mathbf{x}-\mathbf{x}''), \qquad (4.1)$$

where $H(\mathbf{x}-\mathbf{x}')$ and $K(\mathbf{x}-\mathbf{x}'')$ are normalisable functions. The only effect which these factors have is to replace the product $F_\alpha^{(*)}(\mathbf{p}_\alpha)\, F_\beta^{(*)}(\mathbf{p}_\beta)\, G_\gamma{}^*(\mathbf{p}_\gamma)$ in (2.7) by $F_\alpha^{(*)}(\mathbf{p}_\alpha)[F_\beta^{(*)}(\mathbf{p}_\beta)h(\mathbf{p}_\beta)][G_\gamma{}^*(\mathbf{p}_\gamma)k(\mathbf{p}_\gamma)]$, where $h(\mathbf{p})$ and $k(\mathbf{p})$ are the Fourier transforms of $H(\mathbf{x})$ and $K(\mathbf{x})$. Thus the integral (2.7) is effectively unchanged in its nature, except that the extra factors $k(\mathbf{p}_\beta)$ and $k(\mathbf{p}_\gamma)$ may improve its convergence properties. It therefore seems that the theorem extends immediately to almost local changes of variable, and proves that large classes of non-local interactions are equivalent to local interactions.

4.2. THE FAILURE OF THE THEOREM FOR UNRENORMALISED FIELDS

In sect. 3 it was clear that the theorem depended on respectable behaviour of the Fourier transform of the integral $A(x)\ B(x)\ C(x)\ \ldots$ of (2.1) for large values of the momenta. We know in fact that for unrenormalised field operators, operator products fail to have suitable convergence properties; in theory this trouble is remedied by the introduction of renormalisation terms into the Lagrangian which, combined suitably with the divergent integrals, produce convergent ones; put in another way, if one could successfully define "clothed operators" for interacting fields, the integrals over clothed field operators would all be convergent. The failure of the theorem for unrenormalised fields is in fact necessary, for if all the quadratic terms in the Lagrangian were preserved asymptotically, these would include several types of renormalisation terms, which would spoil the free particle properties of the asymptotic fields.

4.3. THE RELATION OF THE THEOREM TO HAAG'S THEOREM

Any change of variables in Lagrangian mechanics generates a canonical transformation in Hamiltonian mechanics, provided that the conjugates of the

original and the new field quantities are defined by the canonical formalism. Hence the theorem proved in this paper can be regarded as the Lagrangian equivalent † of Haag's theorem [3]), which has been proved by Greenberg [4]). It is therefore of interest to compare the scope of the two theorems. First we note again that the theorem proved here does not depend upon relativistic invariance or covariance of the operators, except asymptotically. Second, the theorem extends to almost local changes of variable, and is therefore a generalisation of the result of Ekstein [5]), who has shown that a large class of non-local unitary transformations leave the S-matrix invariant when the Hamiltonian corresponds to non-relativistic particles.

The main restriction on the transformation is the equality of the lowest order terms, which is essential for the preservation of the free-particle parts of the Lagrangian. In a theory where no renormalisation troubles arise, this restriction is reasonable. But, if we wish to perform clothing transformations on our original operators, the corresponding changes of variables must allow for the absorption of renormalisation terms into the other parts of the Lagrangian, and we must expect that the terms $\zeta(x)$ and $\chi(x)$ in (1.4) will be replaced by multiples (possibly zero or infinite) of these terms. The author feels that it may be easier to regard clothing transformations in particular field theories as changes of variables — it seems simpler to discuss arbitrary transformations of n variables rather than restricted transformations of $2n$ variables. One difficulty that has arisen in the discussion of clothing transformations is well-known, and is discussed in sect. 4 of Greenberg's paper: if we assume that a unitary transformation connects the clothed operators with the free field operators, it follows that the field theory is equivalent to one with zero interaction. Greenberg has noted in eqs. (26)—(28) of his paper that the basic hypothesis, when stated clearly, is that the conjugate of a clothed field operator $A(x)$ is its time derivative $\partial A(x)/\partial x_0$. This is equivalent to assuming that, in terms of clothed operators, the interaction Lagrangian does not contain derivatives of these operators; the author agrees with Greenberg that this is a very restrictive assumption, and feels that for any theory normally considered, except for neutral S-V theory, it is very unlikely to be true; changes of variable which result in an interaction Lagrangian with no derivatives are very rare indeed, and it would be extremely fortuitous if such a transformation coincided with the choice of clothed operators as variables.

The author wishes to acknowledge the benefit of discussions he has had on this paper and related work at Birmingham University, University College (London), A.E.R.E. (Harwell) and Cambridge University and with Professor N. Kemmer and Mr. G. M. Dixon. He wishes especially to thank Mr. Dixon for

† The author is indebted to Dr. R. J. N. Phillips and Professor N. Kemmer for clarifying this point.

a number of discussions on Haag's work, and for contributing his improved proof of the inequality derived in the appendix. He is indebted to Professor J. L. B. Cooper for a discussion on the Riemann-Lebesgue theorem and for his constant support and encouragement.

Appendix

It is required to show that if

$$G = [(\mathbf{q}-\mathbf{P})^2+m^2]^{\frac{1}{2}}-[(\mathbf{q}+\mathbf{P})^2+m^2]^{\frac{1}{2}} \tag{A.1}$$

and if $|\mathbf{P}| \equiv P \geqq m\varepsilon^2$ and $|\mathbf{q}| \equiv \mathbf{q} \leqq (m/\varepsilon)$, then we have

$$\left|\frac{\partial G}{\partial \mathbf{q}}\right| \geqq O(\varepsilon^6). \tag{A.2}$$

Differentiating eq. (A.1), we get

$$\frac{\partial G}{\partial \mathbf{q}} = \frac{\mathbf{q}-\mathbf{P}}{[(\mathbf{q}-\mathbf{P})^2+m^2]^{\frac{1}{2}}} - \frac{\mathbf{q}+\mathbf{P}}{[(\mathbf{q}+\mathbf{P})^2+m^2]^{\frac{1}{2}}}. \tag{A.3}$$

Squaring (A.3) and "completing the square", we find

$$\left|\frac{\partial G}{\partial \mathbf{q}}\right|^2 = \left\{\frac{q\mp P}{[(\mathbf{q}-\mathbf{P})^2+m^2]^{\frac{1}{2}}} - \frac{q\pm P}{[(\mathbf{q}+\mathbf{P})^2+m^2]^{\frac{1}{2}}}\right\}^2 \pm \frac{P^2q^2\cos\theta(1\pm\cos\theta)}{[(\mathbf{q}-\mathbf{P})^2+m^2][(\mathbf{q}+\mathbf{P})^2+m^2]}, \tag{A.4}$$

where $\cos\theta$ is defined by

$$\mathbf{P}\cdot\mathbf{q} = Pq\cos\theta. \tag{A.5}$$

Whatever the value of $\cos\theta$, the alternative signs in (A.4) allow us to choose the second term to be non-negative. Understanding that the sign has been chosen in this way, we have

$$\left|\frac{\partial G}{\partial \mathbf{q}}\right| \geqq \left|\frac{q\mp P}{[(\mathbf{q}-\mathbf{P})^2+m^2]^{\frac{1}{2}}} - \frac{q\pm P}{[(\mathbf{q}+\mathbf{P})^2+m^2]^{\frac{1}{2}}}\right| \equiv |X-Y|, \tag{A.6}$$

say, defining X and Y.

We now consider the situations $q > P$ and $q \leqq P$ separately:

THE CASE $q \leqq P$

X and Y are of opposite sign, so that from (A.6), we find

$$\left|\frac{\partial G}{\partial \mathbf{q}}\right| \geqq \left|\frac{P+q}{\max\,[(\mathbf{q}\pm\mathbf{P})^2+m^2]^{\frac{1}{2}}}\right| \geqq \left|\frac{1+(q/P)}{\max\,[(\mathbf{q}\pm\mathbf{P})^2+m^2]^{\frac{1}{2}}/P}\right|.$$

Since $P \geqq m\varepsilon^2$, this gives

$$\left|\frac{\partial G}{\partial \mathbf{q}}\right| \geqq \mathrm{O}(\varepsilon^2). \tag{A.7}$$

THE CASE $q > P$

X and Y are of the same sign, so $X+Y \neq 0$, and we find

$$|X+Y| \leqq \left|\frac{2(P+q)}{\min\,[(\mathbf{q}\pm\mathbf{P})^2+m^2]^{\frac{1}{2}}}\right| \leqq 2\left|\frac{1+(P/q)}{(m/q)}\right|.$$

Since $q \leqq \mathrm{O}(m/\varepsilon)$, we have

$$|X+Y| \leqq \mathrm{O}(\varepsilon^{-1}). \tag{A.8}$$

Also

$$\begin{aligned}|X^2-Y^2| &= \left|\frac{(q\mp P)^2}{q^2+P^2+m^2-2Pq\cos\theta} - \frac{(q\pm P)^2}{q^2+P^2+m^2+2Pq\cos\theta}\right| \\ &= 2\left|\frac{(q^2+P^2)2qP\cos\theta \mp 2Pq(q^2+P^2+m^2)}{[(\mathbf{q}-\mathbf{P})^2+m^2][(\mathbf{q}+\mathbf{P})^2+m^2]}\right|.\end{aligned}$$

The numerator is greater in modulus than $2Pqm^2$, so that

$$\begin{aligned}|X^2-Y^2| &\geqq 4\left|\frac{(q/P)}{[(\mathbf{q}+\mathbf{P})^2+m^2][(\mathbf{q}-\mathbf{P})^2+m^2]/P^2m^2}\right| \\ &\geqq \mathrm{O}(\varepsilon^5),\end{aligned} \tag{A.9}$$

since $(q/m) \leqq \varepsilon^{-1}$ and $(q/P) \leqq \varepsilon^{-3}$.
From (A.8) and (A.9) we have

$$\left|\frac{\partial G}{\partial \mathbf{q}}\right| = |X-Y| = \frac{|X^2-Y^2|}{|X+Y|} \geqq \mathrm{O}(\varepsilon^6). \tag{A.10}$$

Eqs. (A.7) and (A.10) establish the inequality (A.2).

References

1) Coester and Kummel, Nuclear Physics **9** (1959) 225
2) G. M. Dixon, private communication
3) R. Haag, Phys. Rev. **112** (1958) 669
4) O. Greenberg, Phys. Rev. **115** (1959) 706
5) H. Ekstein, Phys. Rev. **117** (1960) 1590

2.C: 2.I

Nuclear Physics **26** (1961) 480—510; © *North-Holland Publishing Co., Amsterdam*

Not to be reproduced by photoprint or microfilm without written permission from the publisher

PROTON CAPTURE GAMMA RAYS IN THE GIANT RESONANCE REGION IN LIGHT NUCLEI

H. E. GOVE, A. E. LITHERLAND and R. BATCHELOR †

Chalk River Laboratory, Atomic Energy of Canada Limited, Chalk River, Ontario, Canada

Received 4 April 1961

Abstract: The 90° yield of capture gamma rays leading to the ground and first excited state of C^{12} and Si^{28} has been measured in the proton energy range from ≈ 3—11 MeV. This covers a range of excitation energy including the peak of the giant dipole resonance. Similar measurements have been made for Mg^{24} except that, in this case the combined yield of capture gamma rays leading to the ground and first excited state was measured. Angular distributions of both gamma rays in C^{12} and Si^{28} have also been measured. The cross section at the peak of the yield for ground state gamma transitions on C^{12} (22.5 MeV excitation energy) is 1.3×10^{-28} cm^2 and the integrated yield is 4.7×10^{-4} MeV · b. No fine structure is observed in the B^{11} (p, γ_0) yield while considerable fine structure is found in the Al^{27} (p, γ_0) and Al^{27} (p, γ_1) yields. The yield of gamma rays to the first excited state does not reach a maximum at the same energy as that for the ground state in either C^{12} or Si^{28}. There is evidence for gross double peaked structure in Mg^{24} and a suggestion of it also in Si^{28}. The angular distributions indicate that direct capture applies, if at all, only for ground state gamma transitions in C^{12}. Forward asymmetry is observed in these distributions which cannot be interpreted as interference between two resonances of opposite parity separated by a spacing greater than their widths.

1. Introduction

Over the past few years a great deal of attention, both experimental and theoretical, has been devoted to what is termed the giant resonance region of nuclear excitation. Most of the information presently available derives from studies of photonuclear reactions [1]) and in particular, from experiments in which the incident photons comprise bremsstrahlung radiation. Despite the considerable problem involved in extracting differential yields from data obtained with continuous bremsstrahlung radiation, a great deal of information about the giant resonance is now available over a wide range of atomic number.

The inverse process in which a nucleon is captured to form a compound nucleus in the region of excitation of the giant resonance, with the subsequent emission of a single gamma ray to the ground state of the compound nucleus has until recently received little or no attention. The reason for this is obvious; low background proton accelerators of variable energy operating up to 12 MeV or higher have only recently been developed and the use of variable energy neutrons would be prohibitively difficult. An indication of the interesting in-

† Seconded from A.W.R.E., Aldermaston, England.

formation to be obtained from such proton capture gamma ray studies is to be seen in recently published work from the Australian National University at Canberra [2]). In these experiments, the beam from a 7.7 MeV proton cyclotron with energy variation by absorption was used to bombard thin targets of Li^7, B^{11}, F^{19}, Na^{23}, Al^{27} and P^{31}. Capture gamma rays to levels near the ground state, and, in the case of the first two targets to the ground state alone of the appropriate compound nucleus, were observed at 90° to the beam as a function of proton energy. Because of the upper energy limit from the Canberra cyclotron only the first two targets which lead to compound nuclei Be^8 and C^{12}, respectively, have sufficiently high Q-values to reach beyond the peak of the giant resonance (22—23 MeV in very light nuclei dropping to about 20 MeV in Si^{28}). The giant resonance region in O^{16} has recently been studied by Cohen *et al.* [3]) for proton energies up to about 15 MeV using a cyclotron and by Tanner *et al.* [4]) using protons up to about 8 MeV from the Harwell tandem accelerator.

Aside from its intrinsic interest, the study of the inverse photonuclear reaction suggests itself as an obvious initial experiment to perform with a tandem electrostatic accelerator. The experimental equipment required is relatively simple and the accelerator is required to operate with considerable stability over its complete voltage range. In the experiments to be described below, targets of B^{11}, Al^{27} and Na^{23} and proton energies up to 11.4 MeV were employed.

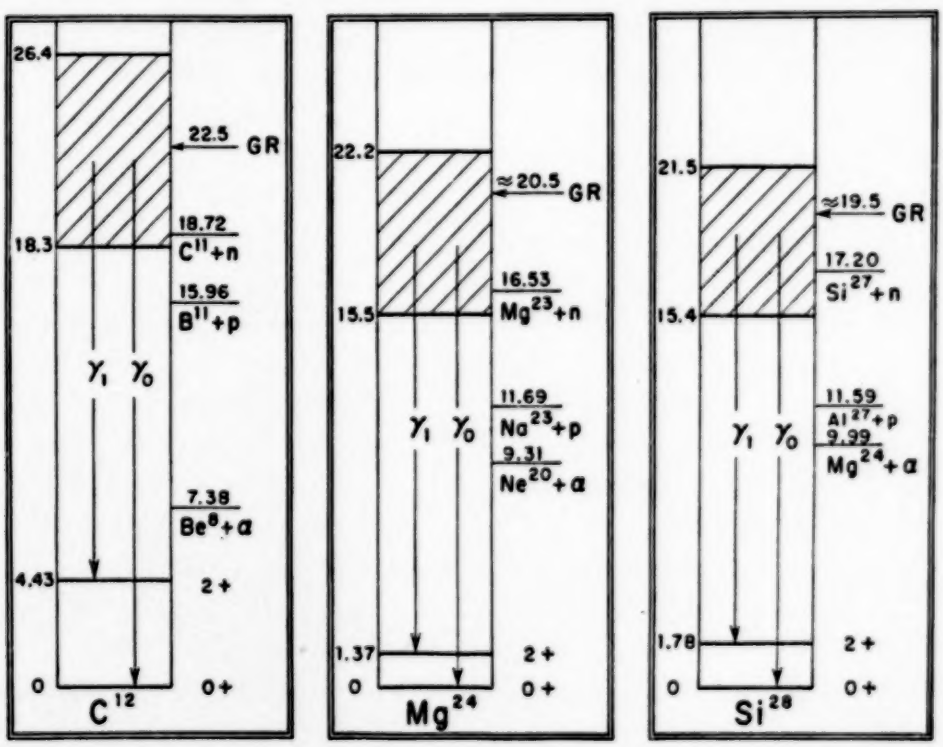

Fig. 1. Partial energy level diagrams for C^{12}, Mg^{24} and Na^{23} showing the region of excitation energy covered (shaded), the positions of the first excited states and the energies at which each nucleus becomes unstable against neutron, proton and alpha particle emission. The approximate position of the peak of the giant resonance (GR) is also indicated.

A preliminary account of this work has been published [5]). The gamma rays studied and the regions of excitation covered in these experiments are shown in the energy level diagrams of fig. 1. In the case of the B^{11} and Al^{27} targets the yield of neutrons was also measured.

2. Apparatus

The measurements were carried out using proton beams variable in energy from 2.6 to 11.4 MeV from Chalk River Tandem Accelerator †. Some details of the machine and target room arrangement, the 90° beam analyzing system and the steering and focussing system along with results of (pn) threshold studies used to calibrate the 90° magnet have been previously published [6, 7]). As in the case of the (pn) measurements the target was located approximately in the centre of a 11m × 15 m target room 175 cm from the floor and approximately 10 m from the centre of the 90° beam analyzing magnet.

The targets, mounted on aluminium frames were contained in the centre of a thin-walled brass cylinder. For most of the work thin targets were employed and, after traversing the target the proton beam passed into an exit tube attached to the cylinder and was stopped in a lead plate behind shielding blocks approximately 4 m from the target. In order to reduce background from protons striking the exit tube after undergoing small angle scattering in the target the exit tube was lined with lead foil. No apertures were employed between the exit slit of the 90° magnet (shielded from the target room by a 0.90 m wall of iron-loaded concrete) and the target itself. The beam spot size on the target was generally about 0.3 cm in diameter.

The gamma rays were detected in a 12 cm diameter by 15 cm long NaI(Tl) crystal ††. No lead shielding was employed around the crystal except for a 0.3 cm thick lead sheet over the front face of the crystal to reduce the intensity of very low energy gamma rays. A 12 cm diameter Dumont K 1659 photomultiplier was optically coupled to the crystal via a quartz window. Pulses were amplified in a preampliflier †††, transmitted some 90 m, further amplified in a double delay line amplifier ††† and displayed on a Chalk River 100-channel transistor pulse-amplitude analyzer ‡. This detector was mounted on a platform which could be driven remotely in angle about the target from 20° to 145°. When the beam was stopped in a heavy element (usually gold) backing the target, the exit tube could be removed and, in this case the detector could be rotated to 0°. For monitoring angular distributions a second NaI(Tl) crystal, 12 cm in diameter and 10 cm long was mounted on the other side and fixed at

† Designed and built by High Voltage Engineering Corporation, Burlington, Massachusetts.
†† Manufactured and canned by the Harshaw Chemical Company, Cleveland, Ohio, U.S.A.
††† Designed by G. G. Kelly, Oak Ridge National Laboratory, Oak Ridge, Tennessee, U.S.A
‡ Designed by Electronics Branch, Atomic Energy of Canada Limited, Chalk River, Ontario, Canada.

90° to the beam direction. Both crystals were located at a distance of 15 cm between the target and the front face of the crystals. The output of this second detector was displayed on a second 100-channel Chalk River pulse-amplitude analyzer. The contents of both analyzers as well as other pertinent information were printed automatically by a typewriter and punched on tape which could be employed for plotting the spectra †.

Measurement of neutrons from the B^{11} (p, n) reaction were made above the neutron threshold energy (E_p (threshold) = 3.019±0.004 MeV) using a modified long counter of the Hansen and McKibben type [8]). This detector measured fast neutrons emitted from the reaction independent of their energy. In addition a 3.8 cm diameter by 3.8 cm long Ne212 liquid scintillator †† with pulse shape discrimination [9]) detected those neutrons leading to the ground state of C^{11}. Pulse-height distributions from the scintillator with the gamma rays eliminated by pulse-shape discrimination were recorded in one of the 100-channel pulse-height analyzers and automatically printed out and plotted after each run. The output of the long counter was measured by counting all pulses above a bias set below the height of the well defined alpha particle peak from the B^{10} (n, α) Li^7 reaction. Neutron yields up to 6.3 MeV from Al^{27} (p, n) Si^{27} have previously been reported [6]) and these have been extended up to 10.5 MeV in the present experiments.

The boron targets were prepared by mixing finely powdered boron of normal isotopic abundance with a colloidal graphite suspension in alcohol. This mixture was spread on a glass plate previously coated with a detergent and then floated off in water. The resulting targets were about 20 keV thick for 10 MeV protons. Some of the preliminary yield curves of B^{11}(p, γ_0) and all the neutron yield curves were made using a separated B^{11} target of approximately 100 $\mu g/cm^2$ deposited on a 4 mg/cm^2 thick gold backing. This was originally on a 0.01 cm thick copper backing which was dissolved off before using. The boron carbon mixture was used in order to obtain a thicker target. Equivalent thicknesses of self-supporting aluminium foil were used. The sodium foil was prepared by rolling it between two sheets of aluminium immersed in oil to a thickness between 30μm to 50μm. The aluminium was stripped in an inert atmosphere and the sodium foil was attached to an aluminium frame. It was transferred quickly to the brass target cylinder which was rapidly evacuated. Oxide and hydroxide surface formation was sufficiently small to cause no trouble. The resultant foil was about 180 keV thick for 10 MeV protons.

3. Experimental Procedure

Yield curves over as wide a range of proton energy as possible were measured

† Designed by Electronics Branch, Atomic Energy of Canada Limited, Chalk River, Ontario, Canada.

†† Manufactured and encapsulated by Nuclear Enterprises, Winnipeg, Manitoba, Canada.

with the 12 cm by 15 cm NaI(Tl) set at 90° to the incident beam. The spectrum at each energy was measured for a constant total charge incident on the target ranging from 5 to 100 μC depending on the target thickness. The beam current was generally limited to values below 0.1 μA to prevent excessive pile-up of pulses. Gamma rays from inelastic proton scattering, (p, n) and (p, α) reactions and neutrons from (p, n) reactions gave rise to counting rates many orders of magnitude greater than those from (p, γ) reactions and it was necessary to keep the beam current both low and relatively constant to prevent gain shifts in the photomultiplier. Particularly in the case of the B^{11} (p, γ) results where the target was not completely uniform in thickness and where yield curves over different regions of energy were measured on different days it was necessary to relate runs with a normalizing factor. This factor was obtained by making several measurements at energies which overlapped previous runs. In the case of angular distribution measurements at fixed incident proton energy 12 cm × 10 cm NaI(Tl) detector fixed in position at 90° to the beam served as a monitor. The 100-channel pulse-amplitude analyzers in which the spectra were recorded were adjusted to analyze only the high energy portion of the gamma ray spectra for yield and angular distribution measurements to avoid counting rate losses in the analyzer.

In a separate experiment the yield of both neutrons leading to the ground state of C^{11} and all fast neutrons from B^{11} (p, n) C^{11} were measured at 90° to the beam for proton energies between about 5 and 10 MeV. The target employed for these measurements was the 100 μg/cm^2 thick separated B^{11} target on a 4 mg/cm^2 gold backing. Total neutron yields were also measured in the Al^{27} (p, n) Si^{27} reaction from below threshold up to 10.5 MeV proton energy.

4. Experimental Results

4.1. THE B^{11} (p, γ) REACTION

Pulse height spectra measured in the 12 cm diameter by 15 cm long NaI(Tl) detector for the two different boron targets are shown in figs. 2 and 3 plotted on a semi-logarithmic scale. They are characterized by the two high energy peaks corresponding to capture gamma rays leading to the ground and first excited state of C^{12}, a fairly steep rise with decreasing pulse-height down to pulse-heights corresponding to about 5 MeV gamma rays which is caused by neutron capture gamma rays in the crystal and superimposed on this a number of sharp gamma ray lines resulting from particle emission from the compound nucleus. The background counts beyond the highest energy gamma ray do not come from the target as demonstrated in fig. 2 but are from cosmic rays. A comparison of these two spectra indicates that the pulses due to neutrons drop off in intensity with increasing pulse height more steeply from the boron plus carbon targets (fig. 3) and hence make it easier to measure the yield of the gamma ray to the first excited state of C^{12}.

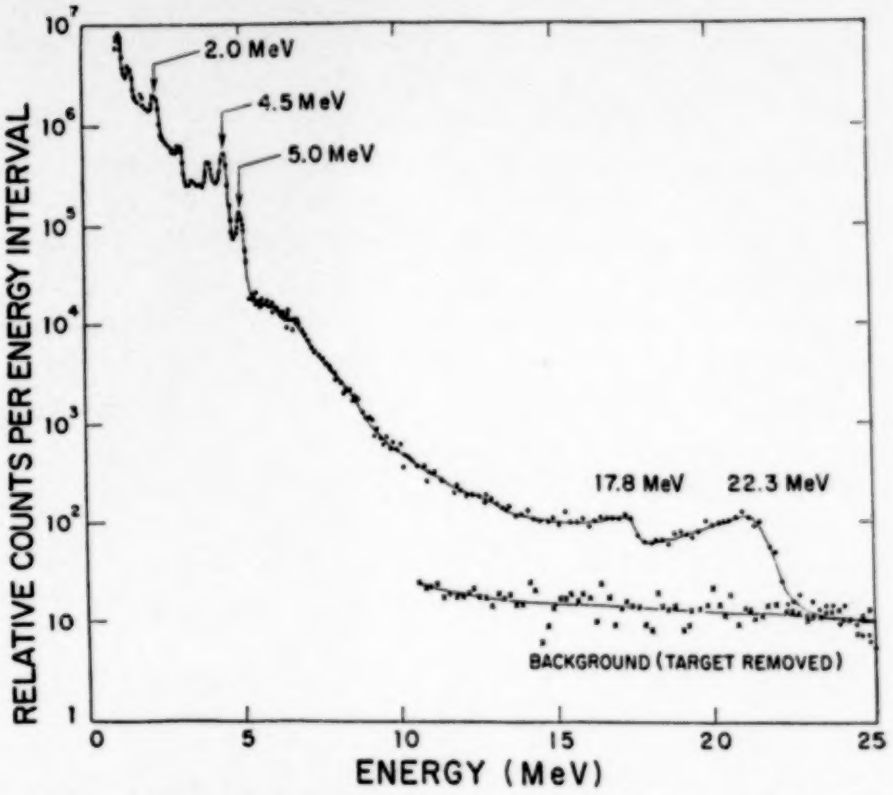

Fig. 2. Gamma ray pulse spectrum from 6.88 MeV proton bombardment of a 100 μg/cm^2 separated B^{11} target on a 4 mg/cm^2 gold backing. The detector was an unshielded 12 cm diameter by 15 cm long NaI(Tl) crystal at 90° to the beam with its front face 15.7 cm from the target centre. The ordinate is a logarithmic scale.

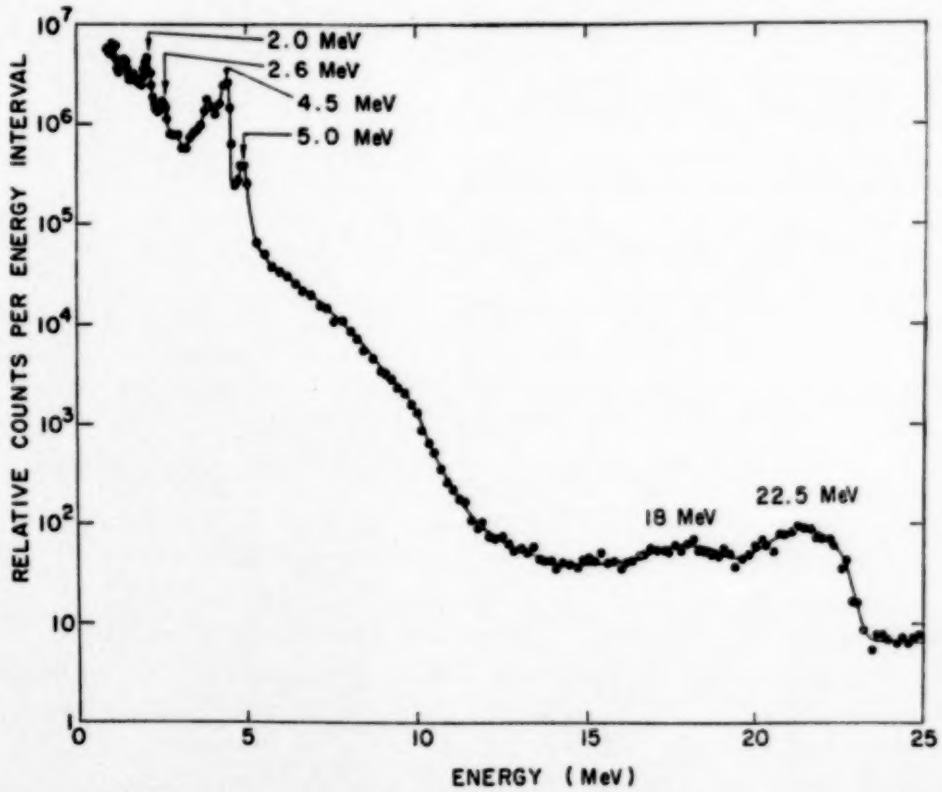

Fig. 3. A gamma ray pulse spectrum from 7.1 MeV proton bombardment of a mixture of boron and carbon of total thickness about 0.7 mg/cm^2 measured under the same conditions as the spectrum of fig. 2. The ordinate is a logarithmic scale.

A linear plot of the upper portion of the gamma ray pulse spectrum for 6 MeV protons incident on the boron-carbon targets is shown in fig. 4. The method used in analyzing the data is indicated on fig. 4 and is discussed below. In order to check that the peak labelled γ_0 arises from capture gamma rays from the B^{11} (p, γ_0) C^{12} reaction, the channel number at which a straight line on the high energy edge intercepted the background line was plotted against proton energy in the range from 3.2. to 8.8 MeV. Between each run the 2.61 MeV total absorption peak from Tl^{208} was recorded to check on gain shifts. The results gave a linear variation for the position of this extrapolated edge with proton energy and were consistent with the kinematics of the reaction assuming that this extrapolated edge was about 1 MeV higher than the true gamma ray energy. Such an assumption appears to be reasonable.

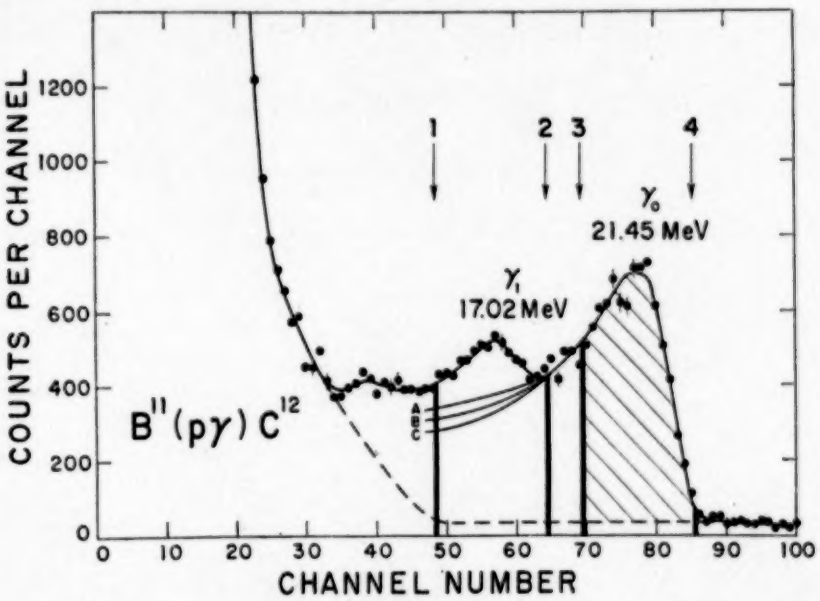

Fig. 4. The gamma ray pulse spectrum plotted on a linear ordinate scale from 6.0 MeV proton bombardment of the boron carbon target in which only the high energy pulses are displayed. The shape of the pulse spectrum for 21.45 MeV gamma rays under the γ_1 peak lies between the lines A and C. The four vertical lines numbered 1 through 4 show the regions used for measuring intensities.

Relative gamma ray yields at each proton energy were obtained in the manner illustrated in fig. 4. The channel number corresponding to the extrapolated end point was obtained and is shown as 4 in fig. 4. To this was added the number of channels biased off in the pulse-height analyzer (40 in this case.) The position of the vertical line 3 was then arbitrarily established as some constant fraction of the end point channel number. The constant was chosen to ensure that no contribution from γ_1 occurred in any channels above the position of this vertical line 3. The average background beyond γ_0 was extrapolated back under γ_0 and γ_1 to meet the extrapolated fall off of pulses caused by neutrons. The shaded area in fig. 4 was then assumed to be proportional to the intensity of γ_0.

To get the intensity of γ_1 it is necessary to subtract the tail of γ_0 which lies under the peak of γ_1. No monochromatic gamma ray pulse spectra in large NaI crystals are available for such high energy gamma rays so it was necessary to estimate the shape. At a proton energy of 6 MeV about the highest ratio of γ_0 intensity to that of γ_1 is obtained in the B^{11} (p, γ) reaction and hence this is the most suitable energy to estimate the shape of the γ_0 pulse spectrum. The three extrapolated curves A, B and C represent the best estimates of the mean and limiting shapes of this pulse spectrum. Since the shape of γ_1 must be

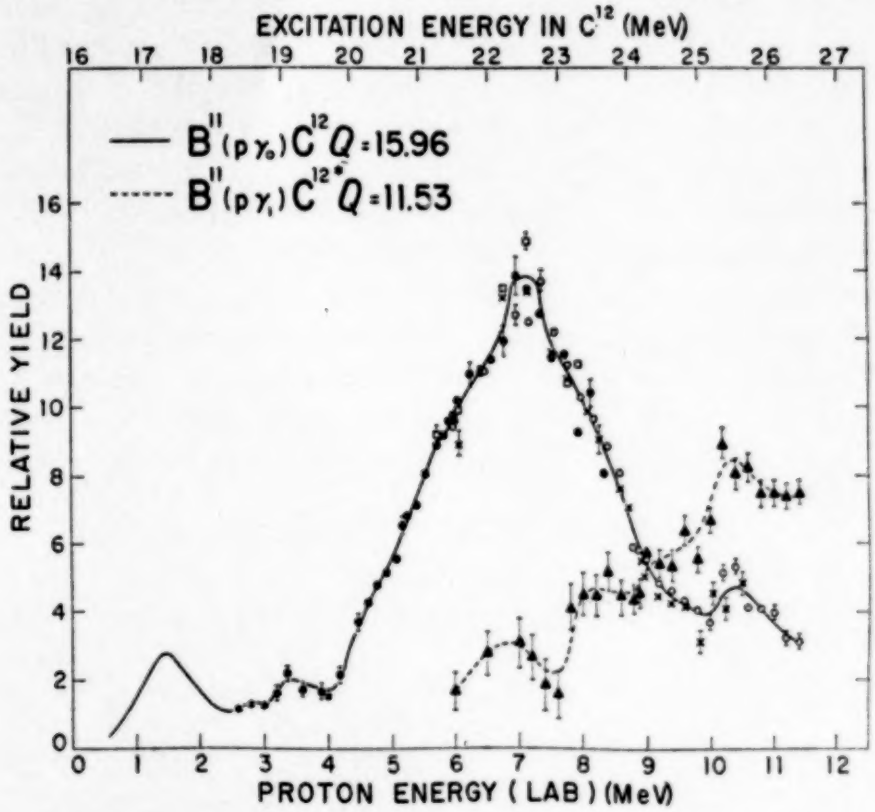

Fig. 5. The yield of gamma rays leading to the ground and first excited state of C^{12} resulting from proton capture in B^{11} and measured at 90° to the incident beam. The different symbols on the γ_0 yield curve represent separate runs. The ordinates of the two yield curves are correct relative to each other. The abscissae are marked both in terms of the incident laboratory proton energy and in excitation energy in the compound nucleus C^{12}

rather close to that of γ_0, one has a self-consistency check on the ABC polations. One can now calculate the area due to γ_0 lying under γ_1 and an subtract both meson background and the contribution of γ_0 from the area between vertical lines 1 and 2 to obtain the intensity of γ_1. The error assigned to this includes the uncertainty displayed by the limiting shapes A and C as well as statistical fluctuations.

The yield curve for gamma rays leading to the ground state and first excited state of C^{12} at 90° to the incident beam measured as described above is shown in fig. 5. The proton energy range employed for this yield curve was 2.5 to

11.4 MeV in the laboratory system. Points on the ground state gamma ray yield curve marked with the same symbol represent individual runs. The solid curve with no points is the yield curve measured by Gove and Paul [10]) which has been fitted to the present measurements in the region of 2.6 to 3 MeV. The ordinates of the two yield curves are correct relative to each other.

From fig. 5 it can be seen that the yield of γ_0 displays a broad resonance centered at an excitation energy of 22.5 ± 0.02 MeV and with a width of about 3.1 MeV in the centre-of-mass system. There is also an indication of a small peak at about 25.5 MeV in excitation. No sharp structure is observed. The yield of γ_1 on the other hand shows somewhat more structure although the statistics are not as good. It continues to climb gradually up to the highest energy available where its yield is approximately twice that of γ_0. At this maximum energy one has still not quite reached an excitation in C^{12} which is 4.43 MeV above the peak position of the giant resonance for γ_0. This occurs at a laboratory proton energy of 12.0 MeV.

In order to search in more detail for structure in the yield curves corresponding to the breaks observed in integral yield curves observed from the photonuclear reaction on C^{12} in several laboratories, the region of excitation from 21 to 22.6 MeV was investigated in smaller energy steps. The results are shown in fig. 6. A break in the integral yield curve of neutrons from brems-

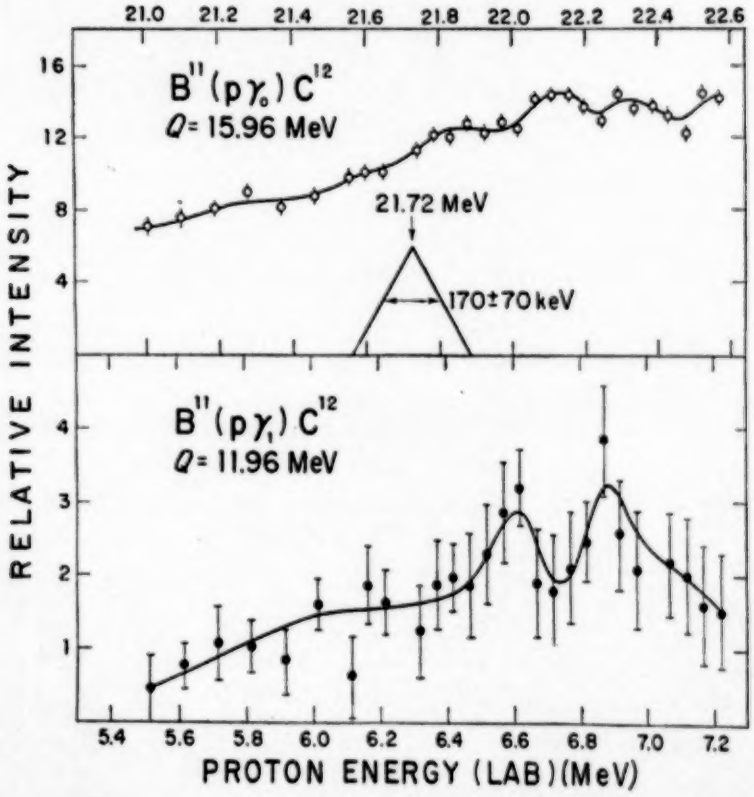

Fig. 6. The 90° yield of gamma rays leading to the ground and first excited state of C^{12} taken in finer energy steps to search for structure in the region of 21.7 MeV. The triangle on the upper curve represents a possible resonance observed in the C^{12} (γ, n) reaction.

strahlung irradiation of C^{12} has been reported by Katz [11, 25]) at an excitation energy of 21.72 MeV. If this break is interpreted as a resonance its width is estimated by Katz to be 170 ± 70 keV. Two or three maxima with widths of 100 or 200 keV and heights about 10 % of the total yield are observed in the upper curve of fig. 5. It is questionable whether such structure would produce sharp breaks in an integral photonuclear yield. However, as is discussed later, the results of the two experiments may not be comparable.

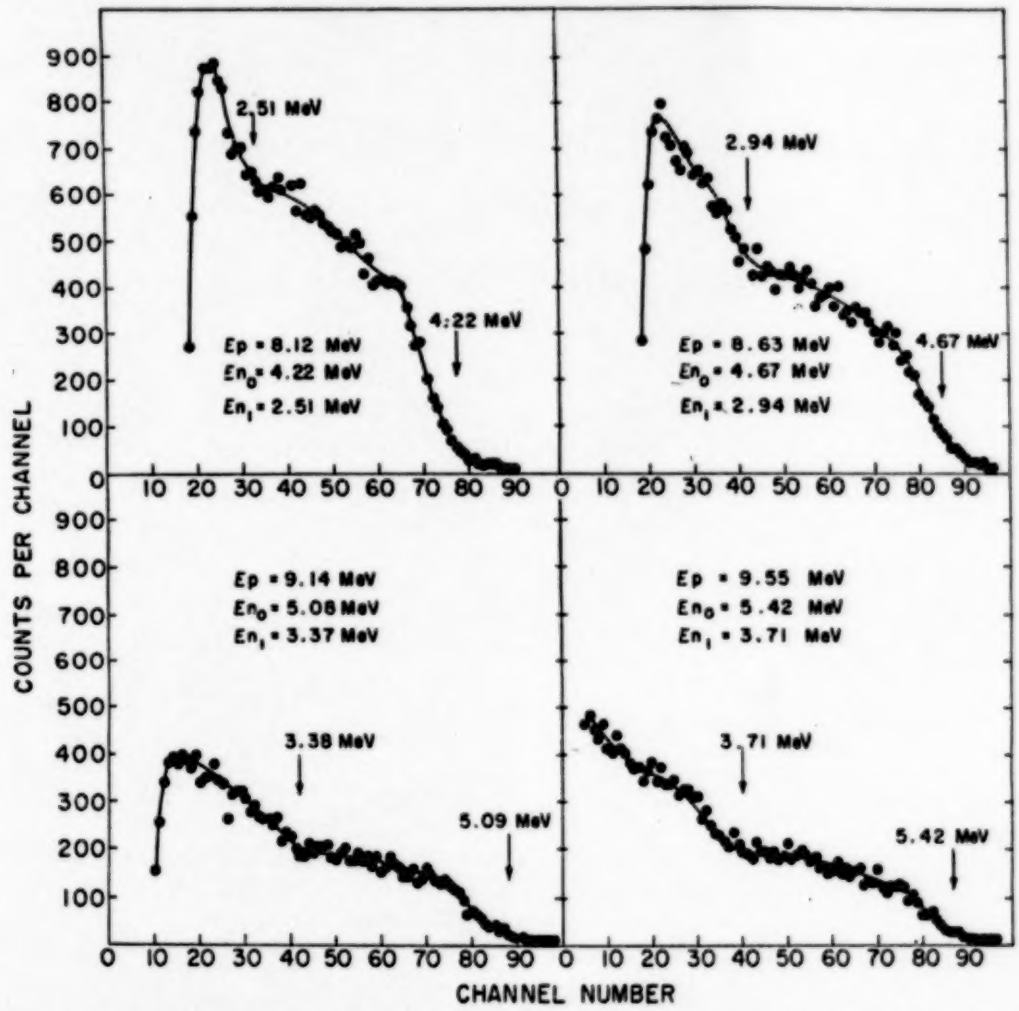

Fig. 7. Pulse height distributions from neutrons incident on a 3.8 cm diameter by 3.8 cm long *NE*212 liquid organic scintillator. The neutrons were produced in the reaction B^{11} (p, n) C^{11} and the detector was set at 90° to the incident beam direction. Pulses due to gamma rays were eliminated by the technique of pulse shape discrimination. Each of the four spectra was measured at different incident proton energies ranging from 8.12 to 9.55 MeV.

Neutrons leading both to the ground state of C^{11} and all neutrons independent of energy from the B^{11} (p, n) C^{11} reaction were measured in the proton energy interval from 4.9 to 9.5 MeV. Typical pulse-height distributions measured at the higher energies with a 3.8 cm diameter by 3.8 cm long NE 212 organic liquid scintillator are shown in fig. 7. Pulses due to gamma rays have been eliminated

from these spectra by the technique of pulse shape discrimination [9]) using a circuit due to Owen [12]). The neutron energy corresponding to the maximum pulse height for the two groups leading to the ground and the 1.90 MeV first excited state of C^{11} are indicated by arrows on each of the spectra. These pulse heights are plotted as a function of neutron energy in fig. 8. This maximum neutron energy corresponds, of course, to the maximum proton recoil energy in the organic scintillator and hence this provides a proton pulse-height calibration curve for this particular scintillator. A similar curve for electrons

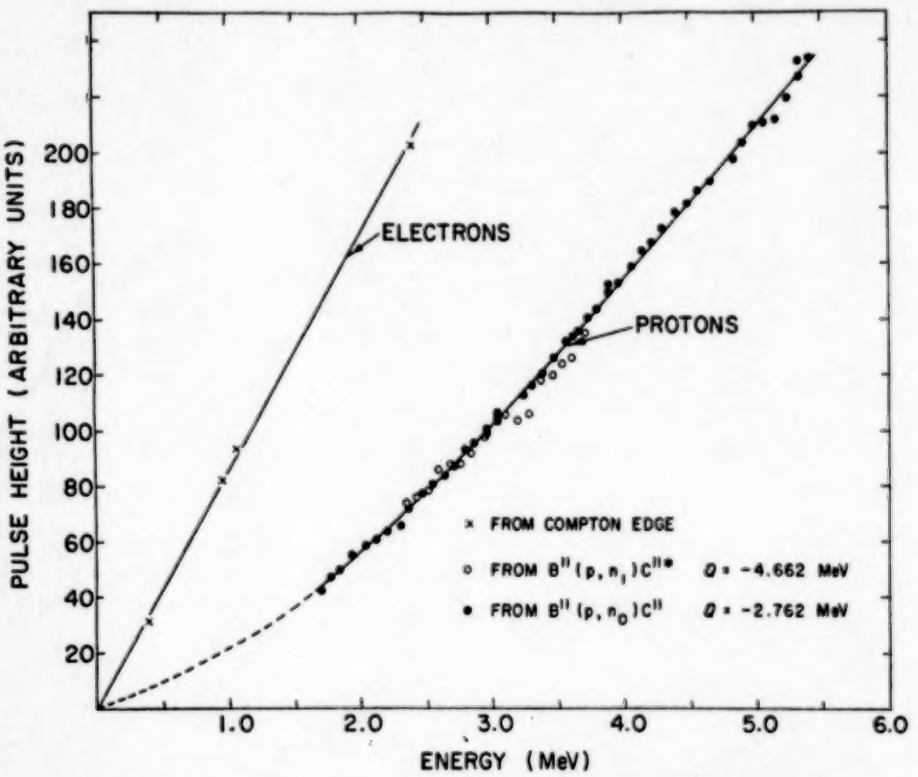

Fig. 8. Pulse height versus energy for protons and neutrons in the liquid organic scintillator NE 212. The crosses are for electrons measured by the Compton edge of standard gamma ray sources. The closed circles are from proton recoils induced by the neutrons leading to the first excited state of C^{11} at 1.90 MeV from the reaction B^{11} (p, n_1) C^{11} while the open circles are from neutrons leading to the ground state of C^{11}.

is obtained from the compton edge of standard radioactive gamma ray sources.

In order to obtain the neutron yield to the ground state of C^{11}, it is necessary to measure the area under the pulse spectrum corresponding to these neutrons shown in fig. 7. This was done in two ways. In the first method the high energy edge was extrapolated to the background base line. Then all pulses lying between 0.7 and 1.0 of this maximum value were counted. In the second method it was assumed that the shape of the pulse height distribution below the end point could be approximated by a hyperbola of the form

$$xy = k.$$

In this case the area between any two limits which are proportional to the neutron energy can readily be shown to be proportional to k. The area analysis proceeds by multiplying the counts per channel by the appropriate channel number. In all cases this was found to yield a constant value to good accuracy and this was taken as being proportional to the area. The yield curves obtained both ways are in satisfactory agreement with each other and the results from the second analysis are shown in the upper half of fig. 9 plotted against incident proton energy in the laboratory system. The total neutron proton scattering

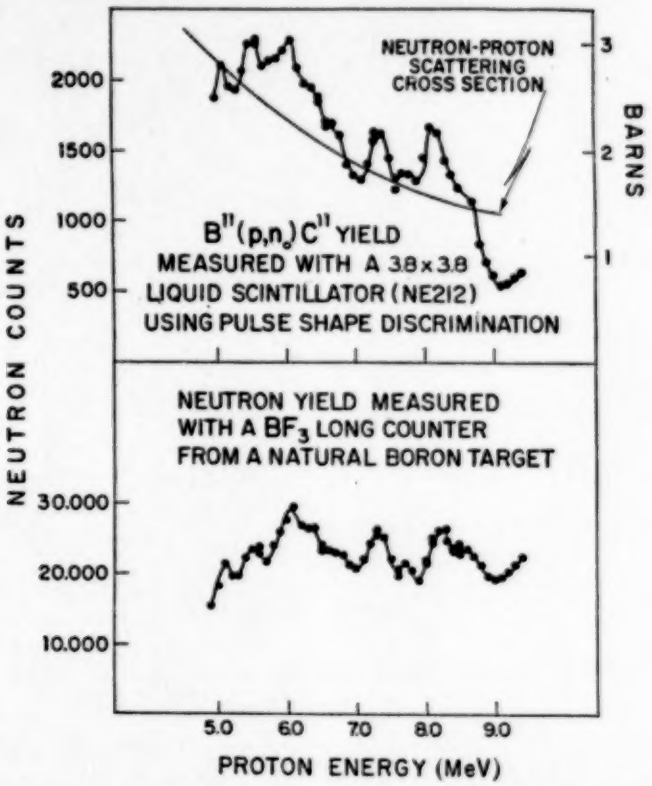

Fig. 9. The upper half shows the yield of neutrons leading to the ground state of C^{11} from the B^{11} (p, n) C^{11} reaction uncorrected for the neutron-proton scattering cross section, i.e. not corrected for the organic scintillator sensitivity. The smooth curve drawn approximately through the average of the measured cross section is the neutron-proton scattering cross section. The lower half shows the total neutron yield from the B^{11} (p, n) C^{11} reaction. In both cases the yields are measured at 90° to the incident proton beam direction.

cross section [13]) is also shown as a smooth curve drawn approximately through the average of the measured cross section. The lower half of fig. 9 shows the total neutron yield measured as described previously with a counter whose sensitivity is substantially independent of neutron energy. Considerably more fine structure is observed in these neutron yield curves than occurs in the capture gamma ray yields.

Angular distributions of gamma rays leading both to the ground and first excited state of C^{12} in the B^{11} (p, γ) C^{12} reaction have been measured at a

number of energies through the giant resonance region. Fig. 10 shows the results for ground state gamma rays at proton energies below, on and above the giant resonance. The results have been fitted by a weighted least-squares method to a Legendre polynomial expansion up to P_2 (cos θ) using the Chalk River Datatron Computer. Since the beam passed through the target into a catcher the minimum forward angle was limited to 22.5° and the maximum backward angle to 145° with the moving counter at 25.4 cm from the target centre. A proton energy of 7.12 MeV corresponds to the peak of the giant resonance

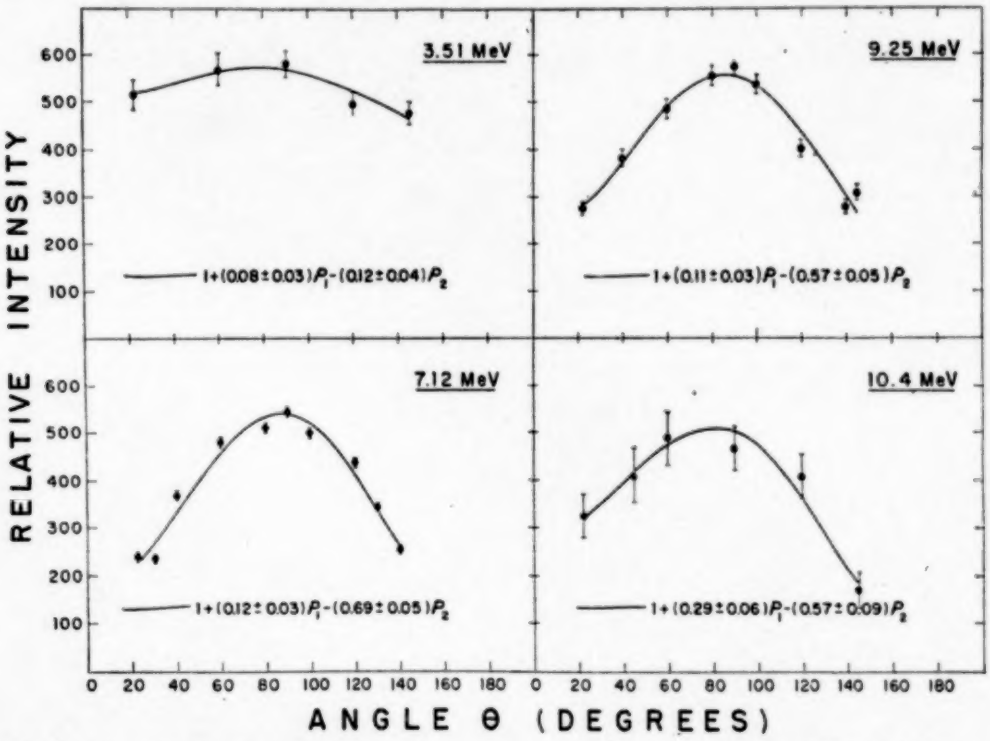

Fig. 10. Angular distributions of ground state gamma rays from the reaction B^{11} (p, γ) C^{12} measured at four incident proton energies below, on and above the giant resonance in C^{12}. The proton energy of 7.12 MeV corresponds to the peak of the giant resonance. The solid lines are least square Legendre polynomial fits and the values of the coefficients are given in the expressions $1+a_1P_1+a_2P_2$.

while 3.51 MeV is off it on the low energy side and 9.25 and 10.4 MeV are off it on the high energy side. The energies of 3.51 and 10.4 MeV correspond to the peaks of small secondary maxima below and above the main resonance. Measurements of the angular distribution of ground state capture gamma rays have also been made at a proton energy of 6.0 MeV with the beam stopped in a gold absorber backing the target. This allowed a geometry which permitted the detector to move through 0° to the beam. In this case measurements were made only from 0° to 90° and the Legendre polynomial expansion obtained was $W(\theta) = 1-(0.47\pm0.02)P_2$ (cos θ). No P_1 coefficient could be measured in this experiment. In addition, preliminary measurements were made at proton energies of 3.5, 6.0, 7.1 and 8.4 MeV with the beam passing through the target.

Within the much poorer statistics of these measurements they were consistent with those of fig. 10. The maximum negative coefficient of P_2 is observed at the peak of the giant resonance although nowhere except at 3.5 MeV is it smaller than about 0.46. At all energies a finite positive coefficient of P_1 (cos θ) is observed reaching its maximum value at the small secondary maximum at 10.4 MeV. As shown in appendix 1 this is, in small part, due to motion of the centre-of-mass and to a good approximation this affects only the coefficient of P_1 (cos θ) and P_3 (cos θ). Table 1 lists the coefficient of P_1 as measured in the

TABLE 1

Kinematic correction to the coefficient of $P_1(\cos\theta)$

E_p (lab)	P_1 coefficient		E_{ex} (C^{12})
MeV	Laboratory	Centre-of-mass	MeV
3.51	0.08 ±0.03	0.07 ±0.03	19.2
7.12	0.125±0.03	0.110±0.03	22.5
9.25	0.106±0.03	0.080±0.03	24.4
10.4	0.291±0.06	0.272±0.06	25.5

laboratory system and also the values corrected for kinematics. The P_1 (cos θ) coefficient is still appreciable after the kinematic correction. Since such a coefficient, if real, means interference between states of opposite parity in the giant resonance of C^{12} it is of importance to establish whether it is arising from experimental misalignment. This was checked in a direct fashion by replacing the boron target with a thin self-supporting carbon foil and measuring the angular distribution of 4.43 MeV gamma rays from the reaction C^{12} (p, p′ γ) at a proton energy of 6.9 MeV. The results are shown in fig. 11. In the centre-of-

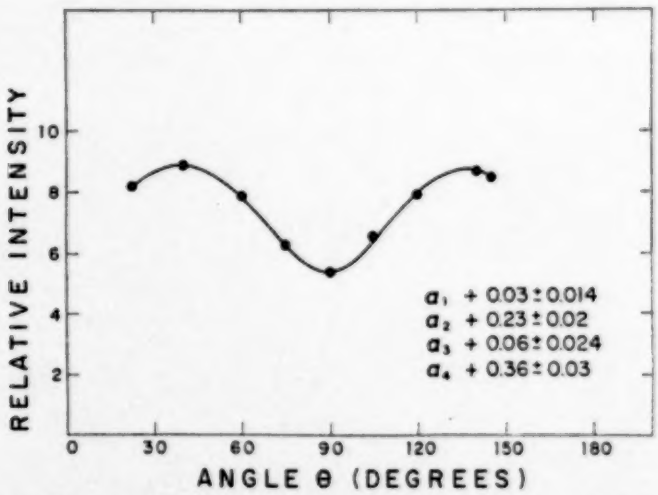

Fig. 11. Angular distribution of 4.43 MeV gamma rays from the reaction C^{12} (p, p′ γ) measured at a proton energy of 6.9 MeV. The solid line is a least square Legendre polynomial fit of the form $W(\theta) = 1+a_1P_1+a_2P_2+a_3P_3+a_4P_4$ and the values of the coefficients are shown.

mass system distributions of this type in which the second radiation is unobserved must be symmetric about 90°. The errors on the experimental data are about equal to the radii of the circles and the Legendre polynomial fit is given as a table of coefficients. The asymmetry about 90° is reflected in the finite size of the P_1 and P_3 coefficients although some of the contributions to both may be due to relativistic centre-of-mass effects which increase the number of gamma rays emitted at forward angles when the gamma source is moving in the beam direction. The maximum value the P_1 coefficient could have from this effect in this case is 0.02 which, within the error accounts for the observed value. The magnitude of the P_1 term in the B^{11} (p, γ_0) reaction can therefore not be accounted for either by experimental misalignment or by kinematic effects. Penner and Leiss [14]) have measured the angular distribution of photo-protons leading to the ground state of B^{11} from the C^{12} (γ, p)B^{11} reaction (the inverse of the B^{11} (p, γ_0) C^{12} reaction) and the Legendre polynomial coefficients they obtained compared with those found in the present are given in table 2. The agreement is remarkable and provides an interesting example of the validity of the principle of detailed balancing.

TABLE 2

Comparison of (p, γ_0) and (γ, p_0) angular distributions in C^{12}

E_p (MeV)	Excitation energy (MeV in C^{12})	a_1	a_2	Reference
7.12	22.5	$+0.12\pm0.03$	-0.69 ± 0.05	Present work
	22.1	$+0.09\pm0.04$	-0.56 ± 0.04	Penner and Leiss [14])
10.4	25.5	$+0.29\pm0.06$	-0.57 ± 0.09	Present work
	25.3	$+0.27\pm0.04$	-0.59 ± 0.06	Penner and Leiss [14])

The distribution is given by $W(\theta) = 1+a_1 P_1(\cos\theta)+a_2 P_2(\cos\theta)$.

The angular distribution of gamma rays leading to the first excited state of C^{12} at 4.43 MeV is more difficult to measure accurately because of the correction which must be made for the contribution of the ground state gamma ray to the pulse spectrum. Fig. 12 shows the distribution measured at a proton energy of 7.12 MeV which corresponds to the peak of the yield curve of gamma rays leading to the ground state. The only other proton energy at which this distribution was measured with any reliability was 8.4 MeV on the high energy side of the ground state giant resonance where approximate spherical symmetry was observed. The significance of the angular distributions is discussed later.

Huus and Day [15]) have measured the cross section for the yield of the B^{11} (p, γ_0) C^{12} reaction for proton energies up to 2.8 MeV. Assuming spherical symmetry for the gamma ray angular distributions they obtain a peak cross section for the resonance at a proton energy of $\approx$ 1.5 MeV of 35 μb. From fig. 5

the 90° ratio of the cross section at 7.15 MeV (the peak of the giant resonance) to that at 1.5 MeV is 5.03. Hence the cross section at 7.15 MeV is 1.75×10^{-28} cm² assuming spherical symmetry. This is to be compared to the value of 2.7×10^{-28} cm² obtained by Gemmel *et al.* [2]) making the same assumptions. From the measured angular distribution at the peak of the giant resonance one can correct the 1.75×10^{-28} cm² figure for the deviation from spherical symmetry and arrive at a cross section for the B^{11} (p, γ_0) reaction at the peak of the giant resonance of 1.3×10^{-28} cm². Using the principle of detailed balance this corresponds † to a cross section at the peak of the giant resonance for the C^{12} (γ, p_0) reaction [16]) of 12 mb.

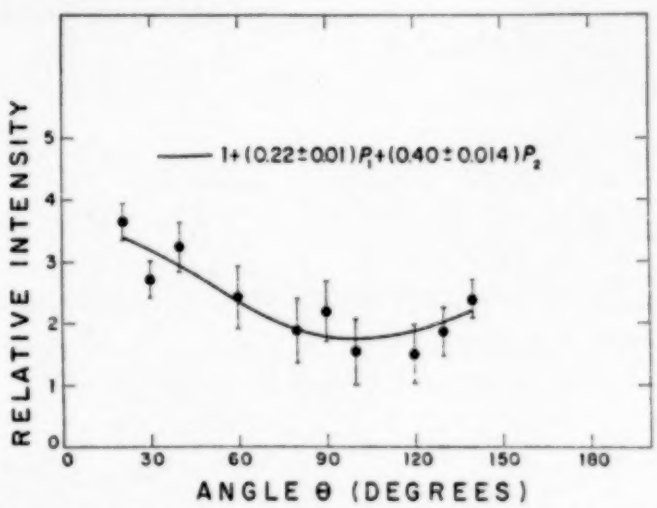

Fig. 12. The angular distribution of gamma rays leading to the first excited state of C^{12} at 4.43 MeV from the reaction B^{11} (p, γ) C^{12*} measured at a proton energy of 7.12 MeV corresponding to the peak of the giant resonance in the yield of gamma rays leading to the ground state. The solid line is a least square Legendre polynomial fit and values of the coefficients are given in the expression $1+a_1P_1+a_2P_2$.

From this peak cross section and assuming a Breit-Wigner shape for the B^{11} (p, γ_0) giant resonance a lower limit for $\Gamma_{\gamma 0}$ the partial width for gamma emission from the giant resonance to the ground state of C^{12} can be obtained. We use the following relations:

$$\sigma_R = 4\pi\lambda^2 \frac{\omega\gamma}{\Gamma}\ \text{cm}^2,$$

$$\omega\gamma = \frac{(2J_1+1)}{(2i_1+1)(2I_0+1)} \frac{\Gamma_p\Gamma_{\gamma 0}}{\Gamma},$$

$$\frac{1}{\lambda^2} = \left(\frac{M_T}{1+M_T}\right) 4.858\times10^{24} E_{\text{Lab}}\ (\text{MeV}\cdot\text{cm}^2),$$

† W. R. Dodge and W. C. Barber, as quoted in ref. [16]) by L. Katz have measured the C^{12} (γ, p_0) B^{11} reaction. They obtain a peak cross section of 1.3 mb/sr [not 13 mb/sr as quoted in ref. [16])] which yields a total cross section at the peak of 11.6 mb. When the energy scales for the C^{12} (γ, p_0) and B^{11} (p, γ_0) reactions are corrected for kinematics the shapes of the two yield curves are almost identical.

where $J_1 = 1$ is the spin of the giant resonance, $i_1 = \frac{1}{2}$ the spin of the proton, $I_0 = \frac{3}{2}$ the spin of the target nucleus, $M_T = 11$ the mass number of the target, $E_{Lab} = 7.15$ the energy corresponding to the peak of the giant resonance, $\Gamma = 3.12$ MeV the centre-of-mass total width and $\sigma_R = 1.3 \times 10^{-28}$ cm^2 the peak cross section. This yields $\gamma = 2.5$ keV from which it follows that $\Gamma_{\gamma 0} \geqq 2.5$ keV.

The electric dipole sum rule can be expressed as

$$\int_0^\infty \sigma(E)\mathrm{d}E = 2\pi^2 \frac{e^2\hbar}{Mc}(1+k)\text{erg cm}^2,$$

where k is an exchange term lying between 0.6 and 0.8 and $\sigma(E)$ is the photonuclear cross section for all (γ, n) and (γ, p) processes. This equation can be written

$$\int_0^\infty \sigma(E)\mathrm{d}E = 0.06 \frac{NZ}{A}(1+k)\text{ MeV} \cdot \text{b};$$

hence for C^{12}, one obtains ≈ 0.3 MeV · b.

Measuring the area under the B^{11} (p, γ_0) C^{12} yield curve of fig. 5 from 4 MeV to 10.5 MeV proton energy in the laboratory system yields a value of 4.7×10^{-4} MeV · b. By the principle of detailed balance this can be related to the integrated yield for C^{12} (γ, p_0) B^{11} giving the value 0.043 MeV · b. This is a factor of about seven lower than the limit of 0.3 MeV · b. but, of course the latter includes all (γ, p) and (γ, n) contributions.

4.2. THE Al^{27} (p, γ) Si^{28} REACTION

A pulse-height spectrum, measured in the 12 cm diameter by 15 cm long NaI(Tl) detector when 6.85 MeV protons are incident on a 400 μg/cm^2 Al^{27} foil plotted on a semi-logarithmic scale, is shown in fig. 13. Like the curves of figs. 2 and 3 it is characterized by the two high energy peaks corresponding to capture gamma rays leading to the ground and first excited state of Si^{28}, a steep rise with decreasing pulse-height down to pulse-heights corresponding to about 5 MeV gamma rays from neutron capture in the crystal and superimposed on this a number of sharp gamma ray lines which follow the emission of particles from the compound nucleus.

A linear plot of the upper portion of the gamma ray pulse spectrum for 7.64 MeV protons incident on an aluminium foil target (20 keV thick for 10 MeV protons) is shown in fig. 14. The line shape of the pulse spectrum for the ground state transition under that for the transition to the first excited state in Si^{28} at 1.78 MeV is taken to be the same as that for the ground state transition in the B^{11} (p, γ) C^{12} reaction shown in fig. 4. The uncertainty about line shape does not exist in this case since in the Al^{27} (p, γ) reaction the energy of two capture gamma rays is much closer and the line shape for the ground state

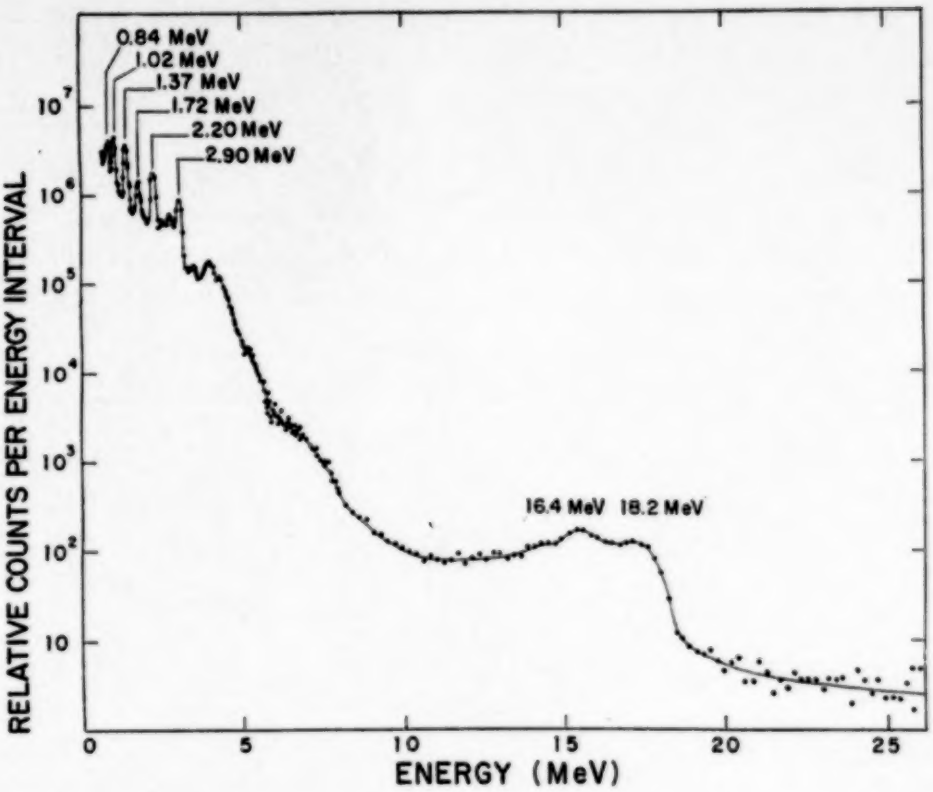

Fig. 13. The gamma ray pulse spectrum from 6.85 MeV proton bombardment of a 400 $\mu g/cm^2$ thick Al^{27} foil. The detector was an unshielded 12 cm diameter by 15 cm long NaI (Tl) crystal at 90° to the beam with its front face 15.7 cm from the target centre. The ordinate scale is logarithmic.

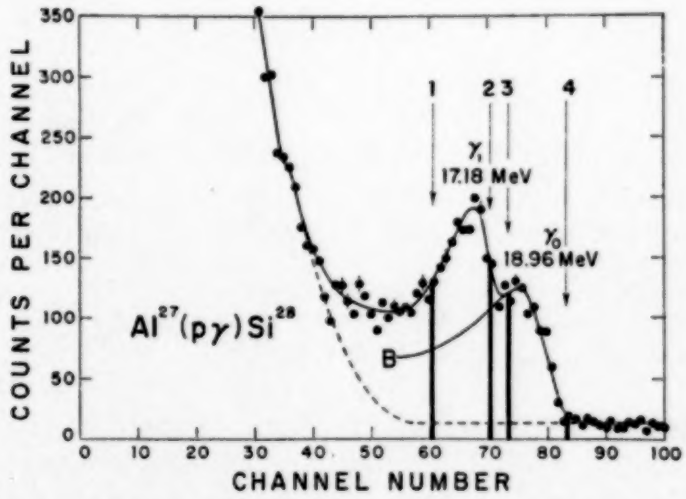

Fig. 14. The gamma ray pulse spectrum plotted on a linear ordinate scale from 7.64 MeV proton bombardment of an aluminium foil target. Only the high energy pulses are displayed. The shape of the pulse spectrum for γ_0 under γ_1 is shown by the line B. The four vertical lines numbered 1 through 4 show the region used for measuring intensities.

transition is directly measured from the B^{11} (p, γ) reaction for energies at least 3 MeV down from the peak. With the contribution of γ_0 under γ_1 established the analysis of the yield proceeds in the same way as that described previously for B^{11} (p, γ)C^{12}.

The yield curves for gamma rays leading to the ground and first excited state of Si^{28} at 90° to the incident beam are shown in the upper and lower half of fig. 15, respectively. The most striking feature of these yield curves is the pronounced narrow resonance structure. Indeed, more structure than indicated

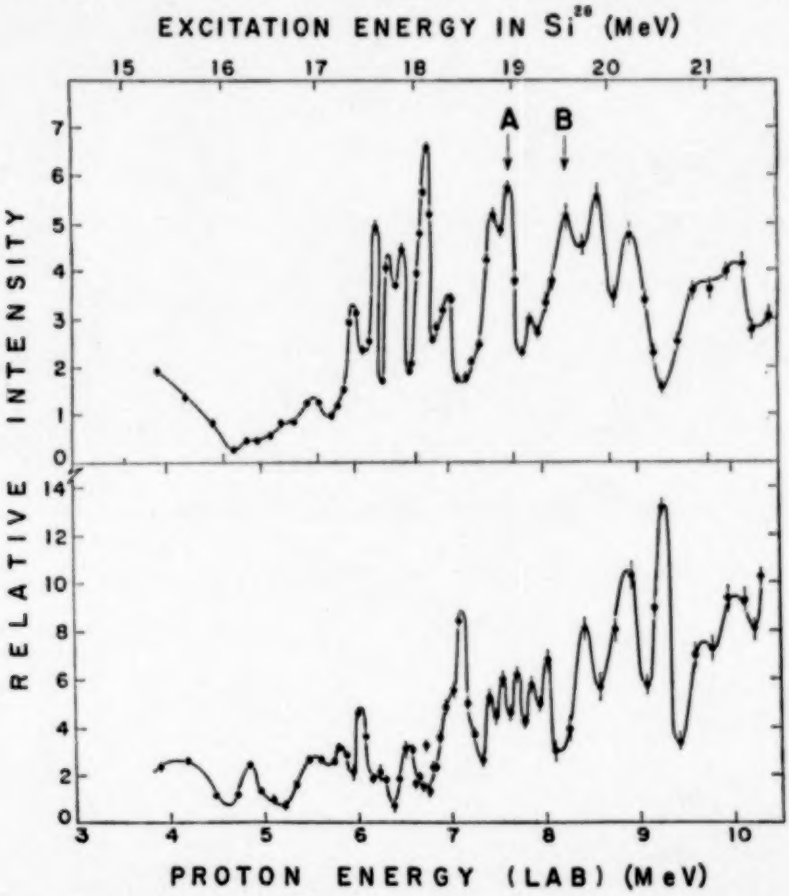

Fig. 15. The yield of gamma rays leading to the ground state (upper curve) and to the first excited state (lower curve) of Si^{28} resulting from proton capture in Al^{27} and measured at 90° to the incident beam. The ordinates of the two yield curves are correct relative to each other. The abscissae are marked both in terms of the incident laboratory proton energy and in excitation energy in the compound nucleus Si^{28}. A and B mark the energies at which angular distributions were measured.

here may be present and to determine this a thinner target and many more points on the yield curve would be required. It is of interest to note that of the approximately 90 resonances observed at proton energies below 3.5 MeV only two or three show ground state capture gamma rays of significant intensity and at least one of the resonances [17]) has spin and parity 1^+. On the other hand most of the resonances emit capture gamma rays to the first excited state

of Si^{28}. As soon as the giant resonance region of excitation is reached, however, ground state transitions compete with and even predominate those to the first excited state.

Measurements of the combined yield of gamma rays leading to the ground and first excited state of Si^{28} have been made by Gemmel *et al* [2]) in the energy range $E_p = 5.75$ to 7.70 MeV and by Kimura *et al.* [18]) in the energy range

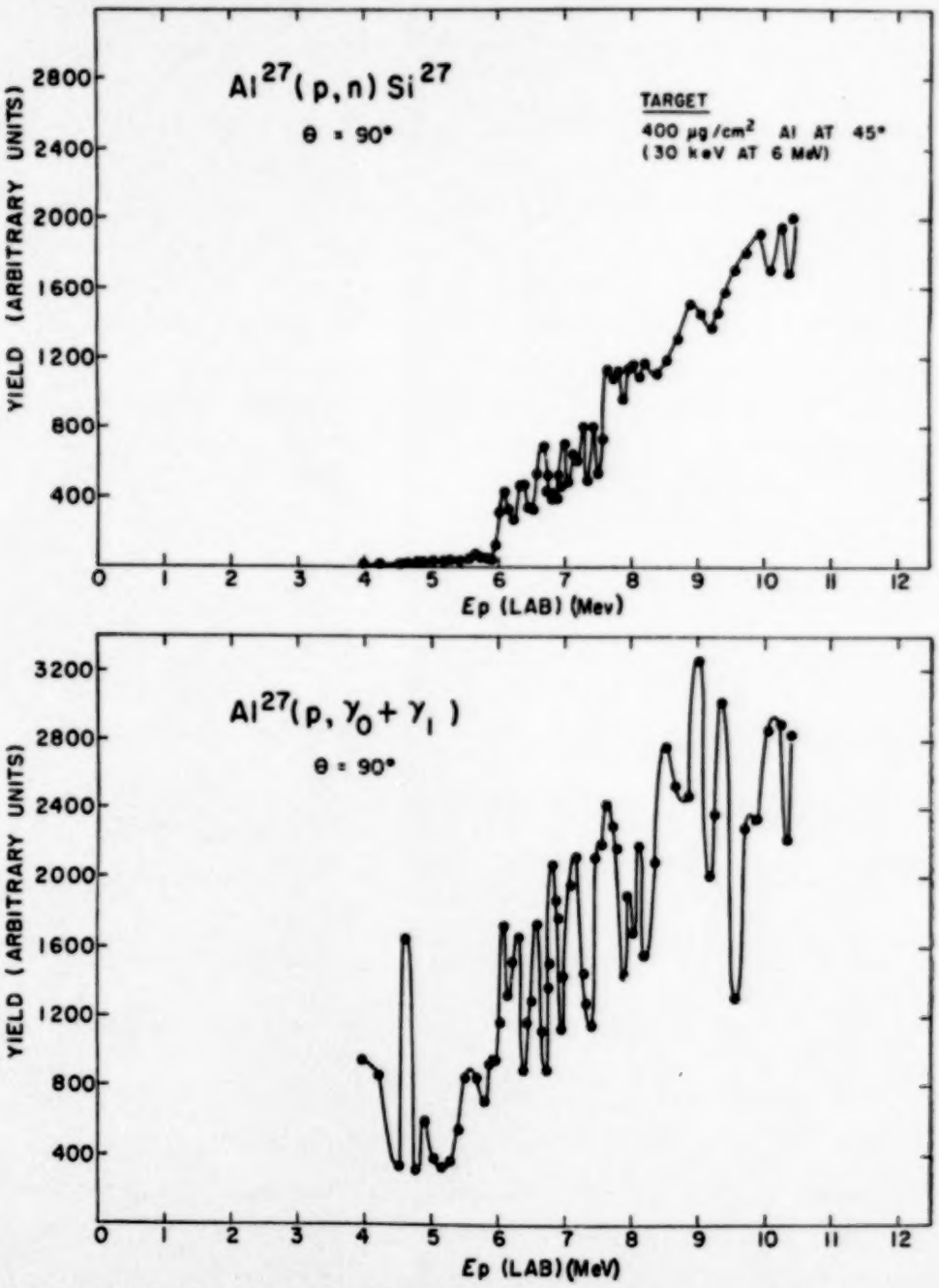

Fig. 16. The combined yield of gamma rays leading to the ground and first excited state of Si^{28} ($\gamma_0+\gamma_1$) at 90° as a function of proton energy in the laboratory system is shown in the lower half. The yield of neutrons from the reaction Al^{27} (p, n) Si^{27} measured at 90° with a modified long counter is shown in the upper half.

$E_p = 7.5$ to 14.7 MeV. In this latter experiment the yield showed three broad maxima of increasing intensity at $E_p = 7.61$, 8.75 and 10.13 MeV followed by a drop off reaching half maximum intensity at about 11.3 MeV. To compare the present results with these the yield of $\gamma_0+\gamma_1$ is shown in the lower half of fig. 16.

In the upper half of fig. 16 the neutron yield from the Al^{27} (p, n) reaction is plotted against incident proton energy in the laboratory system. This was measured by a modified long counter as described previously placed at 90° to the beam. This extends the measurements reported by Gove *et al* [6]) up to a proton energy of 10.5 MeV.

It should be noted in examining the yield curves of figs. 15 and 16 that the envelope of the yield of γ_1 continues to rise to the highest energies as does the neutron yield and the combined yield of $\gamma_0+\gamma_1$. On the other hand the envelope of the yield of γ_0 stays relatively constant and shows some evidence of falling at the higher energy. Strictly speaking it is only the individual gamma-ray yields and not the sum of the intensities of the two gamma rays which has significance as far as the giant resonance phenomenon is concerned. Assuming that the γ_0 yield does drop off at higher energies, the gross structure width observed is greater than 4.3 MeV in contrast to the 3.1 MeV width observed in the B^{11} (p, γ_0) C^{12} yield.

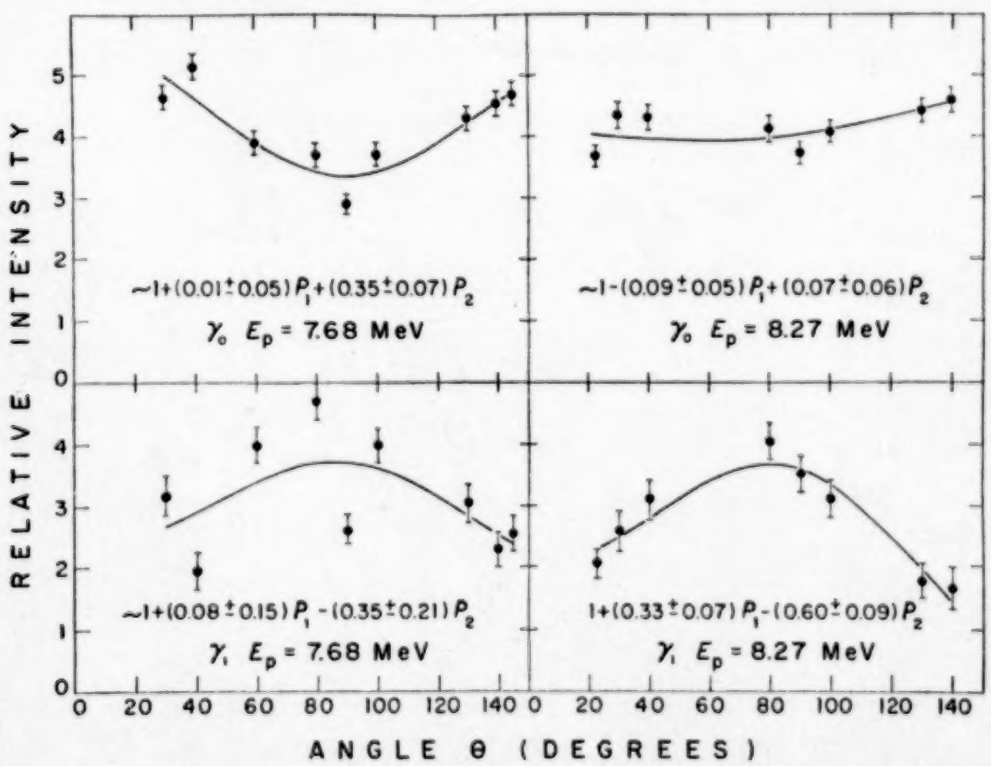

Fig. 17. Angular distributions of gamma rays leading to the ground state (γ_0) and to the first excited state (γ_1) of Si^{28} from the reaction Al^{27} (p, γ) measured at two proton energies of 7.68 and 8.27 MeV (corresponding to the positions A and B on the yield curve of fig. 14). The solid lines are least square Legendre polynomial fits and, in each case, values of the coefficients are given in the expressions $1+a_1P_1+a_2P_2$.

Angular distributions of gamma rays leading to the ground and first excited state of Si^{28} were measured at two energies marked A and B on the yield curve of fig. 15 corresponding to excitation energies of about 19 and 19.6 MeV. These are at the peaks of two of the maxima observed in the yield of γ_0 and the results are shown in fig. 17. The smooth curves through the experimental points are least square Legendre polynomial fits to the distributions and in each case the expansion is given in fig. 17.

4.3. THE Na^{23} (p, γ) REACTION

A linear plot of the upper portion of the gamma ray pulse spectrum for 9.0 MeV protons incident on a Na^{23} target (about 180 keV thick for 10 MeV

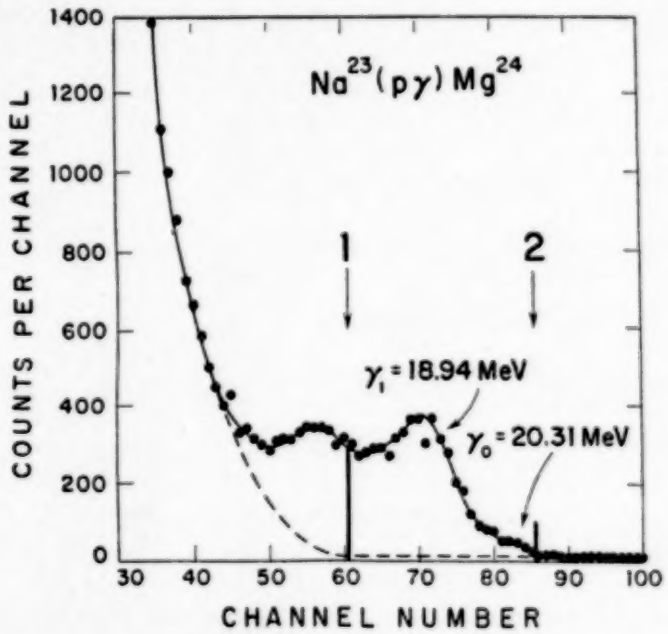

Fig. 18. The gamma ray pulse spectrum plotted on a linear ordinate scale from 9.0 MeV proton bombardment of sodium foil target. Only the higher energy pulses are displayed. In this case the combined yield of γ_0 and γ_1 was measured by taking the area between the two vertical lines 1 and 2 and correcting for estimated background.

protons) is shown in fig. 18. In this case because the separation energy between the ground and first excited state of Mg^{24} is small (1.37 MeV) and also because the yield of the ground state gamma ray is much weaker than that to the first excited state over the whole energy range studied it is more difficult to make any accurate estimate of the yield of γ_0 separately and the combined yield was measured as shown.

The yield curve of $\gamma_0+\gamma_1$ measured in this way, at 90° to the incident beam is shown in fig. 19. Because of the greater target thickness much of the fine structure which is undoubtedly present is largely averaged out. Two gross structure peaks remain however, and, in fact, similar gross structure may also

be present in the Al^{27} (p, γ_0) Si^{28} yield curve of fig. 15. In the Na^{23} (p, $\gamma_0+\gamma_1$) Mg^{24} yield, the two peaks occur at excitation energies of 17.4 and 20.6 MeV while in Al^{27} (p, γ_0) they appear to occur at excitation energies of 17.7 and 19.6 MeV, respectively.

The Mg^{24} (γ, n) Mg^{23} reaction has been re-measured recently [19]). In addition to a broad peak with a large high energy tail, a small peak is observed on the low energy side at an excitation energy of 17.2 ± 0.2 MeV, which may correspond to the peak shown in fig. 19 at 17.4 MeV.

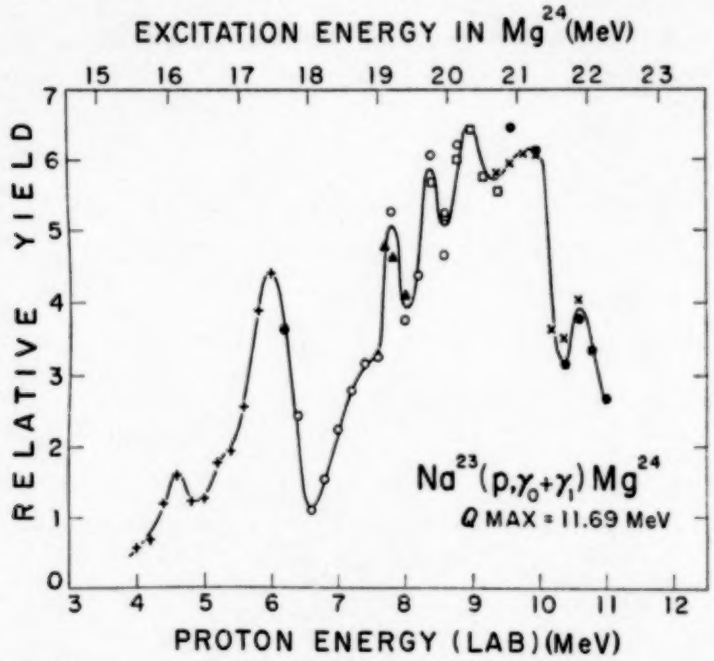
EXCITATION ENERGY IN Mg24 (MeV)
15 16 17 18 19 20 21 22 23
RELATIVE YIELD
0 1 2 3 4 5 6 7
Na23(p,γ0+γ1) Mg24
Q MAX = 11.69 MeV
3 4 5 6 7 8 9 10 11 12
PROTON ENERGY (LAB) (MeV)

Fig. 19. The combined yield of gamma rays leading to the ground and first excited state of Mg^{24} resulting from proton capture in Na^{23} and measured at 90° to the incident beam. The different symbols on the yield curve represent separate runs. The abscissa is marked both in terms of the incident laboratory proton energy and in excitation energy in the compound nucleus Mg^{24}.

5. Discussion of Experimental Results

5.1. ANGULAR DISTRIBUTION

It has been shown by Courant [20]) that, if the (γ, p) reaction in the giant resonance region proceeds by a direct electric dipole photo-disintegration process in which the gamma ray quantum is absorbed by one proton in the nucleus which is then emitted without the formation of an intermediate compound nucleus, the angular distribution of the protons depends only on the orbital angular momentum of this proton in the nucleus. In the (p, γ) reaction, if l is the orbital angular momentum of the incident proton and El radiation is emitted the angular distribution of the gamma rays is given by

$$W(\theta) = 2(l+2)+l\sin^2\theta \text{ for } l \to l+1,$$
$$W(\theta) = 2(l-1)+(l+1)\sin^2\theta \text{ for } l \to l-1.$$

This is equivalent to the more usual form

$$W(\theta) = 1-\tfrac{1}{2}\left(\frac{l}{2l+3}\right) P_2(\cos\theta) \text{ for } l \to l+1,$$

$$W(\theta) = 1-\tfrac{1}{2}\left(\frac{l+1}{2l-1}\right) P_2(\cos\theta) \text{ for } l \to l-1.$$

In these expressions it is assumed that the incident proton jumps from a state in which its orbital angular momentum is l to a final state in which it is $l\pm1$ with the emission of an electric dipole radiation. From these expressions it is clear that in the direct capture process the coefficient of P_2 (cos θ) must be less than or equal to zero. In the case of the B^{11} (p, γ) process the possible transitions are s → p ($W(\theta)$ = constant) and d → p ($W(\theta) = 1-0.5\ P_2$), while for Al^{27} (p, γ) they are p → d ($W(\theta) = 1-0.1\ P_2$) and f → d ($W(\theta) = 1-0.4P_2$).

Experimentally it is found that for B^{11} (p, γ_0) C^{12} the coefficient of P_2 is not far from -0.5 over the whole giant resonance, whereas that for the B^{11} (p, γ_1) C^{12} is positive or approximately spherically symmetric. The positive value of $a_2 = 0.40$ for B^{11} (p, γ_1) at the peak of the giant resonance for γ_0 has a further interesting interpretation. It can be shown that such a coefficient cannot arise from a capturing state of 1− in C^{12} and hence at the peak of the giant resonance for γ_0, the 1− states involved do not emit gamma rays to the first excited state of C^{12}. This is compatible with the suggestion of Brown and Bolsterli [21]) that the giant resonance is intimately related to the final state in the dipole emission, i.e. the ground state for dipole transitions to the ground state.

For the Al^{27} (p, γ_0) reaction, however, the angular distributions bear no resemblance to the direct capture predictions. This is, of course, not surprising since the very considerable resonance structure observed suggests the formation of well-defined compound nucleus states of complicated configurations. It might be useful to perform a poor resolution experiment with the aluminium target to average over many resonances and then to compare the angular distributions with direct capture theory.

As shown in table 1, the coefficient of P_1 (cos θ) in the angular distribution of the ground state gamma ray from B^{11} (p, γ_0) C^{12} when corrections for centre-of-mass motion are made, has a finite positive value which is approximately constant through the giant resonance and has its maximum value of 0.27 ± 0.06 at the small high energy maximum at about 10.4 MeV.

A possible explanation for such an interference term and an estimate of its magnitude has been given by Brown and Levinger [22]). They assume that the interference arises from the electric dipole giant resonance at an excitation energy E_m and an electric quadrupole giant resonance at an excitation energy of about 2 E_m. Under these conditions one would expect an angular distribution

of the form

$$W(\theta) = \sum_{0}^{4} P_n(\cos\theta),$$

where n has all the integral values between 0 and 4. In the vicinity of the dipole resonance the coefficient of P_2 would essentially be that due to the dipole resonance (i.e. $-\frac{1}{2}$ in this case) and the P_4 coefficient would be zero. However, because of the interference between the two resonances, one should also observe both a P_1 and a P_3 term and both these coefficients should change sign upon passing through the dipole resonance.

The angular distributions shown in fig. 10 for B^{11} (p, γ_0) C^{12} at the three highest energies, were also analyzed in a Legendre polynomial expansion which included P_3 and P_4. It was found that the coefficients of P_3 and P_4 were not statistically different from zero. Much more accurate angular distribution data would be required to measure these higher coefficients. However, there is no indication in the measurements that the P_1 coefficient changes sign, although the only measurement below the peak of the resonance is that at $E_p = 3.51$ MeV. It is, therefore, very difficult to explain the observed behaviour of the coefficient of P_1 through the giant dipole resonance in C^{12}. The observation that there is no change in sign of this coefficient through the giant resonance and particularly the fact that it does not even reach a minimum value near the peak, cannot be accounted for by interference with one or two other resonances. It is interesting to note, however, that in this respect the angular distributions of γ_0 in the B^{11} (p, γ_0) C^{12} reaction behave in a similar fashion [10]) for proton energies from 1.0 to 2.6 MeV. The coefficient of a_1 is positive at all energies measured through the broad resonance at $E_p = 1.4$ MeV, which is almost certainly [23]) $J = 1-$. It does, however, show evidence of vanishing at the peak of the 1.4 MeV resonance. The coefficient of P_2 also shows an interesting behaviour in the range from 1.0 to 2.6 MeV. It remains substantially constant at $+0.17$ over the region covered by the 1.4 MeV resonance and then drops rapidly to -0.4 at 2.6 MeV. This may be due to the onset of the tail from the giant dipole resonance.

5.2. STRUCTURE IN THE GIANT RESONANCE

No fine structure is observed in the giant resonance region of the yield from the reaction B^{11} (p, γ_0) C^{12} in which the maxima are greater than 10 % of the yield. This is in marked contrast to the discontinuities reported in the C^{12} (γ, p_0) reaction [24]), which is the inverse to that reported here, although the yield curve of fig. 6 should be extended in both directions to search for the 21.5 and 22.6 MeV resonance reported by Cohen *et al.* [29]). However, a direct comparison between fig. 5 in the present work and fig. 9 of Cohen *et al* [24]) vividly demonstrates the serious discrepancy between the two results. Dis-

continuities are also reported at various energies in the C^{12} (γ, n) C^{11} reaction[11, 25]) but in this case since no energy selection was employed on the neutrons, the yield includes not only the inverse mirror yield C^{12} (γ, n_0) C^{11} but also the yield of neutrons to the first excited state of C^{11} at 1.90 MeV. The total cross section for gamma ray induced reactions on C^{12} has also been measured and marked discontinuities have been observed [26, 27]). The inverse of the B^{11} (p, γ_0) C^{12} reaction has been measured recently by Dodge and Barber [16]). No evidence for fine structure was observed. At the moment, the weight of the evidence suggests that through the giant resonance region no narrow ($\Gamma \approx 100$ to 200 keV) resonances are observed in the B^{11} (p, γ_0) C^{12} reaction or its inverse. The evidence for narrow resonances in the C^{12} (γ, n) C^{11} reaction is still somewhat confused [11, 25]).

Concerning the considerable fine structure observed in the Al^{27} (p, γ) Si^{28} yield curve through the giant resonance and also undoubtedly present in the Na^{23} (p, γ) Mg^{24} yield, not much can be said except that for the first time it has been shown that the giant resonance can consist of a very large number of strong narrow resonances. It is, however, of interest to look for gross structure in the two cases. Definite evidence for this is to be seen in the yield of Na^{23} $(p, \gamma_0+\gamma_1)$ Mg^{24}, shown in fig. 19. Two broad peaks are observed, centred approximately at 20.60 and 17.44 MeV. It has been shown independently by Danos [18]) and Okamoto [28]) that in the case of spheroidal nuclei, one expects the giant resonance to split into two peaks corresponding to the characteristic resonance energy along the major and minor axes. If a and b are the lengths of these semi-axis, then

$$\frac{\hbar\omega_b}{\hbar\omega_a} = 0.911\,\frac{a}{b} + 0.089 = 0.911x + 0.089.$$

The electric quadrupole moment of such a spheroid having a uniform charge distribution is given by

$$Q_0 = \tfrac{2}{5}Z(a^2 - b^2);$$

assuming $R^3 = ab^2 = R_0{}^3A = y$ with $R_0 = 1.4$ fm (so that R is the radius of a sphere having the same volume as the spheroid, A denoting the atomic weight) one can show that

$$Q_0 = \tfrac{2}{5}Z\,\frac{(x^2-1)}{x^{\frac{4}{3}}}\,y^{\frac{2}{3}}. \qquad (2)$$

This relation permits a plot of the intrinsic electric quadruple moment Q_0 vs. the ratio $\hbar\omega_b/\hbar\omega_a$. For the results in Mg^{24} one obtains $\hbar\omega_b/\hbar\omega_a = 1.18$ and hence $Q_0 = 0.32\times10^{-24}$ cm^2. Coulomb excitation measurements [30]) on Mg^{24} yield a value of $B(E2)$ for the transition to the first excited state at 1.37 MeV from which one can derive a value of $Q_0 = 0.59\times10^{-24}$ cm^2. This in turn would

predict $\hbar\omega_b/\hbar\omega_a = 1.34$, which is much larger than can be accommodated by the yield of fig. 19. If one assumes the upper peak to be at 20.6 MeV, this factor of 1.34 would place the lower peak at 15.4 MeV. This is the lower limit of measurements in this work. The Na^{23} (p, γ) reaction has been investigated [31]) over the region of excitation in Mg^{24} from about 11.9 to 14.0 MeV and no evidence for a giant resonance has been observed. In fact, between 13 and 14 MeV capture gamma radiation is either weak or unobservable. However, it would be of interest to explore the region between 14 and 15.5 MeV. It should be noted again that the experiments reported here measure the combined yield of $\gamma_0+\gamma_1$. Since, throughout the whole giant resonance interval the yield of γ_1 is substantially greater than γ_0, the yield curve of fig. 19 is essentially that for γ_1. This complicates the situation since capture states of $J = 1-$, $2-$ and $3-$ can give rise to electric dipole radiation to the $2+$ first excited state of Mg^{24}. Preliminary results [32]) indicate that the Na^{23} (p, γ_0) yield is quite different in detail from that for Na^{23} (p, γ_1). However, the discrepancy between Q_0 measured both ways still remains.

Turning now to the results for Al^{27} (p, γ_0), an examination of the yield curve shown in the upper half of fig. 15, suggests two gross structure peaks centered at about 17.7 and 19.6 MeV, respectively. This yield $\hbar\omega_b/\hbar\omega_a = 1.11$ whence from eq. (2), $Q_0 = 0.22\times10^{24}$ cm. Coulomb excitation [30]) of the 1.78 MeV first excited state of Si^{28} gives $Q_0 = 0.25\times10^{-24}$ cm.

5.3. WIDTHS

From the yield curve of B^{11} (p, γ_0) C^{12} of fig. 5, assuming it to be a single broad resonance one obtains a width of 3.1 MeV in the centre-of-mass system (3.4 MeV in the laboratory system). The angular distributions are reasonably consistent with formation by d-wave protons. The single particle limit for 7 MeV d-wave protons on B^{11} is about 5.3 MeV in the laboratory system [33]). In addition to this contribution to the width there is also that arising from alpha particle and neutron emission as well as inelastic proton scattering. Hence the observed width is rather far from the single particle value.

In this same reaction the ground state gamma ray width at the giant resonance is greater than 2.5 keV. Following Wilkinson's [34]) procedure of analyzing gamma widths in terms of their ratio to the Weisskopf unit [35]) one obtains $|M|^2 \geqq 0.4$. This is to be compared to the classical summed oscillator strength [36]) $NZ/A = 3$.

In the case of the Al^{27} (p, γ_0) Si^{28} reaction the width of the giant resonance is 4.5 MeV in the laboratory system. If only p-wave incident protons participated in the reaction the single particle limit would be about 6.7 MeV. The single particle limit for f-wave protons on the other hand is 2.7 MeV.

5.4. GIANT RESONANCE BASED ON FIRST EXCITED STATE

The yield of gamma rays leading to the ground and excited states of light nuclei resulting from proton capture can be employed to test whether giant

resonances occur for individual primary capture gamma rays. Since the frequency associated with excitation energy of the dipole giant resonance for ground state transitions is a resonance characteristic of each particular nucleus one would expect to find a giant resonance for the capture gamma rays leading to the first excited state of a nucleus at an excitation energy greater than that for the ground state transition by just the energy of the first excited state.

Unfortunately the proton energies available from the Chalk River tandem accelerator are not quite high enough to test this hypothesis in the cases that have been investigated here. The yield curve for B^{11} (p, γ_1) stops just where the peak of the dipole resonance for this gamma ray is expected to occur. However, the yield of γ_1 as shown in fig. 5 is quite low at the peak of the dipole resonance for γ_0 and rises toward the highest energy obtainable showing some tendency to flatten off at the maximum energy. The results, in this case, are at least consistent with the prediction. It would be of considerable interest to continue these yields to higher energy.

The situation for the Al^{27} (p, γ_1) reaction shown in fig. 15 is no better. Again, however, the yield of γ_0 after its initial rise is flat over a fair range and shows some tendency to drop at the highest energy. The yield for γ_1 on the other hand continues to climb to the highest energies available in this experiment. Some useful additional information is however available in this case from the work of Kimura *et al.* [18]). They measured the combined yield of γ_0 and γ_1 for proton energies between 7.5 and 14.7 MeV. This combined yield falls to half maximum at about 11.3 MeV and continues to decline up to the highest energy observed. The conclusion to be drawn from the combination of the present results and those of Kimura *et al.* is that the yield of γ_1 does in fact go through a giant resonance at a higher energy than γ_0 as expected. How much higher one still cannot say.

6. Summary

Measurements have been carried out on the yield and angular distributions of proton capture gamma rays in the giant dipole resonance region of C^{12}, Mg^{24} and Si^{28}. The following summarizes the information obtained and the conclusions drawn:

a) The yield for γ_0 in C^{12} goes through a giant resonance peaked at 22.5 ± 0.02 MeV excitation energy with a width at half maximum of 3.1 MeV in the centre-of-mass system. The peak cross section is 1.3×10^{-28} cm^2 and the integrated area under the peak is 4.7×10^{-4} MeV · b.

The envelope of the yield of γ_0 in Si^{28} is much broader and flatter with a maximum in the vicinity of 19 to 20 MeV excitation and a width of 4.3 MeV or greater in the centre-of-mass.

The envelope of the combined yield of γ_0 and γ_1 in Mg^{24} has a maximum near 20 MeV excitation and a width of 4.9 MeV in the centre-of-mass.

b) No fine structure of height greater than 10 % of the smooth yield is observed in the B^{11} (p, γ_0) yield while considerable fine structure is observed in the Al^{27} (p, γ_0) reaction yield. Target thickness prevented fine structure being observed in the Na^{23} (p, $\gamma_0+\gamma_1$) yield although it is undoubtedly present.

c) Some evidence for gross double peaked structure is observed in both the yield of γ_0 in Si^{28} and of $\gamma_0+\gamma_1$ in Mg^{24}.

d) The yield of γ_1 both in C^{12} and Si^{28} continues to rise up to the highest energies available. It is consistent with the hypothesis of a giant resonance at an energy above that for γ_0 equal to the energy of the first excited state.

Somewhat more fine structure is observed in the yield of γ_1 in C^{12} than for γ_0. The yield of γ_1 in Si^{28} shows as much fine structure as that for γ_0 but there is no correlation between the two.

e) The yield of neutrons from the reaction B^{11} (p, n) C^{11} leading to the ground state as well as that for all neutrons independent of energy shows no evidence for the giant resonance observed in the gamma ray yield. Much more fine structure is observed in the neutron yield curves however.

The yield of all neutrons from the Al^{27} (p, n) Si^{27} reaction continues to rise more or less steadily up to the highest energy observed with a considerable amount of fine structure particularly within 2 MeV of the threshold.

f) The angular distributions of γ_0 in C^{12} are consistent with direct capture of d-wave protons which undergo a transition to p-wave with the emission of dipole radiation. No similar simple explanation applies to γ_1 in C^{12} or γ_0 and γ_1 in Si^{28}.

The angular distribution of γ_1 in C^{12} measured at the peak of the giant resonance for γ_0 indicates that the states responsible for the emission of γ_0 do not predominate in the emission of γ_1.

The angular distribution of γ_0 in C^{12} shows a forward asymmetry which increases with increasing energy. This is inconsistent with interference between two broad resonances of opposite parity whose spacing is larger than their widths.

g) From the measured absolute cross section and assuming the broad peak in the yield of γ_0 in C^{12} is a single resonance one derives a width for emission of ground state gamma rays $\Gamma\gamma_0 \geqq 2.5$ keV. In Weisskopf units this yields $|M|^2 \geqq 0.4$.

The single particle limit to the width for d-wave protons incident on C^{12} at the giant resonance is 5.3 MeV in the laboratory system. It is 6.7 MeV for p-wave protons on Al^{27} and 2.7 MeV for f-wave protons.

It is a pleasure to acknowledge the invaluable assistance of Mr. P. G. Ashbough and his staff for efficient operation of the Chalk River tandem accelerator, Mr. C. E. L. Gingell for his advice and assistance on questions of electronics, Mr. W. Woytowich for target preparation and Miss A. R. Rutledge for data analysis. We would also like to express our gratitude to Dr. E. Vogt and Dr. H. McManus for many helpful discussions of this work and to Dr. W. R. Dodge of Stanford University for several very helpful comments on the manuscript.

Appendix

Appendix 1. Kinematic corrections for Photon Angular Distributions in (p, γ) Reactions

If $d\sigma/d\Omega_0$ is the angular distribution of gamma rays resulting from particle capture in the centre-of-mass system, the distribution in the laboratory system is given to first order in β by

$$\left(\frac{d\sigma}{d\Omega}\right)_{\text{lab}} = \frac{d\sigma}{d\Omega_0}(1+2\beta\cos\theta_0), \tag{1}$$

where $\beta = v/c = m/M+m\sqrt{2E/940}$, m and M are the incident particle and target mass, respectively, and E is the incident particle energy in MeV in the laboratory system. The relationship between angles in the laboratory and centre-of-mass systems is given by

$$\sin\theta_{\text{lab}} = (\sqrt{1-\beta^2}\sin\theta_0)(1+\beta\cos\theta_0)^{-1}.$$

Since for the maximum energy protons available in this experiment the term $2\beta\cos\theta_0$ has a maximum value of 0.03, eq. (1) can be written

$$\frac{d\sigma}{d\Omega_0} = \left(\frac{d\sigma}{d\Omega}\right)_{\text{lab}}(1-2\beta P_1(\cos\theta)).$$

If the measured distribution is written

$$\left(\frac{d\sigma}{d\Omega}\right)_{\text{lab}} = 1+a_1P_1+a_2P_2,$$

we have

$$\frac{d\sigma}{d\Omega_0} = 1+(a_1-2\beta+\tfrac{2}{5}\beta a_2)P_1+a_2P_2-\tfrac{12}{5}\beta a_2P_3,$$

provided $a_1 \ll 1$ and $2\beta\ a_1 \ll a_2$. Hence the main effect of the kinematic correction is to reduce the magnitude of the P_1 coefficient and to add a small P_3 term.

The measured angular distributions were not sufficiently accurate to warrant analysis up to $P_3(\cos\theta)$, and this term has therefore been ignored. In any case, both it and the $\frac{2}{5}\beta\ a_2$ term are considerably smaller than the main kinematic contribution $-2\beta\ P_1(\cos\theta)$.

References

1) See for references M. E. Toms, Naval Research Laboratory Bibliography no. 18, October 1960 (unpublished)
2) D. S. Gemmel, A. H. Morton and E. W. Titterton, Nuclear Physics **10** (1959) 33;
D. S. Gemmell, A. H. Morton and W. I. B. Smith, Nuclear Physics **10** (1959) 45

3) S. G. Cohen, P. S. Fisher and E. K. Warburton, Phys. Rev. Lett. **3** (1959) 433
4) N. W. Tanner, G. C. Thomas and W. E. Meyerhof, (private communication)
5) H. E. Gove, A. E. Litherland and R. Batchelor, Phys. Rev. Lett. **3** (1959) 177
6) H. E. Gove, J. A. Kuehner, A. E. Litherland, E. Almqvist, D. A. Bromley, A. J. Ferguson P. H. Rose, R. P. Bastide, N. Brooks and R. J. Connor, Phys. Rev. Lett. **1** (1958) 251
7) D. A. Bromley, A. J. Ferguson, H. E. Gove, J. A. Kuehner, A. E. Litherland, E. Almqvist and R. Batchelor, Can. J. Phys. **37** (1959) 1514
8) A. O. Hansen and J. L. McKibben, Phys. Rev. **72** (1947) 673
9) A. E. Litherland, E. Almqvist, R. Batchelor and H. E. Gove, Phys. Rev. Lett. **2** (1959) 104
10) H. E. Gove and E. B. Paul, Phys. Rev. **97** (1955) 104
11) L. Katz, private communication
12) R. B. Owen, Nucleonics **16** (1958) 54; (I.R.E. Trans. on Nuclear Sci. NS-5, (1958) 198)
13) D. J. Hughes and J. A. Harvey, BNL 325 July 1, 1955
14) S. Penner and J. E. Leiss, Phys. Rev. **114** (1959) 1101
15) T. Huus and R. B. Day, Phys. Rev. **91** (1953) 599
16) Proc. Int. Conf. Nuclear Structure, Kingston, Canada (1960), ed. D. A. Bromley and E. W. Vogt (University of Toronto Press, Toronto) Chapter VII
17) P. B. Smith and P. M. Endt, Phys. Rev. **110** (1958) 397
18) M. Kimura, K. Shoda, N. Mutsuro, T. Tohei, K. Sato and K. Kuroda, J. Phys. Soc. Japan **15** (1960) 1128
19) J. D. King, thesis, University of Saskatchewan and private communication
20) E. D. Courant, Phys. Rev. **82** (1951) 703
21) G. E. Brown and M. Bolsterli, Phys. Rev. Lett. **3** (1959) 472
22) G. E. Brown and J. S. Levinger, Proc. Phys. Soc. **71** (1958) 733;
J. S. Levinger, Nuclear Photo-disintegration (Oxford University Press, London 1960) chapter VI
23) F. Ajzenberg-Selove and T. Lauritsen, Nuclear Physics **11** (1959) 1
24) Cohen, Mann, Patton, Reibel, Stephens and Winhold, Phys. Rev. **104** (1956) 108
25) V. Emma, C. Milone and A. Rubbino, Phys. Rev. **118** (1960) 1297
26) E. E. Carroll and W. E. Stephens, Phys. Rev. **118** (1960) 1256
27) N. A. Burgov, JETP **37** (1959) 1811
28) M. Danos, Nuclear Physics **5** (1958) 23
29) K. Okamoto, Progr. Theor. Phys. Osaka **15** (1956) 75, Phys. Rev. **110** (1958) 143
30) H. E. Gove and C. Broude, in Proc. Second Gatlinburg Conf. on Heavy Ion Reactions, Gatlinburg (1960), ed. by A. Zucker, E. C. Halbert and F. T. Howard (John Wiley and Sons, Inc. New York 1960) p. 57
31) P. M. Endt and C. M. Braams, Rev. Mod. Phys. **29** (1957) 683
32) H. E. Gove, private communication
33) H. E. Gove, in Nuclear reactions, ed. by P. M. Endt and M. Demeur (North-Holland Publishing Co., Amsterdam, 1959) Chapter VI
34) D. H. Wilkinson in Proc. Rehovoth Conference on Nuclear Structure, ed. H. J. Lipkin (North Holland Publishing Co., Amsterdam 1958)
35) J. Blatt and V. F. Weisskopf, Theoretical nuclear physics (John Wiley & Sons Inc., New York, 1952)
36) J. S. Levinger, Nuclear photo-disintegration (Oxford University Press, London, 1960) Chapt. IV

1.E.5 *Nuclear Physics* **26** (1961) 511—526; © *North-Holland Publishing Co., Amsterdam*
Not to be reproduced by photoprint or microfilm without written permission from the publisher

EXPERIMENTAL STUDY OF THE CHARGE DISTRIBUTION OF O^{16} AND O^{18} BY ELECTRON SCATTERING

F. LACOSTE and G. R. BISHOP
Laboratoire de l'Accélérateur Linéaire, Orsay, S. et O., France

Received 21 February 1961

Abstract: The elastic scattering cross-sections for 150 MeV electrons on O^{16} and O^{18} have been compared for the scattering angles $\theta = 60°$, 90°, 100° and 110°. The inelastic cross-section on O^{18}, up to 6 MeV excitation energy, has been measured for the same angles. From these results one can deduce: 1) The difference between the length parameters of the harmonic well potential for O^{16} and O^{18}. If we write $a_{18} = (1+\varepsilon)\, a_{16}$, this experiment gives $\varepsilon = (2.5 \pm 0.6)\ 10^{-2}$. 2) The lifetime of the 1.98 MeV excited state of O^{18} is $\tau = (3.3 \pm 1.5)\ 10^{-12}$ s.

1. Introduction

The low excitation energy level scheme of O^{18} (fig. 1)[1, 2]) shows a structure which resembles very closely the schemes due to vibrational collective excitations found in heavier nuclei with a few nucleons outside closed shells. The shape oscillations of such spherical nuclei can be classified in multipole orders of which the lowest is in general the quadrupole vibration. In the harmonic oscillator approximation, the energy spacings are equal and excited states

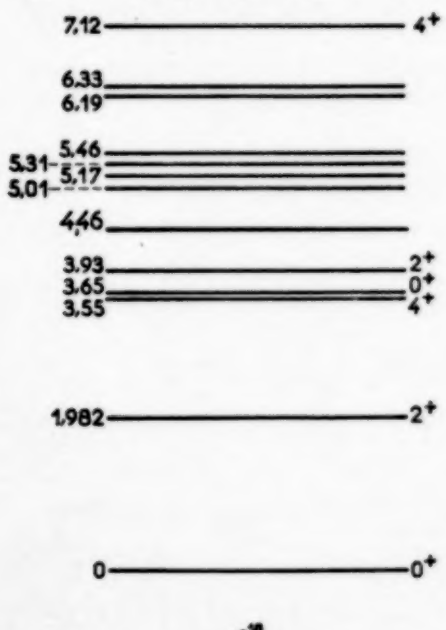

Fig. 1. Level scheme of O^{18} taken from ref. [1]) and modified to take into account recent experimental results [2]).

higher than the first are degenerate. This degeneracy is removed by higher-order terms in the nuclear energy such as are due to particle-core or particle-particle interactions. Thus the characteristic spectra referred to above has a triplet of levels with spins 0^+, 2^+ and 4^+ at approximately twice the energy of excitation of the first excited state [2]).

The vibrational excitations are characterized by enhanced electric transition probabilities. This is especially important when the extra nucleons are neutrons since then the electric transition probabilities between low lying states are due entirely to the "effective" radiating charge resulting from the polarization of the core by the outside nucleons [3]). A polarization of the core could possibly be detected as 1) a modified radius for the charge distribution in the ground state, 2) enhanced transition probabilities to some excited states.

For these reasons, we have attempted to detect a difference of charge radius in the isotopes O^{16} and O^{18}. The method used was the elastic scattering of 150 MeV electrons. We have also measured the cross-section for inelastic scattering of electrons of the same energy, from which the electric quadrupole transition probability to the first excited state can be deduced. The results are analyzed using the Born approximation formulas [4])†. These are known to be reasonably accurate for light elements before the first diffraction minimum. Also it is worth pointing out that in comparing two isotopes, the error introduced by the use of Born approximation should cancel, in first order. In this paper, all the lengths are written in fm and all the momentum transfers in fm^{-1}, if not specified otherwise.

2. Experimental Set-up

As this is one of the first experiments reported from this laboratory, we think it is pertinent to start by describing in some detail our experimental set-up (fig. 2).

The 150 MeV electrons are produced by the first four sections of the linear accelerator of this laboratory ††. The extracted beam is analyzed in energy and focussed on the target by a system of two zero gradient bending magnets [6]). Focussing is obtained by changing the angle of the exit rotating pole face of the first magnet and of the entrance rotating pole face of the second magnet. The first magnet and the energy defining slit are entirely enclosed by a 2 m thick wall of heavy concrete. The second magnet is further separated from the target room by shielding placed around the magnet and by a 50 cm thick wall of ordinary concrete. With this deflecting system, we obtain, on the target, beam spots 2 mm high and 8 mm wide, and an energy definition as good as 0.1 %.

† Hofstadter's review article [4]) contains many references to electron scattering and the literature on Born approximation.

†† An article is under preparation on the design and installation of the linear accelerator by the constructing company, the C.S.F., and with the assistance of the École Normale Supérieure.

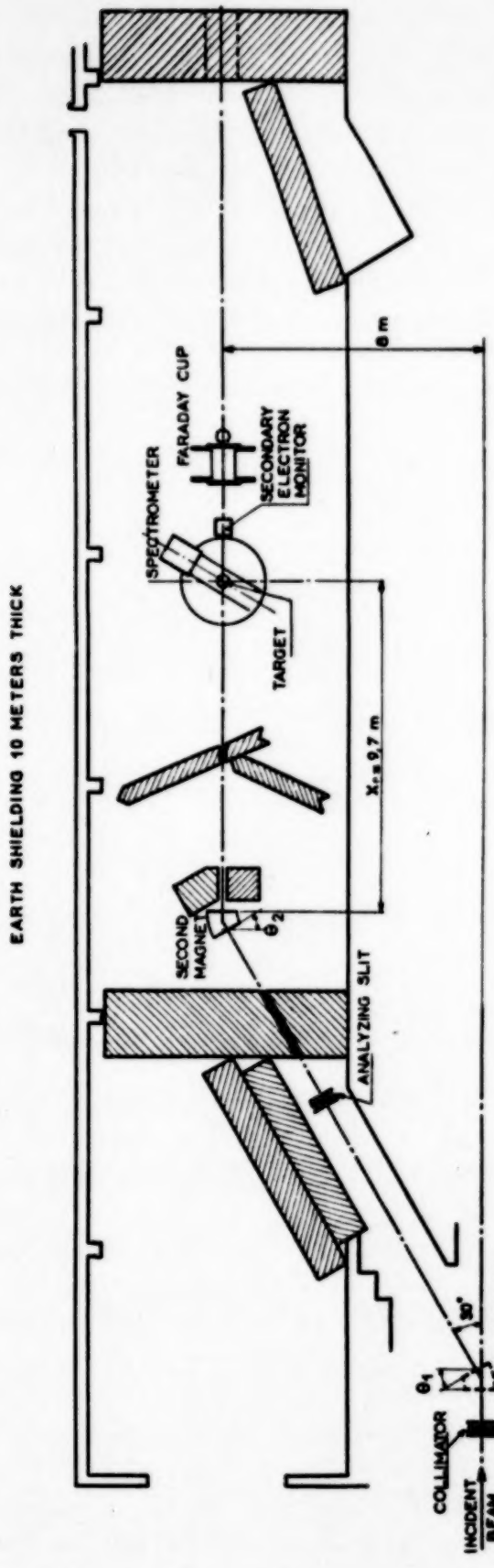

Fig. 2. The lay out of the experimental room at 250 MeV energy, showing the two magnet extraction system, analyzing spectrometer, target chamber, current monitors and shielding.

The analyzed beam incident on the target is monitored by either a Faraday cup of lead or a secondary emission monitor. The latter was calibrated against the Faraday cup and was used during these measurements since the presence of the Faraday cup in the beam considerably augmented the background.

Targets are mounted on a ladder at the centre of the scattering chamber, in a vacuum continuous with the accelerator vacuum. This ladder has telecommanded movements of vertical displacement and of rotation. After traversing the target, the beam leaves the vacuum through a thin aluminium window and enters the monitor. The diameter of the sensitive volume of the secondary

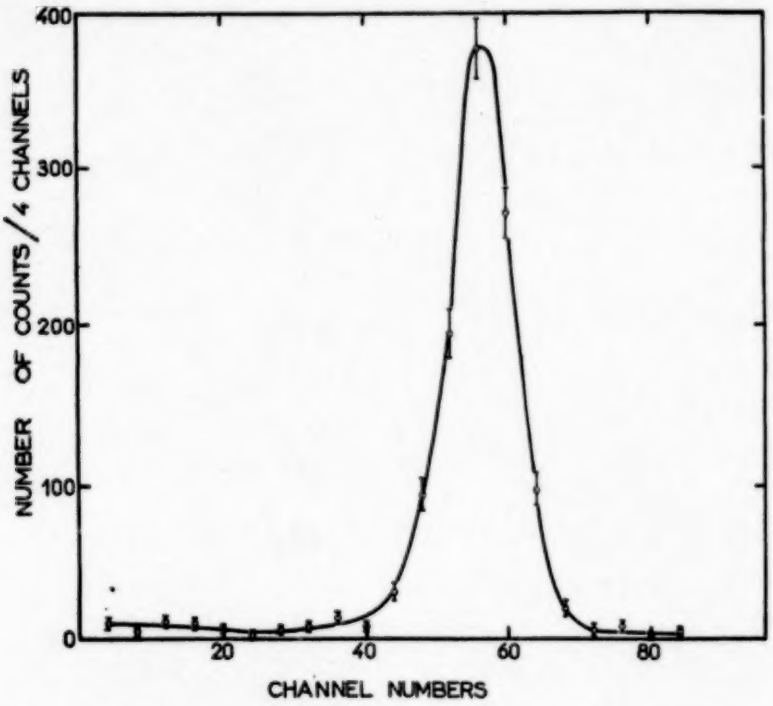

Fig. 3. Pulse height distribution from the lucite Čerenkov counter. Background pulses register in the first fifteen channels only.

emission monitor was 30 cm, which was amply sufficient to contain the direct beam diverging after multiple scattering in the target and window.

Attention was given to the alignment of target, spectrometer and current monitors. The target was situated at the point of intersection of the direct beam with the axis of rotation of the spectrometer. This alignment was carried out before the experiments and verified continually throughout the runs by the use of a fluorescent screen mounted on the target ladder and observed with a closed television system.

Electrons scattered by the target are analyzed in energy by a 180° double-focussing spectrometer. Electrons with the selected energy go through the analyzing slit of tungsten placed after the exit window of the spectrometer and are detected by a lucite Čerenkov counter 10 cm long and 6 cm wide. In fig. 3 is shown the differential pulse-height distribution obtained with this

counter, after a pulse-stretcher insensitive to the pile-up of the numerous background pulses. The pulse-stretcher circuit diagram is shown in fig. 4. For most experiments we used this pulse-stretcher followed by a biased scaler. The overall dead time of the recording circuits is determined by the pulse-stretcher and is long compared to the duration of a beam pulse.

When higher counting rates were measured we used a fast scaler. The basic idea of this scaler is to sum the standardized out-put pulses from a fast discriminator with a diode integrating circuit. With the pulsed accelerator, a scaling circuit based on this principle is relatively easy to build, one can use the long "dead" time between consecutive accelerator pulses to measure the out-put voltage of the integrating circuit with a multichannel pulse amplitude analyzer.

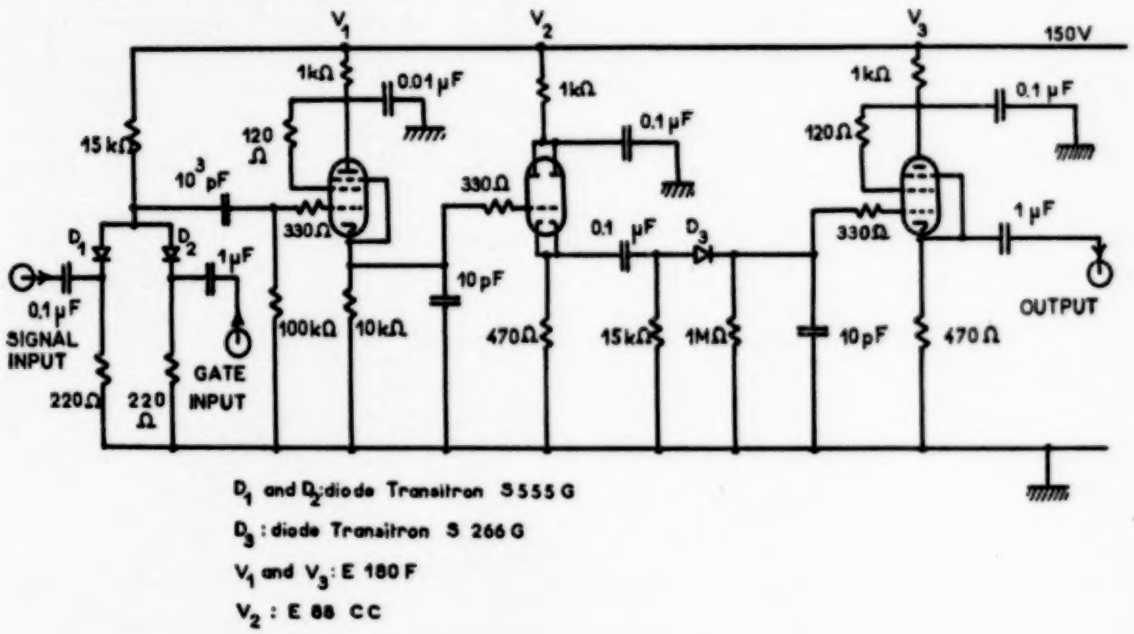

Fig. 4. Circuit diagram of the pulse-stretcher. The stretching is done in two stages by V_1 and D_3.

The fast scaler records the number of accelerator pulses where 0, 1, 2, 3, 4, 5 or more, simultaneous pulses have been registered.

When the accelerator operation is stable, the six numbers found, for a given counting rate, agree very closely with what one would expect assuming a Poisson distribution in the time of arrival of the Čerenkov pulses. When the accelerator operation is not stable, the discrepancy with the expected distribution can be large and it is then that the scaler is especially useful. Table 1 shows the results of a test of the scaler with variable counting rates.

For the experiments described here, we measured at each angle the energy spectrum of the scattered electrons. For the elastic scattering on O^{16} and O^{18}, the first inelastic peaks are well separated from the elastic peaks, thus permitting the use of a wide analyzing slit bracketing the entire elastic peak. The main advantages in this procedure are the following:

TABLE 1

Experimental results of a test of the fast scaler with variable counting rates

m	N_1	N_2	N_3	N_4	N_5	$\sum_{\alpha=1}^{5} N_\alpha$	$\sum_{\alpha=1}^{5} \alpha N_\alpha$	$\frac{1}{50} N_1/t$	me^{-m}
0.177	7090	814	77	8	0	7989	8981	13.9 %	15 %
0.57	4755	1443	345	66	11	6620	8995	30 %	32 %
0.118	7872	547	41	1	0	8461	9093	10.3 %	10.5 %
1.38	2109	1455	764	316	159	4724	9020	32.5 %	35 %
1.50	1917	1361	748	316	159	4501	8942	32 %	33.5 %
0.64	4479	1526	397	62	17	6481	9055	32 %	33 %
0.23	6999	940	91	5	1	8036	9177	18 %	18 %
0.083	8289	387	19	1	0	8696	9124	7.7 %	8 %

N_1, N_2, N_3, N_4 and N_5 give the number of accelerator pulses when 1, 2 . . ., 5 or more Čerenkov pulses were registered. The "true" number of Čerenkov pulses is given with good accuracy by $N = \Sigma_{\alpha=1}^{5} \alpha N_\alpha$. The mean counting rate is then $m = \frac{1}{50} N/t$, if t is the duration of the measurement (in sec). In the last two columns, we compare the predictions based on a Poisson time distribution with the experimental number $\frac{1}{50} N_1/t$. The agreement is quite good because the accelerator was stable during this experiment.

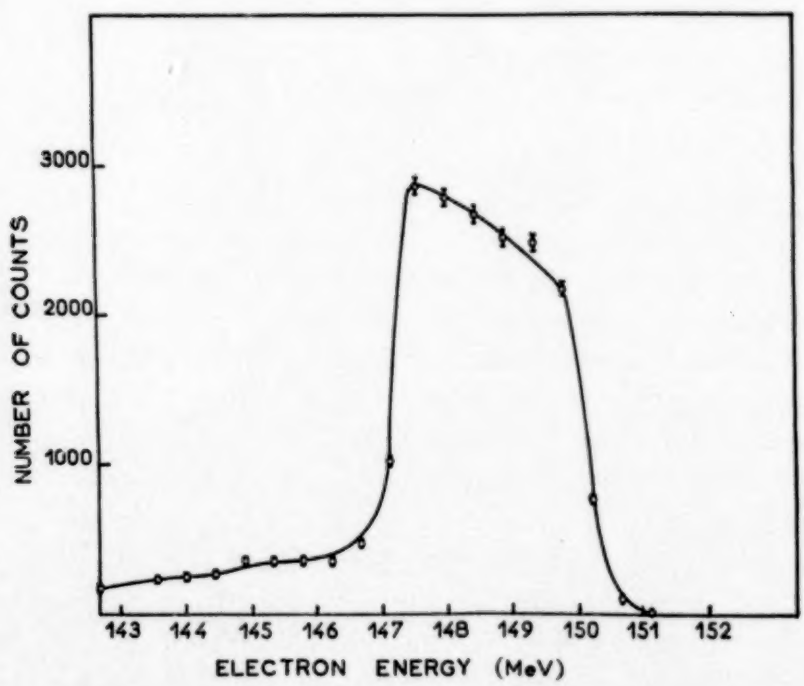

Fig. 5. O^{16} elastic peak measured with the spectrometer energy analyzing slit set at 2 %. The incident beam energy spread was set at 0.2 %.

a) The apparatus is as insensitive as possible to small variations in the energy and the vertical position of the incident beam.

b) The counting rates obtained are directly related to the cross-section.

c) When the cross-section is low, it permits the rapid accumulation of recorded counts, with consequently improved statistical precision.

Fig. 5 shows a typical spectrum obtained with a 2 % wide slit on the O^{16} elastic peak.

A number of preliminary tests were made with our equipment before taking data. The fast scaler was very useful to test to within 1 % statistical precision the overall stability of the equipment, to measure the horizontal profile of the spectrometer and to check the centering of the target.

TABLE 2

Elastic scattering results on hydrogen at 150 MeV

δ	Counts before corrections (in arbitrary units)	Counts after radiative corrections	Ratios of counting rates, normalized to $\theta = 120°$	Calculated ratios using the Rosenbluth formula with $\langle \overline{r^2} \rangle^{\frac{1}{2}}_{\text{proton}} = 0.80$
60°	775.7 ±20	951.2±38	23.1 ±0.9	21.8
80°	198.1 ± 5	246.5±10	6 ±0.24	6.02
100°	71.17± 1.8	89.9± 3.6	2.19±0.09	2.21
120°	32.13± 0.8	41.1± 1.7	1 ±0.04	1

This last experiment was made with a thin polyethylene target of known composition. The quoted errors take into account the statistical accuracy of the measurements and the uncertainty in the subtraction of the carbon tail under the hydrogen peaks.

Measurements of the elastic scattering on hydrogen (using a 2 % wide energy slit) were made with a polyethylene target and gave results summarized in table 2, which agree well with the known hydrogen cross-section [7]).

3. Comparison of the Form Factors of O^{16} and O^{18}

The cross-sections for the elastic scattering of electrons by the nuclei O^{16} and O^{18} were measured so as to compare their charge radii. Since the effect was expected to be small, it was decided to compare the observed cross-sections from similar targets during the same experimental run, rather than to perform separate determinations of them. Thus, for a given scattering angle and a given energy, the elastic peaks were measured from O^{16} and O^{18} consecutively. The advantages of this method are the following:

1) Errors in the measurement of the incident energy and of the beam intensity would cancel out in the ratio of the cross-sections.

2) Errors in setting the scattering angle as well as in the centering of the beam and in the angle of the target with the beam would also cancel.

3) No corrections for changes in counting efficiency need to be made.

By using also targets of similar thickness we reduced the importance of errors in the calculated radiative corrections. In fact, as will be seen, the measured cross-sections from O^{16} agreed very well with the expected ones, so that we might have made quite separate determinations of the cross-sections.

The targets were made of ordinary water containing O^{16} and of water enriched † in O^{18}. The water was enclosed between walls of rolled aluminium of 50 μm thickness, which were held with araldite to a frame of thickness 2 mm, 40 mm wide and 20 mm high. The water was freed of dissolved gases and filled into the targets with a hypodermic syringe through a small hole sealed afterwards with a rubber joint. The pressure in the targets, when these were placed in vacuum, was the saturation vapour pressure of water at the ambient temperature. This pressure produced a slight bulging of the walls. After prolonged bombardment, the bulging would increase, probably due to the decomposition of the water by the beam. The effective thickness at the point of impact of the beam, was found by measuring the elastic scattering by the hydrogen contained in the water. Thus, a determination of the ratio of the form factors, at a given energy and angle, involved the measurement of four elastic peaks. Further auxiliary measurements were made to determine the correction due to scattering from the aluminium walls, which amounted to 5 % at most for this experiment. For the hydrogen peaks, the contribution from the oxygen tail was substracted by admitting that this tail is flat and measuring its size just above and below the hydrogen peak. This assumption would not introduce a big error as the oxygen tail represented at most 20 % of the counting rate in the hydrogen peak.

The measurements were made using the wide slit described in sect. 2, as preliminary runs had shown this procedure to be more reliable than the usual procedure of measuring the differential cross-section and integrating the area under the peaks. Great care was taken to place properly the elastic peaks inside the energy bin defined by the slit. We estimate that the position of each peak was determined with an accuracy of 0.25 MeV, thus introducing an uncertainty in the counting rate smaller than 2 % for each peak.

The data, before corrections, are the ratios of counting rates corresponding to the elastic scattering by hydrogen and oxygen. Corrections smaller than 1 % must be applied to correct the experimental ratios for the finite solid angle subtended by the spectrometer, and for the various electromagnetic interactions of the electrons in the target and the windows between the target and the entrance of the spectrometer. Using the known composition of the enriched target, the ratios $\sigma(O^{16})/\sigma(H)$ and $\sigma(O^{18})/\sigma(H)$ can then be evaluated.

† The water enriched in O^{18} was furnished by the Weizmann Institute of Science, Rehovoth, Israel. It contained 95 % O^{18}, 0.6 % O^{17} and less than 0.1 % deuterium.

The individual cross-sections are given by the following expressions:

$$\sigma(\mathrm{H}) = \left(\frac{e^2}{2E_0}\right)^2 \frac{\cos^2\frac{1}{2}\theta}{\sin^4\frac{1}{2}\theta} \frac{1}{1+\frac{E_0}{M_1c^2}(1-\cos\theta)} \times \left[1+\left(\frac{\hbar q_1}{2M_1c}\right)^2 [2(1+k)^2\,\mathrm{tg}^2\tfrac{1}{2}\theta+k^2]\right] F_{\mathrm{H}}{}^2(q_1),$$

$$\sigma(\mathrm{O}_{16}) = \left(\frac{8e^2}{2E_0}\right)^2 \frac{\cos^2\frac{1}{2}\theta}{\sin^4\frac{1}{2}\theta} \frac{|F_{16}(q_{16})|^2}{1+\frac{E_0}{M_{16}c^2}(1-\cos\theta)},$$

$$\sigma(\mathrm{O}_{18}) = \left(\frac{8e^2}{2E_0}\right)^2 \frac{\cos^2\frac{1}{2}\theta}{\sin^4\frac{1}{2}\theta} \frac{|F_{18}(q_{18})|^2}{1+\frac{E_0}{M_{18}c^2}(1-\cos\theta)}.$$

Here E_0 is the energy of the incident beam, F_{H}, F_{16} and F_{18} are the elastic form factors for scattering by hydrogen, O_{16} and O_{18} and q_1, q_{16} and q_{18} are the momentum transfers for elastic collision and are given by the expression

$$q_\alpha = \frac{2E_0 \sin\frac{1}{2}\theta}{c\hbar\left[1+\frac{E_0}{M_\alpha c^2}(1-\cos\theta)\right]^{\frac{1}{2}}}.$$

From the experimental results and these expressions, one can deduce

1) the elastic form factors $F_{16}(q_{16})$ and $F_{18}(q_{18})$ if one assumes that the hydrogen cross-section is given by the Rosenbluth formula with the form factor measured in Stanford †;

2) the ratios of the form factors for O^{16} and O^{18} for the same momentum transfer q_{16}.

The formulae used for these calculations are the following:

$$|F_{16}(q_{16})|^2 = \frac{\sigma(\mathrm{O}_{16})}{\sigma(\mathrm{H})} \frac{|F_{\mathrm{H}}(q_1)|^2}{64} \frac{1+\frac{E_0}{M_{16}c^2}(1-\cos\theta)}{1+\frac{E_0}{M_1c^2}(1-\cos\theta)} \times \left[1+\left(\frac{\hbar q_1}{2M_1c}\right)^2 [2(1+k)^2\,\mathrm{tg}^2\tfrac{1}{2}\theta+K^2]\right],$$

† See ref. [4]), p. 252.

TABLE 3

Elastic scattering results on O^{16} and O^{18} at approximately 150 MeV

θ	q_{16}^2	$\frac{\sigma(O_{16})}{\sigma(H)}$	$0.95\frac{\sigma(O_{18})}{\sigma(H)}+0.05\frac{\sigma(O_{16})}{\sigma(H)}$	F_{16} (q_{16}) (experimental	$F_{16}(q)$ (calculated)	$\frac{F_{18}\ (q_{16})}{F_{16}\ (q_{16})}$
60°	0.573±0.004	16.44±0.65	15.50±0.60	0.473±0.025	0.483	0.970±0.04
90°	1.163±0.008	3.36±0.2 3.14±0.2 3.06±0.2 } 3.18±0.12	2.80±0.18 2.88±0.18 2.72±0.18 } 2.80±0.10	0.206±0.01	0.208	0.935±0.04
100°	1.356±0.01	1.82±0.12 1.68±0.11 1.60±0.10 } 1.70±0.06	1.38±0.08 1.34±0.08 1.22±0.07 } 1.31±0.05	0.153±0.007	0.153	0.875±0.035
110°	1.507±0.01	0.81±0.06 0.90±0.06 } 0.855±0.04	0.59 ±0.045 0.675±0.055 } 0.63±0.035	0.113±0.006	0.119	0.855±0.035

θ is the scattering angle, q_{16} is defined in sect. 3 F_{16} (calculated) is taken from ref. [9]). The quoted errors on q_{16} take into account the uncertainty in the energy calibration and the exact scattering angle. The quoted errors on F_{16} and F_{18}/F_{16} take into account the statistical accuracy of the measurements, the uncertainty in the subtraction of the oxygen tail under the hydrogen peaks and the possible errors introduced by a bad bracketing of the peaks within the energy bin defined by the slit. As the settings for the measurement of $\sigma(O_{16})/\sigma(H)$ are correlated to the settings for the measurement of $\sigma(O_{18})/\sigma(H)$ this last source of error is nearly cancelled out in the ratio F_{18}/F_{16}.

where

$$(F_H)^2 = \frac{1}{(1+0.05336\,q^2)^4},$$

$$\frac{|F_{18}(q_{16})|^2}{|F_{16}(q_{16})|^2} = \frac{\sigma(O_{18})}{\sigma(O_{16})}\left[1-\left(\frac{E_0}{(M_{16}c^2)}-\frac{E_0}{(M_{18}c^2)}\right)(1-\cos\theta)\left(1+\frac{q\,\mathrm{d}F_{18}}{F_{16}\,\mathrm{d}q}\right)\right].$$

Table 3 summarizes the results for the four values of q_{16} for which the measurements were done. F_{16} (calculated) is the O_{16} elastic form factor found by shell model calculations using a parabolic potential with the value of the length parameter a_{cm} determined by Ehrenberg *et al.* [7]).

This form factor has the simple analytic form

$$F(q) = \left[1-\frac{\alpha}{2(2+3\alpha)}q^2\,a_{cm}^2\right]\exp\left(-\tfrac{1}{4}q^2a^2\ (\text{charge})\right),$$

with $a^2\ (\text{charge}) = (1-1/A)\,a_{cm}^2+\frac{2}{3}\langle\overline{r^2}\rangle_{\text{proton}}$, $\alpha=\frac{1}{3}(Z-2)$ and $\langle\overline{r^2}\rangle_{\text{proton}}=0.64$.

This expression includes the recoil corrections evaluated by Tassie [8]).

For O^{16} we have $a_{cm} = 1.76$ and $F_{16}\,(q)$ is given by

$$F_{16}(q) = (1-0.387q^2)e^{-0.833q^2}.$$

The form factor $F_{16}(q_{16})$ is plotted against q_{16} in fig. 6, which shows also the values of $F_{16}(q_{16})$ determined by this experiment. The agreement is very good.

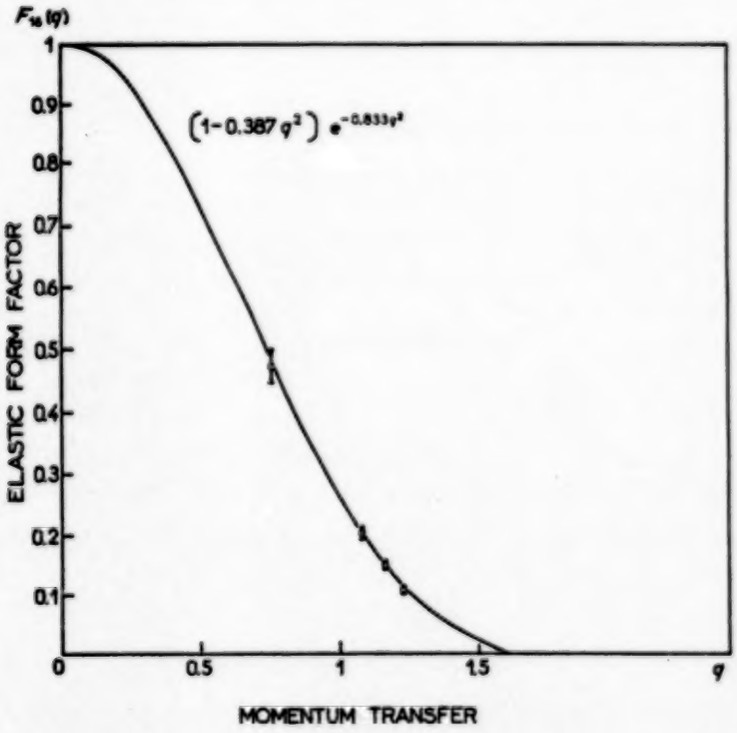

Fig. 6. Experimental values of $F_{16}(q_{16})$ determined by this experiment. The solid curve is the expression $(1-0.387\,q^2)\ e^{-0.833\,q^2}$, which gives the best fit to the data of ref. [9]).

This is interesting as this represents a pseudo-absolute measurement of the O^{16} elastic form factor.

The analytic form that must be used for O^{18} is probably quite similar to that of O^{16} as the protons are also all in the p-shell. The only difference that should exist is a difference in the length parameter a_{cm}. Fig. 7 shows the expected values of the ratio F_{18}/F_{16} assuming that the length parameter a_{cm} (O_{18}) is equal to $(1+\varepsilon)$ a_{cm} (O_{16}).

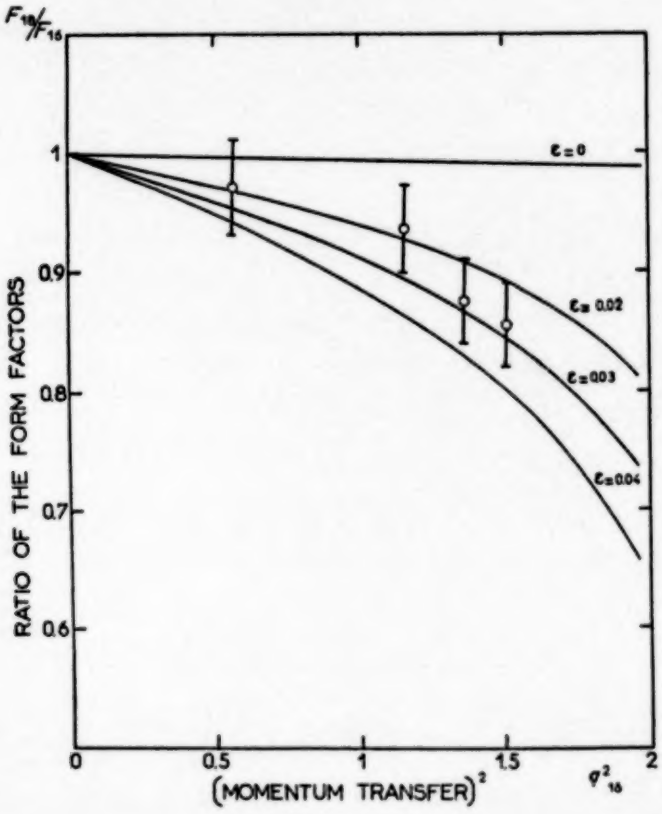

Fig. 7. Experimental ratios of the O^{18} and O^{16} elastic form factors versus q_{16}^2 (defined in sect. 3). The curves labelled $\varepsilon = 0$, $\varepsilon = 0.02$, $\varepsilon = 0.03$ and $\varepsilon = 0.04$ give the shell model predictions assuming a parabolic well potential with a_{cm} $(O^{18}) = (1+\varepsilon)$ a_{cm} (O^{16}).
For $\varepsilon = 0$ the predicted ratio is different from unity because the mass of the two nuclei are different and therefore the recoil corrections are not identical.

From these data, one can certainly conclude that the charge distribution of O^{18} is different from the charge distribution of O^{16}. If one believes in the form factor calculated using the shell model, this difference is expressed very simply by saying that the increase of the length parameter is 2.5 ± 0.6 %.

4. Inelastic Scattering on O^{18}

4.1. GENERAL STUDY OF THE CROSS-SECTION

The differential cross-section for scattering of 150 MeV electrons has been measured for several angles. First, a search with medium energy resolution

was made to find the general appearance of the cross-section up to 20 MeV excitation energy. This search was done at an angle of 110°, which corresponds to a q value near the expected maxima of the form factors for quadrupole excitation. The two most prominent peaks in the inelastic cross-section were located at 2 MeV and around 5.5 MeV. It was therefore decided to study with better resolution and more statistical accuracy the cross-section up to 7 MeV only.

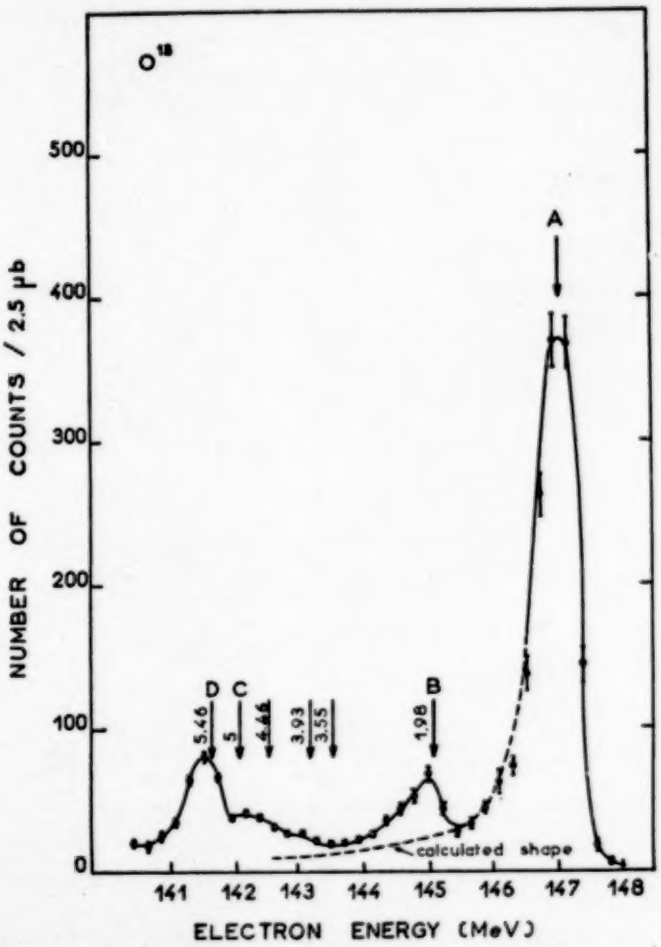

Fig. 8. Energy spectrum of 150 MeV electrons scattered on O^{18} at 90°. Peak A is the elastic peak. Peaks B, C. and D correspond to inelastic scattering with an excitation energy of 2 MeV, 5 MeV and 5.5 MeV. A contribution from the level at 4.46 MeV is probably necessary to explain the shape of the scattering cross-section.

Fig. 8 shows the differential cross-section obtained for a scattering angle of 90°, using an incident beam with an energy spread of 0.2 % and an energy analysing slit set at 0.2 %. Apart from the elastic peak, three peaks are visible with excitation energies of 2 MeV, 5 MeV and 5.5 MeV. These correspond, respectively, to the first excited state of O^{18} and two or more of the complex of levels known to have an excitation energy around 5 MeV. For comparison, the cross-section for scattering on O^{16} for the same angle and energy is shown in fig. 9.

It is interesting to observe that the excitation to the triplet of levels between 3.5 and 4 MeV is very weak as one would expect, in the harmonic potential approximation, for a vibrational excitation of the nucleus involving two phonons.

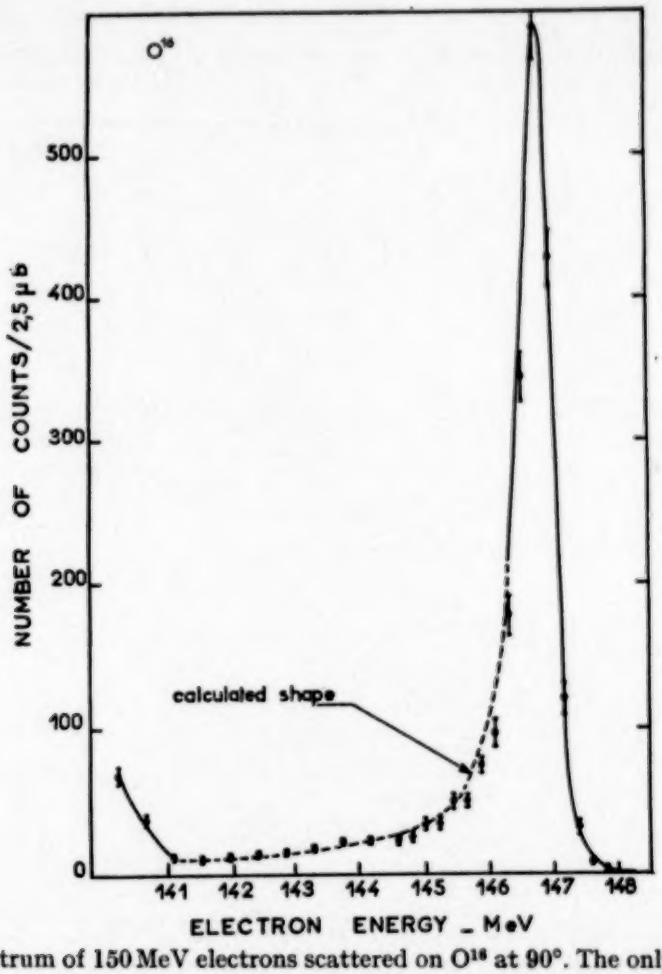

Fig. 9. Energy spectrum of 150 MeV electrons scattered on O^{16} at 90°. The only peak visible is the elastic peak. The dotted line shows the calculated shape of the elastic peak tail normalized to give the best overall fit. We have included in our calculations the Schwinger correction, the bremsstrahlung correction and an approximate formula for the ionisation losses.

4.2. ESTIMATION OF THE REDUCED TRANSITION PROBABILITY TO THE FIRST EXCITED STATE

The angular distribution of the cross-section for exciting O^{18} up to the 2 MeV (2^+) level has been measured between 60° and 100°. As the spin of this level is known to be 2^+, the transition from the ground state can only be electric quadrupole and the analysis is therefore simplified.

The method used was to measure the ratio $\sigma_{\text{inel}}/\sigma_{\text{el}}$ for several angles. If we define the inelastic form factor F_1 by

$$\sigma_{\text{inel}} = \left(\frac{8e^2}{2E_0}\right)^2 \frac{\cos^2 \frac{1}{2}\theta}{\sin^4 \frac{1}{2}\theta} (F_1)^2,$$

we have

$$\frac{F_1^2}{F_{1v}^2} = \frac{\sigma_{\text{inel}}(O^{18})}{\sigma_{\text{el}}(O^{18})}.$$

As F_{18} is known with a good accuracy from sect 3, we can deduce from these measurements the values of F_1^2 for given values of q. The reduced transition probability entering into the expression for the excitation cross-section is then given [9]) by

$$B[E_2, I_1 \to I_b] = \frac{[15]^2}{4\pi} Z^2 e^2 \left[\lim_{q\to 0} \frac{(F_1)^2}{q^4}\right].$$

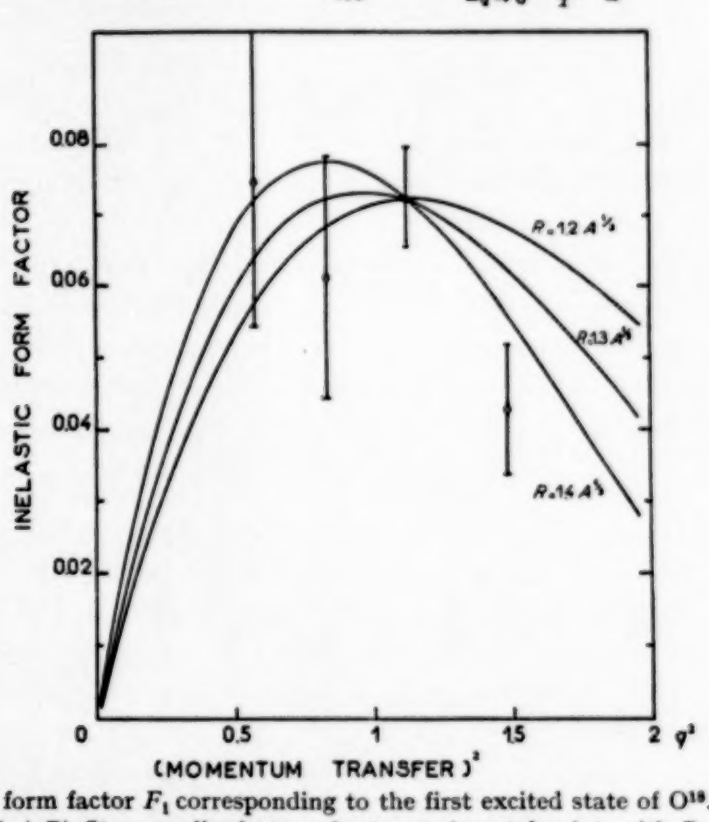

Fig. 10. Inelastic form factor F_1 corresponding to the first excited state of O^{18}. The solid curves are the values of $j_2(qR)$ Ct, normalized at our best experimental point, with $R = r_0 A^{\frac{1}{3}}$ ($r_0 = 1.2$, $r_0 = 1.3$ and $r_0 = 1.4$).

As the measurements were not made for small values of q, we must extrapolate our results. If one assumes that the interaction giving rise to the excitation happens near the surface of the nucleus, it can be shown that the inelastic form factor is proportional to $j_2(qR)$, where R is approximately the nuclear radius.

In fig. 10 we show the experimental values of F_1 plotted against q^2, and the shape of $j_2(qR)$ for $R = r_0 A^{\frac{1}{3}}$ with $r_0 = 1.2$, 1.3 and 1.4. The best fit is obtained for $r_0 = 1.4$, which gives for R a value 36 % bigger than the root mean square radius. This fact has already been noticed by Helm for other electric quadrupole transitions [5]).

If we assume that the shape of the inelastic form factor is given by

$$j_2(1.4A^{\frac{1}{3}}q) = j_2(3.67q),$$

we obtain

$$\lim_{q\to 0}\left[\frac{F_1^2}{q^4}\right] = (0.036\pm 0.015)\text{fm}^4.$$

The quoted uncertainty is intended to give a rough idea of the accuracy of the measurements and of the theory.

From this limiting value and the formulae of ref. [9]), we calculate the lifetime of the first excited state against gamma radiation to be $(3.3\pm 1.5)\ 10^{-12}$ s.

5. Conclusion

The elastic scattering result appears to indicate that the radius of the distribution of charge centres is different in O^{16} and O^{18}, but not as much as an $A^{\frac{1}{3}}$ dependence would give ($\varepsilon = 0.04$).

The inelastic scattering result shows that the effective charge of the neutrons presumably responsible for the E2 transition, is approximately unity as has been noted in O^{17}. To tend support to the vibrational interpretation of the low excitation level scheme, we note that inelastic scattering from the triplet of levels between 3.5 and 4 MeV is very small. This is consistent with a low transition probability from these states to the ground state.

We wish to thank Professor H. Halban for his interest in this work and the use of the facilities of this laboratory. We are especially grateful to Dr B. Milman for his help in the early stages of the experiment and regret that his departure for military service prevented a more complete participation. We are grateful to the staffs of the workshops directed by V. Round and G. Alon for their considerable aid, and to the Accelerator crew, directed by L. Burnod, for many hours of beam time. The assistance of many people in running the experiment and taking data is gratefully acknowledged.

References

1) F. Ajzenberg-Selove and T. Lauritsen, Nuclear Physics **11** (1959) 237
2) S. Hinds, Phys. Soc. Conf., Liverpool (1960);
Jarmie and M. G. Silbert, Phys. Rev. **120** (1960) 914
3) K. Alder, A. Bohr, T. Huus, B. Mottelson and A. Winther, Rev. Mod. Phys. **28** (1956) 535
4) R. Hofstadter, Ann. Rev. Nuclear Sci. **7** (1957) 231
5) Richard H. Helm, Phys. Rev. **104** (1956) 1466
6) J. Pinel, Ann. de radioélectricité **14** no. 57 (1959), **15** no. 59 (1960)
7) H. Ehrenberg, R. Hofstadter, V. Meyer-Berkhout, D. G. Ravenhall and S. E. Sobottka, Phys. Rev. **113** (1959) 666;
U. Meyer-Berkhout, K. W. Ford and A. E. S. Green, Ann. Phys. **8** (1959) 119
8) L. J. Tassie and F. C. Barker, Phys. Rev. **111** (1958) 940
9) L. I. Schiff, Phys. Rev. **96** (1954) 765

10.E *Nuclear Physics* **26** (1961) 527—528; © *North-Holland Publishing Co., Amsterdam*

ERRATA

A. Deloff and J. Wrzecionko, The phenomenological baryon-baryon scattering theory and the relative parity determination (Nuclear Physics **20** (1960) 464).

The following corrections are to be introduced in table 1: the expression for the $M_{10}^{(-)}$ term proportional to $\langle 1\, L|T^L|1\, L+1\rangle$ has plus sign instead of minus and a minus sign is omitted before the expressions for $M_{01}^{(-)}$ and $M_{51}^{(-)}$. These errors influenced strongly our final results concerning the polarizations P_c and P_d which are 0 in both cases of relative parity. This result comes out also from the spherical symmetry of the S wave which does not distinguish any direction. Since the reaction plane is not determined, the polarization must be 0. If in a reaction only one vector is determined (together with the initial or final momentum) there is no sense to introduce **n**, **l**, **m** vectors and to write the polarization tensor in terms of them as was done in a second paper by us (Nuclear Physics **21** (1960) 237). Denoting the distinguished direction by **s** the correlation function of mesons is always of the form $A+B(\mathbf{k}_1\cdot\mathbf{k}_2)+C(\mathbf{s}\cdot\mathbf{k}_1)(\mathbf{s}\cdot\mathbf{k}_2)$ irrespective of the relative parity. The coefficients A, B, C depend only on energy.

We are indebted to Professor Y. Yamaguchi and Dr. M. I. Shirokov for their remarks which helped us to find the error.

J. M. Hansteen, A Remark on the Coulomb Disintegration of Accelerated Heavy Ions (Nuclear Physics **19** (1960) 309).

Equation (8) should correctly read

$$b_{\mathrm{if}}=\frac{4\pi Z_2 e^2}{i\hbar}\sum_{\lambda,\mu}\Big(\sum_{n=1}^{2}a_n{}^{\lambda}Z_1{}^{(n)}(-1)^{(n-1)\lambda}\Big)\frac{1}{2\lambda+1}S_{\mathrm{E}\lambda,\mu}\langle \mathrm{f}|r^{\lambda}Y_{\lambda\mu}(\theta,\varphi)|\mathrm{i}\rangle.$$

This leads to a vanishing dipole disintegration cross section when the two fragments of the disintegrating projectile have the same charge-to-mass ratio.

The cross section for the Coulomb disintegration of accelerated ^{6}Li ions into α-particles and deuterons in the field of gold nuclei has been computed in the quadrupole case with the same simplified model.

In the table below the calculated values of $\sigma_{\mathrm{Coulomb}}^{(\lambda=2)}$ are compared with the data of Anderson *et al.* (Bull. Am. Phys. Soc. **5** (1960) 292) for the total cross section for α-particle emission in the collision σ_{total}.

E_1 (MeV)	25	34	60
σ_{total} (mb)	40	400	500
$\sigma_{\text{Coulomb}}^{(\lambda=2)}$ (mb)	12	70	200

Without going further into the details of the reaction mechanism the calculations with this primitive model still show the usefulness of the cluster picture in this region of the periodic table.

NORTH-HOLLAND BOOKS

Proceedings of the VIIth International Conference

on

LOW TEMPERATURE PHYSICS

Toronto

August 29 - September 3, 1960

editors | G. M. GRAHAM and
A. C. HOLLIS HALLETT
University of Toronto

1. Second Fritz London Award
2. The Mössbauer Effect
3. Magnetic Relaxation
4. Liquid and Gaseous H_2
5. Magnetism below 1°K
6. Further Communications on Magnetism
7. Polarization of Protons
8. Nuclear Orientation
9. Fermi Surface
10. Ultrasonic Attenuation
11. Resistance Minima
12. Further Communication on Transport Properties in Solids
13. Theory of Superconductivity
14. Electrical Properties of Superconductors
15. Superconductivity of Hg and Ta
16. Specific Heat of Alloys
17. Intermediate State
18. Further Communications on Superconductivity
19. Flow Properties of Liquid Helium-4
20. Kapitza Boundary Layer
21. Ions in Liquid Helium
22. Helium Film
23. Further Communications on the Properties of He^4
24. Liquid and Solid He^3
25. Thermodynamic Properties of He^3-He^4 Mixtures
26. Further Communications on He^3-He^4 Mixtures
27. Equation of State and Thermodynamic Properties
28. Thermodynamic Properties of Argon
29. Further Communications on Thermodynamic Properties
30. Proposal for a He^3 Temperature Scale

745 pp. Gld. 57.00 (114s.)

Sole distributors outside U.S.A. and Canada:

NORTH-HOLLAND PUBLISHING COMPANY — AMSTERDAM

NORTH-HOLLAND BOOKS

Just out
Second, revised edition

PLASMA Physics

by **J. G. LINHART**
CERN, Geneva

From reviews of the first edition

The author has the three rare qualifications of experience, mathematical facility and inventive imagination. He also possesses didactic ability, but this will be appreciated only by those readers who share with him the advantages of mathematical ability and of an active mind. It is not a book which can be imbibed passively, or uncritically.

The arrangement is so clear, with full description of the experimental methods and with all the relevant theory required to explain the data, that the book can be equally recommended to the student and to the expert research worker.

Nature

The whole book provides an admirable, if laconic, summary to a vast and important field of work of great topical interest.

Journal of the Royal Institute of Chemistry

6 x 9" 290 pp. 125 figs. Gld. 25.00 (50s.)

NORTH-HOLLAND PUBLISHING COMPANY-AMSTERDAM

Sole distributor U.S.A.: Interscience Publishers Inc. New York